STUDIES IN FRETTING FATIGUE WITH SPECIAL REFERENCE TO THE EFFECT OF STRESS DISTRIBUTIONS ON THE FATIGUE STRENGTH OF ASSEMBLED COMPONENTS

by

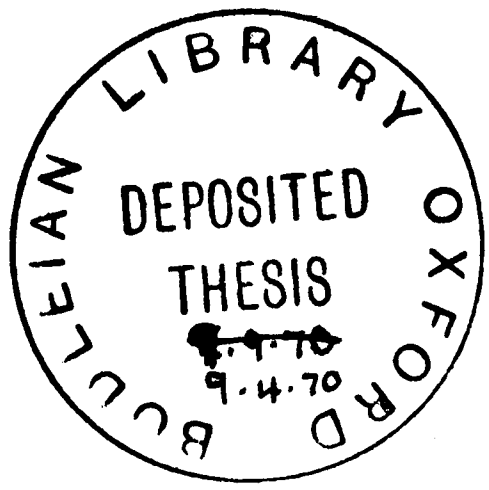
G.P. Wright

BALLIOL COLLEGE

Thesis submitted for the Degree of D.Phil at the University of Oxford

Department of Engineering Science,
Parks Road,
Oxford.

January 1970



STUDIES IN FRETTING FATIGUE WITH SPECIAL REFERENCE TO THE EFFECT OF STRESS DISTRIBUTIONS ON THE FATIGUE STRENGTH OF ASSEMBLED COMPONENTS

by

G.P. WRIGHT

ABSTRACT

When an assembly (such as a shrink-fitted shaft/hub configuration) is subjected to oscillating loads, two components of the assembly may experience oscillating slip relative to each other, giving rise to fretting on the interface between the two components. If, subsequently, a fatigue failure originates in that fretting region, the nominal failure stress is often considerably lower than the fatigue strength of the appropriate material.

The object of the research reported in this thesis was to investigate a hypothesis which explains the (relatively) low magnitude of fretting fatigue strengths as a consequence of macroscopic stress concentrations in the fretted region. Such stress concentrations are a function of the overall geometry of the assembly and it was suggested that, as a result, stress distributions in assemblies should be similar to stress distributions in geometrically similar one-piece (solid) components. In an assembly, high stress concentrations near an interface are partially relieved by slip (which gives rise to fretting) and it was thought that an assembly

should be stronger, therefore, than the equivalent solid. Even so, it was expected that a detailed analysis of the stress distribution in an assembly would predict stress concentrations of sufficiently high magnitude to explain failure under the low nominal stresses found in practice, thus demonstrating that fretting, itself, does not greatly affect fatigue strengths.

Fatigue tests were carried out using solid and assembled specimens of various shapes and a method was developed, using finite element techniques, to analyse the stresses in the assemblies, taking full account of slipping. The theoretical stress analysis showed that, for certain geometries and systems of loading, the stress distributions in an assembly may differ considerably from those in a geometrically similar solid. Furthermore, when the fatigue results were examined in the light of the stress analysis, it was apparent that fretting can reduce the fatigue strength of a material by more than 60%.

To explain this result, a new hypothesis is proposed. It is suggested that under conditions of oscillating slip, the discontinuous contact between two surfaces of an assembly results in large stress concentrations in the regions of actual contact. It is shown that such stress concentrations can be of sufficient magnitude and affect a sufficiently large volume of material to cause failure at a nominal stress considerably lower than the fatigue strength of the material concerned. Such a hypothesis is supported by the results of this investigation and also by the results of several other workers.

ACKNOWLEDGEMENTS

The work described in this thesis was carried out in the Department of Engineering Science at the University of Oxford between April 1967 and December 1969.

I am deeply indebted to Dr. John O'Connor who, besides initiating this research, advised, cajoled and inspired me but never interfered; surely the ideal supervisor.

I was generously financed throughout my three years at Oxford by I.C.I. Ltd. and was encouraged by the interest shown by members of the Plastics Division at Welwyn Garden City. Research contracts were provided by the Science Research Council and the Ministry of Technology.

Messrs. Ted Noel and Peter Mott manufactured specimens and ran the fatigue tests and, despite the repetitive nature of such work, they always contrived to appear enthusiastic.

Mrs. Noel typed the thesis, showing a rare understanding of hieroglyphics.

Finally, I should like to thank all those members of the Engineering Department and the Computing Laboratory who gave advice and assistance during this investigation or who helped with the production of this thesis by, criticising, proof reading and xeroxing.

G.P.W. Jan.1970

CONTENTS

		Page
Abstract		
Acknowledgements		i
Notation		ix
Chapter 1.	A HYPOTHESIS TO EXPLAIN FRETTING FATIGUE FAILURES AND OUTLINES OF TESTS DESIGNED TO INVESTIGATE THE VALIDITY OF THAT HYPOTHESIS	1
1.1	Introduction	1
1.2	The Mechanics of Fretting	3
1.3	Stress Fields Associated with Fretting Fatigue	6
1.4	Proposed Fatigue Tests	10
1.5	The Programme of Investigation	14
Chapter 2.	A SURVEY AND INTERPRETATION OF PREVIOUSLY PUBLISHED WORKS IN THE LIGHT OF THE HYPOTHESIS PROPOSED IN CHAPTER 1	
2.1	Introduction	17
2.2	Investigations into the Mechanics of Fretting	18
2.3	Investigations into Fretting Fatigue	19
2.4	Reports of Service Failures and Related Laboratory Tests	24
2.5	Interpretations of Previously Published Works	27
Chapter 3.	EXPERIMENTAL WORK	
3.1	Introduction	29
3.2	Testing Methods, Equipment and Conditions	29
3.2.1	The Fatigue Testing Machine	29
3.2.2	Material from which Specimens were manufactured	30
3.2.3	The Design of the Basic Specimen	31
3.2.4	Tolerances and Surface Finish	33
3.2.5	Application of Clamping Load	34
3.2.6	Ratio of Axial to Clamp Loads	36
3.2.7	Setting up and Running Tests	38
3.2.8	Measurement of Slip Amplitude	39
3.2.9	Determination of the Coefficient of Friction	43
3.3	Fatigue Tests	47
3.3.1	Series 1. To investigate the effect of changing geometric stress concentration	47
3.3.2	Series 2. To investigate the effect of slip amplitude by changing block length	51

3.3.3 Series 3. Fretting applied in the absence of a propagating load 52
3.3.4 Series 4. Fretting in the absence of macroscopic stress concentration but in the presence of a propagating stress 56
3.3.5 Series 5. Tests carried out following the completion of the Theoretical Analysis of Stress Distributions in Assemblies 58
3.3.6 Series 6. Tests using blocks with 'feet' 59
3.4 Summary 60

Chapter 4. EXPERIMENTAL RESULTS

4.1 Introduction 62
4.2 Series 1 62
4.2.1 S-N Curves 62
4.2.2 Amplitude of slip and size of slip region 74
4.3 Series 2 77
4.4 Series 3 82
4.5 Series 4 83
4.6 Series 5 88
4.7 Series 6 98
4.8 Microscopic Examination of Specimens after Testing 100
4.9 Summary 100

Chapter 5. A METHOD FOR DETERMINING STRESSES IN A CLAMPED JOINT

5.1 Statement of the Problem 102
5.2 Literature Survey 105
5.3 Method of Solution 106
5.4 The Finite Element Method 111
5.5 The Finite Element Method Applied to Plane Stress or Plane Strain 113
5.6 Solution of Finite Element Problems and Evaluation of Method 116

Chapter 6. DETAILS OF THE METHOD OUTLINED IN CHAPTER 5

6.1 Introduction 122
6.2 Solution of the Slip Problem 124
6.2.1 Derivation of Displacement and Equations from Influence Coefficients 124
6.2.2 Boundary Conditions 127
6.2.3 Solution of Nodal Forces 129
6.3 Proportional and Incremental Loading 133
6.3.1 Introduction 133
6.3.2 Incremental Loading 134
6.3.3 The Effect of Load Cycles 137
6.4 Modifications to the Method after Solving some Trial Problems 139
6.4.1 Separation of Surfaces 139
6.4.2 Slip starting at points other than at the edge of the interface 142

6.4.3 Secondary slip 142
6.5 The Determination of Nodal Forces for Various Loads during a Complete Load Cycle 143

Chapter 7. THE DISTRIBUTION OF STRESS AND OTHER VARIABLES IN SOLID AND ASSEMBLED SPECIMENS UNDER FATIGUE LOADING

7.1 Introduction 148
7.2 Division of Continua into Finite Elements and Statement of Boundary Conditions 149
7.2.1 Solid sharp cornered specimens 149
7.2.2 Assembled sharp cornered specimens 149
7.2.3 Assembled radiused specimens 153
7.3 Sharp Cornered Solid 153
7.3.1 Stress distributions 153
7.3.2 Estimate of slip in an assembly 160
7.4 Sharp Cornered Assembly 160
7.4.1 Introduction 160
7.4.2 Slip and separation 164
7.4.3 Solutions to some simplified stress problems compared to those obtained by other methods 172
7.4.4 Stress distributions 174
7.5 Radiused Assemblies 181
7.5.1 Extent of slip region and amplitude of slip 181
7.5.2 Stress distributions 185
7.6 Damping Properties of Assemblies 188
7.7 Comparison of Theoretical Solutions with Experimental Results 190
7.8 Assessment of the Method and some General Comments 194

Chapter 8. DISCUSSION OF RESULTS AND A REVISED HYPOTHESIS TO EXPLAIN FRETTING FAILURES

8.1 Introduction 196
8.2 Strength Reduction Factors Associated with Fretting 199
8.3 A Review of the Hypothesis Proposed in Chapter 1 in the Light of Experimental Results 203
8.4 Stress Concentrations Associated with Discontinuous Contact 204
8.5 A New Hypothesis to Explain Fretting Fatigue Failures 209
8.6 Evidence in Support of the New Hypothesis 210
8.7 The Combined Effects of Fretting and Geometric Stress Concentration 212
8.8 Some Consequences of the New Hypothesis 214
8.9 Suggestions for Further Work 216
8.10 Conclusions 217

Appendix 1. A Computer Program to Solve Plane Stress or Strain Problems 220

Appendix 2. A Program to Solve the Contact Problem 237

Appendix 3. Photoelastic Determination of Stress in Fatigue Specimens 247

References 252

LIST OF FIGURES

Fig.	Title	
1.1	A typical laboratory fretting fatigue specimen	7
1.2	The use of fillet radii to strengthen solid components and assemblies of the same overall shape	11
2.1	Arrangement used to evaluate the effect of fretting on fatigue strength	21
3.1	The basic fatigue specimen	32
3.2	A sharp cornered assembly after failure showing the use of the clamping frame	35
3.3	Measurement of slip, using replicas	40
3.4	Arrangement for measuring dynamic slip	41
3.5	The arrangement used to determine the coefficient of friction	44
3.6	Variation of the coefficient of friction with number of cycles of load	46
3.7	Corner details of specimens used in Series 1	48
3.8	Arrangement for applying fretting to specimens in the absence of a propagating load	54
3.9	Arrangement for investigating the effect of fretting away from a macroscopic stress concentration	57
4.1	S-N curves for sharp cornered specimens	64
4.2	Sharp cornered specimens after failure	65
4.3	Non propagating crack in a sharp cornered solid	67
4.4	S-N curves for fully radiused specimens	69
4.5	Fully radiused specimens after failure	70
4.6	S-N curves for incomplete radiused specimens	71
4.7	Incomplete radiused specimens after failure	73
4.8	Slip amplitudes for assemblies in Series 1	75
4.9	Slip amplitudes for assemblies with different block lengths	75
4.10	S-N curves for sharp cornered assemblies with different block lengths	78
4.11	Sharp cornered assemblies tested with blocks of different length	80

4.12	Specimens of the type used in Series 4	84
4.13	S-N curves for Series 4	86
4.14	S-N curves for sharp cornered assemblies with different ξ	90
4.15	Variation of maximum slip amplitude at fatigue limit with ξ in sharp cornered assemblies	91
4.16	Sharp cornered assemblies tested at different ratios of axial to clamp load	92
4.17	S-N curves for sharp cornered solids with ξ = 1 and 8	93
4.18	S-N curves for Series 6	99
5.1	A plate loaded axially following indentation by rectangular blocks	104
5.2	Continuous pressure distribution represented by n blocks of constant pressure	108
5.3	An element of a continuum in plane stress or plane strain	114
5.4	Plate with central hole	117
5.5	Coarse mesh for plate/hole problem	118
5.6	Fine mesh for plate/hole problem	118
5.7	Solutions for 66 node plate/hole problem	120
5.8	Solutions for 118 node plate/hole problem	120
5.9	Solutions for 118 node plate/hole problem using quadrilaterals	121
6.1	Sharp cornered assembly	122
6.2	Nodes on the interface of an assembly	123
6.3	Slip region in a sharp cornered assembly	125
6.4	Vertical displacement due to a block indenting a plate	128
6.5	Flow diagram for basic iterative process	132
6.6	Flow diagram for iterative process used for solving problem when separation occurs	141
6.7	Boundary conditions during unloading of a sharp cornered assembly	144
6.8	Flow diagram for iterative processes used to solve the general slip problem	146
7.1	Mesh for sharp cornered solid	150
7.2	Mesh for flat plate	151
7.3	Mesh for block	151
7.4	Mesh for full radiused plate	154
7.5	Mesh for incomplete radiused plate	154
7.6	Sharp cornered solid (notation)	155

7.7	Normal stress in a sharp cornered solid	157
7.8	Axial stress in a sharp cornered solid	158
7.9	Shear stress in a sharp cornered solid	159
7.10	Load displacement loop for sharp cornered assemblies	163
7.11	The extent of the slip region in a sharp cornered assembly	165
7.12	Variation of slip amplitude along the interface of a sharp cornered assembly	167
7.13	Change in slip amplitude when $\emptyset$ changes from 1.0 to 0.95 during a cycle with $\lambda^* = 8$	167
7.14	Separation of surfaces during tensile axial loading	168
7.15	Vertical displacement of the interface surface of a block due to point tangential loads on that surface	168
7.16	Normal and shear stresses in a sharp cornered solid and assembly under normal load only	173
7.17	Normal pressure distribution due to a rigid block indenting an elastic plate	175
7.18	Normal stress in a sharp cornered assembly under tension	176
7.19	Normal stress in a sharp cornered assembly under compression	177
7.20	Axial stress in a sharp cornered assembly under tension	179
7.21	Axial stress in a sharp cornered assembly under compression	180
7.22	Maximum shear stress in a sharp cornered assembly under tension	182
7.23	Maximum shear stress in a sharp cornered assembly under compression	183
7.24	Incomplete radius assembly, slip amplitudes	184
7.25	Full radius assembly, slip amplitudes	184
7.26	Stress distributions in an incomplete radius assembly	186
7.27	Stress distributions in a full radius assembly	187
7.28	Load-displacement loops for radiused assemblies	189
7.29	Maximum shear stress determined photo-elastically and theoretically	192
7.30	Comparison between experimental and theoretical slip amplitudes	193
8.1	An idealised model of surfaces on which contact is discontinuous	206
8.2	A cylinder indenting a flat surface	206

A1.1	Flow diagram of program to solve plane stress or plane strain problems using finite elements	221
A2.1	Flow diagram for program to solve nodal forces in the contact region	238
A3.1	Photoelastic model of a full radiused assembly under load	249

NOTATION

A1, A2 B1, B2 C1, C2 D1, D2 E G	Influence coefficients
E	Young's modulus
F_1	Normal force
F_2	Axial force
F	Force
K_t	Stress concentration factor
K_f	Strength reduction factor
L	Load magnitude
N	Number of cycles (fatigue results)
P	Normal force (nodal)
Q	Shear force (nodal)
S	Stress (fatigue results)
U1,U2	Displacement in x direction
V1,V2	Displacement in y direction
a	Length of interface or semi-contact width
a	Radius of hole in plate
d	$1/\Delta$
d_c	Displacement of point in plate originally coincided with the corner of the block
f	F_2/Δ
h	Height of block
l	Total nominal contact length
l_s	Length of slip region
m	Number of nodes slipping
n	Number of nodes on interface
p	Normal pressure
p	P/Δ
q	Q/Δ
r	Radius
s	Slip amplitude
s_p	Separation amplitude
t	Thickness of plate away from blocks
t'	Thickness of plate between blocks
u	Displacement in x direction

v	Displacement in y direction
w	Width of plate or block
x	Co-ordinate or distance along interface measured from corner
y	Co-ordinate
Δ	'y' displacement of point at the centre of the top surface
λ	ratio of nominal axial stress away from blocks to nominal normal pressure
λ	peak positive value of during load cycle
μ	coefficient of friction
σ_a	nominal axial stress on interface
σ_o	nominal axial stress away from blocks
σ_n	nominal normal stress
σ_x	axial stress on interface
σ_y	normal stress on interface
σ_R	maximum range of axial stress
σ_r	radial stress
σ_θ	hoop stress
τ_o	nominal maximum shear stress away from blocks
τ_{xy}	shear stress.
τ_l	(limiting) shear stress before slip occurs
τ_{max}	maximum shear stress on interface
ξ	ratio of nominal axial stress on interface to nominal normal pressure
ν	Poissons ratio

Chapter 1

A HYPOTHESIS TO EXPLAIN FRETTING FATIGUE FAILURES AND OUTLINES OF TESTS DESIGNED TO INVESTIGATE THE VALIDITY OF THAT HYPOTHESIS

1.1 INTRODUCTION

In recent years, several investigations (1 - 6)[+] of the fatigue strength of shafts with shrunk-on or press fitted collars or wheels have been reported. These investigations have usually followed catastrophic service failures at operating loads well below those at which failure was expected. In several instances (1,2,3), the strength reduction has been attributed to the presence of severe geometric stress concentrations associated with rapid changes of section near the origin of failure, whilst in others (4,5,6), the combined effects of the stress concentration, and of fretting damage on the interface, have been suggested as the cause of failure.

Fretting occurs at the interface between metallic surfaces in contact when the surfaces slip relative to each other under the action of an oscillation force. Both the amplitude of slip and the normal force maintaining the surfaces in contact can be very small, but all investigators agree that the essential pre-requisite for fretting to occur is oscillating slip. Depending on the loads that are acting on an assembly in which fretting is occurring, fretting can have a number of effects. If the loads in the components are relatively small and the amplitude of slip low, fretting will simply result in a mild deterioration of the surface (fretting corrosion). With larger slip amplitudes and high normal pressure on the interface but relative low oscillating loads parallel to the interface, the fretting may result in heavy wear and loss of fit between the components of the assembly (fretting wear).

[+]References are given at the end of the thesis.

Neither of the above mentioned effects are likely to be disastrous. However if the oscillating loads parallel to the interface are high enough, the fretting appears to result in premature failure of the assembly - often at nominal stresses well below the unnotched fatigue strength of the material, Such failures are described as fretting fatigue failures.

Laboratory investigations into the effect of fretting on the fatigue strength of several materials have been reported by many authors. Typical of such investigations is the work of Field, Fenner and other co-authors at the National Engineering Laboratories described in (7,8,9,10). They describe tests in which pads were clamped against the surfaces of a fatigue specimen to induce slip on the interfaces when the specimen was loaded axially. Under conditions of an oscillating axial load, fretting damage was produced. The fatigue strength of the fretted specimens was found to be considerably lower than that of plain, polished specimens, the strength reduction being attributed to fretting. Factors such as normal load, slip amplitude, coefficient of friction, atmospheric conditions, specimen-pad material combinations, surface finish and surface treatment have all been considered relevant, to a greater or lesser extent, to the reduction in fatigue strength. However, few investigators consider the effect of the contact stress field associated with the fretting pads on the fatigue strength of their specimens.

Estimates of the strength reduction factor due to fretting vary widely, but those quoted in (7,8,9,10) which

are typical of several investigations, give values of up to five for zero mean load in the specimens and up to seventeen under certain other conditions of mean load. The same references suggest that the amplitude of slip at the edge of the interface is a major factor in determining fretting fatigue strength. It is proposed to put forward a theory which explains such large strength reductions by considering the effect of the stress concentrations usually present in a fretting situation.

1.2 THE MECHANICS OF FRETTING

The considerable strength reduction attributed to even slight degrees of fretting is, at first sight, hardly consistent with the relatively mild nature of fretting damage which can be likened, in surface profile, to a poor surface finish. It therefore seems necessary to examine the stress fields set up during the fretting process.

It has been found (11) that the onset of fretting damage on the interface of an assembled component can often be predicted from the theoretical stress distribution on the interface. It is well established that fretting occurs wherever the surfaces slip relative to each other, in an oscillatory manner, and that a slip amplitude of as little as 10^{-7} inches produces detectable damage. Assume that at each point on the interface, there is a certain limiting shear stress, τ_1 related to the local coefficient of friction, μ, and the local normal pressure p, ($\tau_1 = \mu p$), which the surfaces can transmit across the interface. At all points on the interface,

where the local transmitted shear stress is less than τ_1, the surfaces will remain locked together but elsewhere, the surfaces will slip and the shear stress on the interface, will be limited to τ_1. To predict where slip, and consequent fretting, are likely to occur in an assembly, it is useful to think of the stress fields set up in a geometrically similar, but continuous, solid without an interface under the action of the same loads. Slip and fretting will occur in the assembly wherever the shear stress in the solid, in the region of, and parallel to, the interface in the assembly exceeds the limiting friction, τ_1. Consider, as an example, a solid and an assembly in which the interface is parallel to the x axis. In the solid, the normal pressure, p, will be represented by the y-stress σ_y. Wherever, in the solid, along a line representing the interface in the assembly, the shear stress $\tau_{xy} > \mu\sigma_y$ (where μ is the coefficient of friction in the assembly) slip will occur at the corresponding point in the assembly. In fact it will extend over a larger region than is estimated on this basis because of the redistribution of stress due to slip.

In general then, slip in the assembly will be predicted by shear stress concentrations in the solid at points which coincide with the interface in the assembly.

In the solid, such stress concentrations are relieved by plastic flow and local cracking; in the assembly they are relieved by slip. Thus the onset of fretting in an assembly is controlled by the stress field within the component, the distribution of which is determined by the

geometry, the coefficient of friction and the relative magnitude of the normal and shear forces transmitted across the interface. Most of the examples of fretting reported in the literature fit into this picture. Fretting is found near the edges of the interface where there is usually a rapid change of section.

In applying the results of a theoretical contact stress analysis to a practical situation, there is one obvious complication: contact between real surfaces is not continuous but occurs at the tips of surface asperities. Forces are transmitted from one surface to the other through asperity junctions. The action of fretting continuously shears these junctions and leads to the formation of small pits from which fatigue cracks have been found to propagate. Associated with the junctions and pits are local stress fields which are referred to subsequently as 'microscopic' stress concentrations and which distort the theoretical contact stress field and the associated 'macroscopic' stress concentration. However, the dimensions of such junctions and pits are usually small compared with typical dimensions of the interface, so that the volume of material affected by the microscopic stress concentrations should be orders of magnitude less than that affected by the macroscopic stress field. It has been shown (12) that the bulk deformation of certain assemblies can be closely predicted by a theoretical analysis which ignored the effect of asperity contact, thereby implying that the distortion of the theoretical macroscopic stress field occurs only in shallow layers very close to the interface.

1.3 STRESS FIELDS ASSOCIATED WITH FRETTING FATIGUE

A typical fretting fatigue laboratory specimen is shown in Fig. 1.1. Two rectangular blocks are pressed against the plane faces of a standard fatigue specimen by a clamping force, P, and the specimen is subjected to an alternating axial load, F. Fretting occurs in the region near the edges of the interface, which in a solid would be a region of high stress, and fatigue cracks propagate through the specimen from the fretted areas.

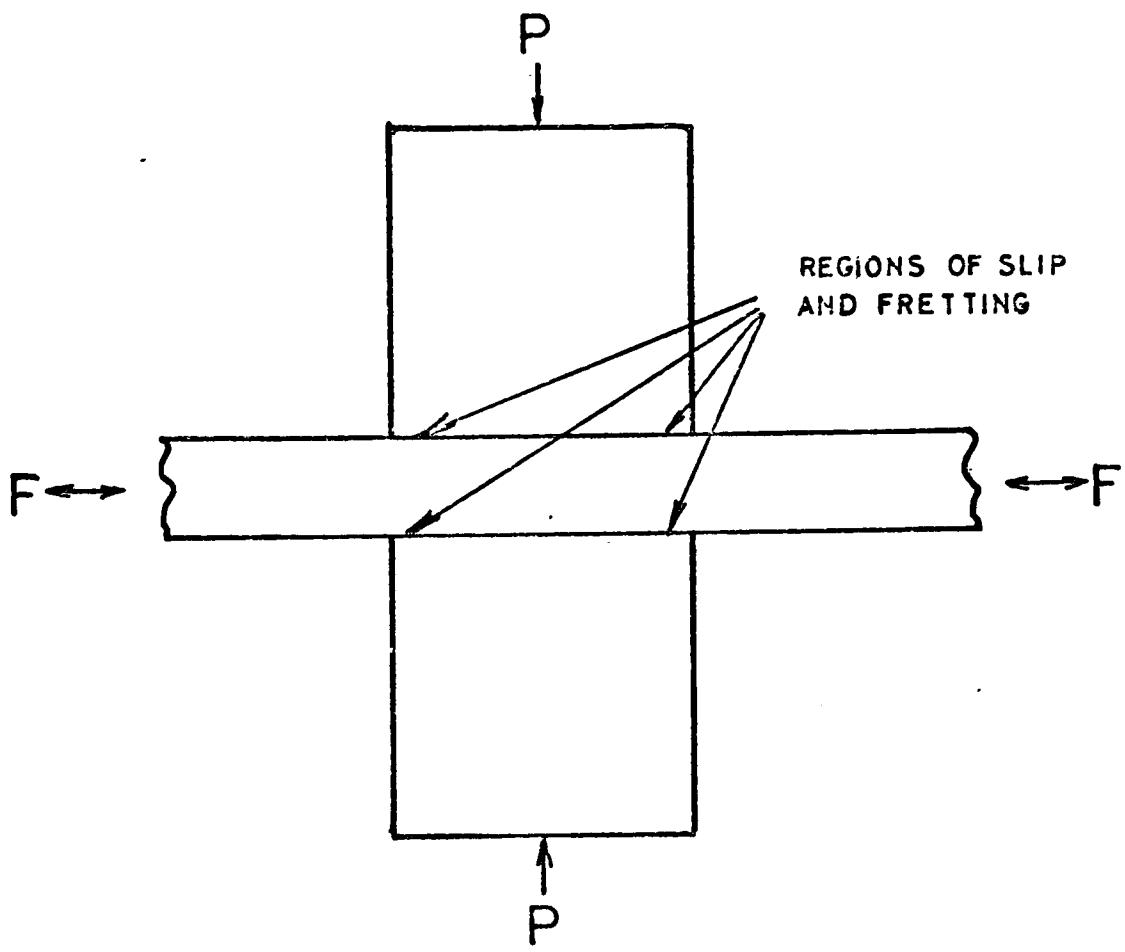
Following the discussion of the previous section, it is useful to think of the stress field, in the vicinity of the cracks, in terms of three components:

(1) The nominal axial stress, σ_o, due to the bulk alternating load (F).

(2) The macroscopic stress field near the interface which depends on P, F, the coefficient of friction (μ), and the geometry.

(3) The microscopic stress-fields associated with asperity junctions and fretting pits.

It is common practice to compare the fatigue strength or fatigue limit (σ_o at 10^7 cycles or runout) of such an assembly with that of a plain polished specimen; to attribute the reduced strength of the assembly to fretting (i.e. to component 3 above); and to ignore altogether the effect of the macroscopic contact stress field. The present work was based on the hypothesis that such a comparison was unrealistic, that the onset of fretting and the reduction of fatigue strength are both effects of a common cause, the macroscopic stress concentration, rather than cause and effect. For example, in the case illustrated in Fig. 1.1 the theoretical stress concentration (based on



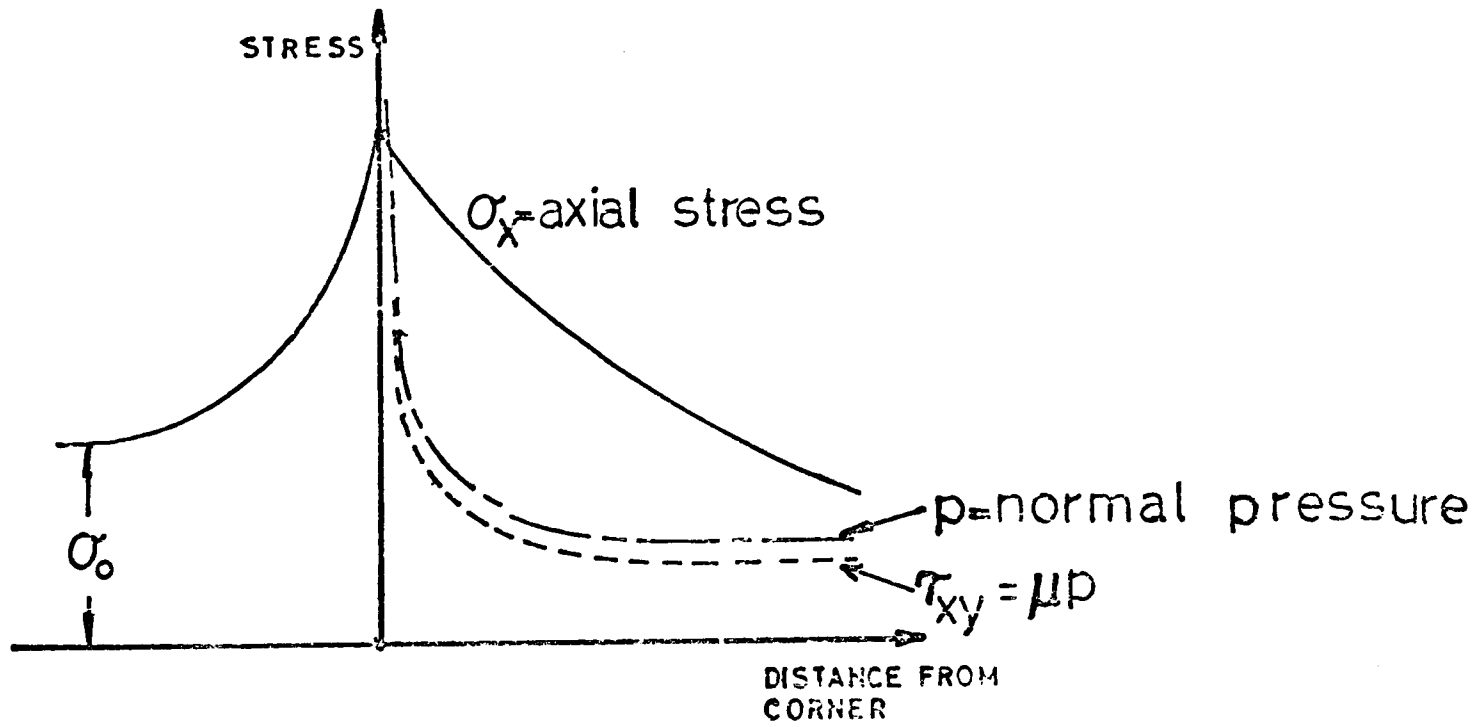


Fig. 1.1 A typical laboratory fretting fatigue specimen

The stress distributions are those originally thought to be present in the slip region. Subsequent analysis showed such estimated distributions to be grossly in error.

elastic analysis) at the corner in a solid of the same shape would be infinite, and it might be expected that, even after slip, the stress concentration at the corner would still be significant in determining the fatigue strength. Thus, it was thought that a more realistic assessment of the effect of fretting on fatigue strength would be obtained by comparing the strength of an assembly with that of a geometrically similar solid of the same material subjected to the same system of loads.

In comparing the fatigue strength of an assembly with that of a geometrically similar solid, there appear to be two main factors which would contribute to a difference in behaviour. On the one hand the stress concentration in the assembly is partially relieved by slip which will tend to strengthen the assembly in comparison to the solid. On the other hand, fretting damage and the associated surface pits should weaken the assembly in comparison to the solid. It is not possible to predict, for a given material, the relative importance of these two factors. However, the volume of material affected by the microscopic stress concentration at a fretting pit should be orders of magnitude less than that affected by the macroscopic stress field. Thus, although fretting may account for the process of crack initiation in the assembly, the rate at which the crack would propagate, and hence the time to failure, should be determined more directly by the macroscopic stress field.

Before the work described in this thesis commenced, a small amount of evidence existed to support the proposed hypothesis.

Unpublished work by J.J. O'Connor, carried out at the University of Minnesota, described experiments in which specimens had been fatigued while fretting was applied to the surface of the specimens by cylinders clamped against them. In this case the elastic contact stress field is well known. The strength of the fretted specimens, when compared to that of unfretted specimens, showed a smaller strength reduction than would be predicted by the (elastic) stress analysis. However, strength reduction factors in fatigue predicted from theoretical stress concentration factors are rarely achieved in practice and the discrepancy is usually attributed to the size effect. From Massonet's experiments on steel plates with holes of various diamters (13, p.138), a measure of the size effect can be obtained. When the results, described above, were interpreted in the light of Massonet's results, it was concluded that the reduction in fatigue strength observed with the fretting specimens was due primarily to a concentration of tensile stress associated with the elastic contact stress field.

The possibility that an assembled component may be stronger in fatigue than a continuous solid of the same shape would have important consequences in the design of clamped joints and shrink or press fitted assemblies. Whether this is so or not will clearly depend on the relative effects of fretting and the contact stress field in determining fatigue strengths. For reasons already explained, the traditional fretting fatigue tests such as those of Field et al (7,8,9,10) produce results

which give a measure of the combined effects of fretting and the contact stress field associated with the particular geometry of the specimens used.

It is difficult to use such results to predict the fretting fatigue strength of other geometries or to deduce from them data which will be useful to designers in the avoidance of fretting fatigue failure. For example, if the effect of fretting on fatigue strength is slight and the major contribution to the strength reduction comes from the contact stress field, assemblies could be strengthened in the same way as solids, that is by the use of stress relieving radii etc. (Fig. 1.2). Alternatively, if fretting is the major factor, then failure might be prevented by various surface treatments or by increasing the normal pressure on the interface so that slip is prevented.

In order to clarify the situation, a programme of fatigue tests was devised to investigate the relative importance of fretting and geometry in determining fatigue strengths of assemblies.

1.4 PROPOSED FATIGUE TESTS

The programme of tests originally proposed (and subsequently carried out) was designed to establish the relative importance of the following features:

(a) the macroscopic stress concentration, both modified and unmodified by slip and fretting,

(b) fretting, applied in the absence of a bulk propagating load in the specimen,

(c) fretting applied in the presence of a propagating load free from macroscopic stress concentrations.

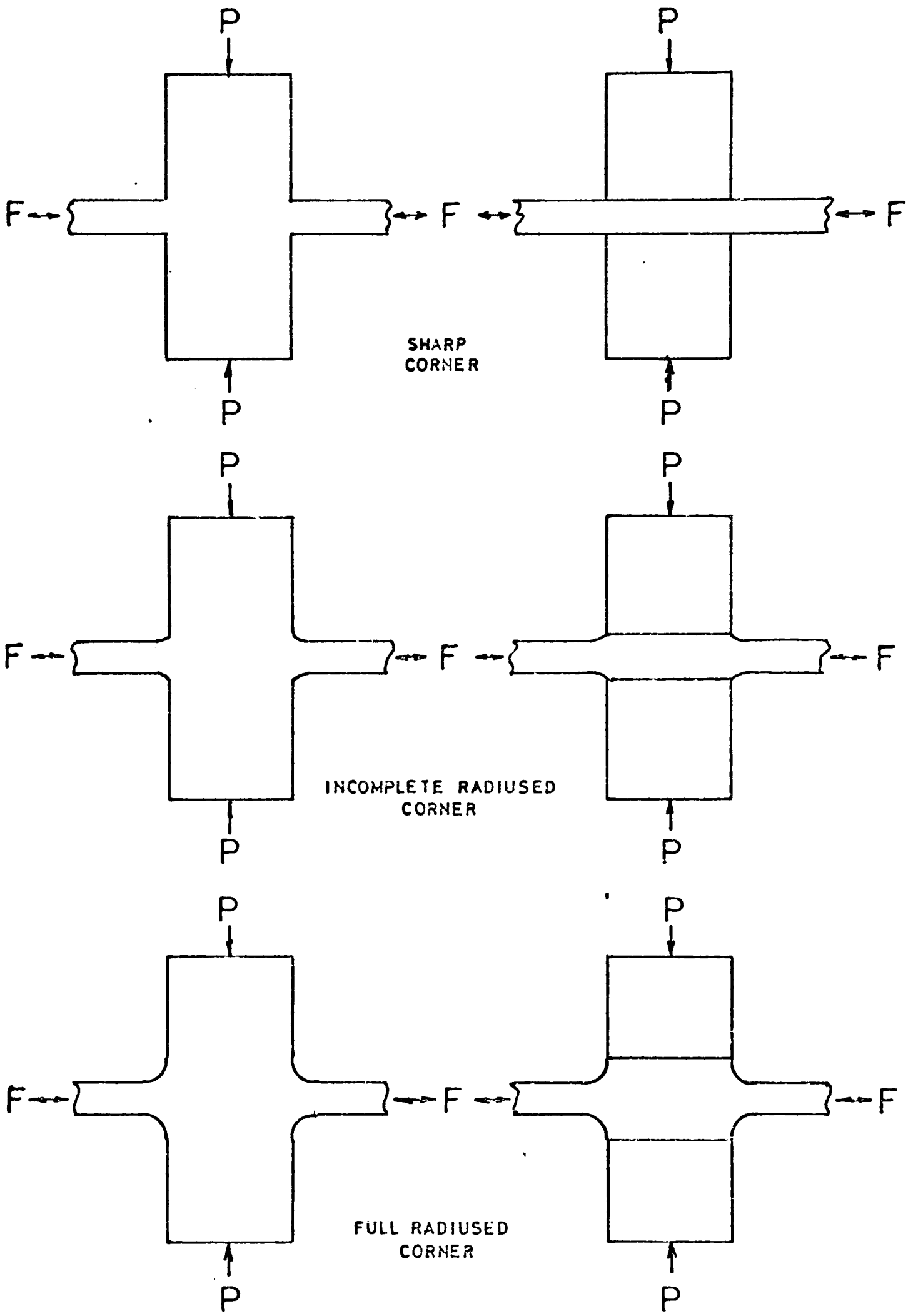


Fig. 1.2 The use of fillet radii to strengthen solid components and assemblies of the same overall shape
Above geometries may be plane or sections through axisymmetric components.

In addition, in view of the emphasis placed on slip amplitude in determining fretting fatigue strengths, it was proposed to carry out tests in which the slip amplitude was varied either side of the mean value of slip amplitude which occurred in the other tests. By this means it was hoped to show that the interpretation of the results was not confused by slip amplitude effects.

Initially, therefore, four series of tests were carried out, using one material, Aluminium alloy to BS L65, for all tests. In the first series of tests, solid and assembled specimens of the same overall shape were tested under identical systems of loads. Three shapes were tested and the macroscopic stress concentration at the edge of the interface was progressively reduced, from that associated with a sharp corner, by the use of fillet radii, i.e. as shown in Fig. 1.2. Thus the fatigue behaviour of solid specimens, having three different theoretical stress concentration factors, was compared with that of assemblies of the same shape, in which slip and fretting occurred during the application of the fatigue load. According to the arguments of the previous section, the following results should have been observed. Assuming that fretting is of secondary importance vis a vis the geometry, the assemblies in which the high stresses are relieved by slip should be stronger than the equivalent solid. Possibly, when the fillet radius is generous so that the stress concentration factor for the solid is very small, the stress relief due to slip (if any) in the assembly will be small and both solid and

assembly will have nearly identical fatigue strengths. If the assumption that fretting is relatively unimportant is not correct, the above predictions will be modified, in practice, to a degree determined by the relative effect that fretting does have.

Because of the importance attached, by other investigators, to slip amplitude, it was proposed to monitor the maximum slip amplitude occurring in each assembly.

In the second series of tests fretting damage was applied to the surfaces of the specimen by moving the pads relative to the specimen. The only load transmitted through the specimen was that load which was transmitted across the interface by friction. Thus the propagating load and, hence, the macroscopic stress concentration, present during the fretting phase was about an order of magnitude less (in terms of actual stress levels) than in the first series. When the surfaces of the specimen were sufficiently damaged, i.e. when 'Talysurf' measurements of surface profile in the fretting region resembled those for the fretted region in the first series, the fretting pads were removed and the specimen then fatigue tested without further fretting. It was argued that, if fretting damage alone is not important, the fatigue strength of these specimens should be very close to that of plain, polished specimens, since the fretting is applied in the absence of either a significant macroscopic contact stress field or a bulk propagating load.

In the third series, the specimens were designed such that the origin of failure was in an area of fretting

remote from the macroscopic stress concentration. Here the stress, very close to the origin of failure, could be measured using strain gauges, and, since the stress gradients are low, this stress will be very nearly the stress at which failure occurred. It was argued that any strength reduction factor, calculated from the value of measured stress at the point of failure and the fatigue strength of a plain unfretted specimen, would be the strength reduction factor due to fretting applied in the presence of a known propagating stress.

A fourth series of tests, carried out in order to assess the effect of slip amplitude, used sharp cornered assembled specimens, such as those used in series 1, with several sets of fretting blocks, each of different length. The maximum slip amplitude depends on the block length, and, provided the change in length was not so great that the block length ceased to be significant compared to the specimen thickness, it was argued that the macroscopic stress concentration would not change appreciably and the results would not be influenced by a fretting area size effect. Therefore, any change in fatigue strength with block length could be assumed to be a function of the changing slip amplitude. As in the first series, it was proposed to monitor the slip amplitude at the edge of the interface during each test.

1.5 THE PROGRAMME OF INVESTIGATION

It was proposed to design the specimens for the tests described above, using values of stress concentrations determined photo-elastically.

Such determinations could be completed quickly and fatigue tests could be commenced without delay, thus leaving ample time to carry out a thorough programme of fatigue testing which must, inevitably, spread over many months. While the fatigue tests were being run, it was proposed to analyse the stresses in the specimens theoretically. It was appreciated that such an analysis would also take many months to complete and there would not be sufficient time to complete the fatigue test programme if testing was not started until after the theoretical stress determinations were complete.

For various reasons described in Appendix 3, the results of the photoelastic stress determinations for assembled specimens were thought to be incorrect. The assembled fatigue specimens were therefore designed on the basis of photoelastic results for solid specimens and the qualitative extension of such results to assemblies, explained in Section 1.2.

The results of early fatigue tests supported the hypothesis proposed earlier in this chapter but it later transpired that these results were misleading. Later tests suggested that the hypothesis was over simplified. Moreover, when the results of the theoretical stress determinations were complete, they showed that the original photoelastic determination of stresses in assemblies was basically correct and that the qualitative estimates of the stress fields in assemblies had, in some cases, been wildly inaccurate. Further tests were therefore run, and some of the original tests re-run in

a slightly modified form, to investigate changes to the original hypothesis suggested by the theoretical results and the early fatigue test results.

The author hopes that by describing the hypothesis in its original form and then showing how it was subsequently modified in the light of the results the reasoning throughout the rest of the thesis will be more easily followed.

Before examining the details and results of the work described, it is interesting to return to the published results of other investigators in the field of fretting fatigue and to see how their results support, or fail to support, the hypothesis described in Section 1.3.

Chapter 2

A SURVEY AND INTERPRETATION OF PREVIOUSLY PUBLISHED WORKS IN THE LIGHT OF THE HYPOTHESIS PROPOSED IN CHAPTER 1

2.1 INTRODUCTION

Broadly speaking,the work of previous authors, in the field of fretting and related topics, can be put into one of three categories: (1) investigation of the fretting process alone, making little or no reference to its effect on fatigue; (2) investigation into the effect of fretting on fatigue strength; (3) work carried out to investigate the fatigue strength of assembled components during which fretting appeared as a contributory factor.

Obviously there is considerable overlap between categories. For instance,investigations into the fretting process, or the mechanics of fretting, often consider the effect on fretting damage of environment, slip amplitude, normal pressure and many other such factors. These parameters are also varied in most fretting fatigue investigations to see whether the consequent change in fretting damage affects the fatigue strength.

There is however one very noticeable and curious dichotomy in the approach to the problem of fretting fatigue adopted by workers in the second and third categories.

Investigations into the fatigue strength of assemblies, such as shrink fitted shafts and hubs or pin and lug attachments, usually start by considering the overall geometric stress concentration of a solid of the same shape, or even the contact stress field in the actual

assembly. If this still does not explain experimental results or service failures, the difference is explained by reference to the debilitating effect of fretting in regions of high stress. On the other hand, workers investigating fretting fatigue as a separate entity, invariably induce it in assemblies which, if analysed as though they were solids of the same overall shape, would exhibit large geometric stress concentrations. However, when interpreting the fatigue results, the contact stresses are usually ignored and the full strength reduction is attributed to fretting.

It appears that people interested in the fatigue strength of assemblies consider fretting as being of secondary importance and predict fatigue strengths on the basis of a theory similar to that described in Chapter 2. This is not usually true of people investigating fretting fatigue in isolation.

2.2 INVESTIGATIONS INTO THE MECHANICS OF FRETTING

Early investigations of fretting, such as those of Tomlinson, Thorpe and Gough, published in 1939 (14), showed fretting to be a mechanical rather than a chemical process and investigated the effect of changing such parameters as slip amplitude and normal pressure. Commenting on the suggestion that fatigue failures may be initiated by fretting, they admit that "there is no strong evidence for or against this view". In 1952 Wright (15) published the results of an investigation into fretting corrosion in which he examined the effect of environment, pressure and surface plating on the severity of damage; again nothing

suggested that fretting should be very detrimental to fatigue strength. In 1956, Ming Feng and Rightmire (16) proposed a mechanism for fretting which was supported by reference to an experimentally determined fretting-weight-loss against number of cycles curve. A four stage process was proposed: in the first stage damage is due to metal transfer and wear but in the second stage the emphasis swings to damage caused by abrasion between the surfaces and the fretting debris, in the third stage the rate of abrasion decreases as the surfaces bed together and the hollows fill with debris until a fourth stage is reached in which the amount of fretting damage increases at a constant rate. Such a mechanism is typical of many proposed but it does introduce one interesting concept which will be referred to when discussing the results reported in this thesis. It is suggested that: "The contact between the two surfaces is established only through a large number of scattered high spots that are grouped into a few companies. The companies of high spots are located in the elevated regions formed by the large scale waviness of the surface". The concept of contact due to large scale waviness will be used later to explain the influence of fretting on fatigue strength.

2.3 INVESTIGATIONS INTO FRETTING FATIGUE

In the second half of a paper by Fenner, Wright and Mann (17), dealing with fretting corrosion and its influence on fatigue failure, the authors mention several instances of service failures of different components where there has been an apparent strength reduction ratio, varying between

2.5 and 20, which they attribute to fretting. In each case except possibly one, there would appear, from the description given, to have been a significant geometric stress raiser associated with the overall shape of the failed assembly. The authors have apparently ignored such stress concentrations when assessing the effect of fretting. Also in the above mentioned paper, when discussing the results of preliminary fretting fatigue tests in which the contact pressure was relatively light, the authors often observed failures away from the fretting region. The stress concentration likely to be present in these tests is not predictable from the outline description of the test but with a light contact pressure it is probably not high. They do not mention any differences in the appearance of the damage compared to that obtained with higher contact pressures and presumably higher stress concentrations, when there was premature failure originating in the fretting zone.

Following the work described in (17) Fenner, Field and Waters, at the National Engineering Laboratories, reported (7,8,9,10) extensive research into fretting fatigue using specimens such as those illustrated in fig. 2.1. Fretting was applied to the specimens by bridge pieces having small pads (feet) at either end and failure originated in the fretting regions at stress levels well below that of polished and unfretted specimens. The reduction in strength was attributed to fretting alone, no allowance being made for the effect of the contact stress field. Apparently no attempt was made to calculate

the theoretical stress distribution associated with such an assembly but the stress concentration in a solid of the same overall shape would be very severe. In fact, the contact pressure used was usually quite low compared to the applied fatigue stress so that the amount of stress relief compared to the solid, due to slip, was probably quite high. However it does not seem justifiable to ignore the contact stress field completely.

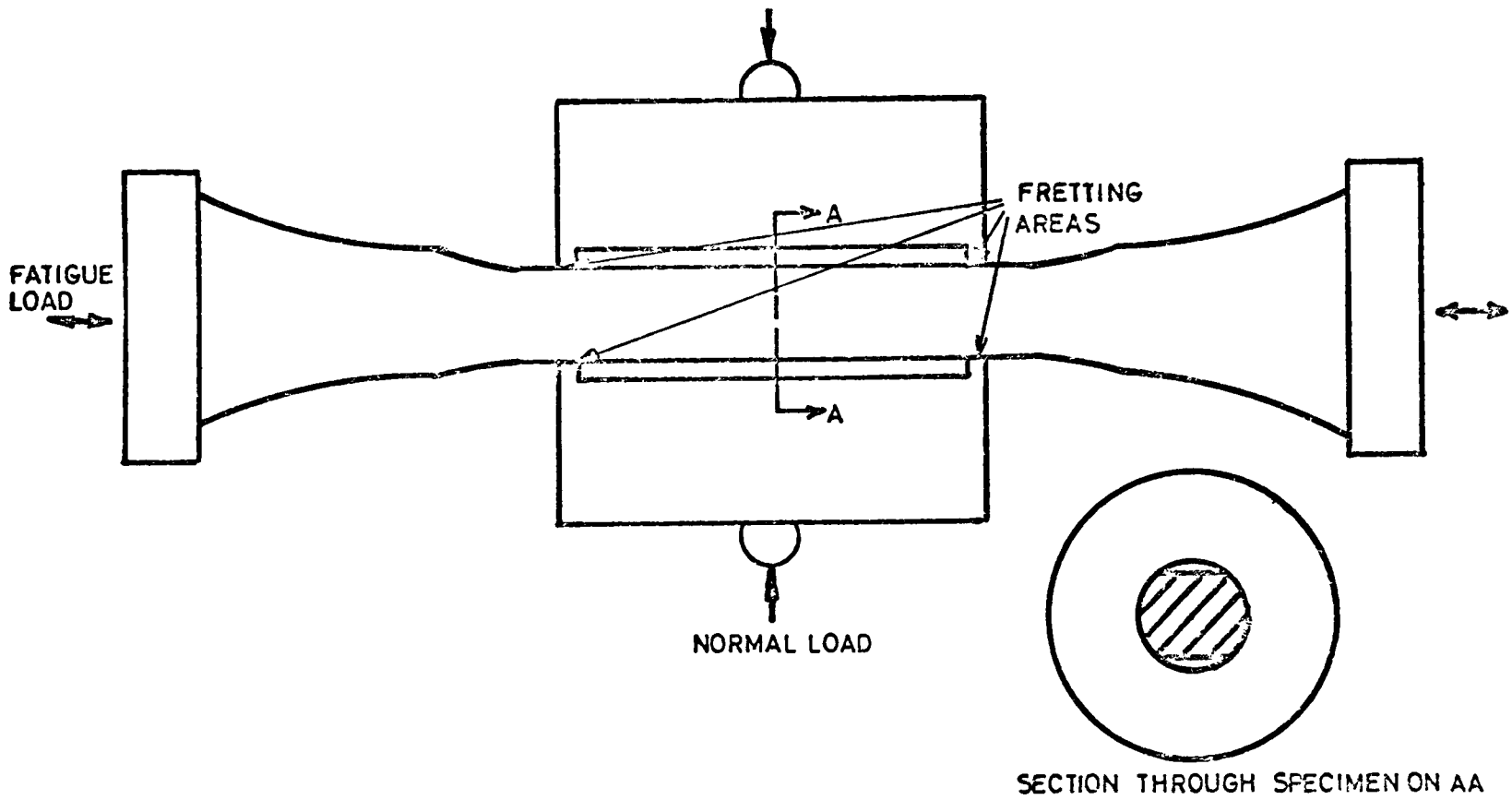


Fig. 2.1 Arrangement used to evaluate the effect of fretting on fatigue strength

Work carried out by Waterhouse (18) and Waterhouse and Brook (19), on the effect of local temperature rise on fretting corrosion of mild steel and the improvement in fretting fatigue strength with certain electrodeposited coatings, employed the same specimen configuration as Fenner et al. Again the effect of the geometry is ignored and improvements in fatigue strength due to various surface coatings is explained in terms of the thermal conductivity of the coating. In (18) it was found that fretting is associated with high local temperature rises.

A coating with high conductivity will conduct the heat away from the contact zone more quickly and the temperature rise will not be so great. However, in general, the materials with high conductivity are also relatively soft (e.g. Cu, Ag). Thus it could equally be argued that the improvement in fatigue strength is due to the surface coating taking up the high strains in the contact zone and isolating the base material from the contact stress field.

Bowers, Finch and Goreham (20), also using the specimen and bridge technique of Fenner et al showed that fretting fatigue strength was improved with various surface coatings and treatments. It can be argued that most of the surface coatings behave in the manner proposed above, in connection with the electrodeposited coatings, and the surface treatments which improve fatigue strength generally induce residual compressive stress in the surface. Such a stress could be expected to improve the fatigue behaviour in the presence of a superimposed tensile stress concentration such as might be associated with the bridge-specimen contact stress field. However, no mention is made of the contact stress field, although one remedy for fretting fatigue was found to be the use of stress relief grooves which reduce the stress on the interface and hence the peak value of the contact stresses.

Marco and Collins (21,22) describe two-stage tests in which fetting was applied to the specimen without the specimen transmitting a large alternating stress. After 10^5 cycles of fretting the specimen was fatigue tested

without further fretting. Tests carried out, in which the mean stress in the specimen during the fretting stage was either compressive or tensile, revealed interesting results. When the mean stress was compressive, the subsequent fatigue strength was reduced by as much as 65%. However, for tensile mean stress during the fretting stage, the subsequent reduction in fatigue strength was only about 6%. A possible explanation, considering residual stresses associated with fretting pits, was offered.

During the fretting stage of these tests, the ratio of the normal pressure to the fatigue limit of the material was low, thus the tensile contact stresses induced in the specimen are likely to have been small and are therefore unlikely to have affected the subsequent fatigue behaviour. Thus, any effect of fretting that was measured is presumably not due to the geometry of the specimen/pad assembly.

When the mean stress during the fretting phase was zero (22), the subsequent fatigue strength was 97% of the unfretted fatigue strength. It seems that fretting damage, considered as a surface finish effect, i.e. fretting applied in the absence of a propagating stress, is not a major factor in determining fatigue strength.

In a thesis by Milestone (23) work is described in which the contact stress fields associated with cylindrical fretting pads are computed. When, subsequently, he discusses the results of fatigue tests, in which such an arrangement was used, he refers to the theoretical contact stress field and concludes that the cyclic contact stresses are of themselves sufficient to explain the reduction

in fatigue strength which is characteristic of fretting. Using a similar geometry of specimen and fretting pad, Nishioka and Hirakawa (24,25) came to the same conclusion. It appears that if the contact area is small, as in the case of cylinders indenting flat plates, the fatigue strength of the assembly can be predicted on the basis of the cyclic contact stresses. Such a result is important and agrees with the hypothesis proposed in the previous chapter. When interpreting the results of the work described in this thesis, reference will be made again to the work described in (23,24,25).

2.4 REPORTS OF SERVICE FAILURES AND RELATED LABORATORY TESTS

As early as 1911 Eden, Rose and Cunningham (26) referred to the failure of fatigue specimens in the grips of fatigue testing machines and the presence, there, of fretting debris. Where the specimen enters the grips there is clearly a sharp change in section and, one would expect, an associated stress concentration. They explained the failures as a consequence of fretting corrosion. In 1932 Kühnel(27), investigating the failure of axles on the German State Railways, realised the potential notch effect associated with shrink fitted wheels, due to the change of section from the wheel seat to the journal and axle. He carried out fatigue tests of such assemblies and showed that a great improvement in fatigue strength was obtained with the use of raised bosses and fillet radii. i.e. as proposed in fig. 1.2. To confirm his views he tested solid specimens, of the same overall shape as the assemblies, and obtained similar fatigue

strengths. He mentions fretting, "Edelrost", only briefly and concludes that it is of secondary importance.

Such conclusions are reached by many other authors. Ouchida (2) predicts fatigue strengths of shrink fitted shaft-disc assemblies from a photoelastic analysis of the contact stresses and recommends the reduction in stress concentration which can be achieved by the use of fillet radii. He suggests leaving a small margin of safety to allow for the effect of fretting. Coyle and Watson (1), McAllen (3), again on the fatigue strength of shaft-disc assemblies, stress the importance of the overall geometry and the similarity between assemblies and geometrically similar solids. In (1) it was observed that steps taken to reduce the stress concentration at the interface also reduced or eliminated fretting. A number of failures, originating in a region of fretting, were observed but although it is appreciated that fretting is potentially a source of failure the authors clearly think that the overall geometry is more important.

Maxwell et al (4) reached similar conclusions when investigating failure of axles on London Underground. They comment qualitatively on the contact stress field associated with a shrink fit and the likely effect of high stresses in the fretting region. Horger (6), (28), again investigating railway axle failures says (28), referring to the axle wheel transition, ..."Such a sharp notch would introduce a high stress concentration. This detrimental shape effect in a simulated one-piece design would be avoided by the designer; yet the fatigue strength

against complete fracture of such a press fitted assembly approaches that of a one-piece design. This weakness due to shape is further aggravated by fretting corrosion ..." He finds that a reduction in the overall geometric stress concentration, by use of fillet radii and raised seat design, considerably improves the fatigue strength.

Peterson and Wahl (29) in an investigation into the fatigue strength of press fitted shaft-disc assemblies with an associated photoelastic stress analysis conclude that .. "the decrease in endurance strength of an ordinary heavy press fit is due to a localised stress system acting on a material weakened by rubbing corrosion". Yet again the beneficial effect of geometric stress relief, this time by the use of stress relieving grooves, is noted.

Recently, work carried out by British Railways (30) has shown the beneficial nature of surface treatments on the fatigue strength of axle wheel assemblies. The surface treatments are applied to the wheel seat and, by careful choice of coating, increases in the fatigue strength of over 100% compared with uncoated seats can be achieved. A possible explanation of the effect of surface treatments, compatible with the idea that macroscopic contact stresses are responsible for fretting fatigue failues has already been suggested in the discussion of (18,19,20). The paper (30), also describes the beneficial effect of improved geometry, using fillet radii and raised wheel seats.

In trying to predict the fatigue strength of small pinned connections, White (31) finds that the predicted

strengths based on photoelastic stress values are not realised in practice and assumes that the difference is due to the effect of fretting from which failure often originates.

2.5 INTERPRETATION OF PREVIOUSLY PUBLISHED WORKS

Considering the previous three sections together, it seems that the following generalisations can be made. From the results of tests which investigate the process of fretting there is no obvious reason why fretting should be very harmful to fatigue strength. The surface damage produced is no worse than a rough machined surface. In (25) it is described how a specimen was indented with a Vickers microhardness pyramid indenter. The resulting pit with its sharp bottom, has the outward appearance of being much more severe than a fretting pit and yet when failure occurred it occurred from the fretting region. It seems that the weakening effect is not due to the stress raising effect of fretting pits.

However, it is quite conceivable that such pits will act as stress raisers to a sufficient extent that cracks are initiated. Many workers have found non propagating cracks under wheel seats, lap joints, etc. and clearly the stresses associated with the fretting damage were not by themselves sufficient to cause the cracks to propagate through unfretted material.

In general, where cracks have propagated and resulted in failure they have done so in a region where, in a solid of the same overall shape, there would be a large concentration of stress. This is not always the case;

in (14) the authors report the failure of a flat plate originating, apparently, from a region where there is no geometric discontinuity. Fractures of wheel-axle assemblies usually start at or near the end of the wheel seat but have been known to occur away from the end.

The main difficulty encountered when interpreting the results of most authors is that, because of complex geometry, the exact stress at the origin of failure is not known, often not even approximately. Few workers support fatigue tests with theoretical or experimental stress analysis which, for assemblies, is usually extremely difficult. It is therefore difficult to evaluate exactly the reduction in fatigue strength due to fretting. However it does seem that there is ample evidence to support the theory that fretting fatigue failures are caused by a combination of fretting (crack initiation) and contact stress field (crack propagation). Certainly, there is enough evidence to warrant an investigation into the relative effects of these two parameters and to justify the development of a fretting fatigue test in which any strength reduction is due only to fretting.

While not suggesting that the results of most fretting fatigue tests are wrong or invalid, it does seem that care should be exercised when interpreting them and applying such results to design problems.

Chapter 3

EXPERIMENTAL WORK

3.1 INTRODUCTION

Fatigue tests were carried out on the lines proposed in Chapter 1. All the specimens were manufactured from one material and, in the main, were derivatives of one basic shape. Where possible, measurements of slip amplitude and size of slip region were made.

After several series of tests had been completed, it was apparent from the results that the hypothesis proposed in Chapter 1 was over-simplified. At about the same time, theoretical determinations of the stress distributions in assembled specimens were completed and showed some unexpected features. The theoretical stress distributions were very different from the qualitative estimates of stress on which the specimen design had been based. Consequently the interpretation of the test results had to be modified and it became clear that fretting, even in the absence of a macroscopic stress concentration, could have a marked effect on fatigue strengh. Tests were carried out to investigate further the magnitude of this effect when acting alone and when coupled with a known, macroscopic stress field.

3.2 TESTING METHODS, EQUIPMENT AND CONDITIONS

3.2.1 The fatigue testing machine

The tests were carried out in a ten ton Amsler Vibrophore, a direct stress fatigue machine, which was equipped with both ten ton and two ton dynamometers. The machine was enclosed in an acoustic chamber which,

besides containing the noise, acted as an enclosed space in which the temperature could be maintained at a constant value of 20°C.

The machine operates on a resonance principle, automatically running at the natural frequency of a spring-mass-spring system, in which the specimen acts as one of the springs. The mass can be changed, to alter this frequency for a given specimen design, but throughout these tests the maximum frequency was utilised. Since the specimens were all similar in stiffness, the frequency altered little from test to test and was about 125 cycles per second.

A rather more significant effect of the Amsler's principle of operation was that, since the system is resonant, the power required to maintain the vibration of the system is normally minimal and hence the power range of the machine is correspondingly low. However, in cases where fretting occurs, there is a relatively high energy absorption by the system, due to frictional energy loss between the contacting surfaces. In practice, it was found that, if the energy absorption was high, there was not enough power available to maintain the desired fatigue load. The effect of this was to limit the specimen size such that loads, near the maximum range of the machine, were not required in order to produce failure within a specified number of cycles.

3.2.2 Material from which specimens were manufactured

The material chosen for these tests was aluminium alloy BS L.65. The reasons for choosing this material were twofold. Firstly, extensive research into the fretting

fatigue characteristics of L.65 has been carried out in recent years by Fenner and Field (7,8), at the National Engineering Laboratories. It was thought that their results could be usefully compared with the work described here. Secondly, the Ministry of Technology, who partly supported this investigation, favoured the use of L.65 due to its aircraft applications.

The material was supplied in extruded bars with 3" x 5/8" section. The specified composition is shown in the table below:

Comp-position	Cu	Mn	Mg	Fe	Si	Ti	Zn	Al
Per Cent	4.26	0.72	0.57	0.36	0.75	0.01	0.06	Balance

The specified heat treatment was as follows:
Solution treated at 507°C (+ 3°/ - 2°C); aged for 5 hours at 175°C (± 3°C) and 1.5 % controlled stretched.

Tests carried out at Oxford determined the following mechanical properties.

Ultimate tensile stress	33 tons/in^2
0.2% Proof stress	28 tons/in^2
Young's Modulus (E)	10.7 x 10^6 lbs/in^2
Vickers Hardness (HV/30)	150-170

3.2.3 The design of the basic specimen

The basic specimen design is shown in Fig. 3.1. The test portion is of rectangular section, ½" x ¼", and 3" in length. Specimens of this type were used to obtain the

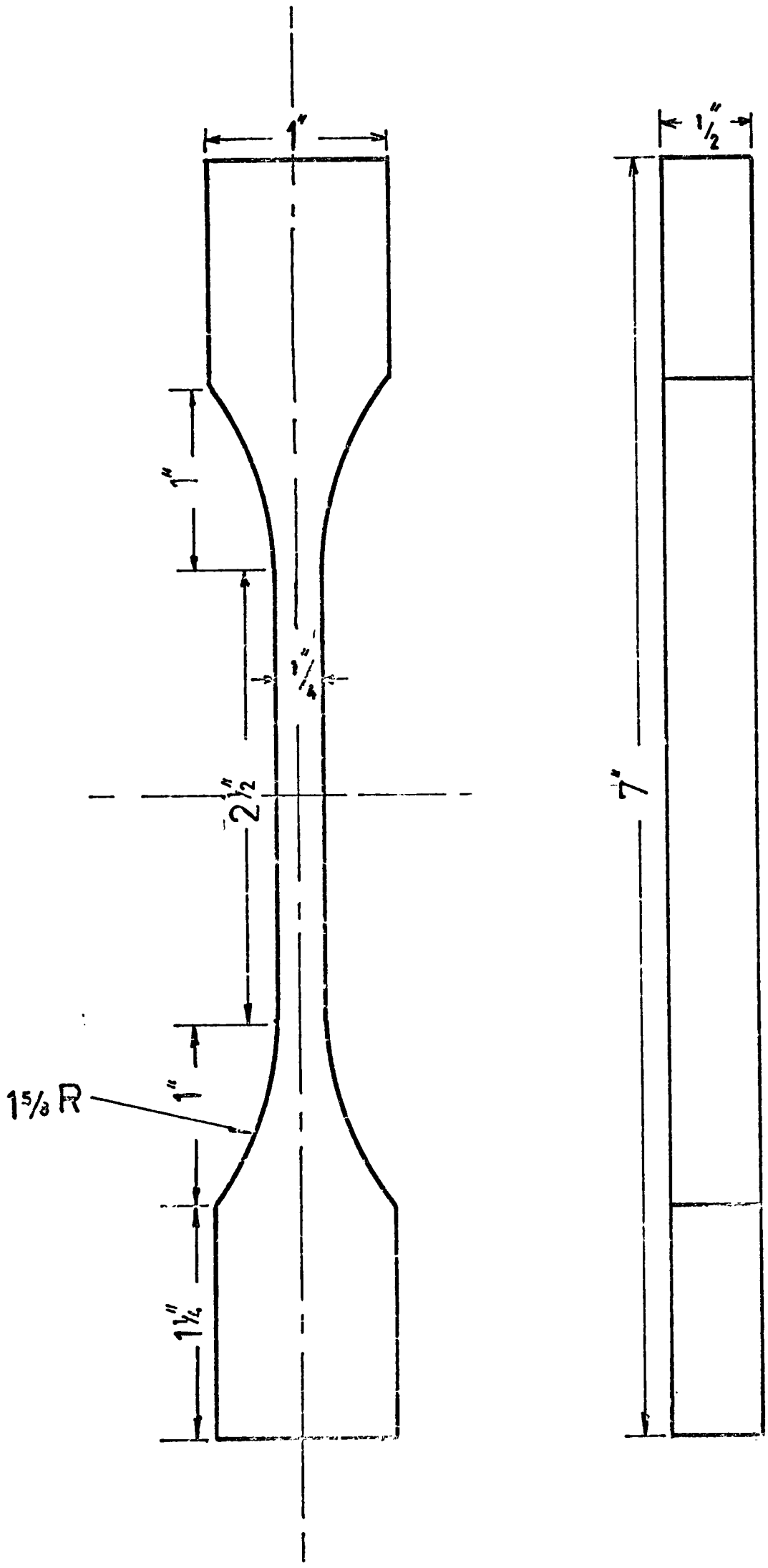


Fig. 3.1 The basic fatigue specimen

control curve, showing the variation of fatigue strength (S) with number of cycles of loading (N), for plain, unfretted and unnotched material. For fretting fatigue tests, two rectangular blocks, 1" x ½" x 1¼", were clamped against the ½" faces of the specimen so that the interface length was 1". The height of the blocks was chosen such that, although the clamp load is applied to each block through a single steel ball, the resulting normal stress on the interface would be effectively uniform if the specimen were rigid and the interface frictionless. Flat specimens, with blocks clamped against them were chosen in preference to round specimens with shrink fit or press fit rings, so that the nominal normal pressure on the interface could be more easily and accurately controlled. Fretting blocks which are in contact with the specimen over the whole block length were chosen, in preference to 'blocks with feet', as used by Fenner and Field (7) and others (Fig. 2.1), for two reasons. Firstly, it was thought that the theoretical analysis of the contact stresses would be easier for blocks with continuous contact and secondly because part of the proposed test programme involved testing solid specimens of the same overall shape as the assemblies; to manufacture a solid specimen, of the same overall shape as the assembly in fig. 2.1, while reproducing the surface finish conditions of the assemblies, would not have been easy.

3.2.4 Tolerances and surface finish

The tolerance on important dimensions was ± 0.0005" and symmetry about the centre line was kept to within

± .001". The specimens were machined in such a way that, where possible, any machining marks ran parallel to the specimen axis. Where this was not possible, for instance in the region of a sharp re-entrant corner, such as those in the sharp cornered solid specimens, the marks were removed with fine emery. In assembly specimens, and specimens used to establish the control curve, the flat surfaces were polished lightly with fine emery. However, care had to be exercised to maintain the flatness of the surfaces otherwise contact between the surfaces of the blocks and the main specimen was lost at the edges.

The contact surfaces of the blocks were ground with the direction of machining parallel to the specimen axis. Blocks were re-used several times and the surfaces re-ground after every test. Usually it was necessary to machine off about 0.010" in order to remove all traces of fretting.

3.2.5 Application of clamping load

The clamping load was applied to each block through a steel ball, loaded by a clamping frame such as that illustrated in fig. 3.2. The frame consists of two rigid end pieces, one of which is recessed to seat a steel ball, while the other has a corresponding tapped hole through which a bolt passes. The bolt is recessed at the end to seat the other ball. The two end pieces are connected by two thin mild steel straps. The load is applied by tightening the bolt, and measured by strain gauges attached to either side of each strap. The two gauges on each strap are connected in series to eliminate bending

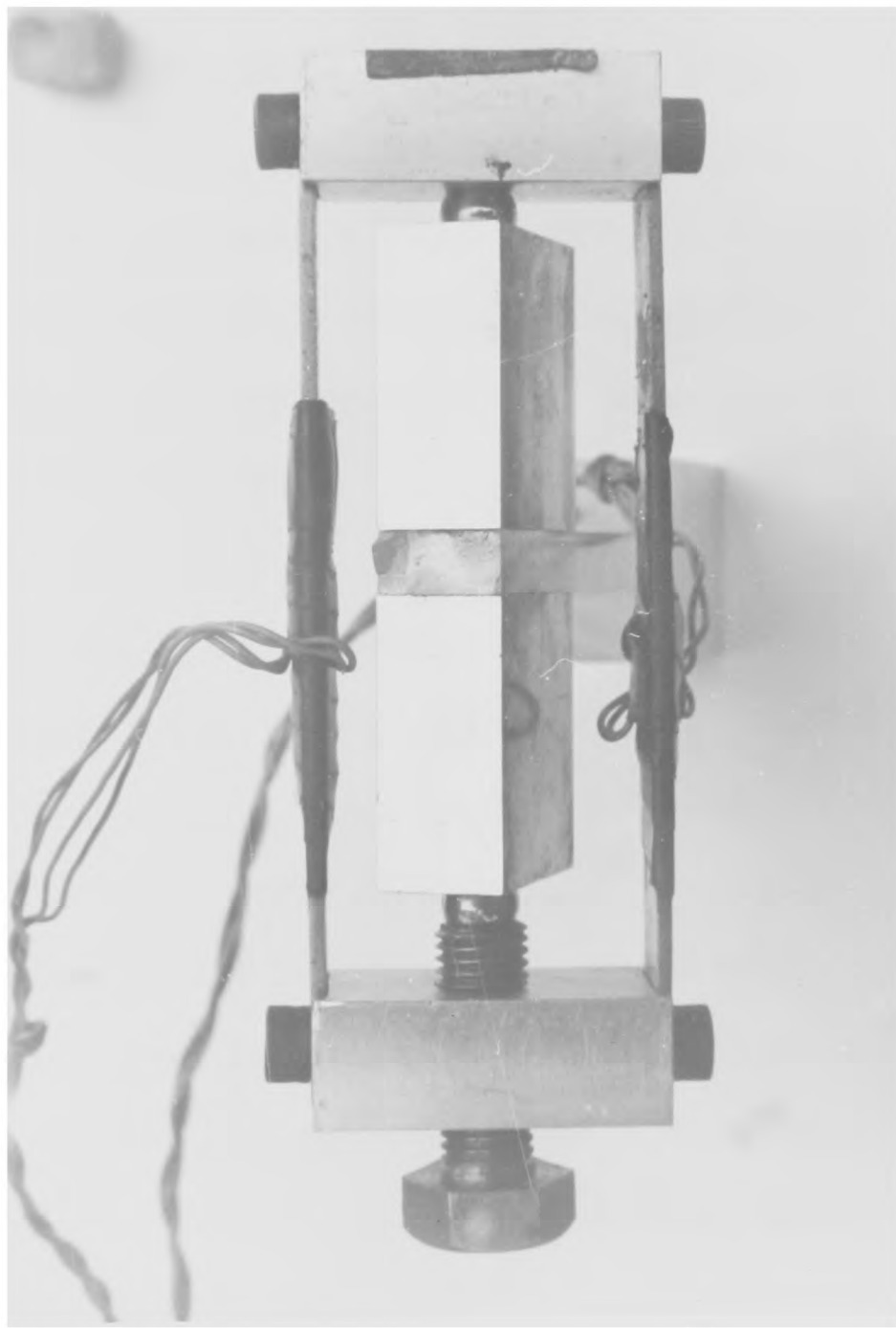


Fig.3.2 A sharp cornered assembly after failure showing the use of the clamping frame.

stress from the readings. The end pieces are made from dural and the whole frame weighs only a few ounces.

Several such frames of differing sizes were used for specimens of different dimensions; each one was calibrated before use.

Early attempts at using a proving ring to apply the clamp load, which gives a more accurate measurement of load, were unsuccessful because the weight of the ring caused rigid body displacements of the blocks during the course of the tests.

3.2.6 Ratio of axial to clamp loads

Initial tests were conducted to determine a suitable ratio of fatigue load to clamping load. Altering the ratio of the clamping load to the axial load changes the length of interface over which slip and fretting occur and also changes the maximum slip amplitude. It was felt that the area covered by fretting should have dimensions comparable with typical dimensions of the specimens and also that the maximum slip amplitude, which occurs at the end of the interface, should not be less than 0.0003" for any fatigue load likely to be used in the tests. (0.0003" is the slip amplitude below which other authors (7) have reported a reduction in the detrimental effect of fretting on fatigue.) It was found that a ratio of nominal peak axial stress (σ_a) to nominal clamping pressure ($-\sigma_n$) equal to 8:1 fulfilled these conditions, the associated fretting region covering approximately one half of the interface. (Nominal peak axial stress (σ_a) is defined as the peak

axial load divided by the cross sectional area of the specimen between the interfaces. In future ($\sigma_a/-\sigma_n$) will be designated by ξ.) Maintaining ξ constant, meant that the clamping load was different in magnitude for each different fatigue load. The alternative scheme in which the clamping load is kept constant for different fatigue loads, is undesirable because the area covered by fretting is then related to the magnitude of the axial load. This has two effects. Firstly the area of fretting associated with each point on the S-N will be different with possible related size effects. Secondly, considering the arguments of Chapter 1, it can be seen that the amount of stress relief due to slip, and hence the macroscopic stress concentration are related to the length of interface on which slip occurs. Thus the macroscopic stress concentration at the end of the interface would be different for each point on the S-N curve. The interpretation of results, in terms of the macroscopic stress concentration, would therefore become correspondingly more difficult. For these reasons the ratio was kept constant throughout each series of tests. In most cases the value of ξ was 8:1 but in certain tests, later in the programme, this was varied. For ξ = 8 the normal stress σ_n, associated with tests run at or near the fatigue limit was about 0.4 tons/in^2 which is the same order of magnitude as that used by Fenner and Field (7). Fenner and Field report little change in fatigue strength with change in normal stress, provided the latter is above a certain minimum level. It therefore seems justifiable to assume

that the results of tests with σ_n between 0.1 and 1.0 tons/in^2 will produce fretting comparable to that found in full scale shrink fit assemblies in which the normal pressure is usually much higher (1).

3.2.7 Setting up and running tests

Since the specimens were rectangular in section they were gripped in the fatigue machine between tapered wedges. These were difficult to tighten without loss of alignment and the imposition of bending stress on the specimen. In order to eliminate bending stresses as much as possible, strain gauges were attached to each specimen before it was placed in the machine. The stress in the specimen was then monitored during the tightening of the grips and the wedges adjusted until the bending component was eliminated. The specimen was initially positioned in the grips using a depth micrometer to ensure that the specimen was aligned (within $\pm$ .002") with the axis of loading of the machine.

Having set up the fretting blocks and applied the clamp load (if required) the specimen was then fatigue tested, under alternating stress of constant peak value, until failure occurred or the specimen had experienced 10^7 load cycles. Failure was said to have occurred when a crack had grown to such a length that the fatigue machine would no longer run. The crack had usually extended through about 75% of the specimen section when the machine stopped running. Specimens which survived 10^7 cycles were retested at a considerably higher load but the results were only used as a guide, and do not

feature in the results presented in the following chapter. In general, about 12 specimens of each type were tested.

3.2.8 Measurement of slip amplitude

Previous investigators have reported that fretting fatigue life is critically dependent on the amplitude of slip. Fenner and Field (7), for instance, found that the fatigue life of L.65 was lowest for slip amplitudes between 0.00035" and 0.002". This result was reproduced by Field and Waters (9) when working with EN.26 steel. In this investigation, two methods of slip measurement were used, one static and the other dynamic.

The first method, which was suitable only for quasi-static conditions, employed a replica technique. With the blocks and specimen clamped together, fine lines were scribed on the surface of the specimen and blocks as close to the corners as possible; usually within about 0.020" of the corner. An imprint or replica of these lines was made by clamping a small piece of sheet acetate, softened with acetone, against the specimen in such a way that the acetate covered the scratch lines. When dry, the acetate was removed, a load applied to the specimen, and a new impression taken. The distance the line on the specimen had moved, relative to those on the blocks, i.e. the slip amplitude, was then measured from the replicas using a measuring microscope.

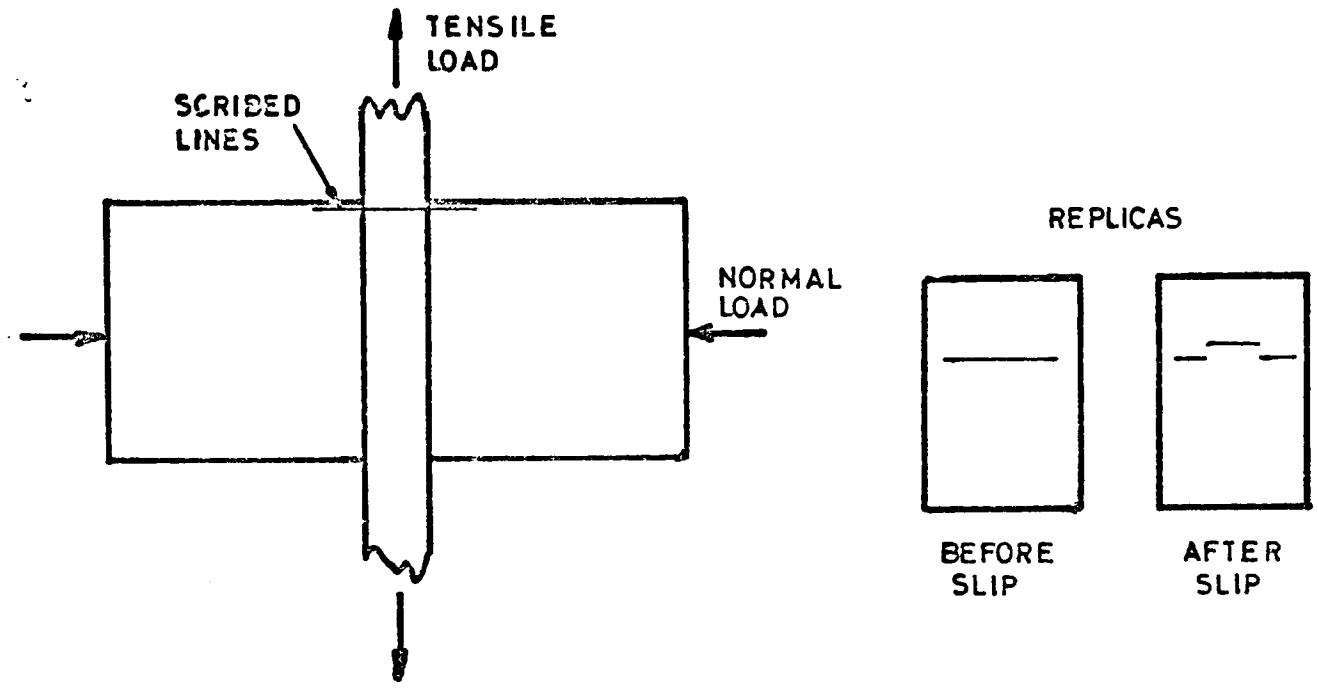


Fig. 3.3 Measurement of slip, using replicas

Using replicas in this way slip amplitudes as low as 0.0003" could be measured to within ± 15%. However, a replica method was clearly not applicable to the measurement of dynamic slip. Since it was thought quite likely that the amplitude of slip would vary during the course of a fatigue test, and might be different under dynamic conditions than static, a method was devised to measure dynamic slip. If a small flat plate is attached to the specimen in such a way that it is parallel to the edge of one of the blocks and separated from it by a small distance, say 0.005" then, as the surfaces of the block and specimen slip relative to each other, the distance between the plate and the block will change giving rise to a linear change in the capacitance between the block and the plate. The change in capacitance can

be measured and related to slip amplitude. A small capacitance probe having an area of 1/16 sq.in. was attached to the specimens with adhesive as shown in fig. 3.4.

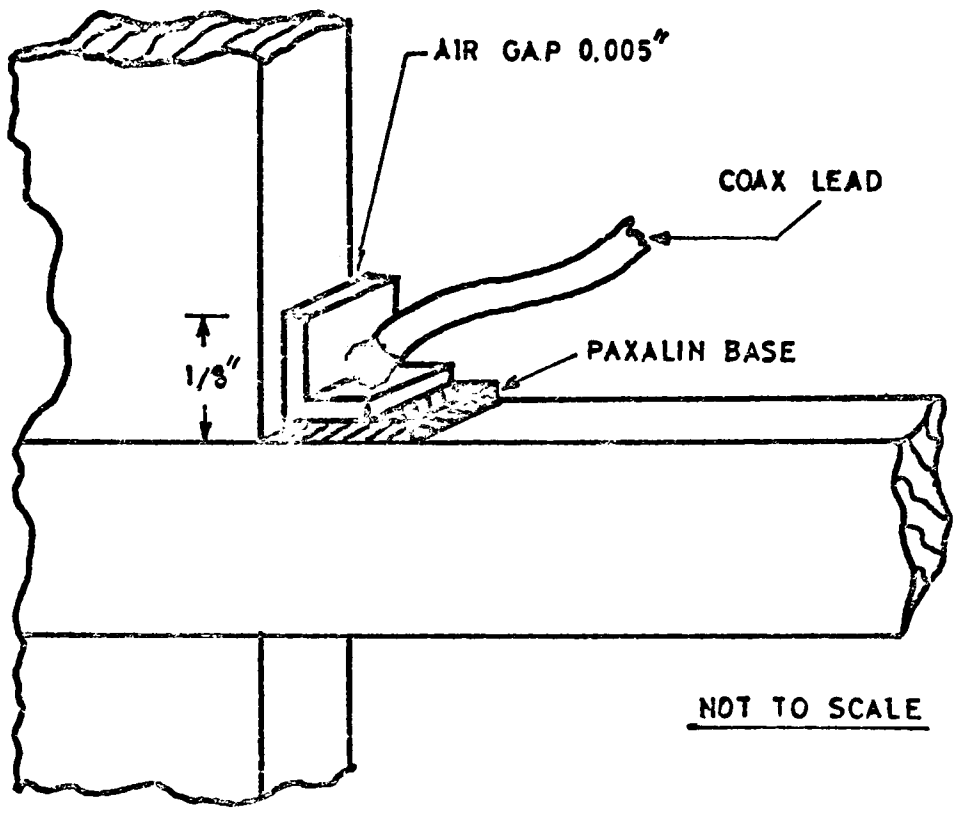


Fig. 3.4 Arrangement for measuring dynamic slip

The probe was used in conjunction with a Fielden Proximity Meter which consisted of a bridge circuit, power supply, and output amplifier. The output could be fed to an oscilloscope or, in cases of static slip, to a meter. The probe made up one arm of the bridge circuit which was balanced before any axial load was applied to the specimen. Subsequent loading and slip caused approximately linear, but uncalibrated, deflection of the oscilloscope trace or the meter. It was necessary to devise a method of calibrating the device so that the oscilloscope or meter deflection could be converted to units of slip amplitude.

In order to achieve the desired sensitivity the mean gap between the probe and the block could not be greater than 0.005". The movement being measured was often as low as 0.0001" so that for reasonable accuracy the full scale deflection of the output device could not be greater than 0.001". Thus if, with a known air gap, the device were calibrated against a known displacement (say 0.001") the probe would have to be positioned on each specimen so that the width of air gap was within, at most, ± 0.0002" of its value during calibration. Positioning the probe with such accuracy proved impossible and an alternative method was adopted which involved re-calibrating for each specimen. With the clamp load reduced to the minimum value required to hold the blocks in place, the strain in the specimen, due to an axial load, is practically unaffected by the blocks. A good estimate of the slip amplitude is then obtained by multiplying the nominal strain in the specimen by half the interface length.

For each specimen the probe was attached so that the air gap was approximately 0.005". With the clamp load reduced so that the blocks were just gripping the specimen, an axial load, calculated to produce a convenient slip amplitude (say 0.0002") was applied and the oscilloscope sensitivity adjusted to give a convenient deflection. Several calibrations, carried out in this way, were subsequently checked against replica measurements and the agreement was good. It appeared that the device was sensibly linear and capable of reading slip amplitudes as low as 0.0001" with an accuracy of about ± 15%, it was assumed that such static calibrations would apply to dynamic

measurement. The oscilloscope used was a Tektronix model 502 A and measurement of the slip amplitude during a load cycle were made from photographs of the trace taken with an Avo-Beattie-Coleman, Polaroid, oscilloscope camera. Measurements were made several times during each fatigue test.

3.2.9 Determination of the coefficient of friction

To determine the coefficient of friction on the interface, the specimen was gripped in the fatigue machine by the top jaws only. The top jaws were then lowered until the blocks just touched two stiff bars which were supported on the bottom grips (fig. 3.5). Further lowering of the jaws causes a compressive load in the top half of the specimen which is transferred by friction across the interface into the blocks. The load is measured by the dynamometer beneath the lower jaws. As the top jaws are lowered the compressive load increases until it equals the maximum value of shear load which the two interfaces can transmit before slipping. The maximum load can be shown to be equal to μpA where μ is the average coefficient of friction, p the average normal pressure on the interface and A the total area of the two interfaces which in this case is equal to 1 sq.in. At this load the blocks start to slip and there is a consequent, slight, drop in the load measured by the dynamometer.

To determine μ, the top jaws were lowered continuously and the maximum load reached was recorded. Knowing that the maximum load is equal to μp, and knowing p the calculation of μ is simple. It should be noted that the

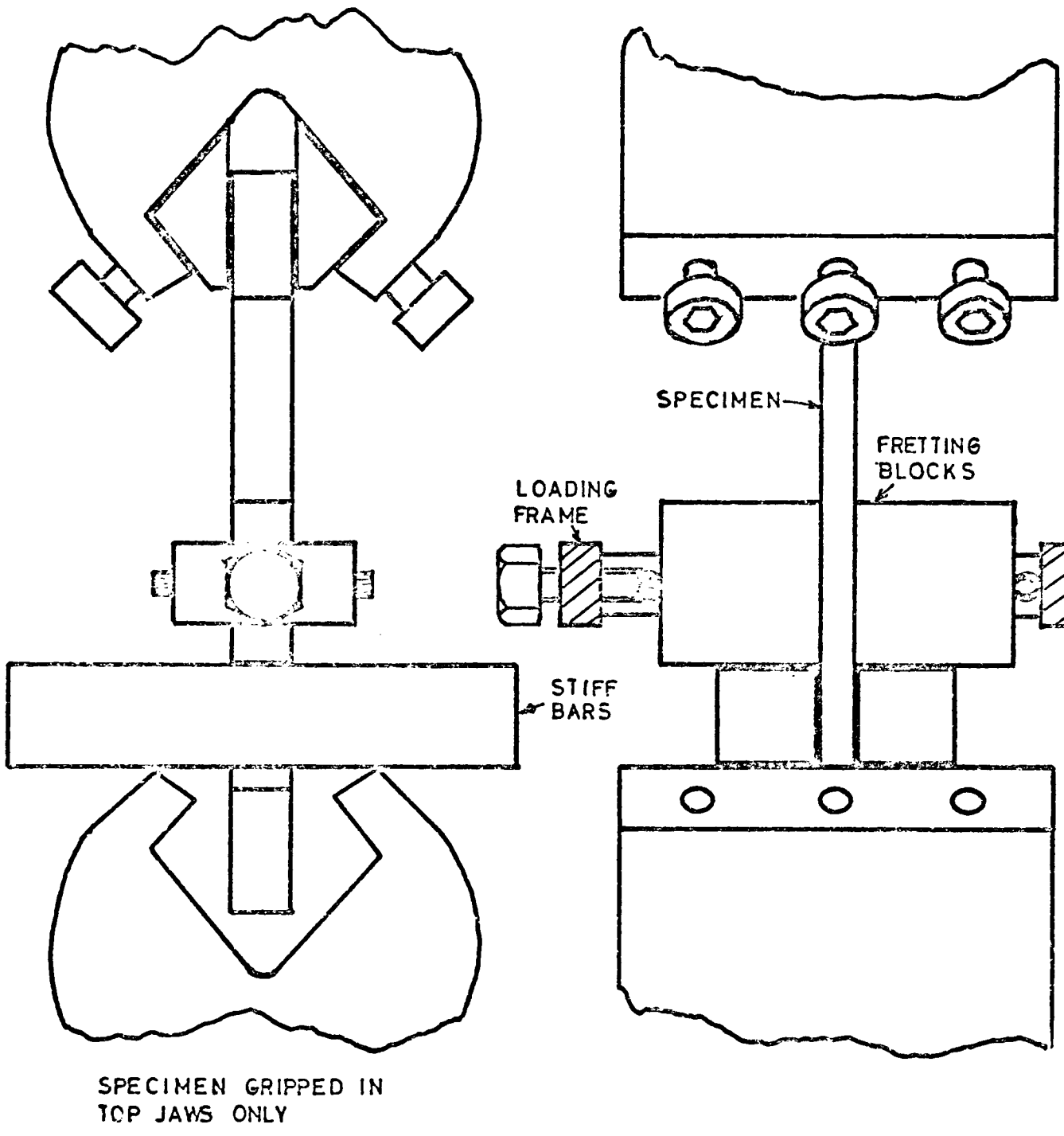


Fig. 3.5 The arrangement used to determine the coefficient of friction

value of μ obtained by this method is an average value for the coefficient of friction over the two (whole) interfaces. It is almost certain that μ will vary over the interface especially when, during a fatigue test, only part of the interface is experiencing slip. However calculations based on average values of μ, determined experimentally, showed good agreement between experimental and theoretical slip amplitudes and slip regions.

Tests, such as those described above, were carried out on several specimens after they had experienced various numbers of load cycles. The value of the clamp load was such that fretting covered most of the interface. The results indicate the variation of the average coefficient of friction between two fretting surfaces with the number of cycles of slip. Fig. 3.6 shows a typical plot of the variation of μ with number of cycles. The mean value for the average coefficient of friction after 10^6 cycles of fretting, obtained by averaging the results from several tests, was 0.8. This value was used in subsequent stress calculations.

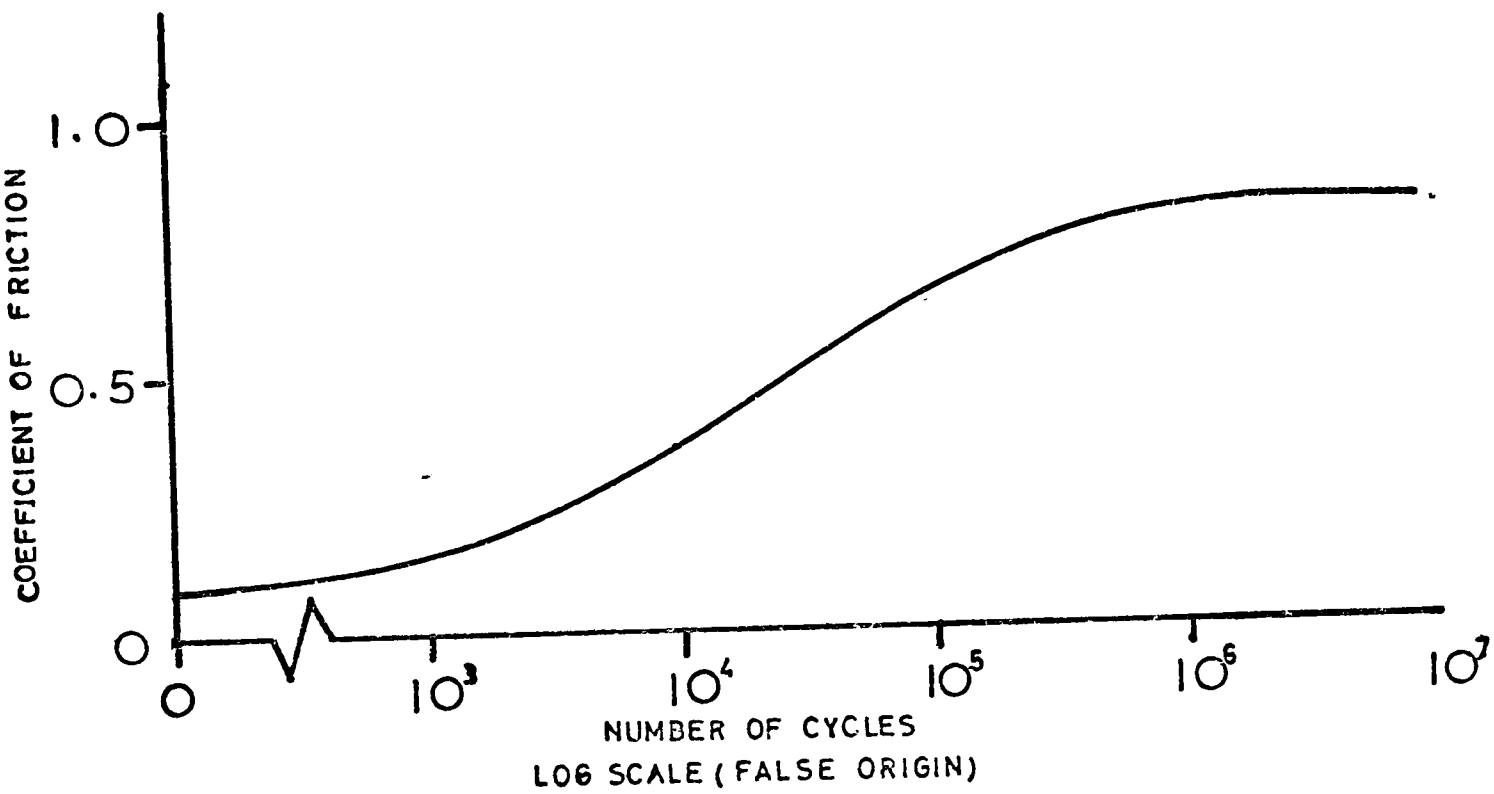


Fig. 3.6 Variation of the coefficient of friction with number of load cycles

3.3 FATIGUE TESTS

3.3.1 Series 1. To investigate the effect of changing geometric stress concentration

The first series of tests were designed to show the effect of changing the geometric stress concentration in the fretting region and, it was hoped, to demonstrate that the (fretting) fatigue strength of an assembly could be predicted closely by considering the fatigue strength of a geometrically similar solid.

To this end three designs of specimen, having different stress concentrations, were tested in both solid and assembly form and their fatigue strengths compared to that of plain unfretted and unnotched specimens. The various specimens are illustrated in fig. 3.7.

Their geometries differ only at the corners formed by the blocks and the specimen. When the corner is sharp the stress concentration in the solid is infinite at the corner* and, by the arguments of Chapter 1, it was thought that in the assembly there would exist, at the end of the interface, a corresponding high (but not infinite) stress concentration. In the case of the incomplete radius the discontinuity at the point where the radius meets the vertical face of the block, gives rise in the solid, to a finite stress concentration with the consequence that the stress there is slightly greater than that in the specimen away from the blocks. Again, for the assembly, it was thought that there would be a

---

*In the specimens tested, the corners, although nominally sharp, had an average radius of about 0.002". This still results in a theoretical stress concentration that is sensibly infinite.

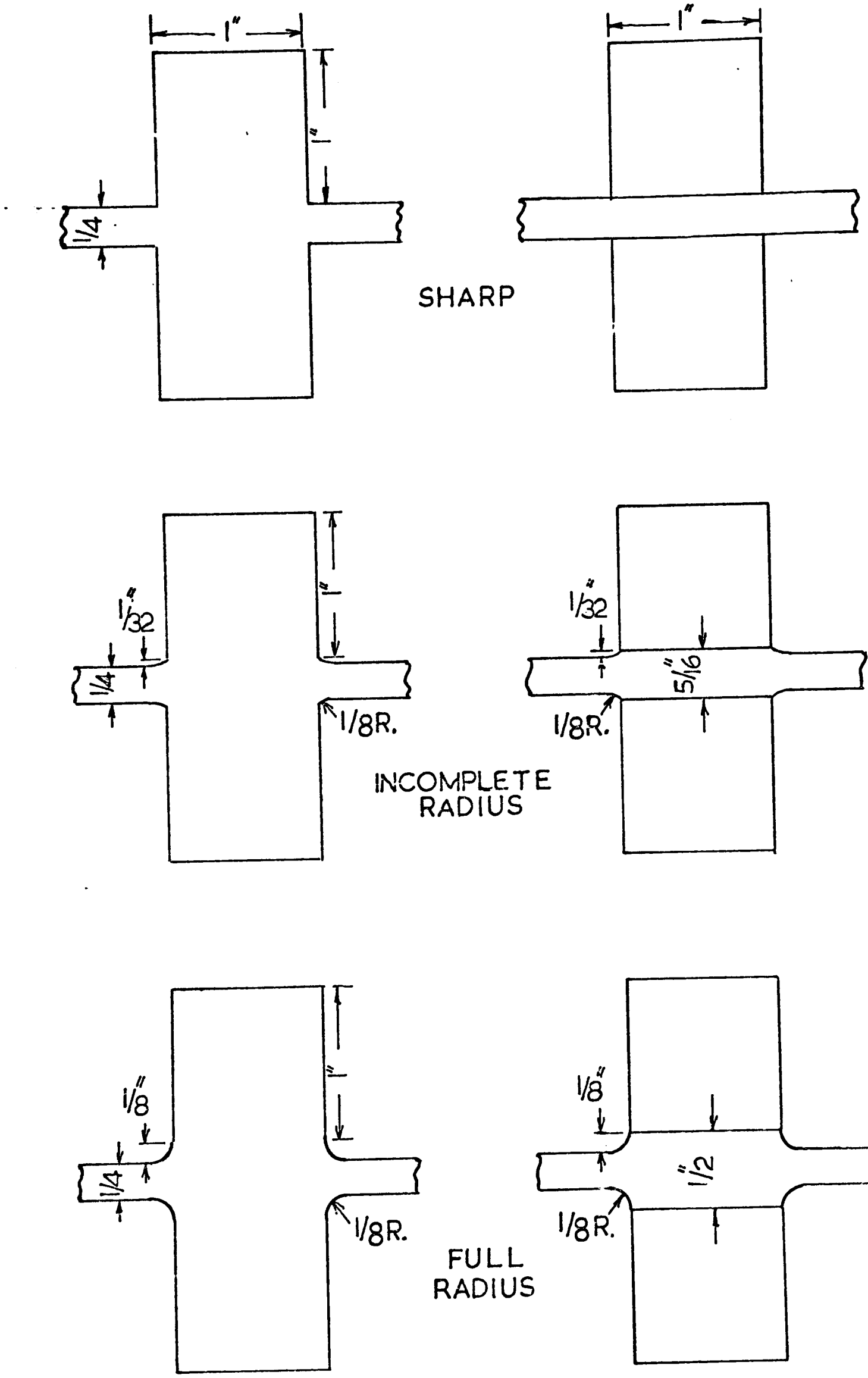


Fig. 3.7 Corner details for specimens used in Series 1

certain amount of stress relief on the interface due to slip so that the maximum stress in the assembly would be less than that in the solid.

In the fully radiused specimens, the maximum stress concentration is in the toe of the radius and has a value of about 1.2 for both the solid and the assembly. The interface is now in a region of relatively low stress and it was thought that the slip in the assembly would not, therefore, greatly affect the overall stress distribution.

The designs of these specimens were based on photoelastic tests (described in Appendix 3) in which values of maximum shear stress concentrations were determined for both the solid and assembled specimens. However, the results for the assemblies, particularly the sharp cornered assembly, did not appear to be correct. No stress concentration was discernible at the corner under tensile load, a result which, at the time, did not seem reasonable. It was decided that the cause of such unexpected results must be the low coefficient of friction - about 0.2 - on the interface of the araldite assemblies, which allowed almost complete stress relief to occur by slipping. In the fatigue specimens, it was argued, the coefficient of friction would be much higher and an appreciable stress concentration would exist.

Thus the design of the fatigue specimens just described were based on the photoelastic results for the solid specimens, the stress distributions in the assemblies being estimated on the assumption that high

stress concentrations found in the solid, in the region of the interface, would be (only) partially relieved by slip.

Remembering the arguments of Chapter 1, it was thought that the series of tests described above would give the following results. In the cases where the corner is sharp the solid specimen will have a very low fatigue strength due to the high stress concentration in the corner. In the assembly of the same shape the stress concentration will be relieved to a certain degree by slip. Therefore, ignoring fretting, at this stage thought to be of secondary importance, the assembly should be slightly stronger in fatigue than the solid. For the incomplete radiused specimens the same arguments apply. However, since the stress concentration in the solid is lower than in the sharp cornered case, the difference between the solid and assembly was expected to be less marked. For the fully radiused specimens the point of highest stress is in the toe of the radius in both the solid and the assembly. Failure should, therefore, occur at that point in both solid and assembly and the S-N curves for both should be identical.

These expected results, it was argued, would demonstrate that, so called, 'fretting fatigue' is really a consequence of macroscopic stress concentrations and that in the absence of a geometric stress raiser, e.g. in the fully radiused case, fretting has no effect on the fatigue strength. As explained in the following chapter, these predicted results did not materialise and a different hypothesis had to be advanced to fit the experimental results.

Each of the tests in this series were run under conditions of alternating fatigue load. The ratio of nominal peak axial stress on the interface to nominal clamping pressure was constant for all tests and equal to 8. Since in the assemblies the specimen width between the blocks increases as the geometric stress relief increases, the ratio of clamp load to axial load will decrease as the geometric stress relief increases. For example, for a given axial load, the clamp load for the fully radiused assembly will be only a half of that for the sharp cornered assembly.

Since one aim of these tests was to compare the fatigue behaviour of solid and assembly having identical overall geometries and loading conditions it was necessary to apply a clamp load to the solid specimens. The ratio of this clamp load to the peak fatigue load was the same as that in the corresponding assembly.

3.3.2 Series 2. To investigate the effect of slip amplitude by changing the block length

As mentioned in Chapter 2, several authors have noted the effect of slip amplitude on fretting fatigue strength. The results of the first series of tests led the author to believe that, contrary to his original belief, fretting did, indeed, have some effect on fatigue strength.

It seemed desirable therefore, to investigate the effect of slip amplitude on fatigue strength with particular reference to the tests of series 1. To this end, several series of tests on sharp cornered assemblies were carried out using blocks of different length in each series. Again ξ was maintained at 8 for all

tests. The slip amplitude was measured using the device described earlier (fig. 3.4). Specimens were tested using blocks of $1\frac{1}{2}$", $\frac{1}{2}$", $\frac{1}{4}$" and $\frac{1}{8}$" in length and the results were compared to those obtained in series 1 using 1" blocks. It was thought, however, that for a block length of $\frac{1}{8}$" the ratio of block length to specimen thickness had changed so radically that changes other than that of slip amplitude might be affecting the results. To investigate this possibility a series of solid specimens having a block length of $\frac{1}{8}$" were tested.

3.3.3 Series 3. Fretting applied in the absence of a propagating load

One theory that has often been put forward, suggests that the strength reduction due to fretting is a consequence of the surface damage which characterises fretting; in other words, that the strength reductions associated with fretting occur for the same reasons as strength reductions associated with poor surface finish. Thus fretting pits are analagous to pits or scratches in a poor surface. Such pits give rise to stress concentrations which are high enough to initiate and propagate cracks through regions where the nominal stress is too low to initiate cracks.

It seemed, however, that the strength reductions due to fretting, which were estimated from the results of series 1, were too high to be thus explained. At this stage in the test programme strength reduction factors, estimated to be greater than 2, were being found which could, apparently, only be explained as a consequence of fretting. Talysurf readings of surface roughness for

several fretted surfaces indicated that the fretting was equivalent to a rough machined surface. According to results quoted by Forrest (13), the fatigue strength of rough machined specimens is unlikely to be less than 70% of the fatigue strength of polished specimens.

In Chapter 1 it was suggested that the effect of fretting damage is, at most, a secondary factor, the major fatigue damage being caused by stress concentrations associated with the overall geometry. However, if the bulk stress in the specimen is sufficiently low, there will be no point in the specimen, even in regions of macroscopic stress concentration, where the stress is high enough to cause crack propagation. If fretting is applied to a specimen in such a way that any bulk stress in the specimen is of low magnitude, the damage would be restricted to the surface and would not be a function of any macroscopic stress concentrations.

Fretting, thus applied, is referred to as fretting in the absence of a propagating stress. If a specimen, which has previously been subjected to (say) 100,000 cycles of such fretting, were to be subsequently fatigue tested without further fretting (and therefore macroscopic stress concentrations), the result should indicate the damaging effect of the fretting pits etc, acting as surface imperfections.

The arrangement used to apply fretting to a specimen, without simultaneously producing a propagating stress in the specimen, is shown in fig. 3.8. Two specimens of the type used to establish the control curve (fig. 3.1) are fretted at one time. The specimens are clamped, in the

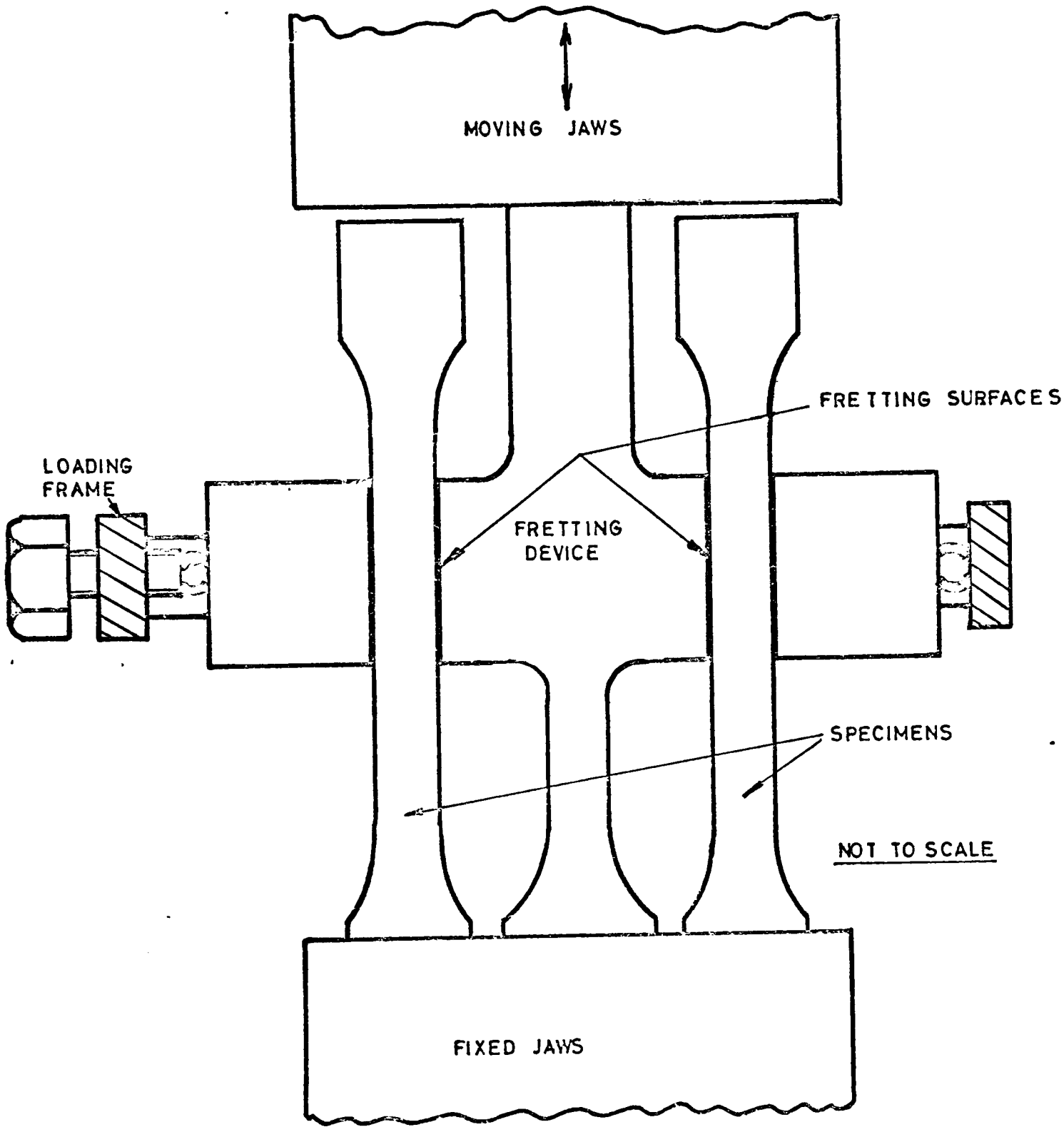


Fig. 3.8 Arrangement for applying fretting to specimens in the absence of a propagating stress

manner shown, against the faces of the cruciform shaped fretting device. When this assembly is gripped in the machine, only the lower end of the specimens are gripped, the top ends being free. When a load is applied to the cruciform, the faces clamped against the specimens move relative to the stationary lower grips, and hence relative to the specimens. The slip on the interfaces produces fretting on the surface of the specimens. The load carried by the specimens during this process is limited to that which can be transmitted across the interface by friction.

The clamping stress used in these tests was equal to that used in the sharp cornered assembly of series 1 for an axial stress equal to the fatigue limit of the material (based on 10^7 cycles). The clamping stress, therefore, is equal to $\frac{1}{5}$th of the fatigue limit for the material, and since the coefficient of friction under these conditions is 0.8, the axial stress in the specimen during this process is only about 1/10 of the fatigue limit. Even in the region of the stress concentration at the edge of the interface, the stress in the specimen is unlikely to approach the fatigue limit.

The amplitude of slip during this process can be controlled by altering the load applied to the cruciform and for these tests was approximately equal to 0.0005".

Specimens were fretted in this way for 10^5 and 3×10^6 cycles and then fatigue tested in the normal way without further fretting.

3.3.4 Series 4. Fretting in the absence of macroscopic stress concentrations but in the presence of a propagating load

From the first three series of tests it was apparent that fretting in the presence of a propagating stress was detrimental to fatigue life, to an extent that could not be explained by the presence of macroscopic stress concentrations. It therefore seemed necessary to determine the strength reduction factor due to fretting in the absence of any macroscopic stress concentration. This could best be done by arranging a fretting fatigue failure to occur in a region of nominally uniform stress where this stress could either be determined theoretically or measured.

The arrangement used is shown in fig. 3.9. The fretting blocks overlap the thinnest section of the specimen so that the stress concentrations associated with the corners of the blocks occur in a region of low nominal stress. In order that the fretting area should spread well into the narrowest section of the specimen, the blocks were prevented from slipping at one end by a high clamp load applied there. This load was prevented from affecting the normal stress on the thin part of the specimen by the cutout in the blocks, and the normal stress in the failure region is then a function solely of the clamp load applied in the centre of the main part of the blocks. By this arrangement all the slip occurs at one end of the blocks and therefore extends over a greater area at the free end than it would if both ends were free to slip.

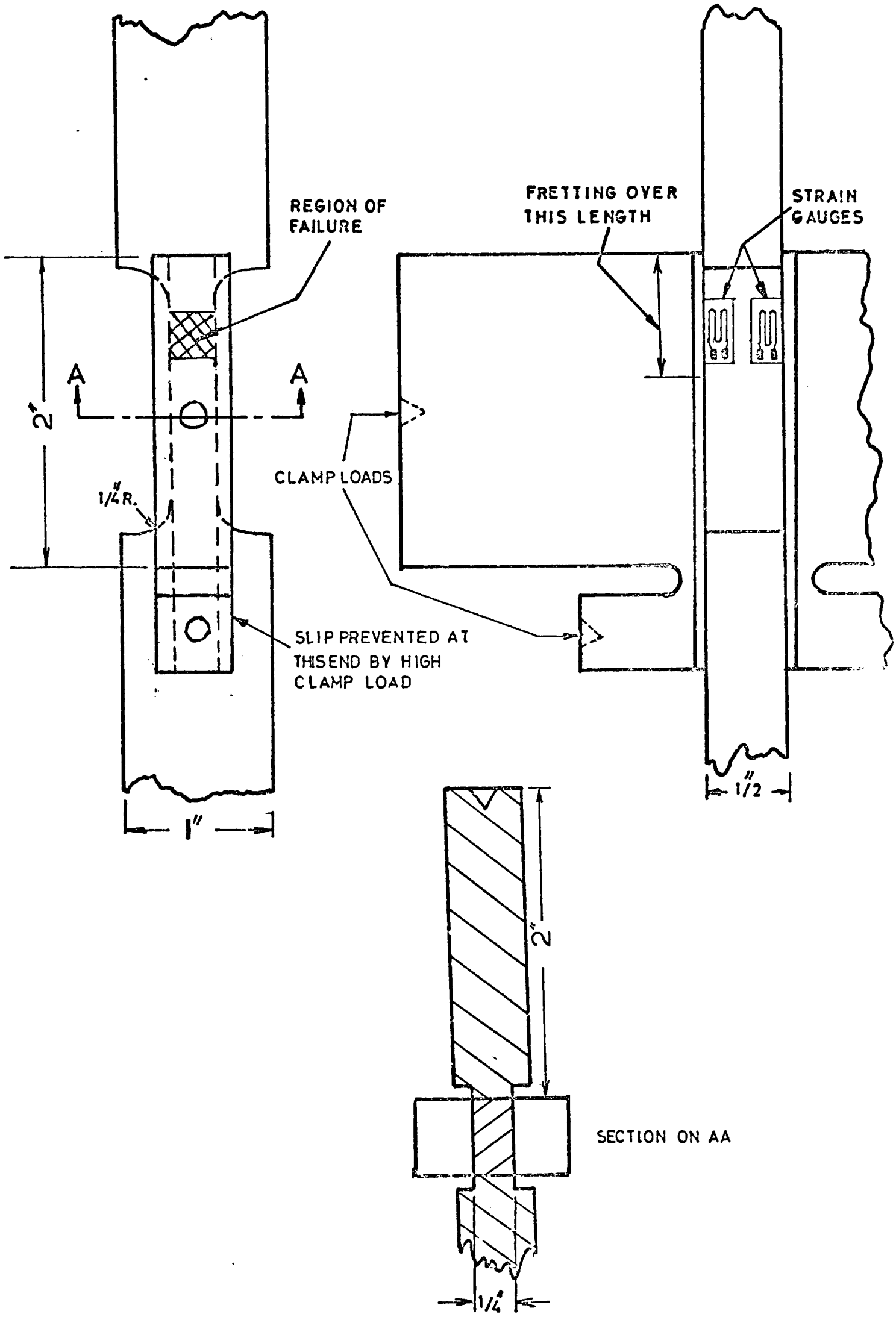


Fig. 3.9 Arrangement for investigating the effect of fretting away from a macroscopic stress concentration

In these tests the ratio of the nominal axial stress to nominal normal pressure was again 8:1.

Initial tests showed that failure, originating from the fretting zone, occurred at a point in the test section just clear of the radius. In following tests four strain gauges were attached to the specimen at this point and as close to the interfaces as possible, (fig. 3.9). The gauges were monitored during tests to determine the stress range at the point of failure. The local stress range differed from the nominal stress range by an amount proportional to the load transferred, by friction, across the interface and into the blocks. Knowing the stress at the origin of failure and comparing it to the fatigue strength of the unfretted material should enable the strength reduction due to fretting in the absence of a macroscopic stress concentration to be determined.

3.3.5 Series 5. Tests carried out following the completion of the Theoretical Analysis of stress distributions in Assemblies

While the tests of the first four series were being run, a theoretical analysis was made of the stresses in the fatigue specimens tested in series 1. The results of this analysis (Chapter 7) showed that, to achieve a high stress concentration at the corner, in a sharp cornered assembly, the normal load would have to be greater than it was in series 1. In order to achieve conditions of fretting in a region of high stress concentration, which was the original aim of the tests in series 1, tests of sharp cornered assemblies were

run using higher clamp loads. The ratios of nominal axial stress to nominal normal pressure (ξ) used were 4, 2 and 1. In addition to testing assemblies under high clamping load, tests using solid sharp cornered specimens with $\xi = 1$ were carried out to determine the effect of a high static normal stress on the fatigue strength under alternating axial stress. With $\xi = 1$ the nominal normal pressure is equal in magnitude to the nominal peak axial stress and it seemed likely that a stress of such magnitude, even though static, might have a significant effect on the fatigue strength. A further series of tests designed to investigate the effect of high static clamp loads used sharp cornered assemblies which had been assembled with a sheet of thin rubber (thickness 0.004") separating the blocks and the specimen. (The rubber used was, in fact, cut from a toy balloon.) The fatigue tests were run with $\xi = 1$. It was thought that the rubber would take up the high strains in the assembly at the end of the interface, and thus prevent any macroscopic stress concentrations occurring there. As a result, the specimen would be subjected only to a sensibly uniform static normal stress and the cyclic axial stress.

3.3.6 Series 6. Tests using blocks with 'feet'

One outcome of the arguments in Chapter 1, was a criticism of traditional methods of investigating fretting fatigue phenomena.

In many of these investigations blocks are used which have small feet at either end (fig. 2.1). The contact area is very small and the arrangement appears

to have an associated stress distribution which is far from uniform. The exact stress at the point at which failure originates is, therefore, not known and the small contact area introduces a further unknown associated with 'size effect'.

Fatigue tests were therefore carried out using 'blocks with feet' to cause fretting and the results were compared to those obtained in the tests comprising series 1 to 5. The blocks used in these tests were one inch long with pads 0.05" long and 0.02" high at each end.

The value of ξ chosen was again 8.

3.4 SUMMARY

This chapter has described in detail the fatigue tests carried out in the course of this investigation. For quick reference when reading following chapters the tests are summarised below.

Series 1: Fatigue tests to investigate the effect of fretting in a region in which there is a macroscopic stress concentration and a bulk propagating stress. The results of such tests were compared to tests using solid specimens with the same overall shape.

Series 2: Fatigue tests to investigate the effect of changes in slip amplitude on fretting fatigue strength.

Series 3: Fatigue tests to evaluate the effect of fretting applied in the absence of a bulk propagating stress.

Series 4: Fatigue tests to evaluate the effect of fretting applied in the absence of a macroscopic stress

concentration but in the presence of a bulk propagating stress.

Series 5: Fatigue tests carried out following the completion of the theoretical stress analysis, to investigate the combined effect of fretting and high macroscopic stress concentration. Also tests to determine the effect on fatigue strength of high static normal stress in the absence of fretting.

Series 6: Tests modelled on those of other investigators using blocks with small fretting pads at either end.

Chapter 4

EXPERIMENTAL RESULTS

4.1 INTRODUCTION

The tests described in the previous chapter aimed at producing S-N curves in the range between 10^5 and 10^7 cycles for the various types of specimens tested. Usually, about twelve specimens of each type were tested and an estimated best-fit curve was drawn through the points. From such curves estimates were made of the fatigue limit for each type of specimen. The fatigue limits of notched and fretted specimens were compared to that of plain unnotched and unfretted specimens (the control curve) to obtain strength reduction factors.

The results are presented in historical order. The first tests gave results which appeared to support the original hypothesis (Chapter 1) but, as more tests were carried out, it became clear that this was merely coincidence and the supposition, that fretting in the absence of a geometric stress concentration is not detrimental to fatigue strength, was not true. Furthermore, the theoretical stress analysis of the assemblies showed that the original aim, to investigate the combined effect of fretting and geometric stress concentration on fatigue strength, had not been achieved. Later sections of this chapter describe the results of some tests in which this aim was partially achieved.

4.2 SERIES 1

4.2.1 S-N curves

The S-N curves for the six types of specimen tested in series 1 are plotted in three separate graphs, each

of which shows the fatigue results for one geometric shape, both solid and assembly, and the control curve. The control curve, a plot of the fatigue strength of plain, unnotched and unfretted specimens of the type illustrated in fig. 3.1, showed that the material had a fatigue limit of about 10 tons/in^2. The S-N curves are plotted on semi log axes and show life (in cycles) plotted against the nominal stress in the specimen away from the influence of the blocks. Clearly, in cases where there are large changes of section or high stress concentrations, the nominal stress will not be the stress which initiates failure and account is taken of this when discussing strength reductions.

Considering first the sharp cornered specimens (fig. 4.1), it is seen that, at low endurances, the fatigue strength of the solid is less than that of the assembly. At high endurances this difference becomes progressively less and eventually the two curves become coincident. The fatigue limit for both solid and assembly, based on the nominal stress in the specimens is 2.8 tons/in^2 which corresponds to a strength reduction factor (K_f) of 3.5. In all cases of both solid and assembly, failure occurred at the corner (fig. 4.2). These results fitted the original hypothesis well. It appeared that the assembly was slightly stronger than the solid and this was assumed to be due to stress relief associated with slip. Since the assembly failed at the corner it seemed likely that this was due to high stresses associated with the corner. The fact that, at high endurances, the two

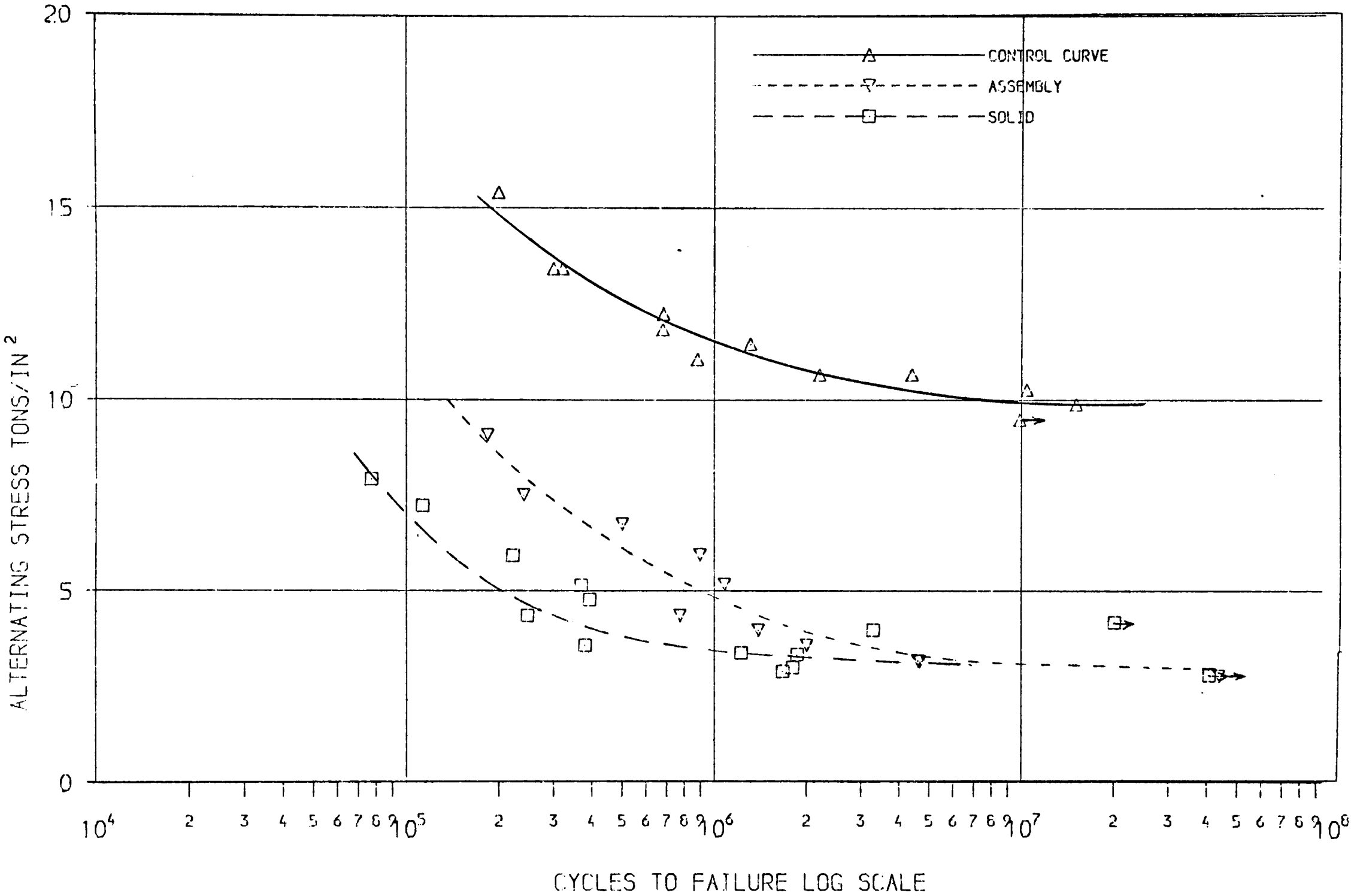


FIG.4.1 S-N CURVES FOR SHARP CORNERED SPECIMENS

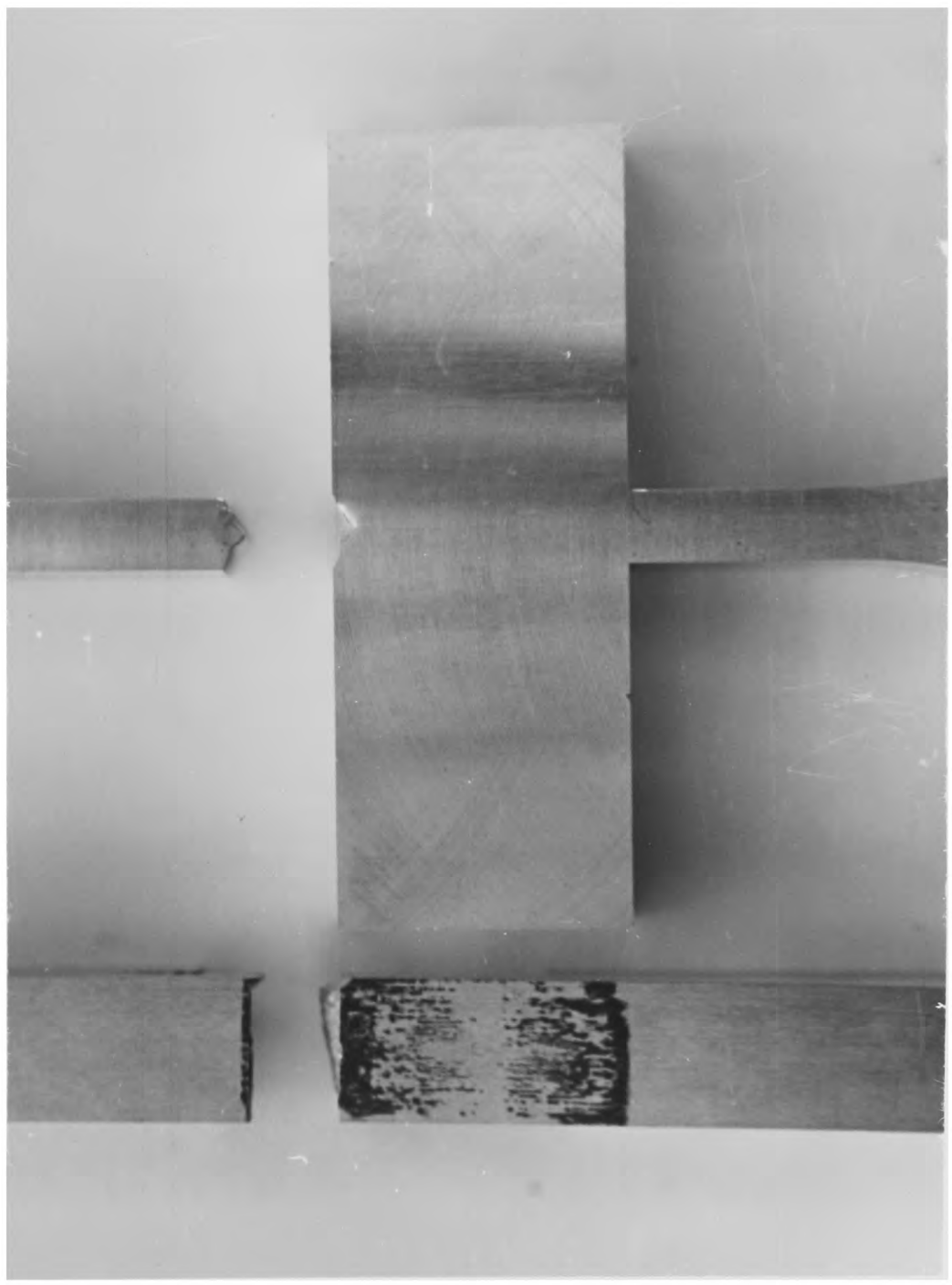


Fig.4.2 Sharp cornered specimens after failure,both solid and assembly failed at corner.Note severe fretting in assembly.

curves were coincident can be explained either by assuming that fretting damage increases with number of load cycles, so that at high endurances the assembly is relatively weaker, or by assuming that the solid is relatively stronger at low stresses due to the formation of non propagating cracks.

The presence and effect of non propagating cracks in regions of high stress gradient but relatively low nominal stress are described in detail by Harris (32). He predicts, and supports his theory with experimental results by other authors, that the relationship between stress concentrations (K_t) and fatigue strength reduction factor (K_f) is such that as K_t increases K_f increases to a maximum and then falls again due to the formation of non propagating cracks. In the sharp cornered solid specimens, (in which K_t is very high) tested by the author, non propagating cracks were found in specimens run to long endurances without failure (fig. 4.3).

So far the experiments fitted the hypothesis; the strength reduction in the fretting specimen had been explained without reference to the effect of fretting, and it seemed that the fatigue strength of an assembly could be predicted from that of the solid.

Of course, had the stress distribution in the assembly been known at this time, the interpretation would have been different. But the photoelastic results which had been obtained were not thought to be representative of the fatigue specimens and the theoretical analysis had not yet been completed.

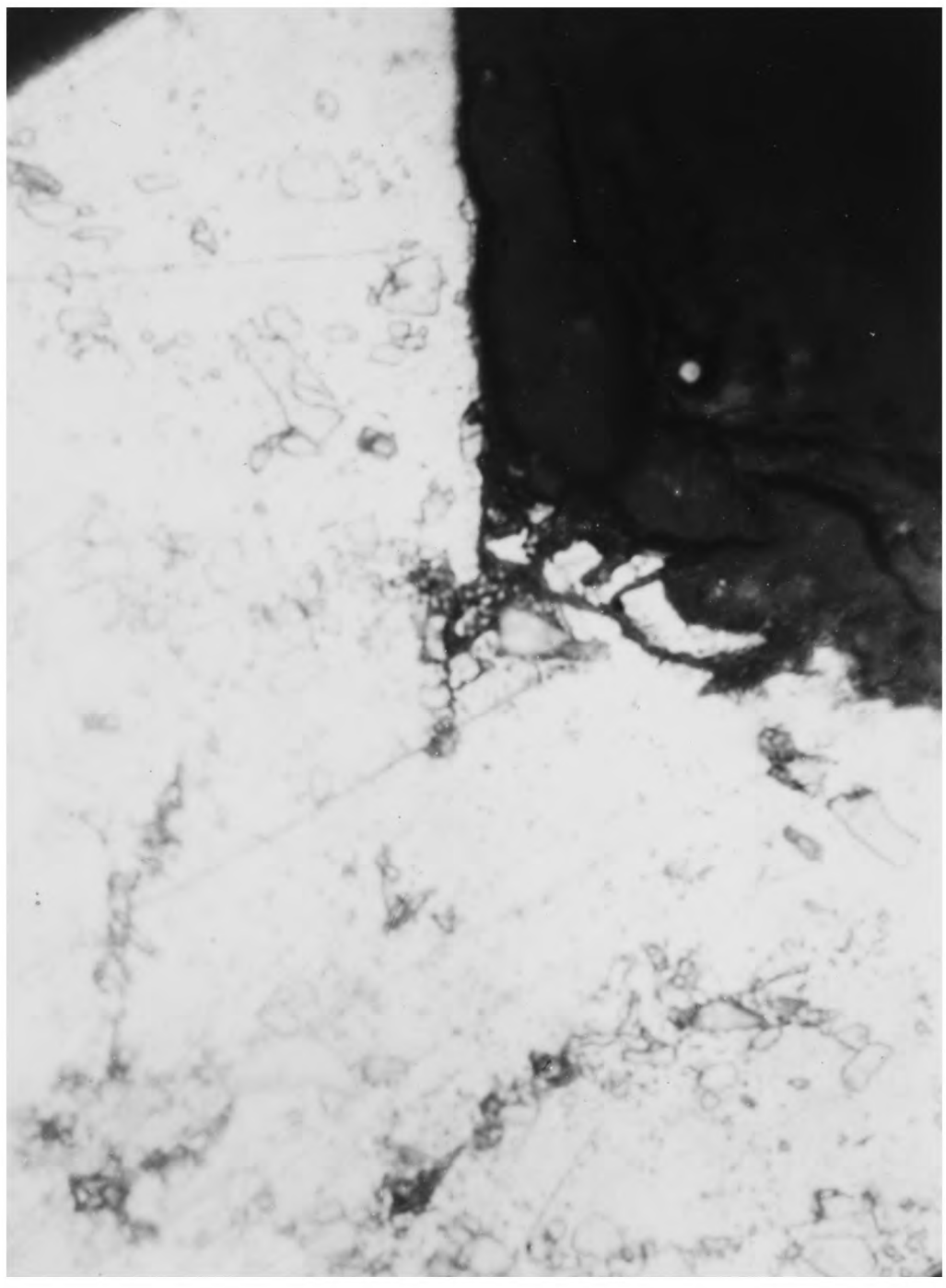


Fig4.3 Non propagating crack in a sharp cornered solid tested for 10^7 cycles at a stress just below the fatigue limit for such specimens.

The results for the fully radiused specimens are shown in fig. 4.4. The curves for both solid, assembly and the control specimens are virtually indistinguishable. The majority of the assembly specimens failed in the radius as did all the solids (fig. 4.5). However, four of the assemblies, run for long endurances, (life $> 10^6$ cycles) failed in the section between the blocks, the failure originating, in each case, about $\frac{1}{4}$" from the end of the interface, in a region of severe fretting (fig. 4.5). These four, so called, fretting failures gave the first indication that all was not well with the original hypothesis. The nominal axial stress at this point of failure was only one half as great as the stress away from the blocks and the geometry was such that it seemed unlikely that the stress at the origin of failure could be higher than the nominal stress. Thus, it appeared that in cases, where fretting had been allowed to develop for over 10^6 cycles, it was responsible for reducing the strength of the material to under one half of its unnotched value.

The results for the incomplete radiused specimens plotted in fig. 4.6 also indicated that fretting could reduce the fatigue strength significantly. Except at very low endurances, the solid was stronger than the assembly and always failed in the radius. In every case but one (for which the load was highest and the endurance lowest), failure of the assembly occurred across the widened section of the specimen, about 3/32" from the end of the interface. Again the crack originated within a region of

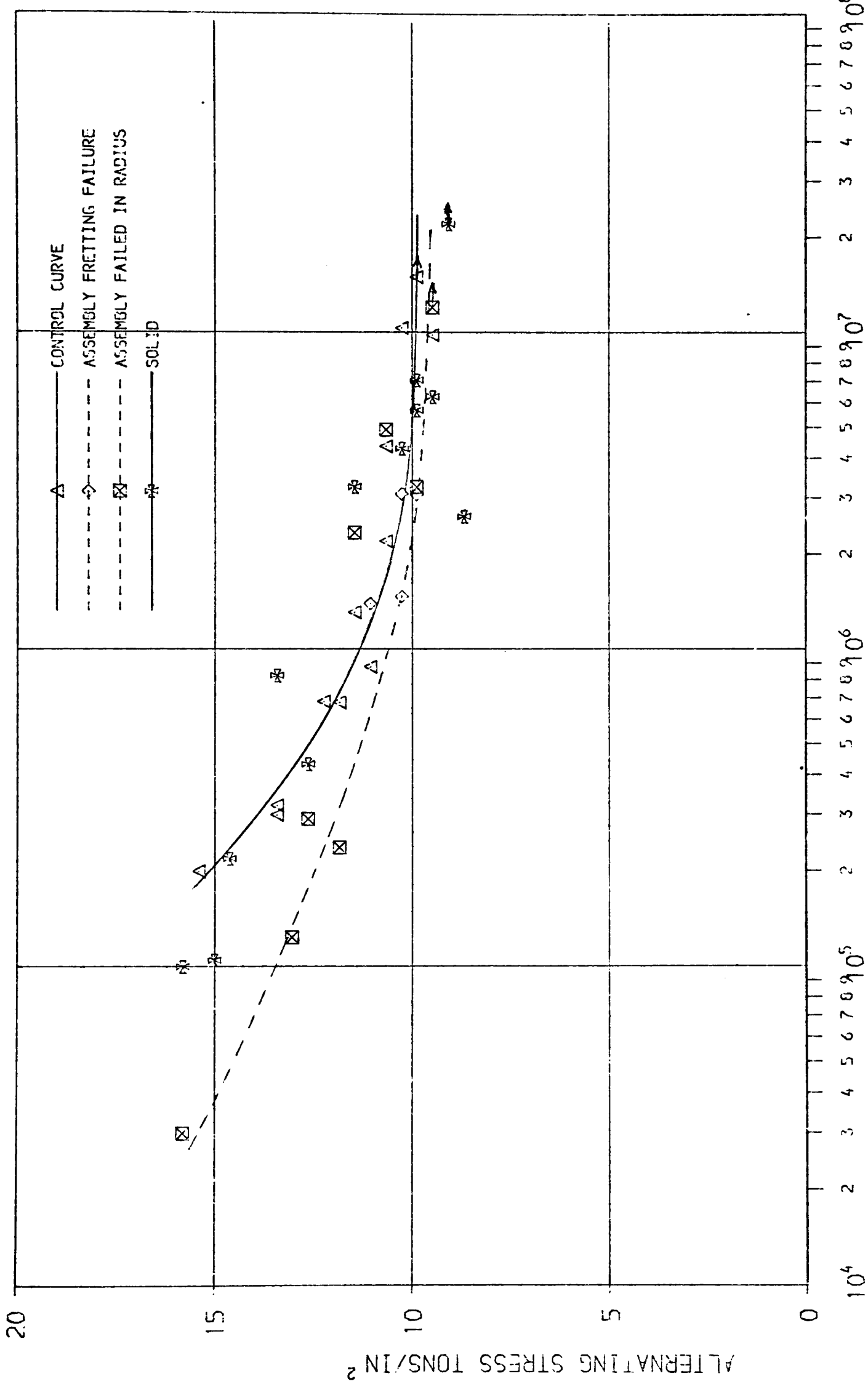


FIG. 4.4 S-N CURVES FOR FULLY RADIUSED SPECIMENS



Fig.4.5 Fully radiused specimens after failure.The solids and most assemblies failed in the radius.The remaining assemblies failed from the fretting region.

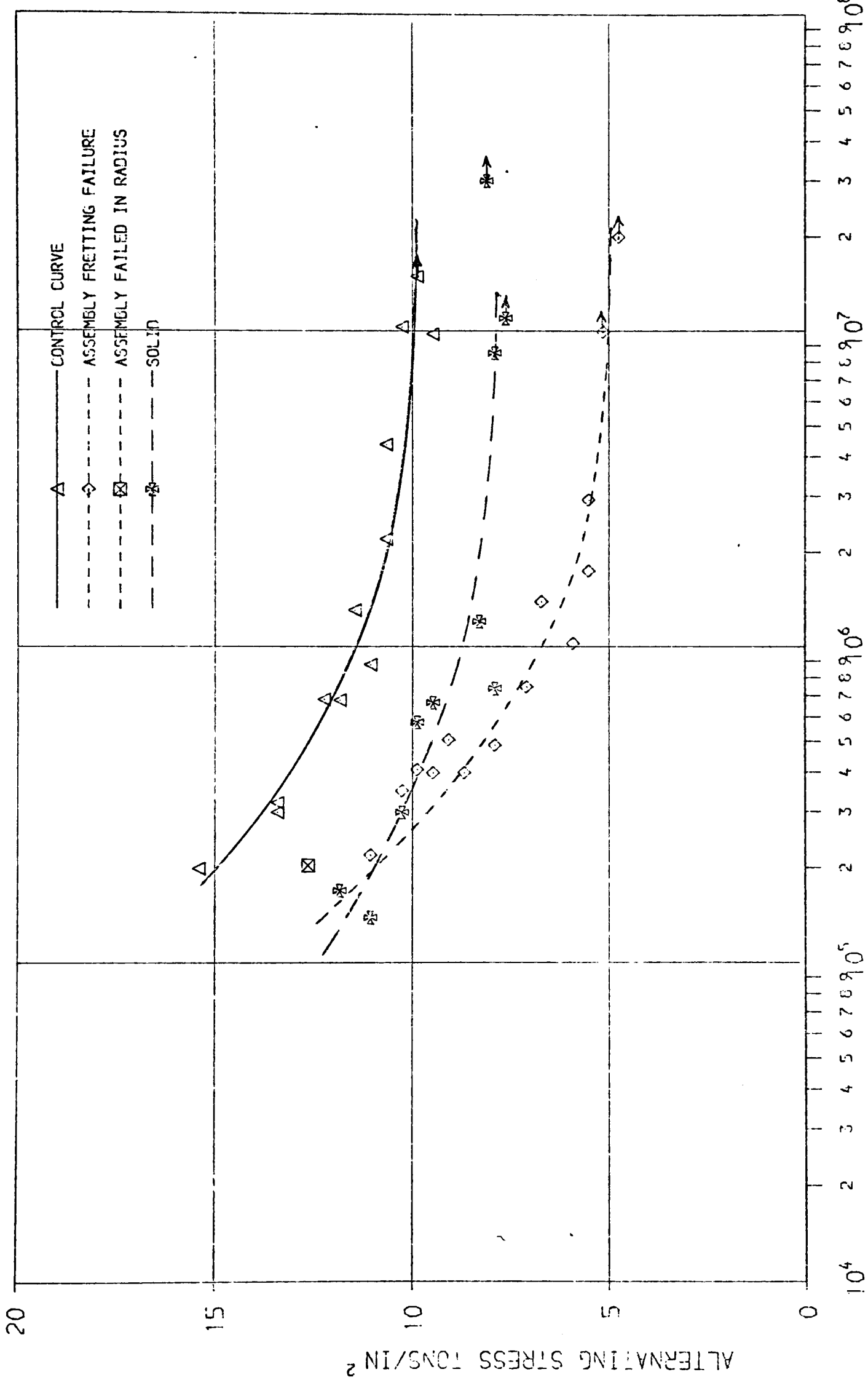


FIG.46 S-N CURVES FOR INCOMPLETE RADIUSED SPECIMENS

intense fretting, fig. 4.7. With these specimens, it was more difficult to estimate the stress at the origin of failure, due to the proximity of the origin of failure to the corner. However, the nominal stress at the origin of failure, based on the specimen width there, is 4/5 of that away from the blocks and the specimens broke at loads only half as great as those required to break unnotched specimens in the same number of cycles. Again it appeared that the strength reduction factor due to fretting can be at least 2. In addition, the fact that the only assembly to fail in the radius had the shortest life, supported the theory, suggested by the results for the full radius series, that fretting takes time to develop its maximum strength reduction effect.

At this stage it began to look as though the photoelastic results, or at least those for the radiused assemblies, were more representative of the fatigue specimens than had been supposed.

In both the full and incomplete radiused assemblies, failure originated from a point on the interface close to the point at which the maximum shear stress, as predicted photoelastically, is apparently greatest.

If, now, it is assumed that the photoelastic results give a close approximation to the stress in the fatigue specimens, it is possible to estimate more accurately the real effect of fretting on fatigue strength. From the S-N curves the bulk axial stress required to produce failure in 10^7 cycles is estimated and the corresponding stress at the point of failure is calculated, using the

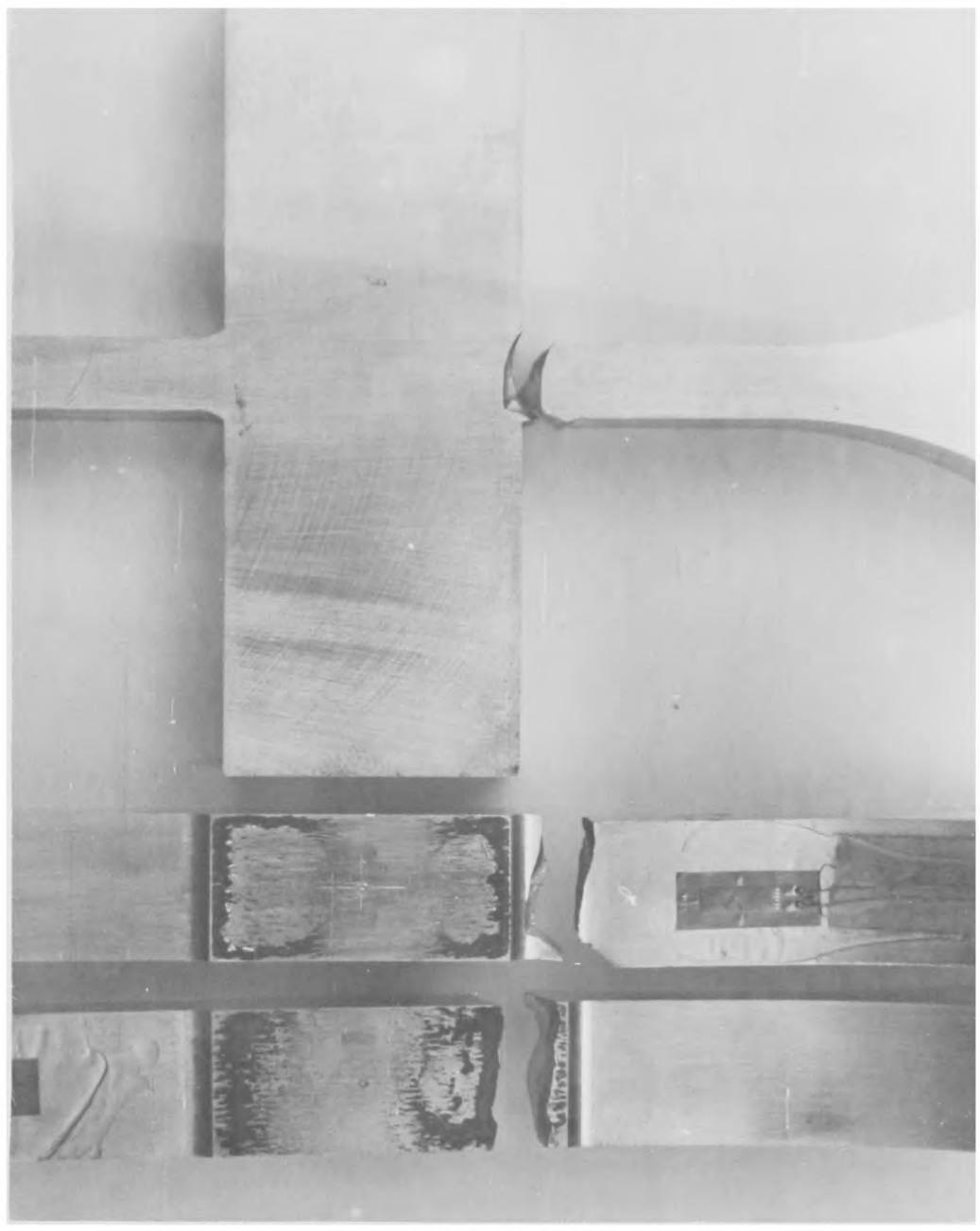


Fig.4.7 Incomplete radius specimens after failure.The solids and one assembly failed in the radius.The remaining assemblies failed from the fretting region.

photoelastic results. This stress is then compared to the unnotched fatigue strength to obtain a strength reduction factor, (K_f) due, presumably to fretting. The above method was applied to both the full and incomplete radiused assemblies and the figures obtained for K_f due to fretting were 2.42 and 2.34 respectively. If the same calculation is made for the sharp cornered assembly, the value of the K_f due to fretting is estimated to be greater than 3. However at this stage in the programme, the author still believed that the photoelastic results, especially those for the sharp cornered specimen, were in error due to the different conditions on the interface of photoelastic and fatigue specimens. While beginning to admit that fretting on its own was more serious than originally thought, the author was not yet prepared to believe that the value of K_f greater than 3, found with the sharp cornered assembly, was entirely due to fretting.

4.2.2 Amplitude of slip and size of slip region

Several other interesting features emerged from the tests of series 1. Amplitudes of slip at the edge of the interface were recorded for each assembly tested and are plotted in fig. 4.8. In practically every test, the maximum slip amplitude fell within the critical range of 0.0001" to 0.001" mentioned by Fenner and Field (7), although along each interface the slip amplitude varied from zero to some maximum value. However in none of the series of tests was there any tendency for the origin of failure to shift in a way that indicated a relationship

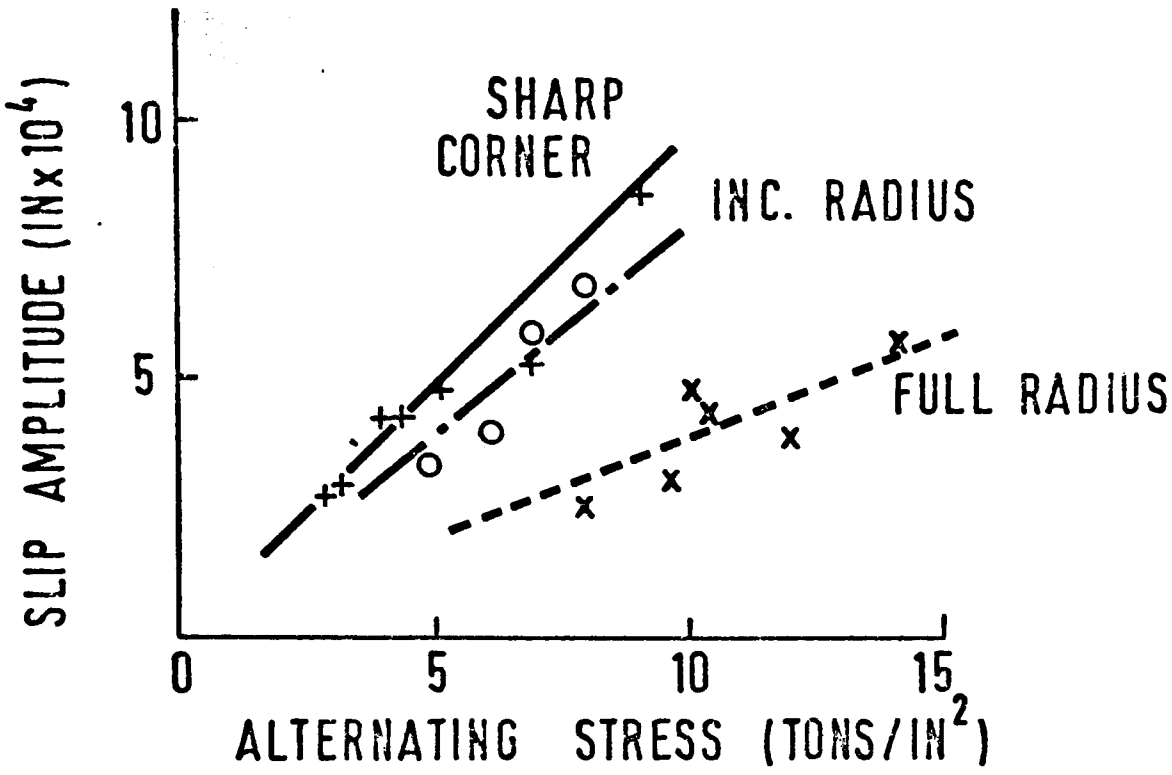


Fig. 4.8 Slip amplitudes for assemblies in Series 1

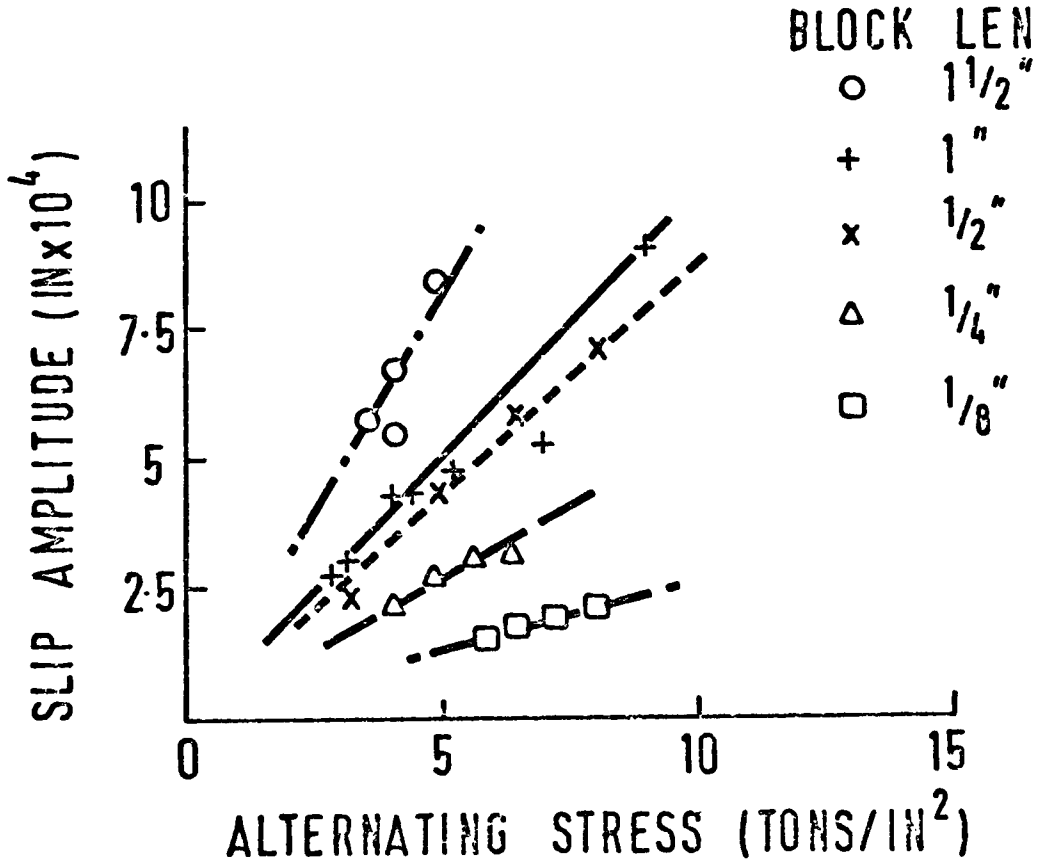


Fig. 4.9 Slip amplitudes for sharp cornered assemblies with different block lengths

between the origin of failure and slip amplitude. In the fully radiused specimens, the stress gradients on the interface are small over quite a large region and, if slip amplitude is a major parameter, one would expect that the position of the origin of failure would move within this region as the load, and hence the maximum slip amplitude, changed. This was not observed.

From the readings of slip amplitude recorded, it is possible to estimate the slip amplitude at the origin of failure for the various fretting failures observed. In the case of the sharp cornered assemblies which all failed at the edge of the interface, the measured values were obviously the require slip amplitudes and these showed that, at the fatigue limit of $\pm$ 2.8 tons/in^2, the slip amplitude was 0.0003". In the incomplete radiused assemblies failure occurred so close to the edge of the interface that it could be assumed that the slip there was the measured slip. In this case, at the fatigue limit of $\pm$ 5.0 tons/in^2, the amplitude of slip was 0.0004".

In those fully radiused assemblies in which failure occurred in the fretting zone, it originated about halfway along the interface and the slip amplitude is therefore difficult to estimate. However at a later date, using the theoretical analysis of the assemblies, it was possible to calculate the ratio of slip amplitude at the corner to that at the point of failure. From this, and the measured values at the corner, an estimate was made of the desired slip amplitude which, at the fatigue limit of $\pm$ 10 tons/in^2, was found to be about 0.0003".

In most tests of assemblies fretting covered about one half of the contact area and became progressively more severe towards the edge of the interface. (Highly polished surfaces showed slight burnishing between the fretting area and the no-slip area, indicating that slip was occurring there although the amplitude was not sufficient to cause fretting. The total slip area appeared to cover about 90% of the interface.) It has already been mentioned that the sharp cornered assemblies failed at the corner where fretting damage was most severe. However, it was often observed that with radiused assemblies in which failure originated on the interface the fail crack, although starting from a fretting pit did not originate in the area where fretting appeared to be most severe.

4.3 SERIES 2. TESTS TO INVESTIGATE THE EFFECT OF SLIP AMPLITUDE

The purpose of the tests comprising Series 2 was to investigate the effect, if any, of slip amplitude on fretting fatigue strength. Fig. 4.9 shows the variation of maximum slip amplitude with nominal axial stress for the various block lengths used and their respective S-N curves are plotted in fig. 4.10. For block lengths of $1\frac{1}{2}$", 1" and $\frac{1}{2}$" the maximum amplitude of slip, when the specimens were being stressed to their fatigue limit, was found to be 0.0005, 0.0003 and 0.00025" respectively. Despite this variation in slip amplitude, the fatigue limits of all three assemblies were found to be identical and equal to 2.8 tons/in^2. For blocks of $\frac{1}{4}$" and $\frac{1}{8}$" in length however, the fatigue limits rise to 4.6 and

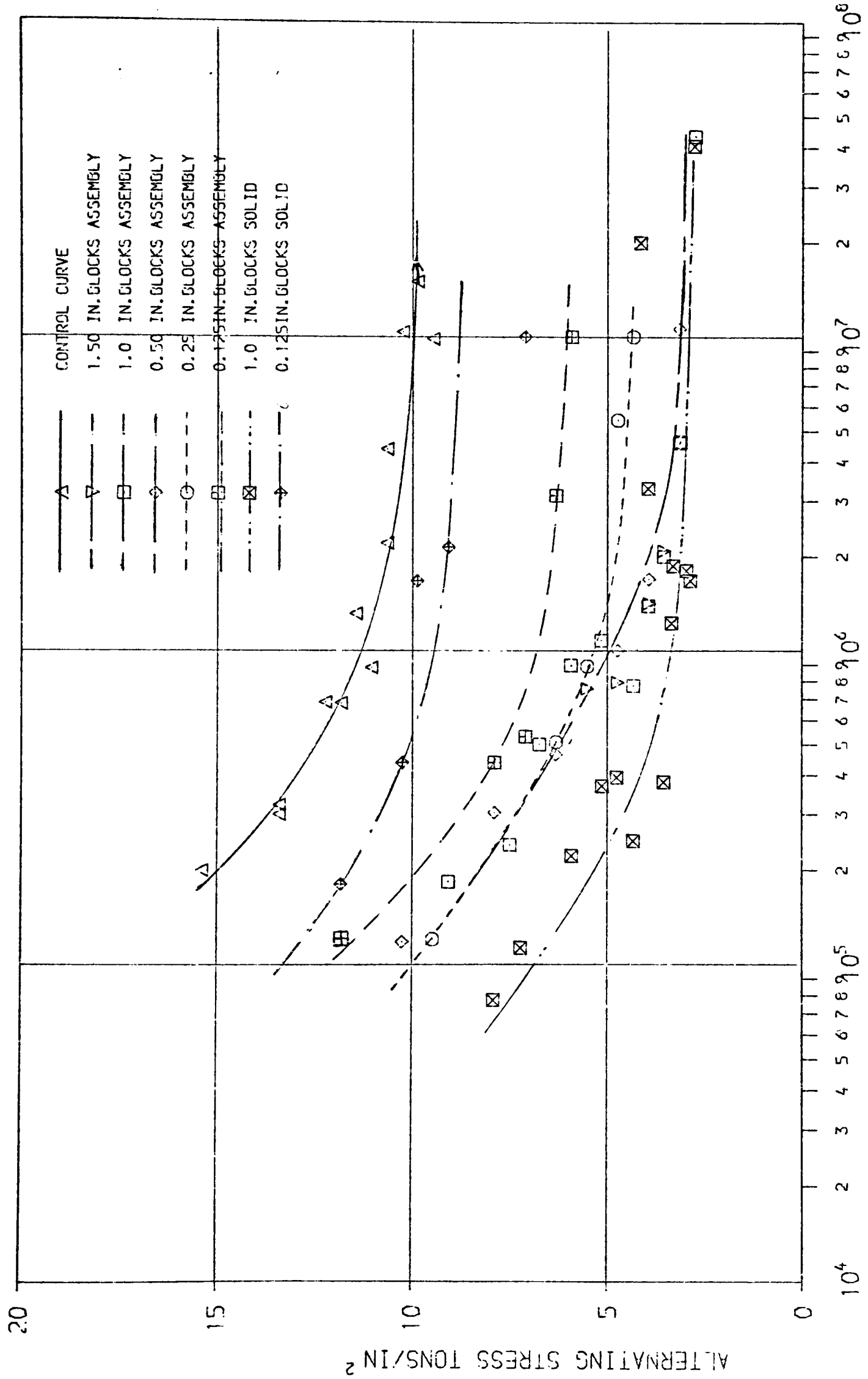


FIG. 4.10 S-N CURVES FOR SHARP CORNERED SPECIMENS WITH DIFFERENT BLOCK LENGTHS

6.0 tons/in^2 respectively while the maximum amplitude of slip at these stresses is found to be 0.00025" and 0.00015". This rise in fatigue strength however, cannot immediately be attributed to the fall in slip amplitude, for it is apparent that changing the block from 1½" to ⅛" changes other parameters besides slip amplitude. Clearly, the stress distribution near the blocks, in assemblies in which the block length is large compared to the specimen thickness, will be very different to that associated with specimens in which the block length is less than the specimen thickness. One might also expect there to be a 'size effect' due to the change in area of fretting. When the blocks are large the area is large compared to the cross sectional area of the specimen but with ⅛" blocks the area of fretting is reduced to little more than a line (fig. 4.11). One might expect a 'size effect' analagous to that found with more conventional stress raisers.

In an attempt to assess the effect of such size related phenomena, a series of solid specimens having ⅛" blocks was tested. These were found to have a fatigue limit of 9.2 tons/in^2, (fig. 4.10) very close to that of the unnotched specimens, which suggests that the effect of the geometric stress concentrations, associated with the sharp corner, has become virtually insignificant due, presumably, to the size effect. Consequently, the difference between the solid and assembly having ⅛" blocks must be due entirely to fretting which, therefore, appears to be less sensitive to the size

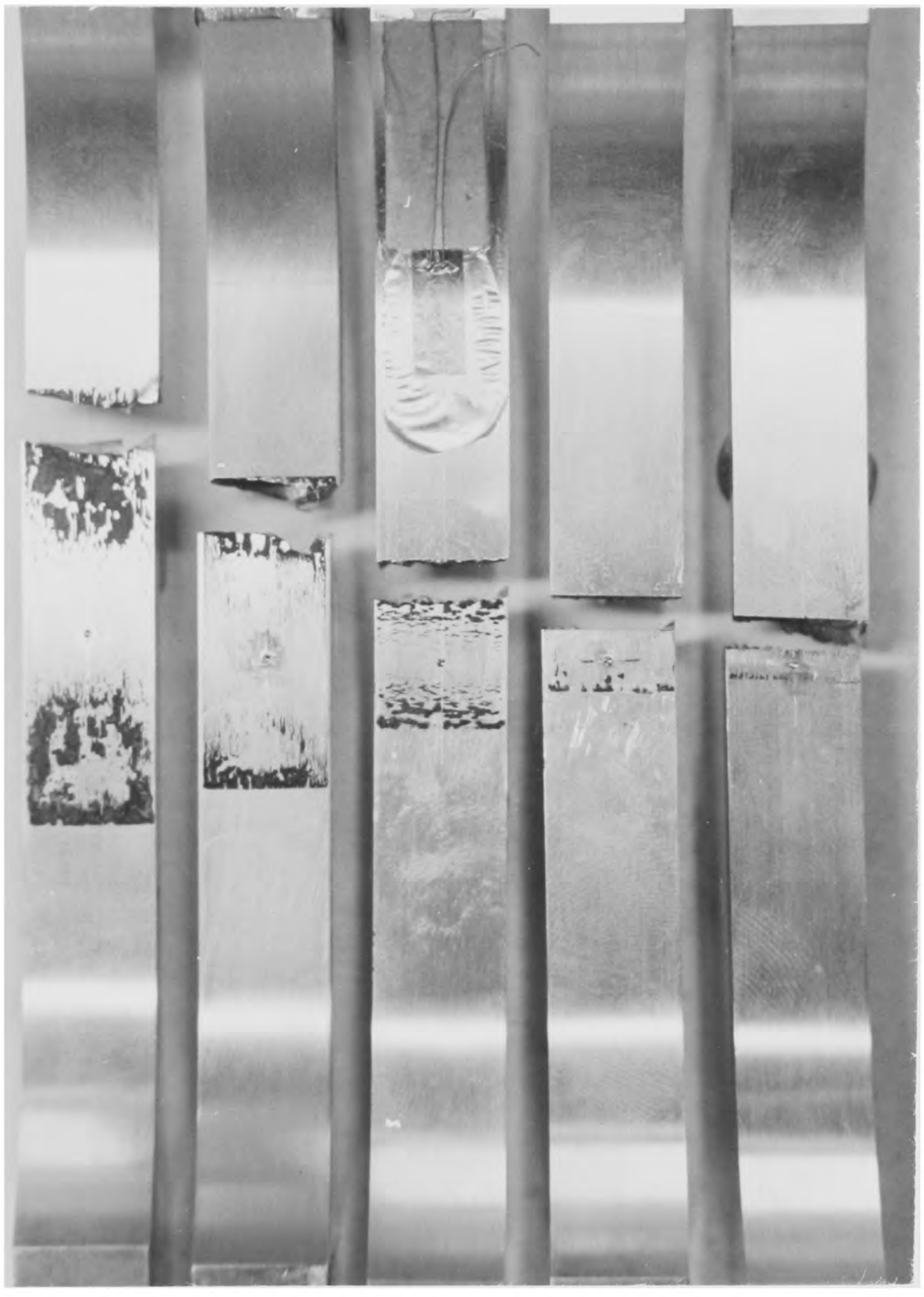


Fig.4.11 Sharp cornered assemblies tested with blocks of different length (Series 2).From **left,**block length=$1\frac{1}{2}$";1";$\frac{1}{2}$";$\frac{1}{4}$"and $\frac{1}{8}$".

effect phenomenon. Comparing the two fatigue limits, fretting alone appears to have reduced the fatigue strength by a factor of 1.5 although the slip amplitude was only 0.00015" and the area covered by fretting almost immeasurably small (fig. 4.9).

At the time that these test results were being analysed it was still thought that the strength reduction found in the assemblies with longer blocks was caused by a combination of both fretting and geometric stress concentration, with fretting no more than comparable with the geometric effect. Comparing the results for solid and assembly with $\frac{1}{8}$" blocks had again demonstrated that fretting by itself is, apparently, a major factor in determining fatigue strength. The value for the S.R.F. due to fretting found in the $\frac{1}{8}$" block tests was less than those found in series 1, for radiused specimens, but it was not possible to say whether this was an effect of the reduced slip amplitude or the reduced size of the fretted region. The tests with longer blocks had however demonstrated that, provided the slip amplitude is above 0.00025", variations in slip amplitude do not, of themselves, affect the fretting fatigue strength. Since, in all the tests of series 1, the slip amplitude had been greater than this value, those tests were presumably representative of fretting at its most damaging.

Later, when the theoretical stress distributions for the sharp cornered assemblies became available, it was apparent that, with long blocks, there was no appreciable geometric stress concentration during tensile

loading and that therefore most of the strength reduction was due to fretting. However, even in the light of the theoretical results, it was not possible to separate the effects of reduced slip amplitude and reduced fretted area. All that could be definitely concluded from the results of Series 2, was that, for changes in slip amplitudes, between 0.00025 and 0.0005, there is no noticeable change in fretting fatigue strength.

4.4 SERIES 3. TESTS TO EVALUATE THE EFFECT OF FRETTING IN THE ABSENCE OF A PROPAGATING LOAD

As explained in the previous chapter, the purpose of the tests of Series 3 was to investigate the effect of fretting applied in the absence of a propagating load. By taking surface roughness measurements using a Talysurf the damage to the surface of the specimen produced during the fretting stage of these tests was compared to that found in sharp cornered assemblies after failure. The damage in both cases seemed to be comparable, both as regards the size and depth of the pits and their spacing. However, when specimens are fretted for both 10^5 and 3×10^6 cycles were fatigue tested without further fretting, the control curve was reproduced. Indeed, in several cases, failure originated at a point outside the fretted region.

It therefore seemed that in the absence of a significant propagating load (both static and alternating) fretting damage does not affect the fatigue strength. As has been mentioned in the previous chapter the specimens were not highly polished and so the fatigue limit for the unnotched specimens (control curve) is probably lower

than the maximum obtainable for this material. Had the unnotched specimens been highly polished it is likely that a small strength reduction would have been recorded with the pre-fretted specimens. (In (22) a reduction in fatigue strength of only 3% was reported for similar tests.)

4.5 SERIES 4. TESTS TO EVALUATE THE EFFECT OF FRETTING IN THE ABSENCE OF A MACROSCOPIC STRESS CONCENTRATION

The tests in series 4 were designed to evaluate the effect of fretting in the presence of a propagating load but in the absence of any geometric stress concentrations.

In each case, the failure occurred in the narrowest section of the specimen close to the toe of the radius (fig. 4.12). This was about $\frac{3}{8}$" from the end of the interface which is thought to be far enough away to avoid any stress concentrations associated with the corner. The dynamic readings from the four strain gauges, positioned at the point of expected failure, were averaged and, from this, the stress at the origin of failure was evaluted. It was found that these strain measurements changed during the first ten to fifty thousand cycles but thereafter remained fairly steady. The readings used to compute the stress at the point of failure were therefore taken after 100,000 cycles.

It was found that the peak stress reached during the compressive half cycle of loading was considerable less, numerically, than the corresponding stress during the tensile half cycle. In other words, the stress cycle at the origin of failure took the form of an alternating stress superimposed on a mean tensile stress. From the

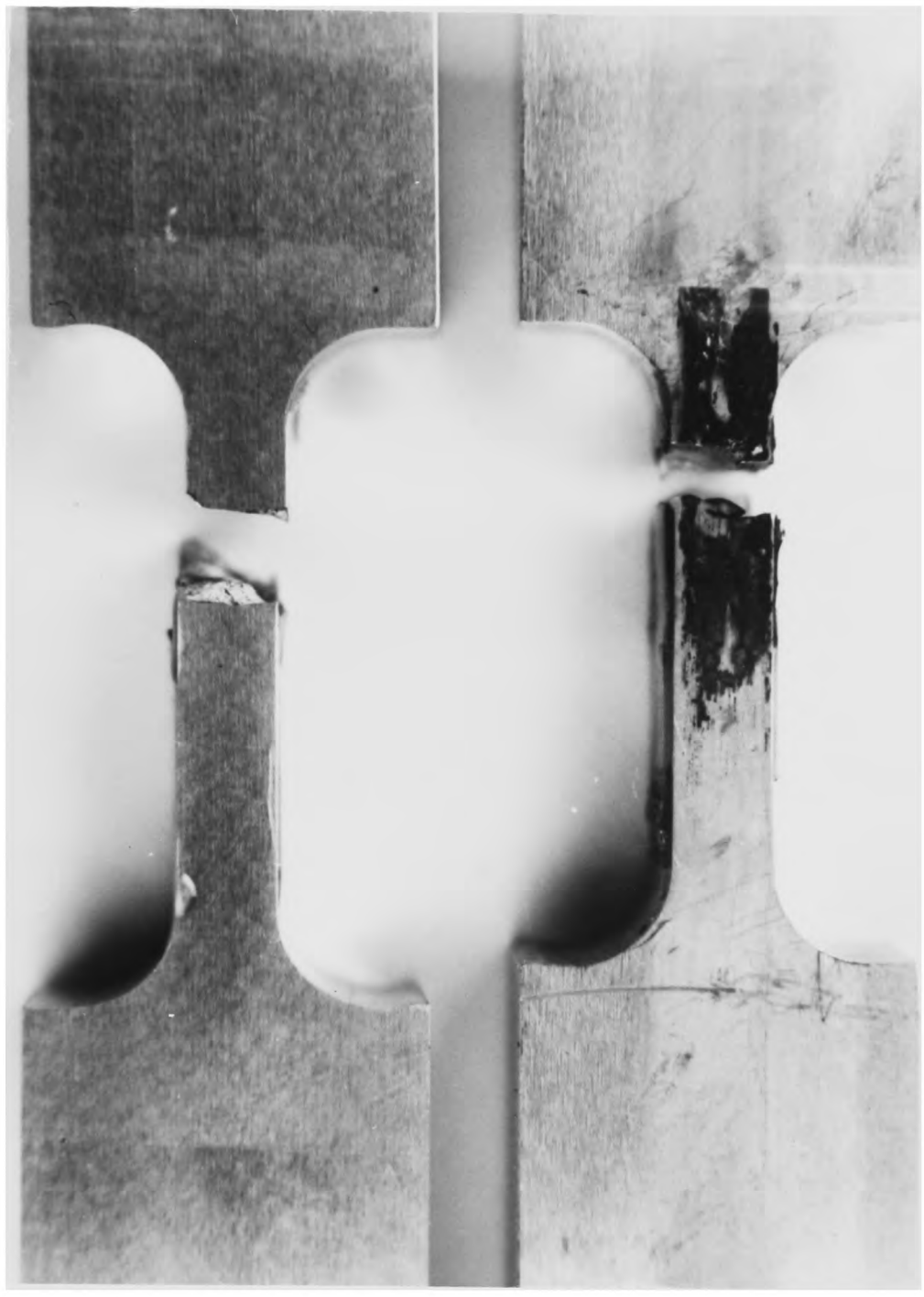


Fig.4.12 Specimens of the type used in Series 4 in which fretting failures occurred away from the corner of the blocks. The specimen on the left was tested without fretting.

theoretical stress determinations for the sharp cornered assembly of Series 1, which were, by this time, nearly complete, it is seen that such a result is predicted. At a point some distance away from the corner the peak tensile axial stress during a cycle is greater than the peak compressive axial stress (figs. 7.20, 7.21).

The deviation from true alternating stress somewhat reduces the value of these tests which were intended to evaluate the effect of fretting under zero mean stress. The estimation of fatigue strengths under zero mean load from those evaluated under non zero mean loads is difficult and unlikely to be very accurate. There is also a problem in presenting the results of the fatigue tests. The endurances can be plotted against either the nominal stress based on load, as in all the previous tests, or against the true stress obtained from the strain gauge readings. The same problem was to arise with the earlier tests since the analytic stress determinations from specimens of Series 1, revealed similar departures from pure alternating stress. However, for consistency the endurances of Series 4 specimens are plotted against the nominal stress based on load but the curve based on the semi axial stress range is also included (fig. 4.13).

(Note that specimens of the type used in this series, tested without fretting blocks, virtually reproduced the control curve.)

The fatigue limit for these specimens, based on the nominal stress is 4.3 tons/in^2. However, evaluating K_f due to fretting in the presence of a propogating

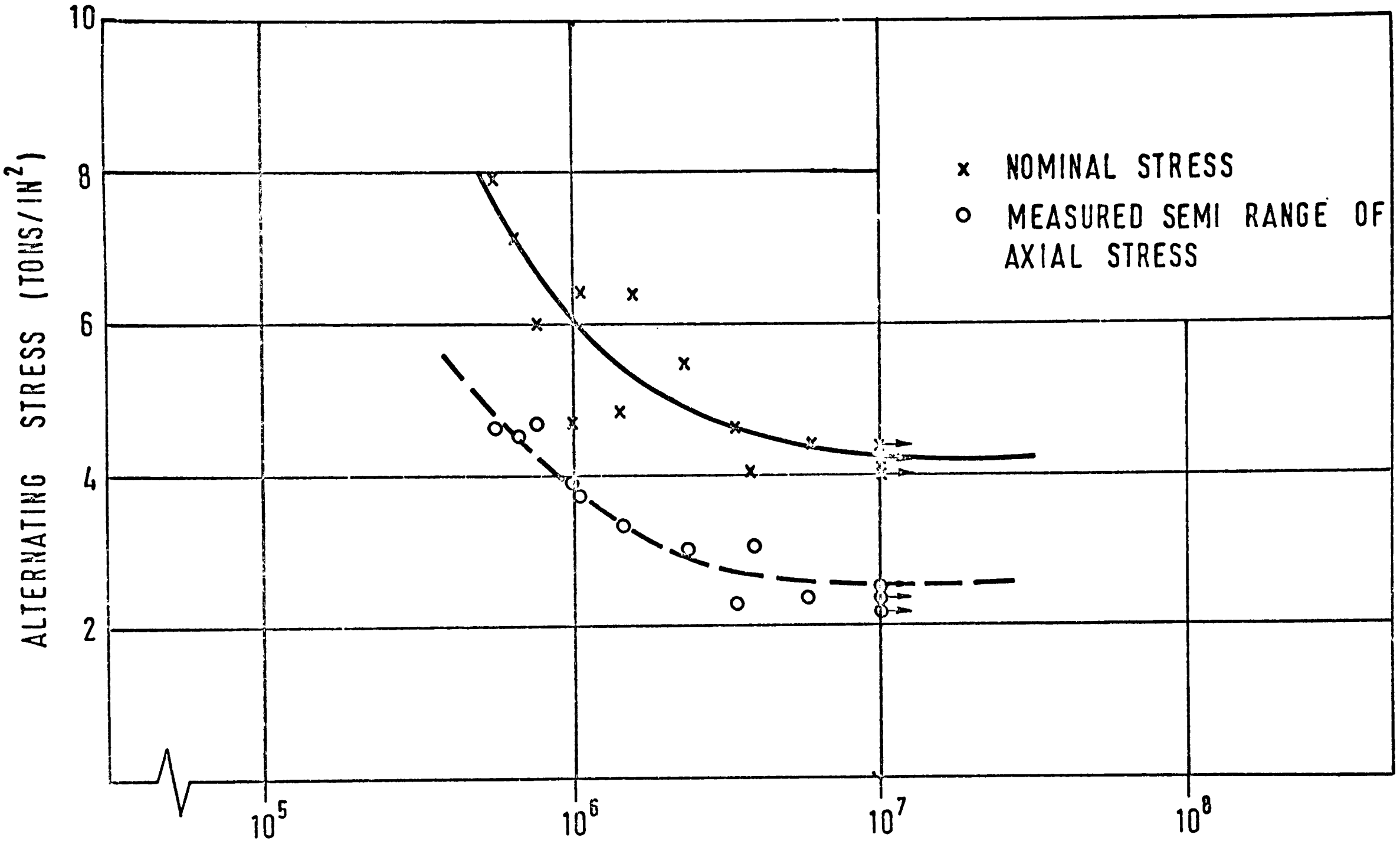


FIG. 4.13 S-N CURVES FOR SERIES 4.

stress using the measured axial stress at the point of failure gives values greater than 3.

Another drawback of this test is that, since failure occurs between the blocks, some way from the end of the interface, it is not easy to measure the slip amplitude at the point of failure. Furthermore, theoretical calculations are also difficult due to the complex geometry. However, in these tests, values of strain, at or near the point of failure, were recorded as has already been mentioned. From the calculations of slip for the specimens of Series 1 (fig. 7.12) it is seen that the variation of slip within the slip region is nearly linear and that, for the ratio of nominal axial stress to nominal normal stress used in these tests, the strain in the blocks is small compared to that in the specimen. One can therefore estimate the slip amplitude from the strain readings and the (observed) distance between the point of failure and the slip-noslip boundary. On this basis, the slip amplitude in the specimens of Series 1, at the fatigue limit, was about 4×10^{-4} inches. According to the results of Series 2 strength reductions due to fretting reach their maximum value at this amplitude of slip. These tests are thought, therefore, to be indicative of the greatest strength reductions likely to be found due to fretting alone.

In Chapter 8 the results of this and previous series will be examined more closely in the light of the theoretically determined stress distributions and values of K_f due to fretting will be calculated from the theoretical stress cycle rather than the nominal stress cycle.

However it was quite clear, from the results of the tests so far described, that the original hypothesis had severely underestimated the damaging nature of fretting when accompanied by a propagating stress. Furthermore, at about this stage in the test programme, the theoretical stress determinations for Series 1 revealed that the stress concentration, supposedly present at the corner in the sharp cornered assembly, was considerably reduced by the application of the axial fatigue load. So far, the author had failed to do the test that he set out to do, which was to investigate the combinded effects of fretting and a severe stress concentration. However, the original suggestion, that fretting by itself was not a major contributory factor in determining fatigue strength, had clearly been shown to be false.

4.6 SERIES 5. TESTS CARRIED OUT AFTER COMPLETION OF THE THEORETICAL STRESS ANALYSIS

Following the theoretical determination of the stresses in the specimens used in Series 1, it was realised that the geometric stress concentration in a sharp cornered assembly is strongly dependent on the ratio of the axial to normal stress(ξ). With this ratio equal to 8, as in Series 1, the surfaces at the corner of the block actually separate during the tensile half cycle of loading (see Chapter 7, fig. 7.20). The maximum tensile stress, equal to 1.07 times the nominal axial stress, actually occurs just inside the interface where real contact starts. On close examination, the sharp cornered assemblies in Series 1 were found to have failed just inside the

fretting area, failure originating roughly at the point at which the maximum tensile stress was predicted. It was now clear that fretting could result in strength reduction factors as high or higher than 3 even in the absence of obvious macroscopic stress concentrations. However it still seemed desirable to investigate the combined effects of fretting and a large geometric stress concentration - the original aim of the sharp cornered specimen tests in Series 1. Theory showed that increasing the nominal normal pressure (i.e. the clamp load) would increase the stress concentration at the corner of sharp cornered assemblies (see fig. 7.20 and 7.21) although at the same time the slip amplitude and size of slip region would be reduced. Tests on sharp cornered assemblies were therefore carried out with different ratios of nominal axial stress to nominal normal pressure (ξ).

Fig. 4.14 shows the S-N curves for sharp cornered assemblies with 1" blocks tested with the ratio of nominal axial stress to nominal normal pressure (ξ) equal to 8, 4, 2 and 1. It is seen that the effect on fatigue strength of changing (ξ) is small. However, it has a marked effect on the slip amplitude and the area covered by fretting fig. 4.15 and 4.16. As in the sharp cornered assemblies of Series 1, all failures occurred at the corner formed by the blocks and specimen.

In fig. 4.17 the S-N curves for solid sharp cornered specimens tested with ξ = 1 and ξ = 8 show that even increasing the static normal load to the same value as the peak axial load has only a small effect on the fatigue strength. Surprisingly, perhaps, it in fact causes a

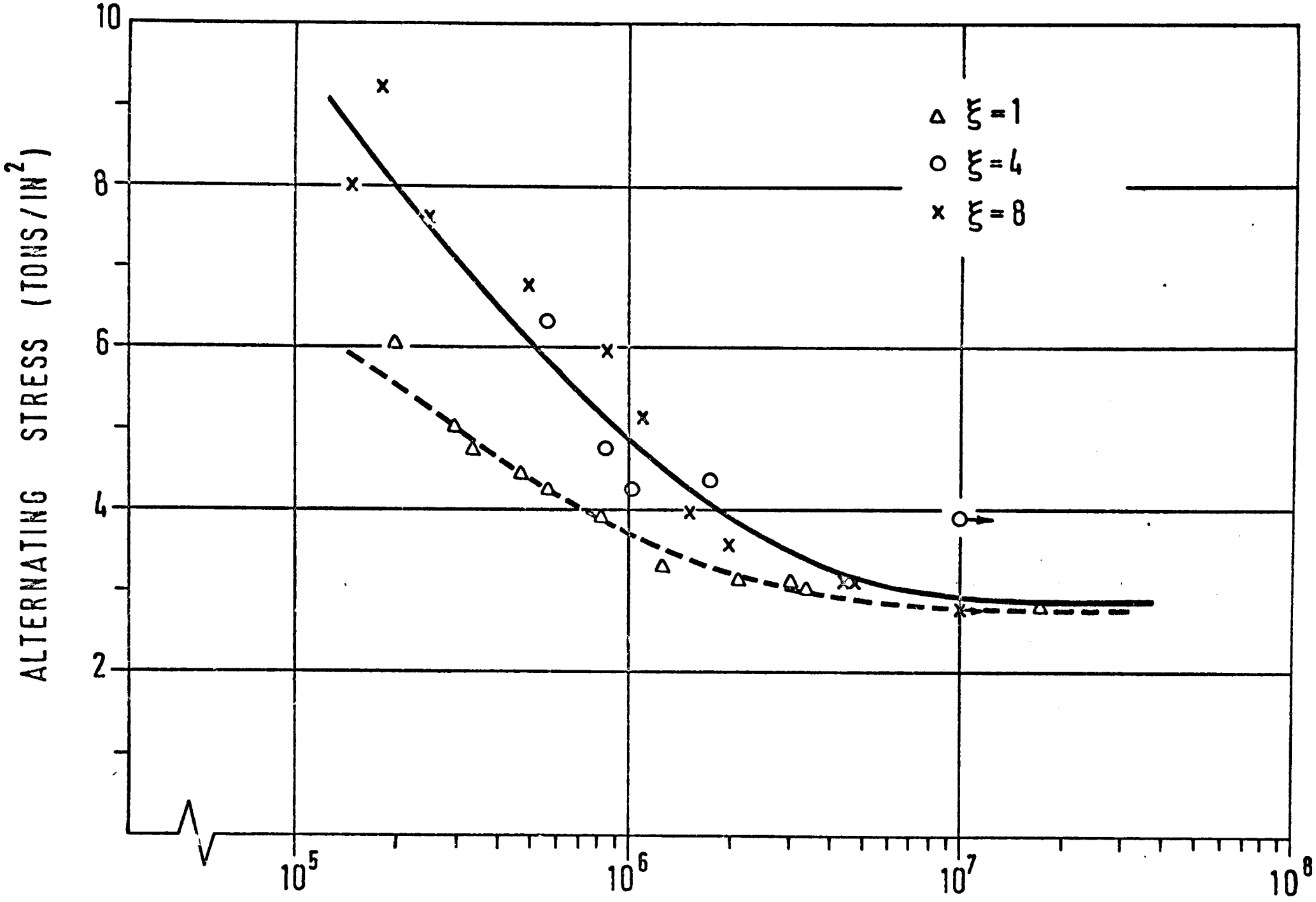


FIG. 4.14 S-N CURVES FOR SHARP CORNERED ASSEMBLIES WITH DIFFERENT ξ

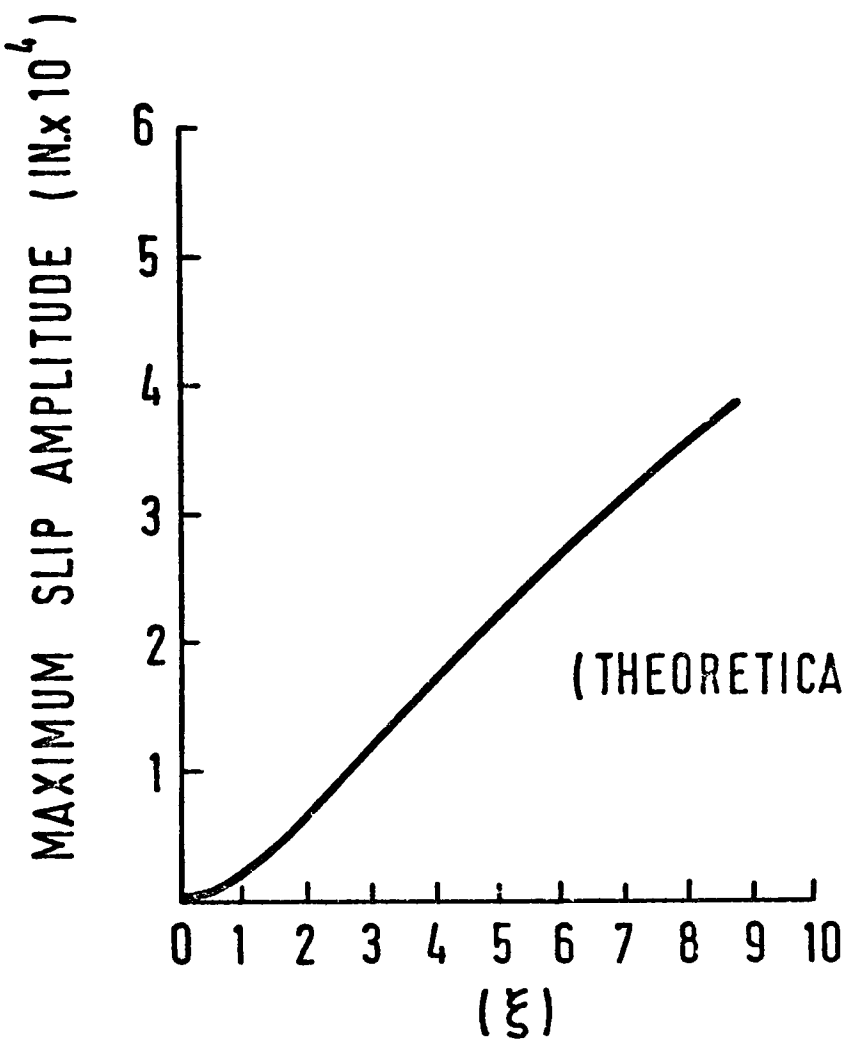


Fig. 4.15 Variation of maximum slip amplitude at fatigue limit with ξ in sharp cornered assemblies

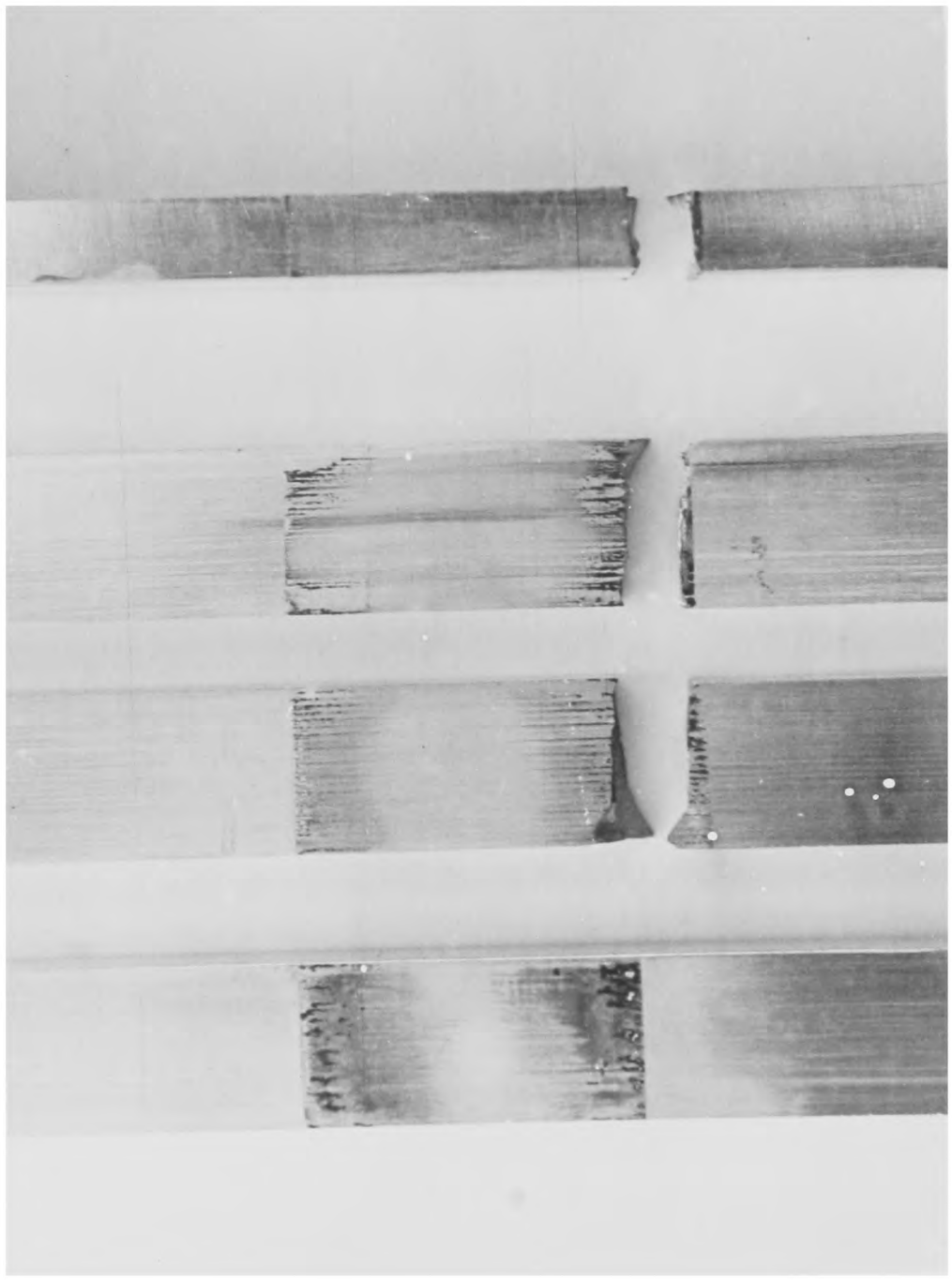


Fig.4.16 Sharp cornered assemblies tested at different ratios of axial load to clamp load.From top to bottom ξ =1,2,4and8.

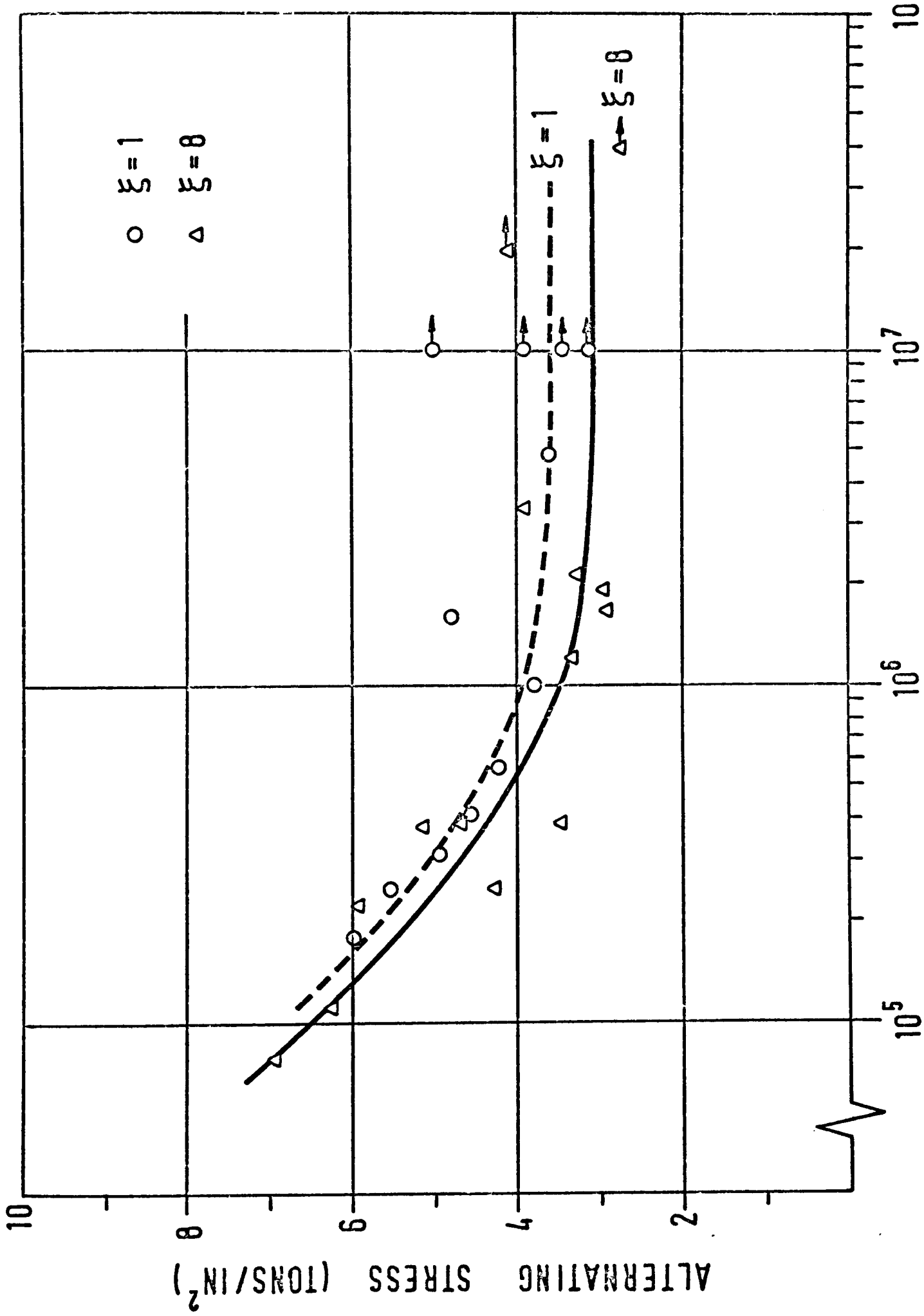


FIG. 4.17 S-N CURVES FOR SHARP CORNERED SOLIDS WITH $\xi = 1 \& 8$

slight rise in strength but checking with the theoretical results for a solid sharp cornered specimen under normal load only, shows that, at the corner, both principle stresses associated with this loading are compressive. Thus one could expect that increasing the normal load would have the effect of imposing an increased static hydrostatic pressure at the corner which will inhibit crack propagation and increase the fatigue strength.

The purpose of these tests on sharp cornered solid specimens was to examine the effect of the increased normal pressure and to relate this to the results for the assmblies tested at various ξ. From these tests, it appeared that increasing the normal pressure would not of itself reduce the fatigue strength. This result was confirmed by the series of tests in which a rubber interleave was inserted between the blocks and the specimen of a sharp cornered assembly having 1" blocks. The tests were run at $\xi = 1$ and in effect reproduced the control curve. Failure often occurred away from the region of the blocks and there was no fretting damage. (Although it was not the purpose of these tests, they did demonstrate the efficacy of rubber interleaves as a fretting preventative.)

The results for the tests described above, confirmed that the slight change in fatigue strength of the assemblies with change in ξ, illustrated in fig. 4.14, was not due to the increased static normal load but rather to changes in stress concentration and slip amplitude.

Comparing the results for $\xi = 8, 4$ and 1 it is seen that decreasing ξ from 8 to 4 has a negligible effect on

fatigue strength, but for ξ = 1 the fatigue strength, particularly at low endurances, has been slightly reduced. However, when ξ = 1, the amplitude of slip has been reduced to an order of magnitude less than that found for the $\frac{1}{8}$" block assemblies in Series 2. In that case, fretting was apparently reducing the fatigue strength by a factor of 1.5 (see Section 4.3) so that in this case the contribution to the overall strength reduction due to fretting is probably even less than 1.5. Thus, with ξ = 1 resulting in an overall S.R.F. of 3.5, it would seem that the geometric stress concentration at the end of the interface is contributing significantly to the overall strength reduction.

Such a result, explains why the difference between S-N curves for assemblies with ξ = 1 and ξ = 8 is greatest at low endurances. It has already been observed, with radiused assemblies in Series 1, that fretting takes some time to develop its maximum effect. However, the effect due to the geometric stress concentration will remain constant however long the test runs (neglecting any initial yielding). Thus assemblies for which ξ = 8, in which the strength reduction is almost entirely due to fretting, are relatively stronger at low endurances, because the fretting has not fully developed, than those for which ξ = 1, which are, at most, only partially dependent on fretting for the loss in strength.

Also of interest is the result that the assemblies in which ξ = 1 have almost identical fatigue strengths at all endurances to the solids for which ξ = 8. The differences between solid and assembly for ξ = 8 have

already been noted and explained as being a consequence of either non propagating cracks formed in the solid at low nominal stress, or of the time required for fretting to develop fully in the assembly. Increasing the normal load in the assembly so that ξ = 1 reduces the fatigue strength at low endurances to that of the solid for which ξ = 8 but has little effect on the fatigue limit. It appears from the theoretical stress analysis that in an assembly with ξ = 1 the stress concentration will not be high enough to produce non propagating cracks (Harris (32) suggests that non propagating cracks only develope when the stress concentration factor is greater than 6), and it has been shown, experimentally, that the increased normal stress has no effect by itself. It has already been shown that the strength reduction in the assemblies with ξ = 1 is due more to geometric stress concentration than fretting, and so the similarity between assemblies with ξ = 1 and solids with ξ = 8 suggests that the differences between solid and assembly with ξ = 8 are almost entirely due to fretting requiring several hundred thousand cycles to develop fully. The effect of non propagating cracks mentioned in Section 4.2.1 would seem to be of secondary importance.

In the light of the above reasoning, it is interesting to refer back to the results for the sharp cornered assemblies and solids of Series 1, in which ξ = 8, and compare their S-N curves to the control curve. It is seen that the curve for the solid is similar to the control curve but shifted down the stress axis, i.e. the strength reduction factor is sensibly the same for all

endurances. For the assembly, however, this is not so, the strength reduction factor varies from 1.6 at 10^5 cycles to about 3.5 at the fatigue limit. This immediately suggests that the fretting damage increases steadily over a considerable number of cycles.

Unfortunately this point was not appreciated at the time the tests were carried out - the coincidental equality of the fatigue limits of the solid and the assembly blinding the author to the more subtle aspects of the results until later.

Returning to the results of Series 5 it is interesting that, with $\xi = 1$, the solid is stronger than the assembly. It has already been suggested that the solid increases in strength as ξ decreases due to the hydrostatic nature of the stress at the corner due to the normal load. In the assembly this stress, which inhibits crack propagation, may be destroyed by the slip, thus making the assembly stronger than the solid. Alternatively it may be that the effect of any hydrostatic stress is more than compensated for by fretting.

Summing up, it seems certain that in the tests of the assemblies in which $\xi = 1$ the strength reduction was due almost entirely to the geometric stress concentration, fretting being at most of secondary importance. Unfortunately, in order to achieve a satisfactory stress concentration, the slip amplitude has had to be reduced to such an extent that the full effect of fretting at its worst is not realised and the two effects together add up to little more than severe fretting alone. With this

particular geometry it appears that as one effect increases in significance the other decreases in proportion so that the overall S.R.F. remains fairly constant for all values of ξ. Ways of overcoming this and combining severe stress concentrations with severe fretting are suggested in Chapter 8 but must, unfortunately, be the subject of research outside the scope of this thesis.

The tests of this series have shown that, under certain conditions, failure of an assembly from a region of fretting is due to the geometric stress concentration associated with the overall shape of the assembly and not to fretting. However this was an isolated result; in general it has been shown by the other tests that fretting can be responsible for strength reductions as high as 3 even in the absence of a macroscopic stress concentration.

4.7 SERIES 6

A series of tests, similar to those carried out by other authors (7), was run to see whether the criticism of such tests levelled in Chapter 1, was justified. The S-N curve for fretting applied by blocks with feet is shown in fig. 4.18 with the curve obtained using blocks with continuous contact. The fatigue limits are 3.5 and 2.6 tons/in^2 respectively. Clearly the fretting applied by the feet is less damaging than that associated with the continuous blocks and the S.R.F. due to fretting computed from these tests would not appear to be the maximum possible. It was originally suggested that these tests would overestimate the true strength reduction due to fretting because of the complex stress distribution

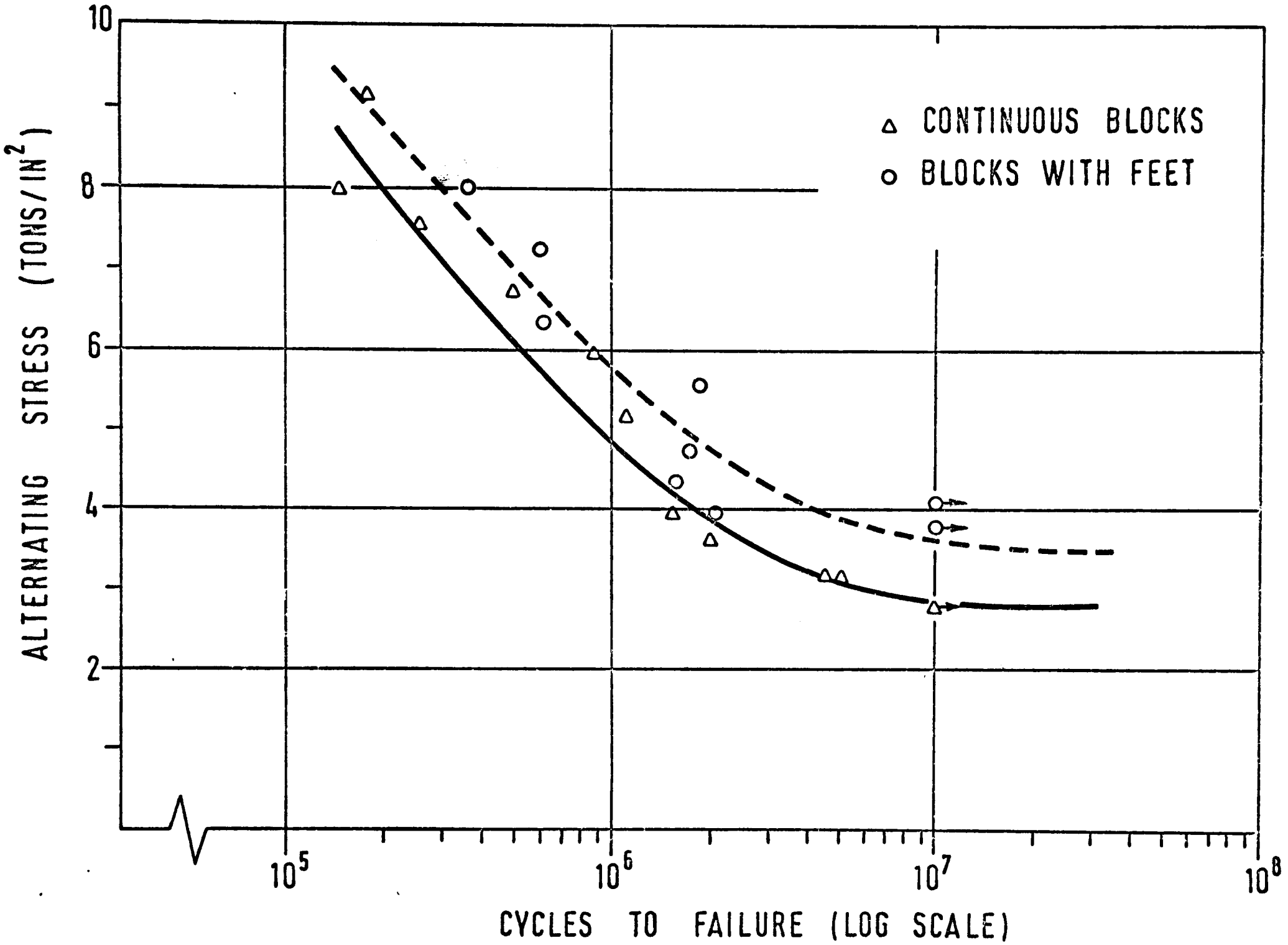


FIG 4.18 S-N CURVES FOR SERIES 6.

around the contact area. This does not appear to be the case and the low value for the S.R.F. may be due to a size effect. This Series and its implications are discussed further in Chapter 8, following a more detailed discussion of the results of this investigation taken as a whole.

4.8 MICROSCOPIC EXAMINATION OF SPECIMENS AFTER TESTING

Sections were taken through the fretted areas of several specimens of various types. When viewed through a microscope these sections revealed little that has not already been reported extensively by other investigators. It was observed that all fatigue cracks originating in fretting zones leave the surface inclined to the surface at angles varying between 30° and 60°. Cracks which have propagated well away from the surface change direction just below the surface and then run perpendicular to the direction of the bulk propagating stress. In general there were fewer cracks in specimens in which stress gradients are high e.g. some sharp cornered assemblies, than in specimens in which the stress gradients are low. The density of cracks in any one specimen was always highest in the region of highest stress. In specimens in which the stress gradients were high all the cracks except the failure crack were very short and at failure were still inclined to the surface. In specimens with low stress gradients there were often several relatively long cracks as well as the failure crack.

4.9 SUMMARY

The results of the fatigue tests indicated that fretting, applied in the presence of a propagating stress,

can reduce the fatigue strength of a material by as much as 60%. However without a precise knowledge of the stress at the origin of failure quantitative evaluation of the fatigue results is not possible.

A method for the theoretical determination of stresses in the fatigue specimens is described in the following two chapters and the results of such a determination are presented in Chapter 7. In Chapter 8 the fatigue results are examined in the light of the theoretical stress distributions. The reader who is primarily interested in the fatigue results may wish to turn directly to Chapter 8 in which relevant results from Chapter 7 are usually quoted again.

Chapter 5

A METHOD FOR DETERMINING STRESSES IN A CLAMPED JOINT

5.1 STATEMENT OF THE PROBLEM

In order that the conclusions resulting from the fatigue work should be quantitative rather than simply qualitative, it was necessary to know the stress distributions in the fatigue specimens. For reasons described in Appendix 3, the validity of the results obtained from photoelastic tests was doubtful and it was apparent that a theoretical analysis was required.

A model which was rigorously representative of the fatigue specimens seemed to be impracticable. For example, there is no obvious way of representing asperity contact on the interface, nor of including the effect that fretting debris would have on the coefficient of friction and the normal pressure distribution.

The simplified model chosen for the analysis was based on the following assumptions:-

(1) Both the blocks and the specimen are perfectly elastic at all times.

(2) The surfaces of the interface are perfectly flat and contact is continuous.

(3) The coefficient of friction is constant over the whole interface but can have any value from zero to infinity.

(4) The axial stress in the specimen is uniform in regions remote from the blocks.

(5) The normal load is applied at a point on the centre line of the blocks.

Using this model it was hoped to obtain values for the stress distributions along the interface for various loading systems and, from these, to plot the stress variations during a complete fatigue cycle. By comparing computed values of slip amplitude, size of slip region, and displacement of points on the interface to values obtained experimentally, an estimate can be made of how closely the model represents the actual fatigue specimens.

The problem, then, was to determine the contact stresses and displacements which arise when an elastic plate is compressed between two elastic blocks and then subjected to cyclic axial loading. Coulomb's law of friction is assumed to hold, relating the normal and shearing stresses on the interface.

Work by other authors (33,34,35) on contact stress problems in half spaces, has shown that the interface between the half space and the indenter can be thought of as having two distinct regions, one where the surfaces slip relative to each other and one where they do not.

If it is assumed that the same will be true of contact between a plate of finite thickness and a rectangular indenter, boundary conditions on the plate/block interface can be formulated.

One example of such a problem is illustrated in Fig. 5.1. Clearly because of symmetry about both the x and y axes, only one half of one interface need be considered.

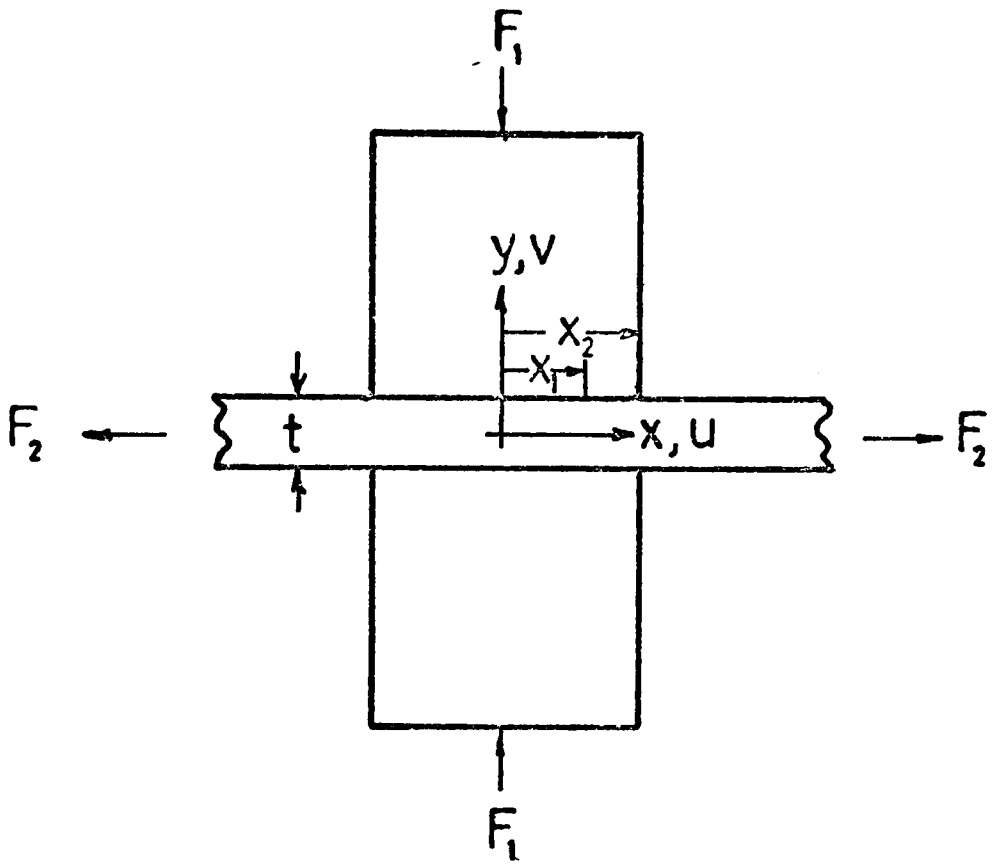


Fig. 5.1. A plate loaded axially following indentation by rectangular blocks

The no slip region is assumed to extend from $x = o$ to $x = x_1$ and the slip region from $x = x_1$ to $x = x_2$.

The following notation is used:-

p = the normal pressure on the interface

τ_{xy} = the shear stress on the interface

σ_x = axial stress in the plate

U_1 = the surface displacement of the block parallel to the axis of the plate

U_2 = the surface displacement of the plate parallel to the axis of the plate

V_1 = the surface displacement of the block normal to the axis of the plate

V_2 = the surface displacement of the plate normal to the axis of the plate

μ = the coefficient of friction

F_1 = the clamping(hormal) load

F_2 = the axial load

t = the plate thickness

w = the plate width

The displacements are relative to the axes of symmetry. The boundary conditions in this case can therefore be written as follows:

(1) $\tau_{xy} = \mu p; \quad x_1 < x < x_2$ 5.1

(2) $\tau_{xy} < \mu p; \quad 0 < x < x_1$ 5.2

(3) $V_1 = V_2; \quad 0 < x < x_2$ 5.3

(4) $U_1 = U_2; \quad 0 < x < x_1$ 5.4

(5) $2w \int_{-o}^{x_2} p \, dx = F_1$ 5.5

(6) $2w \int_{o}^{t/2} \sigma_x \, dy = F_2; \quad x \gg x_2$ 5.6

Clearly for arbitrary values of F_1, F_2, and μ, the value of x_1 is not known and will be part of the solution. The above equations describe the problem that the author set out to solve. It was found that in certain circumstances the boundary conditions had to be slightly modified. However, equations 5.1 to 5.6 represent the basic problem and it remained to find a method of solving them.

5.2 LITERATURE SURVEY

The literature contains very little information which is directly applicable to this boundary value problem. Most contact problems, dealing with blocks indenting plates and for which solutions are available have been

simplified by assuming that the blocks are rigid and that the coefficient of friction is either zero or infinite. In addition a great number of contact stress problems associated with half spaces and also problems involving cylindrical or spherical contact have been solved analytically (33-35). Such solutions can be used to predict, qualitatively, the location of slip and fretting regions and the damping capacities of clamped joints, but clearly are of only limited application in this very different boundary value problem. They do, however, exemplify the great complexity of purely analytic methods.

The closest approach to solving the general plate/block problem is probably the recent work of Conway, Farnham, So, and Vogel (36,37). They use a numerical method to solve the problem of a rigid indenter compressing a flat strip assuming Coulomb friction on the interface. The strip however is not loaded axially.

5.3 METHOD OF SOLUTION

As mentioned above the analytic solution of contact problems is extremely complex and usually requires simplifications to be made that significantly reduce the utility of the answers.

What was required in this work was a method of solution that would give reasonable, but not necessarily exact, answers to the problem while allowing all the important parameters to have realistic values.

Furthermore, it was obviously desirable that a solution should be found capable of dealing with specimens of complex shape such as those with stress relieving radii.

The alternative to an analytic solution was one or other of the now well tried and (since the advent of fast digital computers) widely used numerical techniques. These have several disadvantages. For example, they do not produce algebraic expressions for the unknowns in terms of variable parameters; each change of parameter requires the whole problem to be recomputed. In addition numerical methods do not give exact solutions and produce values for the unknowns only at a number of discrete points.

Against these disadvantages however, it appeared that only by using a numerical technique would it be possible to solve the problem while limiting the assumptions to those listed in Section 5.1. Because only relatively few cases needed to be solved to determine the stress distributions in the fatigue specimens and 100% accuracy was not essential, the application of numerical techniques was acceptable in this context.

A numerical technique for solving plane contact problems, used by several authors including Conway et al (36) assumes that the interface is subdivided into (n) short lengths. The normal pressure distribution between the block and the plate is considered to be equivalent to a series of n blocks of pressure (p_1, p_2 -- p_n) constant over each such length (Fig. 5.2).

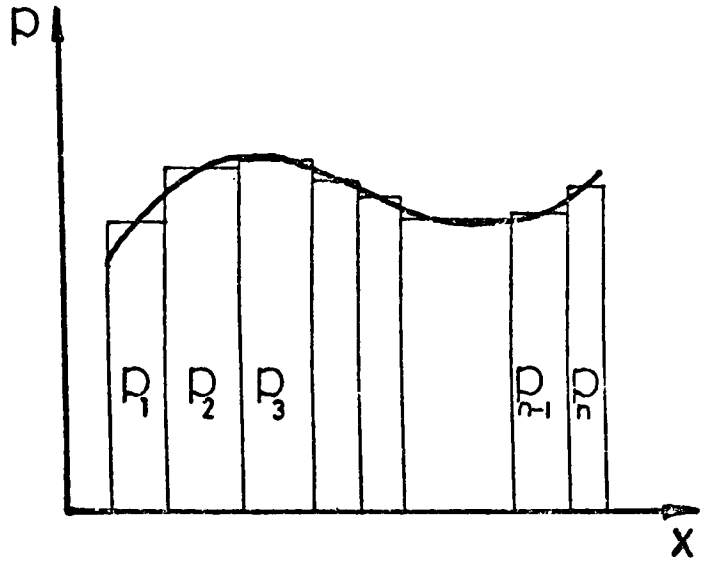


Fig. 5.2. Continuous pressure distribution represented by n blocks of constant pressure

Horizontal and vertical displacements of the interface are computed for unit blocks of pressure acting one at a time on each of the interface subdivisions. Depending on the method used the displacements will be either in the form of displacement of discrete points (influence coefficients) or continuous functions of position (influence functions). The interface shear stress can be treated similarly (q_1 q_2 -- q_n) and a corresponding set of influence coefficients or functions computed. The problem is now to solve for p_i and q_i where i takes values from 1 to n. Interface displacements can now be expressed in terms of the n discrete pressures and n discrete shear stresses and the influence coefficients. The boundary conditions can therefore be expressed in terms of the discrete

pressures and shear stresses, thus forming a set of simultaneous algebraic equations with the p_i and q_i as unknowns. Having solved for p_i and q_i the computation of the interface displacements is straightforward. The method described above assumes that continuous pressure and shear stress distributions can be replaced by blocks of constant pressure and shear stress. If the continuous stress distributions are replaced by a number of discrete forces, acting parallel and normal to the interface at severl points along the interface, similar arguments to those used above can be applied to formulate equations which can be solved for the unknown forces.

The influence coefficients or functions can be determined in a number of ways. Analytic solutions involving infinite integrals and series have been used to calculate displacements in both plate and block respectively (ref. 36,38) but the inevitable truncation of the series introduces errors when matching boundary conditions on the interface. In addition, the algebra required to deal with both an elastic plate and an elastic block would be very lengthy. However, the chief argument against using analytic methods in this work was their inherent inability to deal with any but the simplest geometries. It was hoped to consider complex geometries such as those typified by the specimens with stress relieving radii described in Chapter 3. Finite difference or finite element techniques are known to have the fewest limitations in respect of geometry and it appeared that, if used with caution, they would be suitable for determining the influence coefficients

for the various geometries of the fatigue specimens. Furthermore, having solved for p_i and q_i by the method outlined above, finite element or difference methods could then be used to determine the contact stresses in the specimens resulting from the p_i and q_i.

In their paper on "The Finite Element Method for Analysis of Elastic Isotropic and Orthotropic Slabs" (39) Zienkiewicz and Cheung, discussing the advantages of the finite element method, note that "... in general the resulting system of equations is better conditioned than that corresponding to a finite difference system" and that certain boundary conditions ... "notorously difficult to deal with by finite difference do not present any problem here". They also note that "standard structural procedures (stiffness analysis) can be used for the solution of the (finite element) problem" and go on to mention that use can therefore be made of known computer techniques and programs. (In this Thesis the word program is used in the context of computer program and is distinct from programme which is used only in its original sense.)

It seemed, therefore, that the technique of Conway et al (36), modified in as much as the influence coefficinets would be computed using a finite element solution, could be used to solve the contact stress problem of the type found in the fretting fatigue specimens. Influence coefficients, computed using finite elements, are clearly not exact and this must affect the final answers correspondingly. Where possible, Conway et al have compared their solutions with existing, exact solutions to similar problems in order to assess the accuracy of their technique.

In the case of an axially loaded, rigid, cylindrical indenter compressing a half space with frictionless contact the Boussinesq solution of the pressure distribution is well known. Conway and Farnham reproduce the Boussinesq pressure distribution with apparently negligible error. In (39) and again in (40) Zienkiewicz and Cheung attempt assessments of the accuracy of the finite element technique by comparing their solutions with available, exact, solutions. From the examples quoted, it appears that with careful choice of element size very close approximation can be obtained. It did not seem that the use of finite element methods to compute the influence coefficients would seriously affect the accuracy of the final answers.

5.4 THE FINITE ELEMENT METHOD

A very good description of the finite element method is given by Zienkiewicz (40) and only a brief outline of the method will be given here. (40) will be quoted extensively. The method is based upon the proposition that a continuum can, if certain assumptions are made, be analysed as though it were an assembly of finite elements using well known techniques of structural analysis. The main steps are as follows:-

(a) The continuum is separated by imaginary lines into a number of finite elements.

(b) The elements are assumed to be interconnected at a number of discrete nodal points situated on their boundaries. The displacements of these nodal points are the basic unknown parameters of the problem.

(c) A function is chosen to define uniquely the state of displacement within each 'finite element' in terms of its nodal displacements.

(d) The choice of the displacement functions defines uniquely the state of strain within an element in terms of the nodal displacements. These strains, together with any initial strains and the elastic properties of the material, will define the state of stress throughout the element and, hence, also on the boundaries.

(e) A system of forces concentrated at the nodes and equilibrating the boundary stresses and any distributed loads is determined, resulting in a stiffness relationship of the form:

$$\{F\}^a = [k]^a \{\delta\}^a + \{F\}^a_p + \{F\}^a_o$$

where $\{F\}^a$ is the column matrix of the nodal forces, $\{F\}^a_p$ represents the nodal forces required to balance any distributed load acting on the element and $\{F\}^a_o$ the nodal forces required to balance any initial strains. ('a' takes values 1 to n where n is the number of elements.)

The matrix $[k]^a$ is known as the element stiffness matrix. This system of equations is of the form found in structural analysis problems ([illegible]). By considering the equilibrium of each node under the action of the nodal forces contributed by the elements meeting at that node and any external nodal forces, a system of equations is established with the nodal displacements as unknowns. When these have been solved the determination of the stresses is easily carried out.

The stiffness matrix $[k]^a$ is a function of the element shape and its elastic properties and an expression for it in terms of these may be determined by equating the external and internal work done by the various forces and stresses during the application of an arbitrary nodal displacement.

Clearly a series of approximations has been introduced. Depending on the choice of displacement functions, continuity of displacement between adjacent elements may or may not be achieved. Thus the compatibility condition on the lines between elements may not be satisfied. Secondly, since the forces are concentrated at the nodes, equilibrium conditions are satisfied in an overall sense only and will usually be violated within each element and on its boundaries.

Thus the choice of element size and shape and of displacement functions will affect the accuracy of the solution and it is in this respect that care must be taken when using the method.

5.5 THE FINITE ELEMENT METHOD APPLIED TO PLANE STRESS OR PLANE STRAIN

In the case of plane problems it is convenient to divide the continuum into triangular elements. A typical element is shown in fig. 5.3.

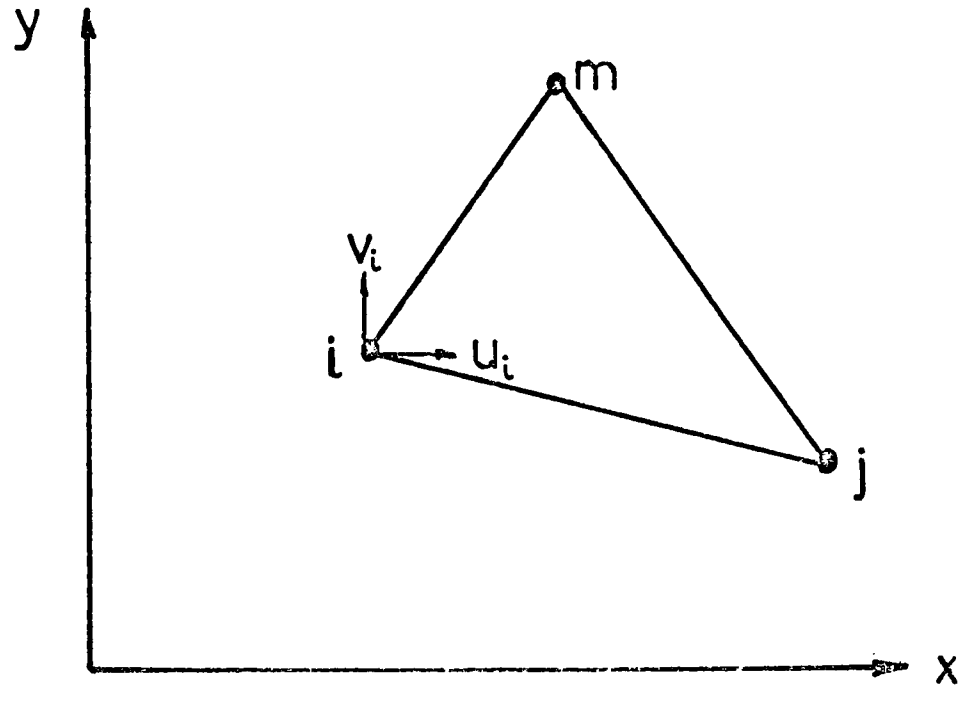


Fig. 5.3 An element of a continuum in plane stress or plane strain

The displacement of a node has two components

$$\{\delta_i\} = \begin{Bmatrix} u_i \\ v_i \end{Bmatrix}$$

and there are six components of element displacement

$$\{\delta\}^e = \begin{Bmatrix} \delta_i \\ \delta_j \\ \delta_m \end{Bmatrix}$$

It is necessary now to define the displacements within the element in terms of these six nodal displacements and this can be done most simply by two linear polynomials

$$u = \alpha_1 + \alpha_2 x + \alpha_3 y$$

$$v = \alpha_4 + \alpha_5 x + \alpha_6 y$$

where α_1 etc can be evaluated in terms of the u_i, v_i and the corresponding co-ordinates $x_i y_i$ from the six equations of the form

$$u_i = \alpha_1 + \alpha_2 x_i + \alpha_3 y_i$$

It is clear that, with the chosen linear displacement

functions, continuity of displacements between adjacent triangles is guaranteed since the displacements in two adjacent triangles are equal at the nodes and will vary linearly along the interface. Having selected the displacement function, the solution then proceeds along the lines outlined above to produce the desired nodal displacements. The element stresses are computed using the relationship

$$\{\sigma\} = [S]\ \{\delta\}$$

where $\{\sigma\}$ represents the column matrix of stresses, $[S]$ is defined as the overall stress matrix and $\{\delta\}$ is the column matrix of displacements. Like the stiffness matrix, the stress matrix is assembled from the individual element stress matrices, the elements of which are simple functions of element shape and elastic properties.

Since the chosen displacement functions are linear, it follows that the strains and hence stresses are constant within the element. The convention adopted is to assign these stress values to the centroid of the element. This arbitrary choice may, in regions of high stress gradients, be a small source of error and may lead to an oscillation of stress values about the true solution. Zienkiewicz notes this and mentions that an improvement is often obtained by averaging the stress values from two adjacent elements. The averaged value of stress is allocated to the centroid of the quadrilateral formed by the two triangles.

5.6 SOLUTION OF FINITE ELEMENT PROBLEMS AND EVALUATION OF METHOD

In plane stress or strain, there are two unknown displacements for each node. Thus, most problems involve the solution of a large number of simultaneous equations. This is only practicable if done by computer.

The "Centre for Numerical Methods in Engineering" at the University of Wales, Swansea, kindly supplied the author with their program, devised by Y.K. Cheung, for the solution of problems in plane stress or plane strain using Finite Elements (42). This program was modified to run on the University of Oxford KDF9 computer and the modified version is listed and described briefly in Appendix 1. The program as received solved problems in which any node could have prescribed, in-plane loading or displacement. The output gave solutions for the nodal displacements and for stresses σ_x, σ_u, σ_{xy} as well as the principal stresses and directions at each element centroid. In this form, the program was directly applicable to the problem of the solid fatigue specimens and also to the calculation of the influence coefficients required in the solution of the assembly problem.

In order to gain experience of using finite element techniques and to assess the order of accuracy which could be obtained, the method was first applied to two problems, having known solutions. The first of these was a bar of uniform rectangular cross section in simple tension. Since, for this problem, the stress is uniform throughout the bar, the solutions should be exact whatever the mesh size. This was found to be so.

The second problem was that of a flat plate with a central hole under a tensile load applied parallel to the x axis (fig. 5.4). The hole diameter to plate width ratio (2a/w) was 6:1 and the solution was compared with the exact solution for a hole in an infinite plate in tension which, according to Timoshenko and Goodier (43), should be within 6% of the exact solution for (2a/w) = 6. Two mesh sizes were used, figs. 5.5, 5.6. Since the system is

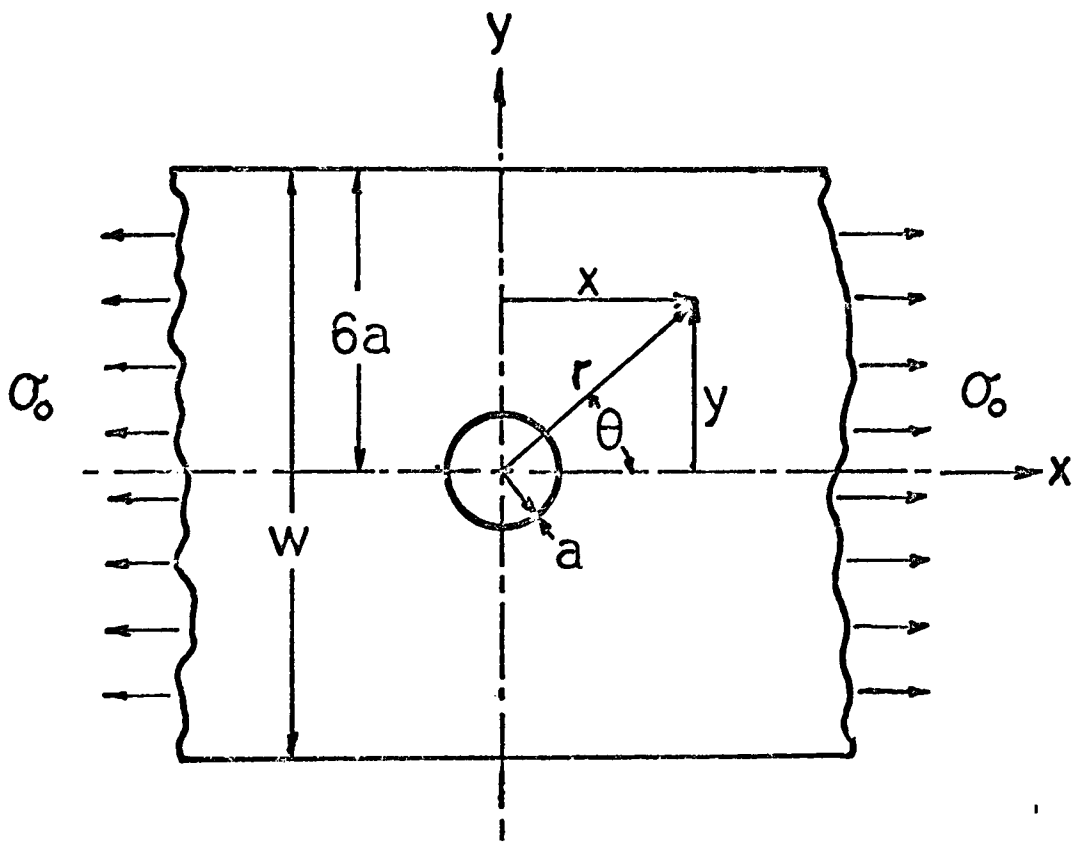


Fig. 5.4 Plate with central hole

symmetric about both x and y axes, only one quarter of the whole need be considered. At the nodes on these axes the displacements perpendicular to the axis and the shear stress parallel to the axis are prescribed to be zero.

Taking advantage of the symmetric properties in this way, considerably reduces the input data and computing time but has the one disadvantage that values of stress on the axes of symmetry will not be given and, if required, must

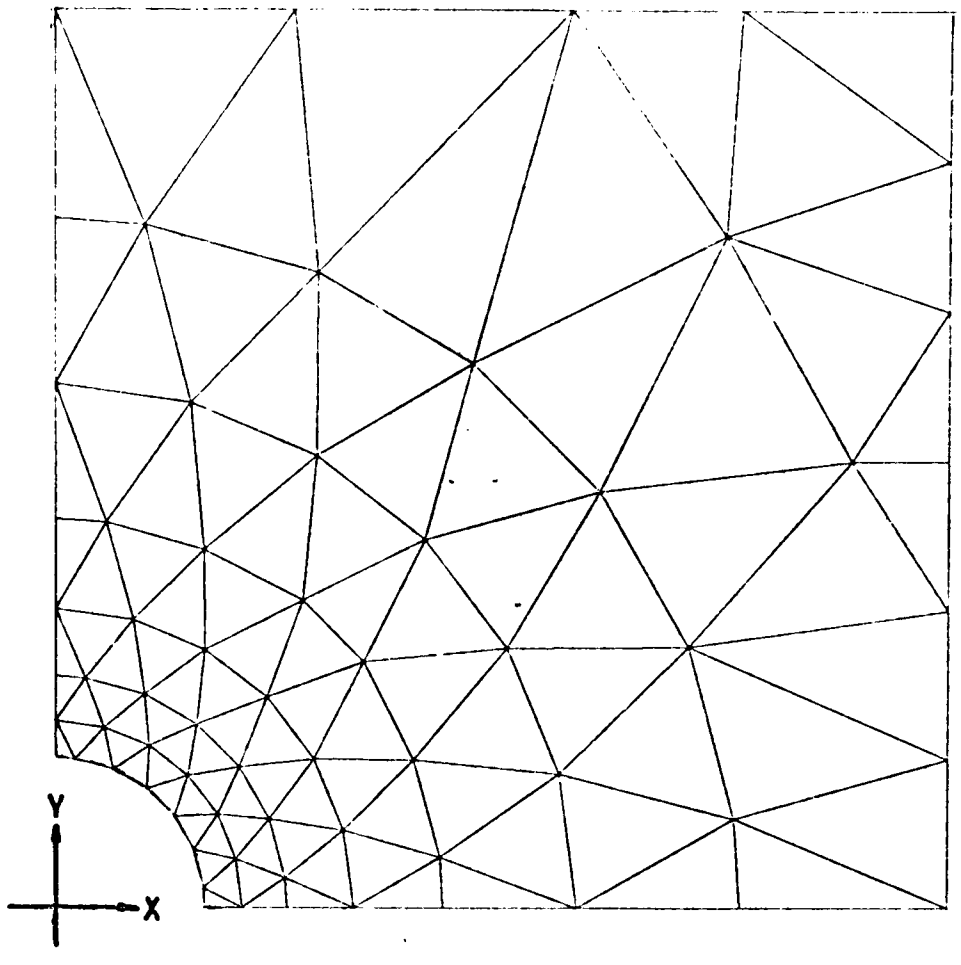


Fig. 5.5 Coarse mesh for plate/hole problem (66 nodes)

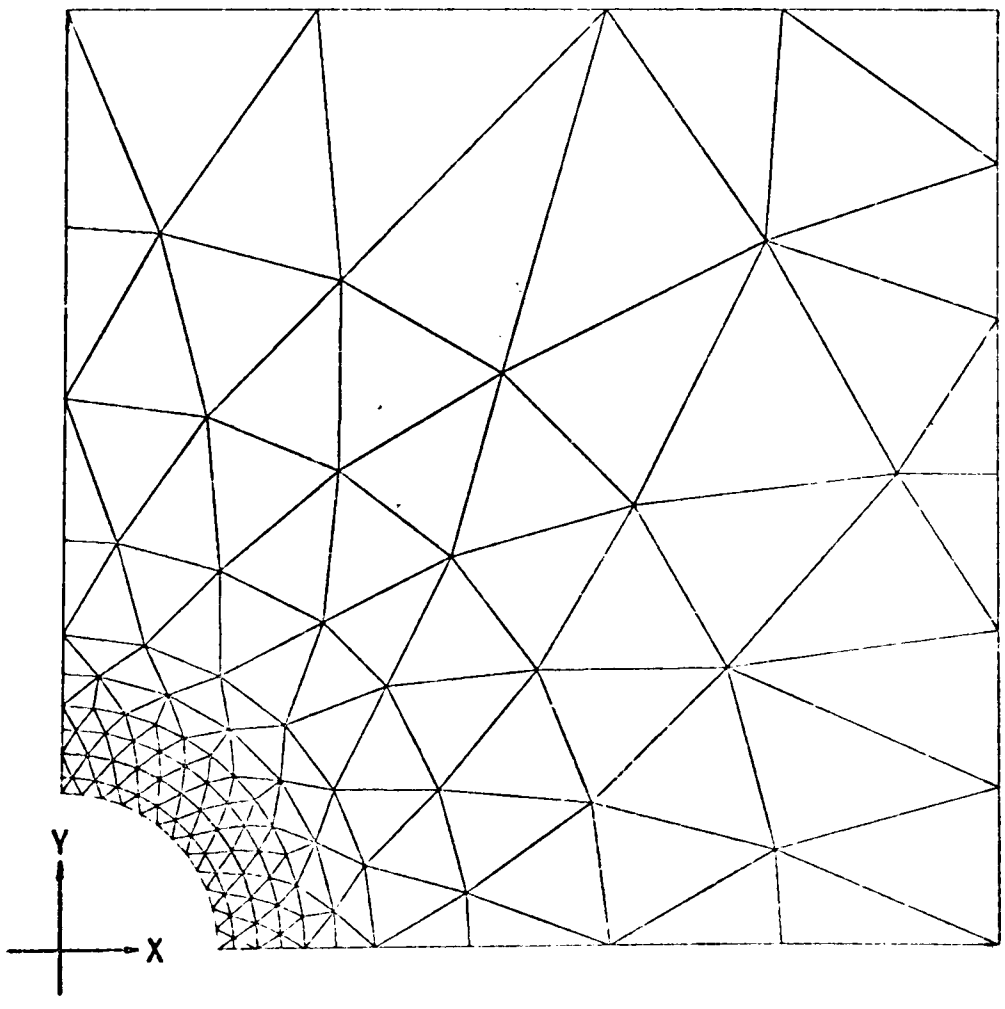


Fig. 5.6 Fine mesh for plate/hole problem (113 nodes)

be extrapolated from the values at the centroids of immediately adjacent elements.

Some results are plotted in figs. 5.7, 5.8. Radial (σ_r) and hoop (σ_θ) stresses are non-dimensionalised with respect to the average tensile stress in the plate away from the hole (σ_o) and plotted against θ for several values of r. Graphs of the theoretical solutions for an infinite plate are shown as a continuous curve with point values from the finite element solutions superimposed. The results for the finer mesh are clearly better than those for the coarse, however in both cases oscillation about the true values is noted as r increases. For the lowest value of r the values of stress from the finite element solution are higher than predicted analytically; for the next lowest value of r the finite element solutions are lower than the analytic solutions; and so on. As mentioned at the end of Section 5.5, Zienkiewicz has observed this phenomenon in regions of high stress gradients and improved the results by averaging the values given by adjacent elements. The averaging technique was applied to the fine mesh solutions and produced a considerable improvement in the accuracy of the results, fig. 5.9.

The indications from this preliminary investigation were that, with careful choice of mesh size and use of the averaging device, good approximations to exact solutions can be obtained using finite elements. The accuracy will clearly depend upon many factors and will vary from problem to problem but to assume a maximum error of 10% would not appear to be unrealistic.

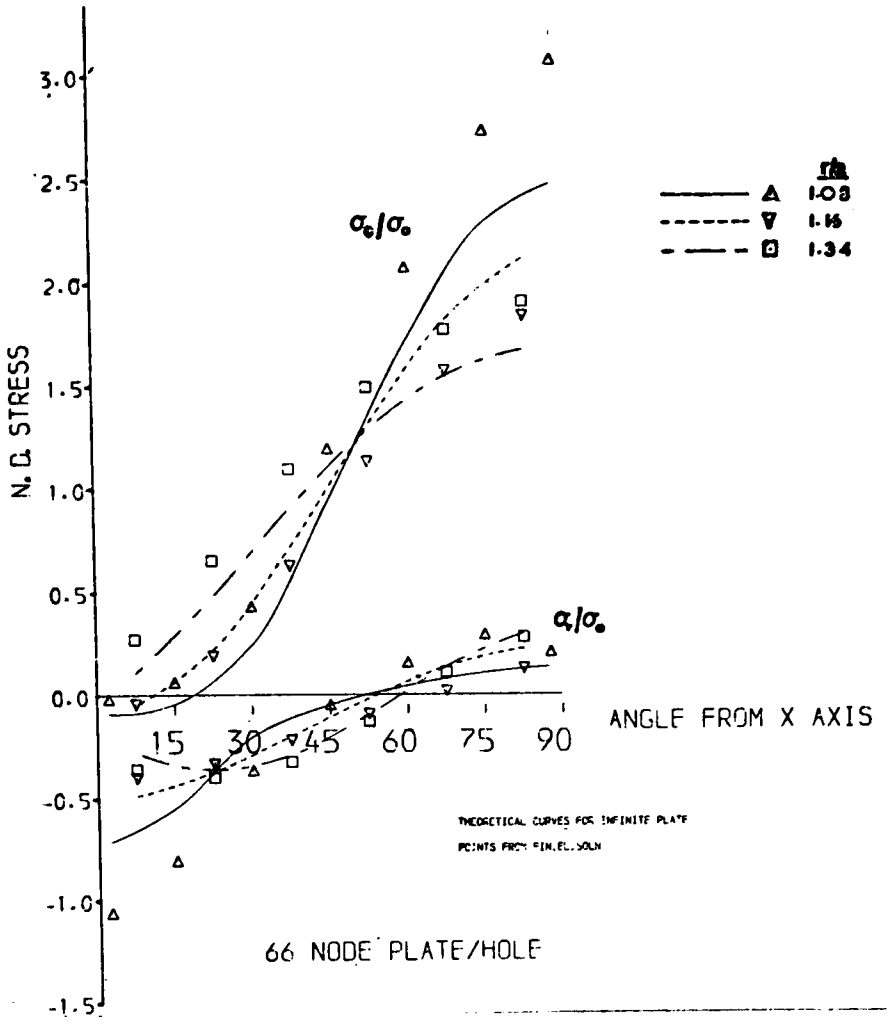

N. D. STRESS
3.0
2.5
2.0
1.5
1.0
0.5
0.0
-0.5
-1.0
-1.5
$\sigma_\theta/\sigma_\infty$
α/σ_∞
r/a
1.03
1.15
1.34
15
30
45
60
75
90
ANGLE FROM X AXIS
THEORETICAL CURVES FOR INFINITE PLATE
POINTS FROM FIN.EL.SOLN
66 NODE PLATE/HOLE

Fig. 5.7

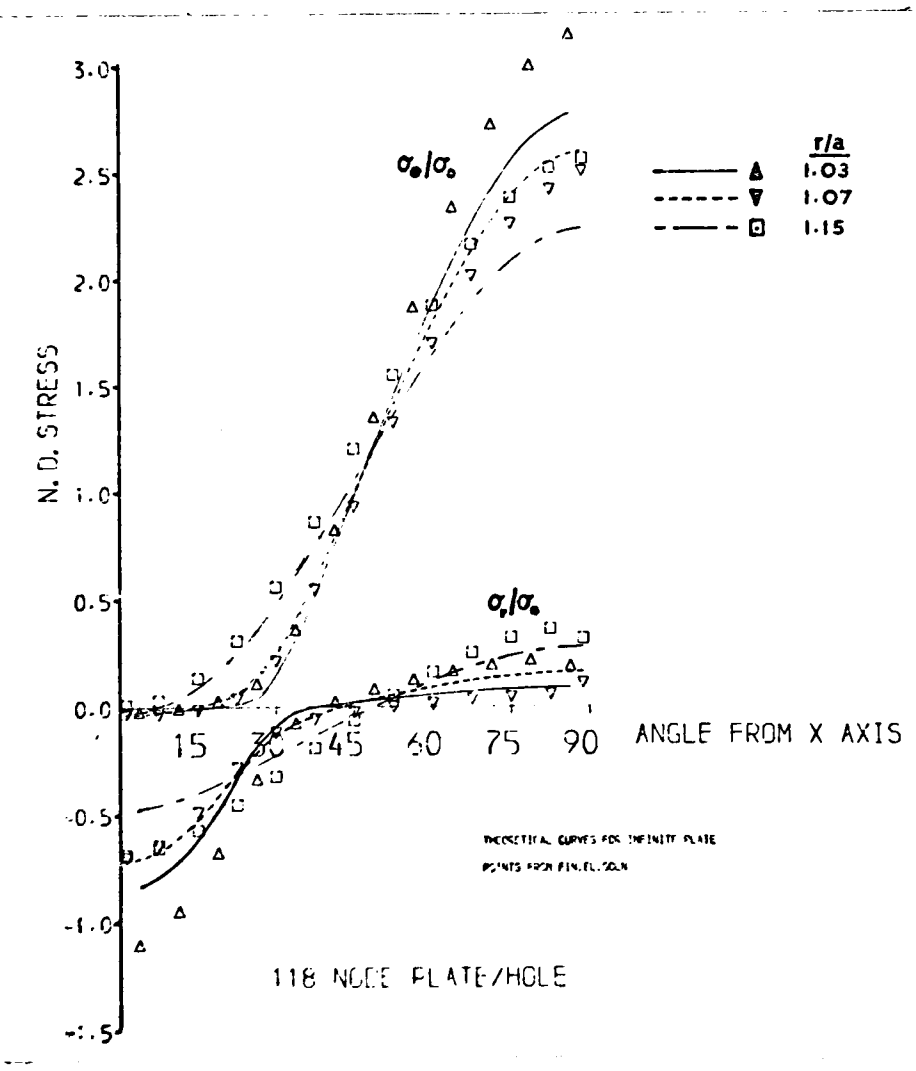

N. D. STRESS
3.0
2.5
2.0
1.5
1.0
0.5
0.0
-0.5
-1.0
-1.5
$\sigma_\theta/\sigma_\infty$
σ_r/σ_∞
r/a
1.03
1.07
1.15
15
45
60
75
90
ANGLE FROM X AXIS
118 NODE PLATE/HOLE

Fig. 5.8

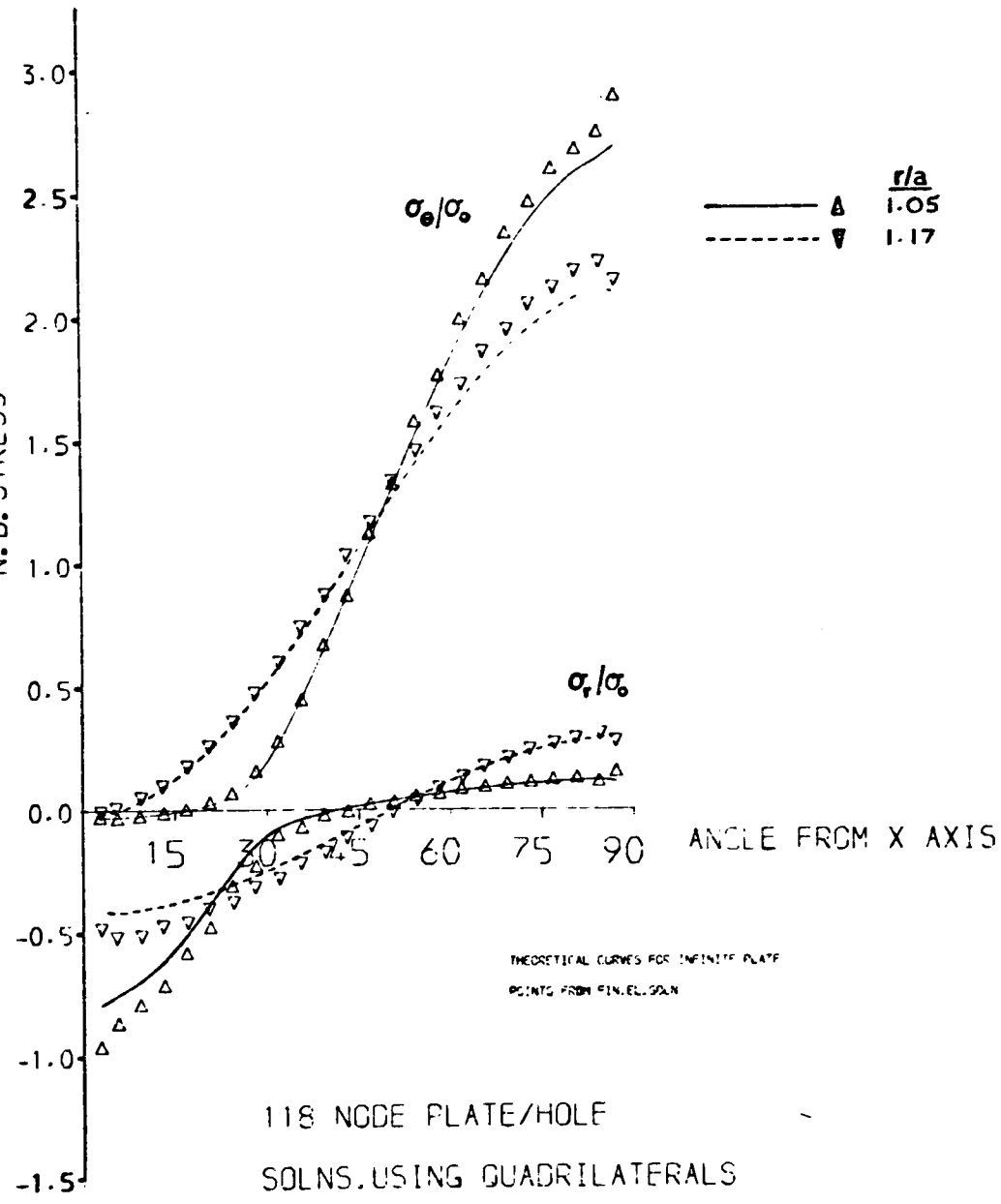

3.0
2.5
2.0
1.5
1.0
0.5
0.0
-0.5
-1.0
-1.5
N.D. STRESS
$\sigma_\theta/\sigma_\infty$
σ_r/σ_∞
r/a
1.05
1.17
15
30
45
60
75
90
ANGLE FROM X AXIS
THEORETICAL CURVES FOR INFINITE PLATE
POINTS FROM FIN.EL.SOLN
118 NODE PLATE/HOLE
SOLNS.USING QUADRILATERALS

Fig. 5.9

CHAPTER 6

DETAILS OF THE METHOD OUTLINED IN CHAPTER 5

6.1 INTRODUCTION

In the previous chapter a method was outlined for solving the problem of a block indenting a plate which is subsequently loaded axially. The method, is applied, to the specific problem of the fatigue specimens used in this investigation.

Because of symmetry, only one quarter of the whole problem need be examined, and, using the case of the sharp cornered assembly as an illustration, the area of interest is shown shaded (fig. 6.1).

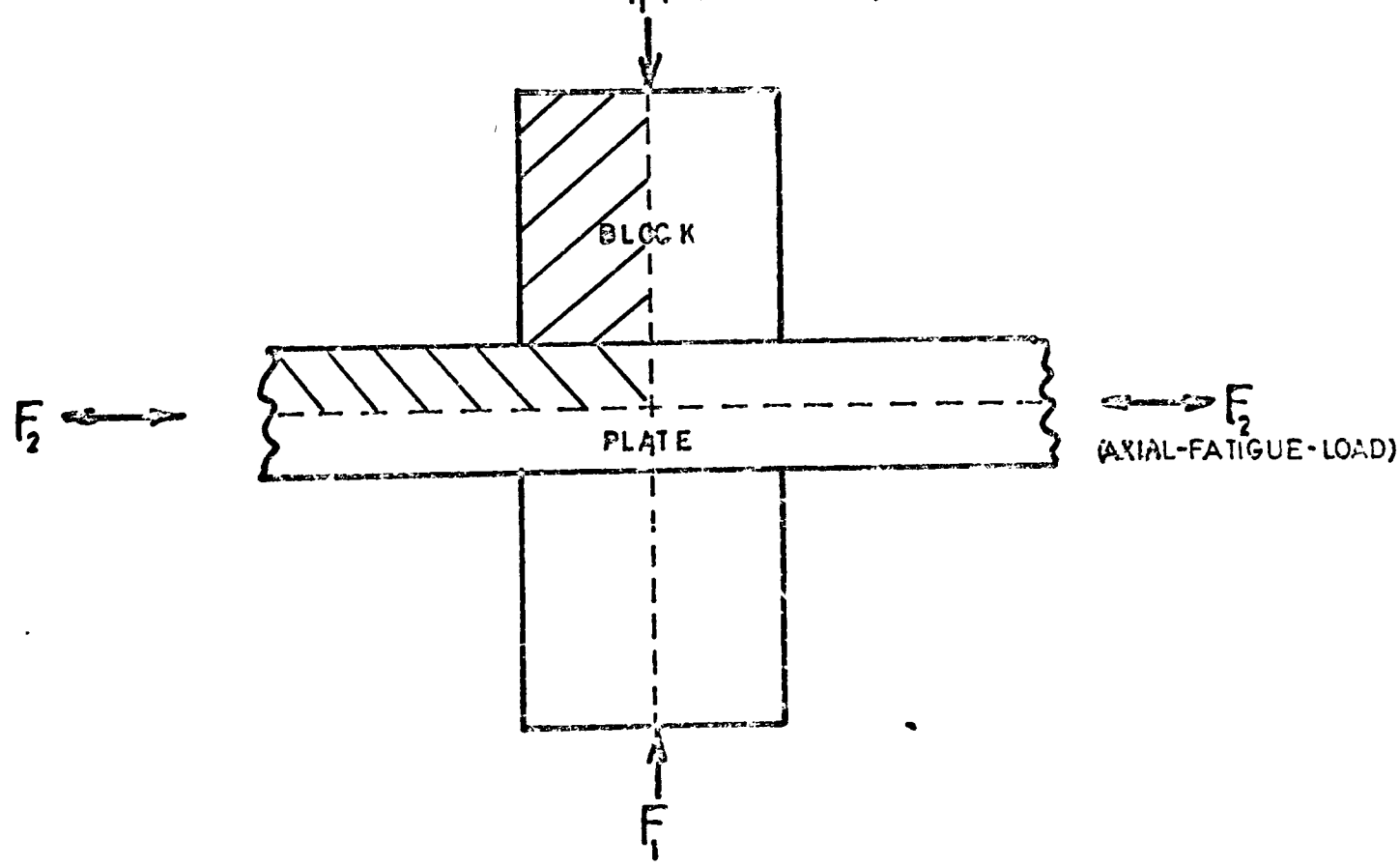


Fig. 6.1 Sharp cornered assembly

The component parts of the assembly will be referred to as the plate and the blocks.

The plate and block are divided into separate meshes such that the (n) nodes along the interface in the plate are coincident with those in the block when the system is unloaded (fig. 6.2). The continuous distribution of pressure and shear stress on the interface is replaced by discrete forces acting normal and parallel to the interface at each of the n nodes.

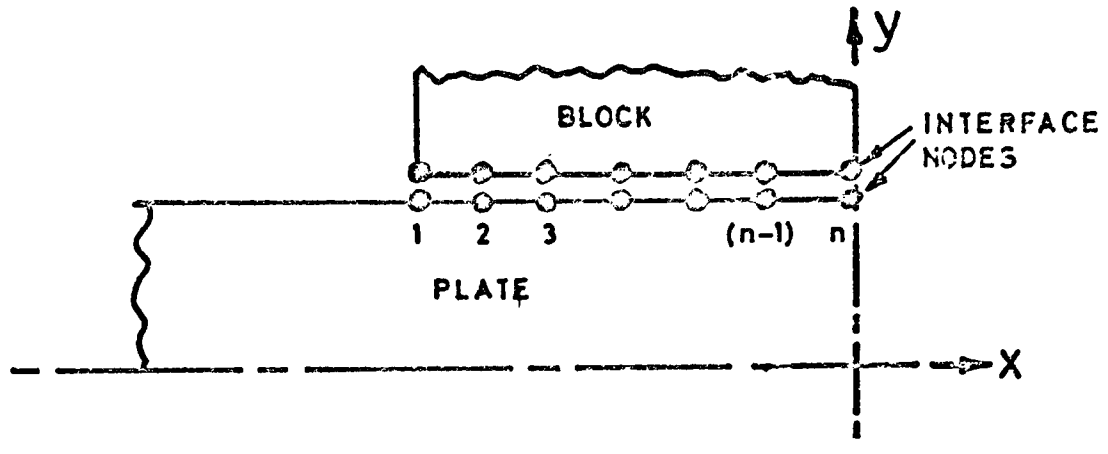


Fig. 6.2 Nodes on the interface of an assembly

The problem is solved in three distinct stages:

1. The x and y displacements at each interface node are computed, firstly, for unit shear (x) loads and then for unit normal (y) loads, applied successively at each interface node. This is done for both the block and the plate producing a set of influence coefficients for each. In the case of the plate, influence coefficients on the interface due to the axial load F_2 are also computed. The computation in this stage is carried out using the Swansea program in a slightly modified form. (See Appendix 1.)

2. Using the influence coefficients computed in stage 1 and knowing the boundary conditions on the interface (see Section 5.1), simultaneous equations are set up and solved for the unknown nodal forces on the interface.

The general form and derivation of these equations is outlined in Section 6.3 and they are solved by computer using the program described in Appendix 2.

3. The calculated interface nodal forces are now used to compute the resulting stress distribution in the plate, again making use of the Swansea program in a virtually unmodified form (Appendix 1).

It should be noted that the influence coefficients are dependent only on the elastic properties of the material and the shape of the assembly. Having been computed once they can then be used in stage 2 with any combination of boundary conditions. This means that, in solving the problem for any one assembly, stage 1 will be used once only and stages 2 and 3 as many times as there are changes of boundary conditions. It was therefore convenient to separate the stages and run them as three quite separate programs. Besides being presented in a printout of answers, the influence coefficients from stage 1, and the nodal forces from stage 2, were punched on cards in a suitable form for use as input to the next stage. (See Appendices 1 and 2.)

6.2 SOLUTION OF THE SLIP PROBLEM

6.2.1 Derivation of Displacement Equations from Influence Coefficients

The solution of the slip problem (i.e. stage 2) involves the determination of the unknown nodal forces acting on the interface nodes of the plate. The equations for these unknowns are derived as follows.

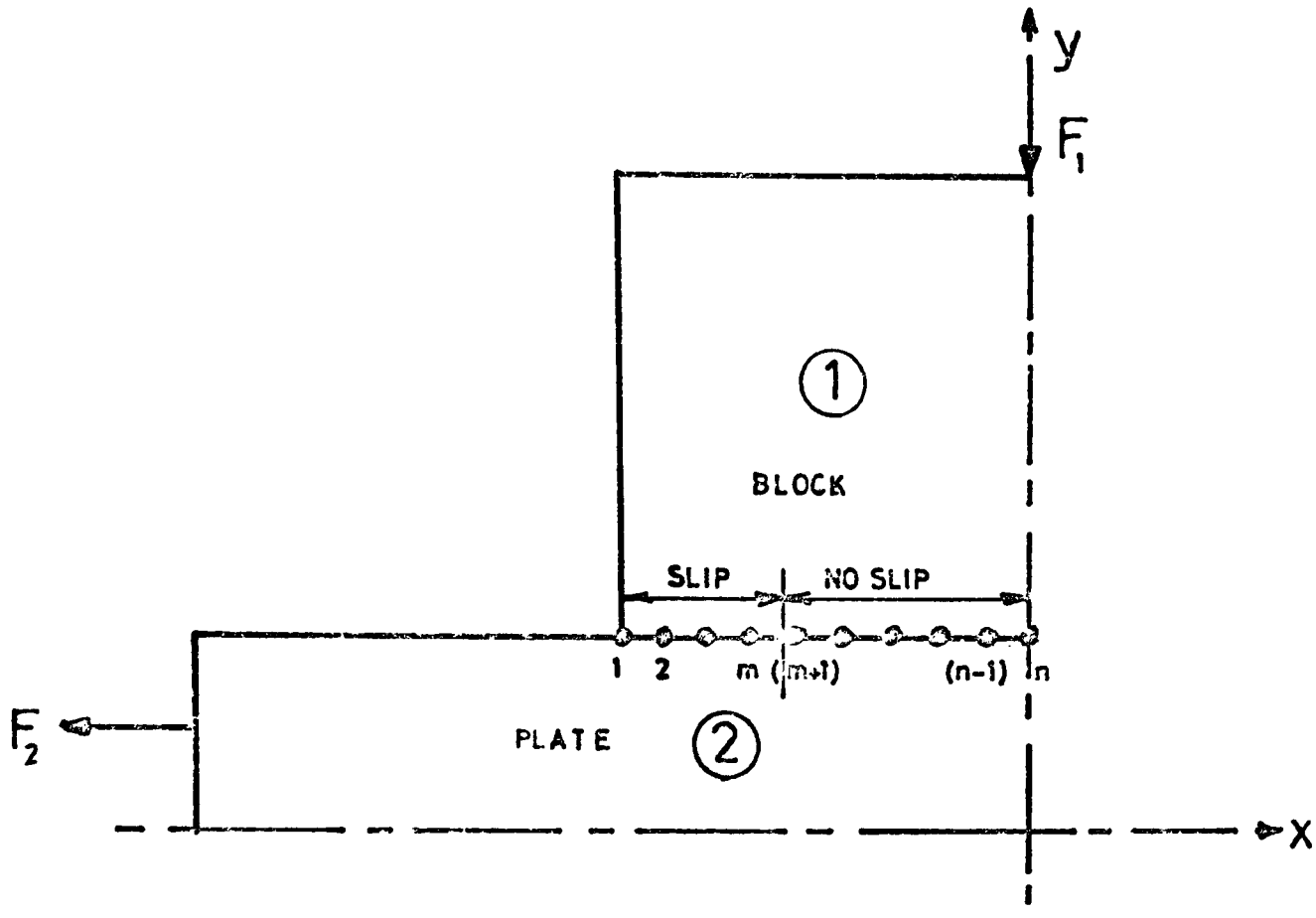


Fig. 6.3 Slip region in a sharp cornered assembly

As previously explained, it is only necessary to consider one quarter of the whole assembly as shown in fig. 6.3. The x and y axes are coincident with the axes of symmetry of the whole assembly and are respectively parallel to and normal to the interface between the block and the plate. In the following derivations, variables related to the block are followed by numeral 1 and to the plate by numeral 2.

Assume that there are n pairs of corresponding nodes on the interface as in fig. 6.2, the first pair being located at the edge of the interface and the nth pair on the y axis.

Let the first m pairs of nodes be slipping relative to each other and assume that Coulomb's Law of friction is obeyed in that region.

The normal force, F_1, is assumed to act at the point x = o on the top of the block and is positive in the y negative direction. The axial force F_2 is assumed to be evenly distributed over the half cross sectional area of the plate and is positive in the x negative direction. (i.e. F_1 and F_2 are positive when the block is pressed against the plate and the plate is in tension.)

Let the nodal forces parallel to the x axis be Q_i)
Let the nodal forces parallel to the y axis be P_i) i = 1,n

(N.B. on the plates, Q_i are positive in the direction x positive and P_i are positive in the direction y negative; the reverse is true on the block.)

Let the x displacement of the nodes in the block be $U1_i$)
Let the x displacement of the nodes in the plate be $U2_i$) i=1,n
Let the y displacement of the nodes in the block be $V1_i$)
Let the y displacement of the nodes in the plate be $V2_i$)

The displacements in the block, $U1_i$ and $V1_i$, are measured relative to the point x = 0 on the top surface of the block and displacements in the plate $U2_i$ and $V2_i$, are measured relative to (0,0).

In stage 1 of the calculation, the following sets of influence coefficients are assumed to have been calculated.

$A1_{ij}$ = the x displacement of the i^{th} node in the block due to a unit negative x force at the j^{th} node.

$B1_{ij}$ = the x displacement of the i^{th} node in the block due to a unit positive y force at the j^{th} node.

$C1_{ij}$ = the y displacement of the i^{th} node in the block due to a unit negative x force at the j^{th} node.

$D1_{ij}$ = the y displacement of the i^{th} node in the block due to a unit positive y force at the j^{th} node.

$A2_{ij}$ = the x displacement of the i^{th} node in the plate due to a unit positive x force at the j^{th} node.

$B2_{ij}$ = the x displacement of the i^{th} node in the plate due to a unit negative y force at the j^{th} node.

$C2_{ij}$ = the y displacement of the i^{th} node in the plate due to a unit positive x force at the j^{th} node.

$D2_{ij}$ = the y displacement of the i^{th} node in the plate due to a unit negative y force at the j^{th} node.

E_i = the x displacement of the i^{th} node in the plate due to a unit positive axial force F_2.

G_i = the y displacement of the i^{th} node in the plate due to a unit positive axial force F_2.

Note that the displacements are relative to axes within the block or the plate and do not include any rigid body displacements such as the block will undergo when indenting the plate.

For a general system of nodal forces the nodal displacements are determined by summing the effects of each nodal force:-

$$\left.\begin{aligned} U1_i &= \sum_{j=1}^{n} (A1_{ij}Q_j + B1_{ij}P_j);\ i = 1, n \\ V1_i &= \sum_{j=1}^{n} (C1_{ij}Q_j + D1_{ij}P_j);\ i = 1, n \\ U2_i &= \sum_{j=1}^{n} (A2_{ij}Q_j + B2_{ij}P_j) + E_iF_2\ ;\ i = 1, n \\ V2_i &= \sum_{j=1}^{n} (C2_{ij}Q_j + D2_{ij}P_j) + G_iF_2\ ;\ i = 1, n \end{aligned}\right\} \quad \ldots\ 6.1$$

6.2.2 Boundary Conditions

As a first attempt at solving the problem the following assumptions were made:-

1. The surfaces of the block and the plate experience the same y displacement relative to the x axis of the assembly. i.e. the surfaces do not separate.
2. The half interface has two regions, an outer region where relative slip between the block and the plate occurs and an inner region where there is no relative slip. In the slip region, Coulomb friction is assumed to apply and the coefficient of friction (μ) is assumed to be constant.
3. In order to differentiate between this problem and one of a solid of the same overall shape with a crack corresponding to the slip region, it is necessary to assum continuity of shear stress between the slip and no-slip regions.

These assumptions give rise to the following five boundary conditions:-

1. Referring to fig. 6.4, when the block is pressed into the plate the point B, relative to which displacements in the block are measured is displaced an amount Δ relative to the x axis of the assembly. Thus for all nodes on the interface, remembering that $V1_i$ are positive and $V2_i$ negative,

$$V1_i - V2_i = \Delta ; \quad i = 1, n \qquad 6.2$$

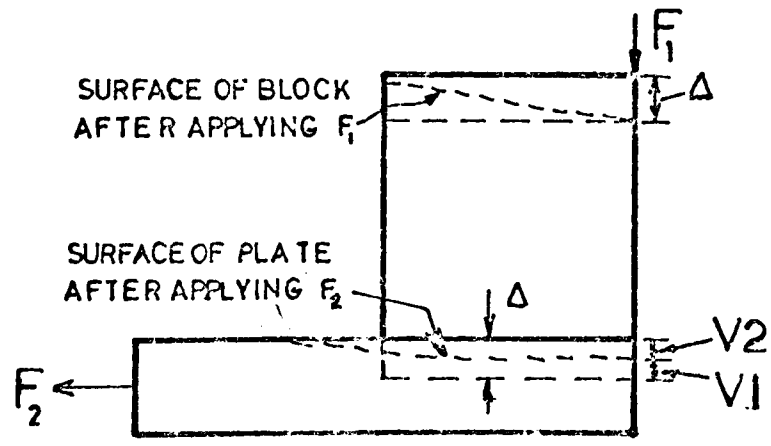


Fig. 6.4 Vertical displacements due to a block indenting a plate

2. For points in the no-slip region the displacements parallel to the interface of nodes on the surface of the block must be equal to those of corresponding nodes in the plate. Thus if m nodes have slipped:

$$U1_i = U2_i;\ i = (m + 1),\ n \qquad 6.3$$

3. For points in the slip region the shear force acting on a node is μ times the normal force acting on the node where μ is the coefficient of friction.

   Thus:

$$Qi = \mu P_i;\ i = 1,\ m \qquad 6.4$$

4. To ensure continuity of shear, the shear force at the first no slip node is assumed to be μ times the normal force. This implies that the slip region extends right up to the first node in the no-slip region. Thus:

$$Q_{(m+1)} = \mu P_{(m+1)} \qquad 6.5$$

(N.B. for the plate in compression the sign of the L.H.S. of both equations 6.4 and 6.5 will be changed.)

5. A final condition can be imposed by considering the equilibrium of the block. The only vertical forces acting on the block are F_1 and the nodal forces P_i. Thus

$$\sum_{i=1}^{n} P_i = F_1 \qquad 6.6$$

6.2.3 Solution of nodal forces

Substituting the displacement equations 6.1 into the boundary conditions (1) and (2) gives:

$$\sum_{j=1}^{n}(Cl_{ij} - C2_{ij})Q_j + \sum_{j=1}^{n}(Dl_{ij} - D2_{ij})P_j - G_iF_2 = \Delta; \quad i = 1,n \qquad 6.7$$

$$\sum_{j=1}^{n}(Al_{ij} - A2_{ij})Q_j + \sum_{j=1}^{n}(Bl_{ij} - B2_{ij})P_j - E_1F_2 = 0; \quad i = 1, n \qquad 6.8$$

It is now convenient to define the following variables:-

$$p_j = P_j/\Delta;\ q_j = Q_j/\Delta;\ f = F_2/\Delta;\ d = 1/\Delta$$

The problem is now defined by (2n + 5) variables;

$$q_j,\ p_j,\ (\text{for } j = 1,n)\ f,\ d,$$

the number of slipped nodes m, the coefficient of friction μ, and the clamping force F_1. It will not reduce the generality of the method if F_1 is put equal to unity since it is clearly the ratio between F_1 and F_2 that is important, not their absolute value. This reduces the number of variables to (2n + 4). Using equations 6.2 to 6.8 (2n + 2) equations can be set up with (2n + 4) variables.

From equation 6.7 dividing both sides of the equation by Δ, n equations are obtained of the form:-

$$\sum_{j=1}^{n}(Cl_{ij} - C2_{ij})q_j + \sum_{j=1}^{n}(Dl_{ij} - D2_{ij})p_j - G_if = 1;\ i = 1,n \qquad 6.9$$

Similarly from equation 6.4 a further m equation:-

$$q_j - \mu p_j = 0;\ i = 1, m \qquad 6.10$$

followed by (n - m) equations from equation 6.8:-

$$\sum_{j=1}^{n}(Al_{ij} - A2_{ij})q_j + \sum_{j=1}^{n}(Bl_{ij} - B2_{ij})p_j - E_if = 0; \quad i = (m + 1),n \qquad 6.11$$

From equation 6.5, one equation:-

$$q_{(m+1)} - \mu p_{(m+1)} = 0 \qquad 6.12$$

and from equation 6.6 remembering that F_1 = unity:-

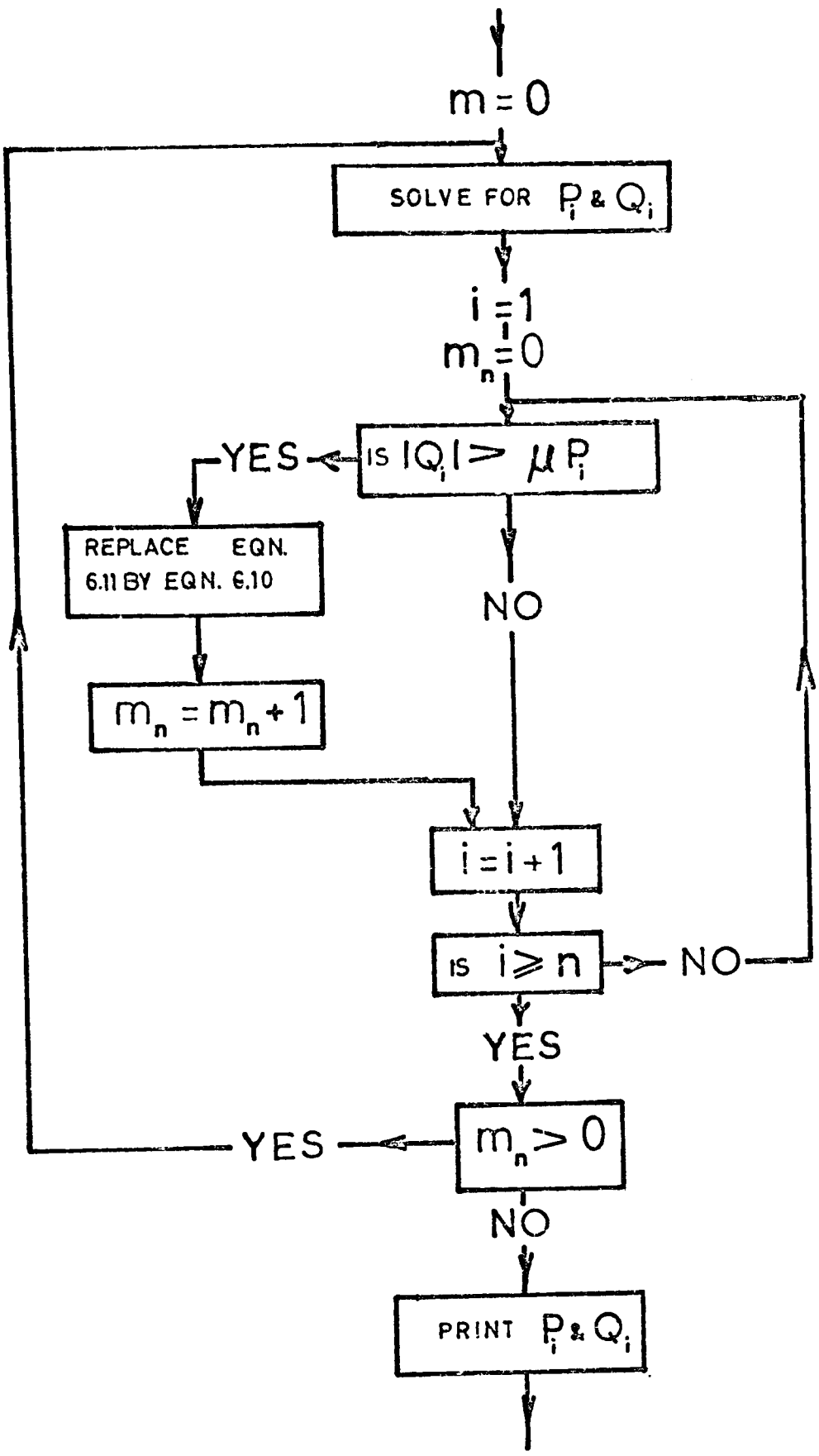
$$\sum_{j=1}^{n} p_j - d = 0 \qquad 6.13$$

Clearly, if m and μ are specified, there are (2n + 2) linear equations on (2n + 2) unknowns, p_i, q_i, f and d, which can be solved by a single matrix inversion. Such a solution is very desirable; it is economic on computing time and eliminates problems of convergence etc. implicit in iterative methods; however it has the disadvantage that m is specified and F_2 is part of the solution.

In general, the problem is to find the slip length (m) for a given load F_2. Solutions appropriate to a specific value of F_2 can only be obtained by solving for several values of m and estimating the desired P_i and Q_i by interpolation - an inelegant form of solution. An alternative form of solution involves an iterative process. F_2 and μ are specified and initially it is assumed that m is zero. This clearly makes one equation, equation 6.12, redundant and eliminates all equations 6.10. (In fact, in order to keep generality, equation 6.12 is replaced by an equation specifying F_2 i.e.

$$f - (F_2)d = 0.)$$

The iterative process is illustrated by a flow diagram in fig. 6.5. The 2n + 2 equations are solved for p_i and q_i. Each node, starting from node 1, is now examined and if $|q_i| > \mu p_i$ the appropriate equation 6.11 is replaced by equation 6.10. The new set of equations is now solved and the process is repeated until a solution is reached in which there are no nodes where $|q_i| > \mu p_i$. The resulting



(1) Equation 6.11 expresses the boundary condition for surfaces that are not slipping.

(2) Equation 6.10 expresses the boundary condition for surfaces which are slipping. i.e. $Q_i = \pm \mu P_i$ the sign depending on the sense of the slip.

Fig. 6.5 Flow diagram for basic iterative process

P_i and Q_i are the nodal forces associated with the specified F_2. In this case the exact location of the slip/no-slip boundary is not known, only that it lies somewhere between the last slipped node and the first non-slipped node. In the exact solution, where m is specified, the slip region extends up to the (m + 1) node.

As mentioned previously this type of solution can be extravagant with computing time, but trial solutions showed that convergence was quite rapid and, in most cases, required only two or three iterations for each value of F_2.

In the event both methods of solution described above were used. However, before solving real problems the manner in which the system is loaded must be considered in greater detail.

6.3 PROPORTIONAL AND INCREMENTAL LOADING

6.3.1 Introduction

Because slip occurs in the assembly, the problem is non linear. That is to say dsiplacements are not simply functions of the loads which are acting at any given time, but are functions of the load history. Strictly speaking, the equations which have been derived above apply only to the case of proportional loading. i.e. only if, starting from an unloaded state, F_1 and F_2 are applied simultaneously, increasing in magnitude from zero to their maximum values proportionally. Clearly in the fatigue tests this is not

the case, the constant load F_1 being applied before the alternating load F_2. To solve the problem of proportional loading, equations must be derived which solve for the effect of an incremental change in F_2 on an already loaded system.

6.3.2 Incremental loading

When solving the equations exactly (rather than iteratively) the slip length must be specified by the (integral) number of nodes m, on which slip is occurring. The smallest increment of load that can be considered is therefore that increment which will cause the number of nodes slipping to change by 1. Assume that the problem has been solved for $m = m_1$ to give values of p_{1i}, q_{1i}, f_1 and d_1 and that up to this point in the load history F_2 has increased or decreased monotonically from zero. The solutions are required for $m = m_2$ where $m_2 = m_1 \pm 1$. To change m from m_1 to m_2 requires an incremental change of in f and will result in changes δp_i, δq_i δd in p_i, q_i, and d respectively. Clearly, by specifying the new value of m, the problem can be solved for proportional loading using equations 6.9 - 6.13 with $m = m_2$ to produce new values, p_{2i}, et.

If the change in F_2, i.e. f, required to change m by 1 is such that it represents a further monotonic change and hence increases the slip region, (i.e. $m_2 = m_1 + 1$), the incremental loading equations are as follows:

$$\sum_{j=1}^{n} (C1_{ij} - C2_{ij})(q_{1j} + \delta q_j) + \sum_{j=1}^{n} (D1_{ij} - D2_{ij})(p_{1j} + \delta p_j) -$$

$$G_i(f_1 + \delta f) = 1; \quad i = 1,n \qquad 6.9A$$

$$(q_{1j} + \delta q_j) - \mu(p_{1j} + \delta p_j) = 0;\ i = 1,\ m_2 \qquad 6.10A$$

$$\sum_{j=1}^{n} (A1_{ij} - A2_{ij})(q_{ij} + \delta q_j) + \sum_{j=1}^{n} (B1_{ij} - B2_{ij})(p_{1j} + \delta p_j)$$

$$- E_i(f_1 + \delta f) = 0;\ i = (m_2 + 1),\ n \qquad 6.11A$$

$$q_{1(m+1)} + \delta q_{(m+1)} - \mu(p_{1(m+1)} + \delta p_{(m+1)}) = 0 \qquad 6.12A$$

$$\sum_{j=1}^{n} (p_{1j} + \delta p_j) - (d_1 + \delta d) = 0 \qquad 6.13A$$

If now p_{2j}, q_{2j} etc. are substituted for $(p_{1j} + \delta p_j)$, $(q_{1j} + \delta q_j)$ etc. it is clear that the equations are identical to those for proportional loading and hence p_{2j} etc. will be the same for both proportional and incremental loading.

However, if the change in F_2 had not been monotonic and had, therefore, not resulted in an increase in m, the above incremental equations would not apply. For, if after slip has spread over m nodes, the load is reduced, the slip length does not decrease from m to m - 1 to m - 2 etc. (i.e. as the reverse of the loading process), rather, the nodes which were slipping when the axial load was at its maximum, become 'stuck' in their slipped positions and slip in the reverse direction starts at the outside edge of the interface.

Thus, a change of -1 in m has no physical meaning and a new variable, m_r, equal to the number of nodes experiencing reversed slip must be considered. If the slip amplitude at node i when $m = m_1$ is defined as S_i three new boundary

conditions can be set up which will apply when a change in axial load is such that it will reverse the direction of slip.

In the region of reversed slip

$$Q_j = -\mu P_j; \qquad j = 1, m_r$$

which becomes $q_j + \mu p_j = 0; j = 1, m_r$ 6.14

N.B. the change of sign of the R.H.S. This is assuming that the original slip was due to a tensile load. If the original loading is compressive the signs of equation 6.10 and 6.14 will be reversed.

At the end of the reversed slip boundary there will be a condition analagous to equation 6.12.

$$q_{(m_r + 1)} + \mu p_{(m_r + 1)} = 0 \qquad 6.15$$

Again the sign of this equation and equation 6.12 are dependent on the sign of F_2.

In the region between the end of the reversed slip region and the slip/no-slip boundary which existed when F_2 was a maximum, the surfaces remain slipped by the amount that they were slipped at the instant of maximum $|F_2|$

$$\text{i.e. } U1_i - U2_i = S_i; \; i = m_r, m$$

which becomes:-

$$\sum_{j=1}^{n} (A1_{ij} - A2_{ij})q_j + \sum_{j=1}^{n} (B1_{ij} - B2_{ij})p_j - E_i f = S_i; \quad i = m_r, m \qquad 6.16$$

It is clear now that proportional loading equations can only be applied to problems which are really incremental if the increment of load being considered is such that it does not cause, or tend to cause, a reversal of the

direction of slip.

Applying this argument to the problem of the plate and block, in which the clamping load is applied first, the following observations can be made. If the application of the clamp load alone does not result in the interfaces slipping, the proportional loading equations can be used to compute the effect of subsequent monotonic axial loading in either compression or tension. However, if slip were to occur due to the clamp load, the proportional loading equations could only be used for monotonic compressive axial loading (which would increase the slip already caused by the clamp load) and would give false answers for tensile loading.

In the cases considered in this work it was found that, with the clamp load only, there was no slip on the interface. The proportional loading equations were, therefore, used to compute the effect of loading the assembly, once, to peak values of tensile and compressive axial stress. Such loading is equivalent to the first $\frac{1}{4}$ cycle of a fatigue test only and may not be indicative of peak stress values reached after the completion of several load cycles. To investigate the effect of complete load cycles, it was necessary to use the non proportional loading equations 6.14-6.16 together with equations of type 6.9, 6.11 and 6.13 which apply for both types of loading.

6.3.3 The effect of load cycles

Using the proportional solution for S_i due to a peak value of F_2 (if the iterative solution was used) or a peak value of m (if the direct solution was used), solutions can be obtained for the subsequent unloading process

corresponding either to load increments or progressive increase in m_r depending on whether the iterative or direct solution is used.

From this point it is a simple step to solve the problem at any point around a complete load cycle. It was found that the change in load to change m or m_r by 1 was often large so that solutions could only be obtained at a few points on the load cycle. This, together with the convenience of obtaining solutions for specific loads associated with the iterative method, made that the best form of solution. Also, for convenience, the incremental equations were used for the whole load cycle. To illustrate the technique, imagine that the problem has been solved for $F_2 = F_{2(k-1)}$. If the definition of Si is now changed slightly to be the relative displacements of pairs of nodes coincident in the unloaded state. $S_{(k-1)i}$, $i = 1,n$ will define the nodal slip amplitudes (whether actually slipping, slipped due to previous loading, or unslipped) for $F_2 = F_{2(k-1)}$. If now it is assumed that no further slip occurs when F_2 is changed to $F_{2(k)}$, the following equations can be written.

The equation of type 6.9:-

$$\sum_{j=1}^{n} (C1_{ij} - C2_{ij})q_{kj} + \sum_{j=1}^{n} (D1_{ij} - D2_{ij})p_{kj} - G_i f_k = 1; \; i = 1,n \qquad 6.17$$

Combining equations 6.11 and 6.16:

$$\sum_{j=1}^{n} (A1_{ij} - A2_{ij})q_{kj} + \sum_{j=1}^{n} (B1_{ij} - B2_{ij}) - E_i f_k = S_{(k-1)i} \qquad 6.18$$

The equation of type 6.13:

$$\sum_{j=1}^{n} p_{kj} - \delta_k = 0 \qquad 6.19$$

The solutions at each node are now examined to check whether

$$|q_{kj}| > \mu p_{pj}$$

For values of j for which this is so, the equation of type 6.18 is replaced by:-

$$q_{kj} \pm \mu p_k = 0 \qquad 6.20$$

the sign being dependent on the sign of p_{kj} from the first set of solutions.

The new set of equations are solved again and the iterative process continued until the solutions satisfy the boundary conditions. Amongst the solutions will be a set of S_{ki} which is carried forward to be used to solve the problem when $F_2 = F_{2(k+1)}$ and so on. For the actual cases solved, the process started with $S_{oi} = 0.0$ i = 1,n, a specified value of F_1, and the problem solved for $F_2 = 0.0$. Solutions were obtained for various loads during 1¼ cycles of axial load during which F_2 went from zero up to a maximum of F , down to - F and back up to F . At this point (i.e. after 1¼ cycles) the solutions were found to be identical to those after ¼ cycle and the shakedown process was assumed to be complete.

6.4 MODIFICATIONS TO THE METHOD AFTER SOLVING SOME TRIAL PROBLEMS

6.4.1 Separation of surfaces

After solving some initial problems for the sharp cornered case it was found that under certain combinations

of F_2 and μ negative values of P_i were found on nodes near the edge of the interface. This, literally interpreted, means that the pressure there is negative and since the adhesive forces between the surfaces are assumed negligible it must mean that the surfaces there will separate.

It was therefore necessary to modify the boundary conditions to include this phenomenon. A new variable is introduced, n_s, being the number of nodes separated. Two new boundary conditions are also necessary since, where separation has taken place, both nodal forces, Q_i and P_i, must be zero. Thus:-

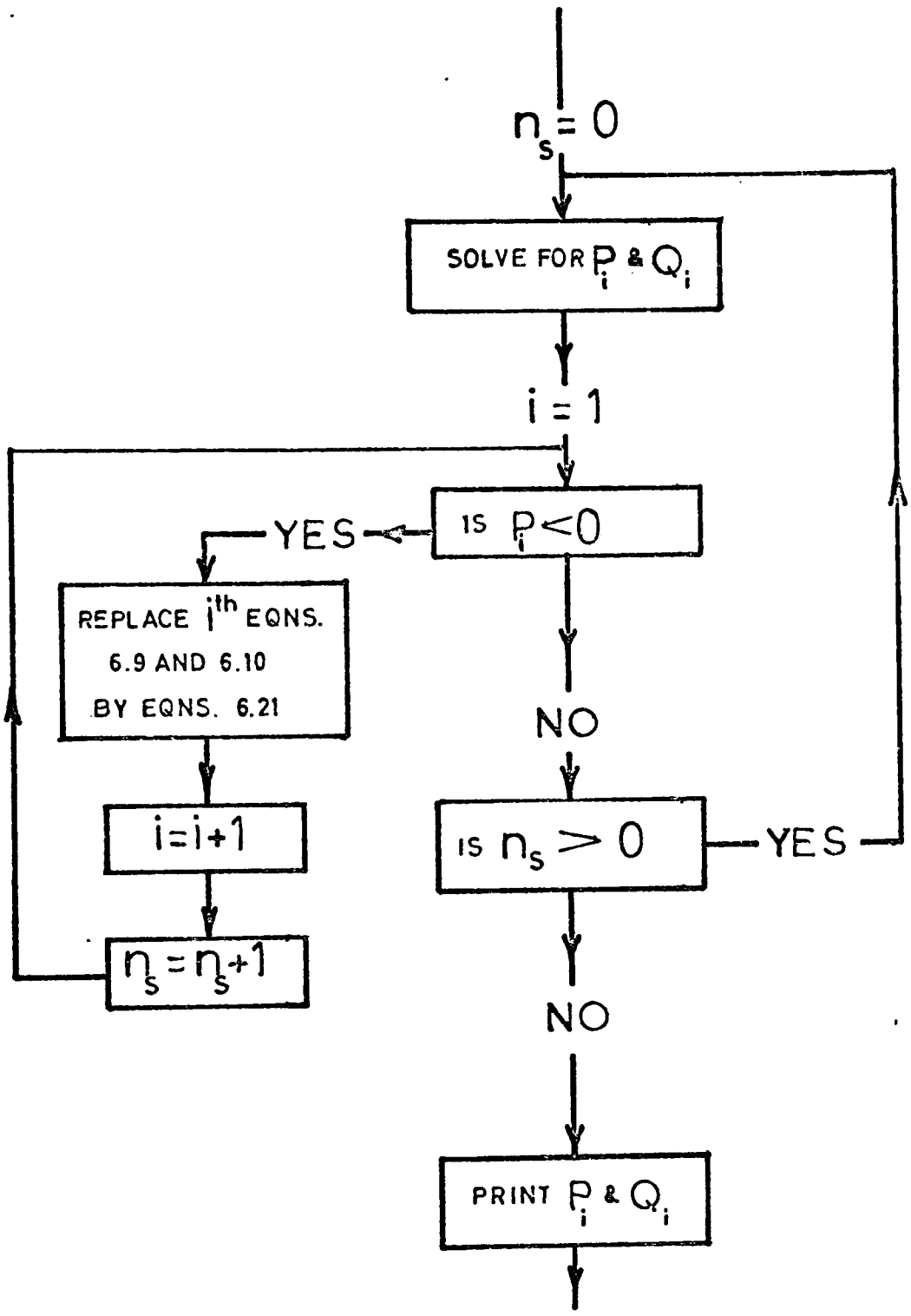
$$\left.\begin{matrix} P_i = 0 \\ Q_i = 0 \end{matrix}\right) \; i = 1, n_s \qquad 6.21$$

(This assumes that separation occurs from the edge of the interface (node 1) inwards. In all cases investigated this was the case.) These two equations replace the relevant equations 6.9 and 6.10.

Since the relationship between the lengths over which separation, slip and noslip occur cannot be predicted, the problem must be treated iteratively.

The process is outlined on a flow diagram in fig. 6.6

Initially it is assumed that separation does not occur and at nodes where P_i is found to be negative the equations 6.21 are substituted for equations 6.9 and 6.10. The modified set of equations are then solved for new values of P_i etc. This is repeated until all the $P_i \geq 0$. Although this part of the problem must be treated iteratively, it can be used with either the direct or iterative solution of the whole problem.



(1) Equation 6.9 and 6.10 express the boundary conditions that the y displacements of nodes in the block and the plate which were originally coincident are equal and that the magnitude of the nodal shear force is equal to μ times the nodal normal force in the slip region.

(2) Equation 6.21 express the boundary condition that the surfaces have separated. i.e. $P_i = Q_i = 0$.

Fig. 6.6 Flow diagram for iterative process used for solving problem when separation occurs.

6.4.2 Slip starting at points other than at the edge of the interface

In the case of the fully radiused specimens, described in Chapter 3, it was found, when solving by the direct method, that for short slip lengths some points in the assumed no-slip region had values of $|qi| \geq |\mu p_i|$. This suggested that the slip did not start at the edge of the interface. Such a situation does not present any problems if an iterative solution is used since the problem is first solved assuming no slip anywhere.

The boundary conditions are changed appropriately wherever $|qi| > |\mu p_i|$ and the problem re-solved. Thus, the full radius problems were always solved iteratively.

6.4.3 Secondary slip

When examining the problem of a sharp cornered assembly going through a complete load cycle it was found that, during the initial period of the second quarter cycle, as the load F_2 began to fall, the region of forward slip extended further along the interface. This was indicated by values of $Q_i > \mu P_i$ for $i > m + 1$ during this part of the cycle. As with separation, continuation of forward slip cannot be predicted and therefore has to be dealt with iteratively. Thus, if an initial solution gives $Q_i > \mu P_i$ for $i > m + 1$, the boundary condition at these points is changed from one equating horizontal displacement on opposite sides of the interface (equ.6.3) to one relating the nodal shear and normal forces (equ.6.4) and the problem is solved again. To aid the following discussion, slip of this nature occurring away from the outer edge of the interface, will

be referred to as secondary slip and the more usual and expected slip, at the outer edge of the interface, as primary slip.

6.5 THE DETERMINATION OF NODAL FORCES FOR VARIOUS LOADS DURING A COMPLETE LOAD CYCLE

With the above mentioned modifications it is possible to determine the nodal forces at any point in a load cycle. However the problem has now become very complex, and, in the general case, there will be five distinct regions on the interface, each with different boundary conditions as follows:-

(1) surfaces have not slipped at any time during the preceding part of the cycle. For these nodes:-

$$U1_i = U2_i$$

(2) surfaces have slipped earlier in the cycle but are not slipping at the point in the cycle being considered. Here $U2_i - U1_i = S_i$

(3) surfaces are slipping at the outer edge of the interface i.e. primary slip is taking place and on these nodes $Q_i = -\mu P_i$

(4) surfaces are slipping at points away from the edge of the interface and in the opposite direction to the slip in (3) above. i.e. secondary slip. Here

$$Q_i = \mu P_i.$$

(5) surfaces have separated at the edge of the interface and $P_i = Q_i = 0$

(6) at all nodes except those where separation occurs the normal displacements satsify the equations $V1_i - V2_i = 0$

Such a general situation is illustrated in fig. 6.7

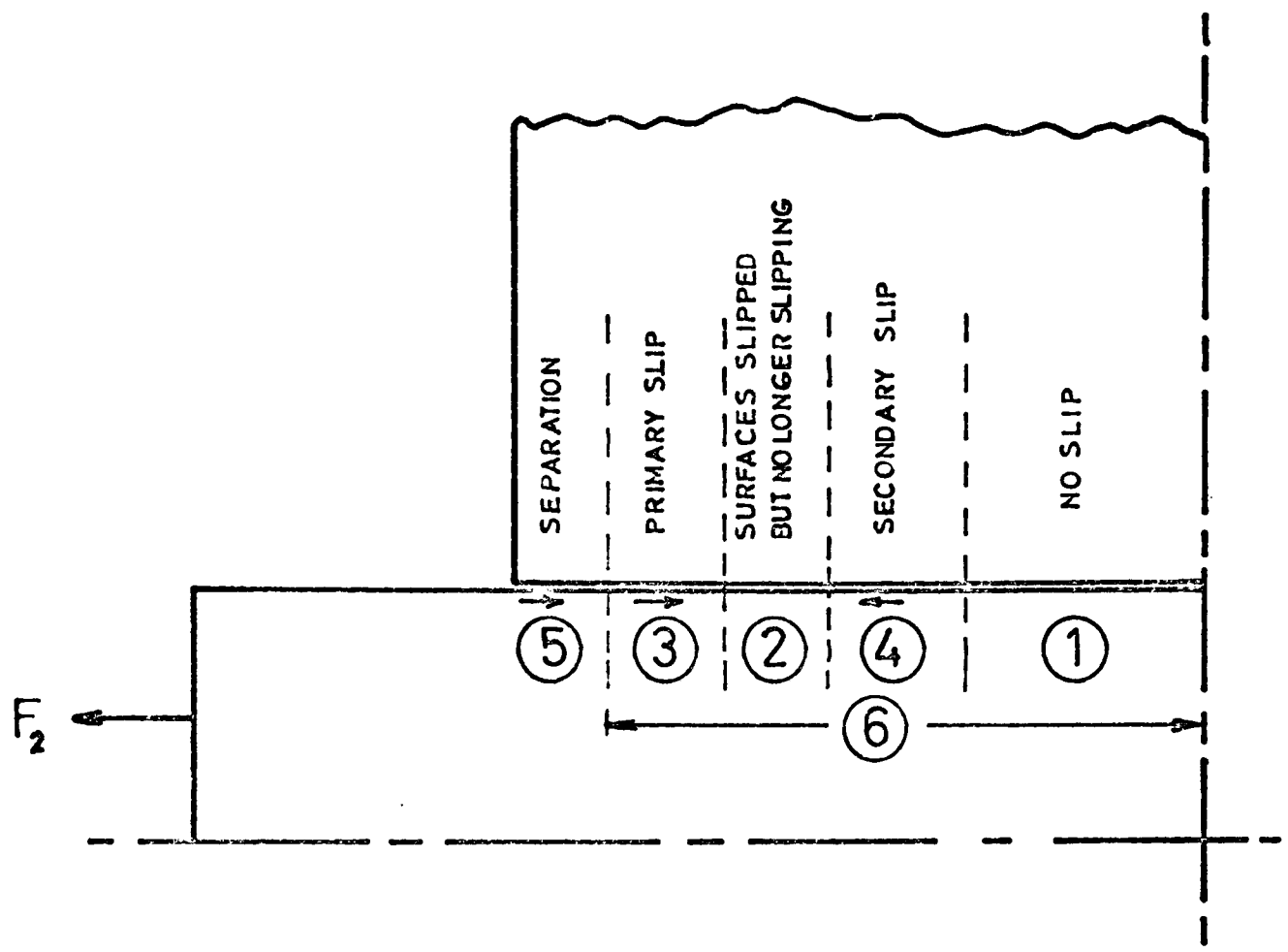


Fig. 6.7 Boundary conditions during unloading of a sharp cornered assembly

The load F_2 is taken to be decreasing from a maximum tensile value thus causing primary and secondary slip in the directions shown. However it has not fallen sufficiently to prevent separation at the corner or to cause reversed (primary) slip over the whole of the interface region on which forward (primary) slip occurred while F_2 was increasing. In view of the complexity of the problem when separation, etc. are involved, care must be taken to ensure that the boundary conditions are satisfied over the whole interface. The method of solution used was basically the iterative, incremental one that was described at the end of Section 6.3. However, there it was assumed that only primary slip would occur. When separation and secondary slip are possible, further iterative processes are required. The process of

iterating for separation and secondary slip have been described in isolation in previous sections and their inclusion into the general method of solution is not, in principle, difficult.

Having solved equations 6.17, 6.19 for p_j, q_j, etc. an additional check must be made to see if at any point $p_j < 0$ and the check on whether $|q_j| > \mu p_j$ must be split to separate the regions of primary and secondary slip. So far there are no complications but at this stage a problem arises. The boundary conditions have to be satisfied by iteration in three separate regions, but satisfying the boundary condition in one region will affect the solutions over the whole interface and it is quite possible that the final solutions will depend on the order in which the three iterative processes are carried out. Further possibilities must be considered since simultaneous iteration to satisfy the boundary conditions in two or more regions at once is also possible.

In practice it was found that convergence was most rapid when iterating initially for primary slip followed by secondary slip and then separation. The iterative loops are nested as shown in the flow diagram in fig. 6.8 so that, after each interim solution, all nodes are checked to see that the previous iteration has not resulted in further violation of boundary conditions in a region in which they had previously been satisfied. For example, after the first iteration for separation, the nodal forces are examined to see if this has resulted in a need for further iteration for primary or secondary slip before continuing with the iteration for separation.

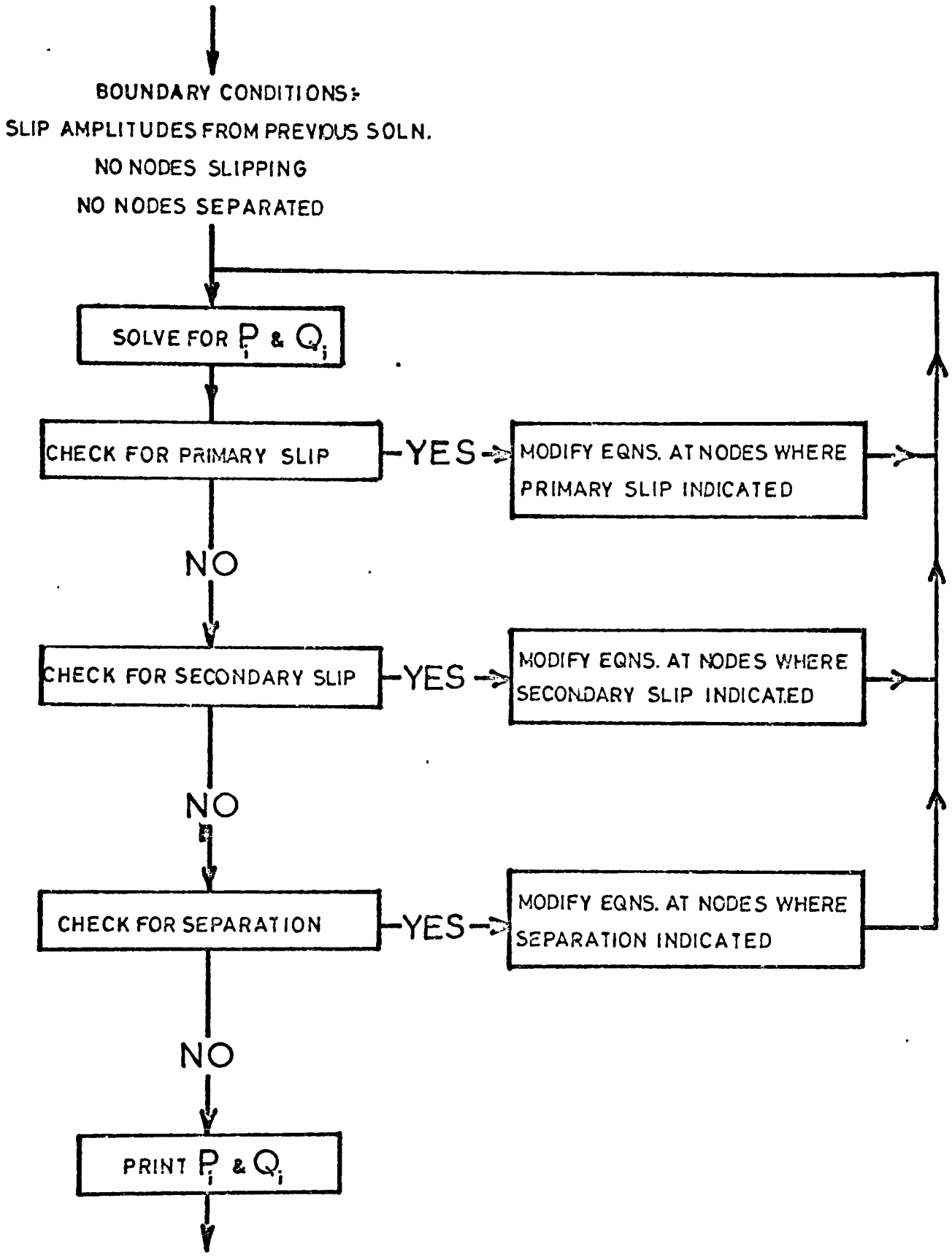


Fig. 6.8 Flow diagram for iterative processes used to solve the general slip problem

The program for solving the nodal forces during a complete load cycle is described in detail in Appendix 2.

Chapter 7

THE DISTRIBUTION OF STRESS AND OTHER VARIABLES IN SOLID AND ASSEMBLED SPECIMENS UNDER FATIGUE LOADING

7.1 INTRODUCTION

The methods outlined in the previous two chapters are applied to four geometries used in the fatigue tests. These are the solid sharp cornered specimen, the corresponding assembly and the assembled full and incomplete radiused specimens. In each case, the ratio of block length to plate thickness away from the blocks is 4:1 and the ratio of block height to length is 1:1. In the radiused specimens, the ratio of the radius to the plate thickness is 1:2 and, for the fully radiused specimen, the ratio of the plate thickness inside the block to that outside is 2:1. The corresponding ratio in the incomplete radius specimens is 5:4. The fatigue specimens are illustrated in fig. 3.7 and the calculations were based on non dimensionalised models of these configurations.

The elastic properties used in the calculations of stress were those of L.65 aluminium alloy; i.e. E = 10.7×10^6 lb/in^2 and Poissons ratio = 0.32. Displacements were computed assuming conditions of plane stress.

For each case, stresses on the interface are computed, and for the assemblies, values of slip amplitude and size of slip region are determined. Solutions are obtained for several ratios of clamp load to axial load which occur during a complete load cycle. Where possible, computed results are compared with experimental results and in a few special cases, worked solely for this purpose, to the results of other authors. Finally, by

considering the displacement of a point in the plate during a complete load cycle, the damping capacities of the different assemblies are compared.

7.2 DIVISION OF CONTINUA INTO FINITE ELEMENTS AND A DESCRIPTION OF THE BOUNDARY CONDITIONS

7.2.1 Solid sharp cornered specimen

The finite element method can be used directly to solve for stresses and displacements in the solid specimens. Fig. 7.1 shows the element mesh in the region of one corner in a sharp cornered solid specimen. Lines GF and DF are axes of symmetry. The mesh size is reduced as the corner is approached since this is clearly a region of high stress gradients. The line BE corresponds to the interface in an assembled specimen and a series of elements are arranged with their centroids on this line so that values of stress there may be computed directly. The boundary conditions were as follows:-

1. Surfaces AB, BC, CD are stress free.
2. Zero normal displacement on lines GF and FD.
3. Zero shear stress on lines GF, FD and AG.
4. A unit load is applied at point D representing the clamping load.
5. A unformly distributed load representing the fatigue load F_2 acts along surface AG.

7.2.2 Assembled sharp corner specimen

For this problem, two separate meshes are required, one for the block and one for the plate, and they are illustrated in figs. 7.2 and 7.3. Again, lines DC, BC and GH are lines of symmetry. Contact between block and plate occurs along line KB and the nodes in the plate on

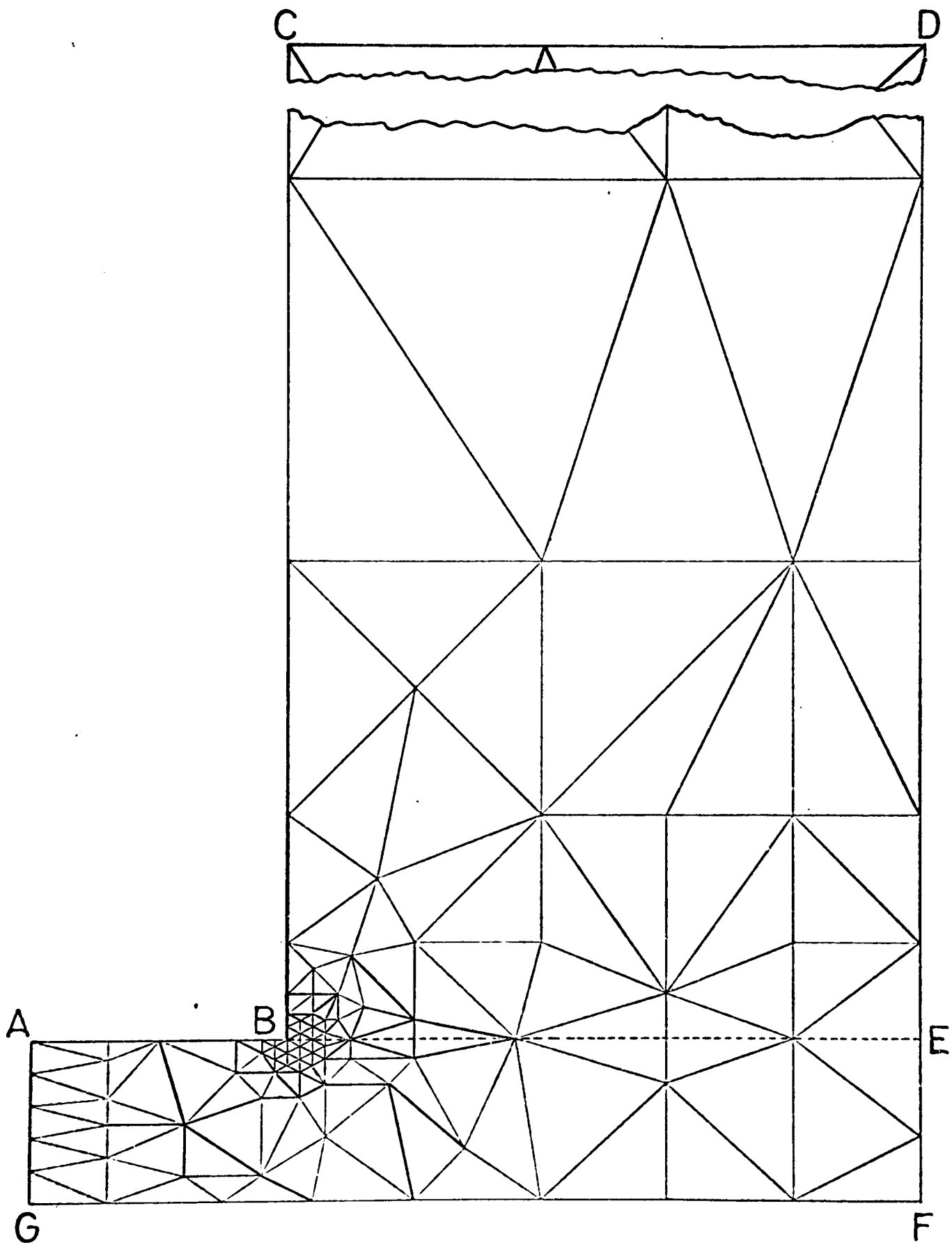


Fig. 7.1 Mesh for sharp cornered solid (93 nodes)

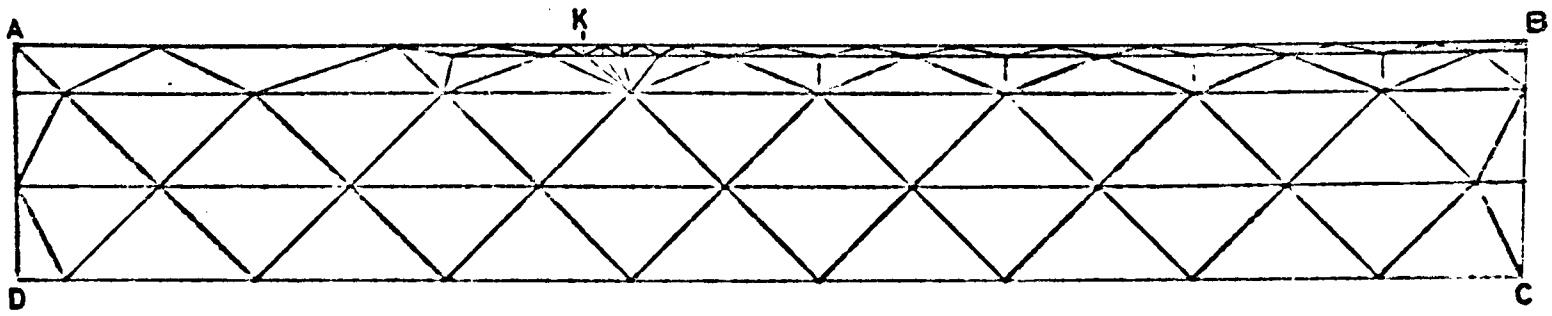


Fig. 7.2 Mesh for flat plate (14 Interface Nodes)

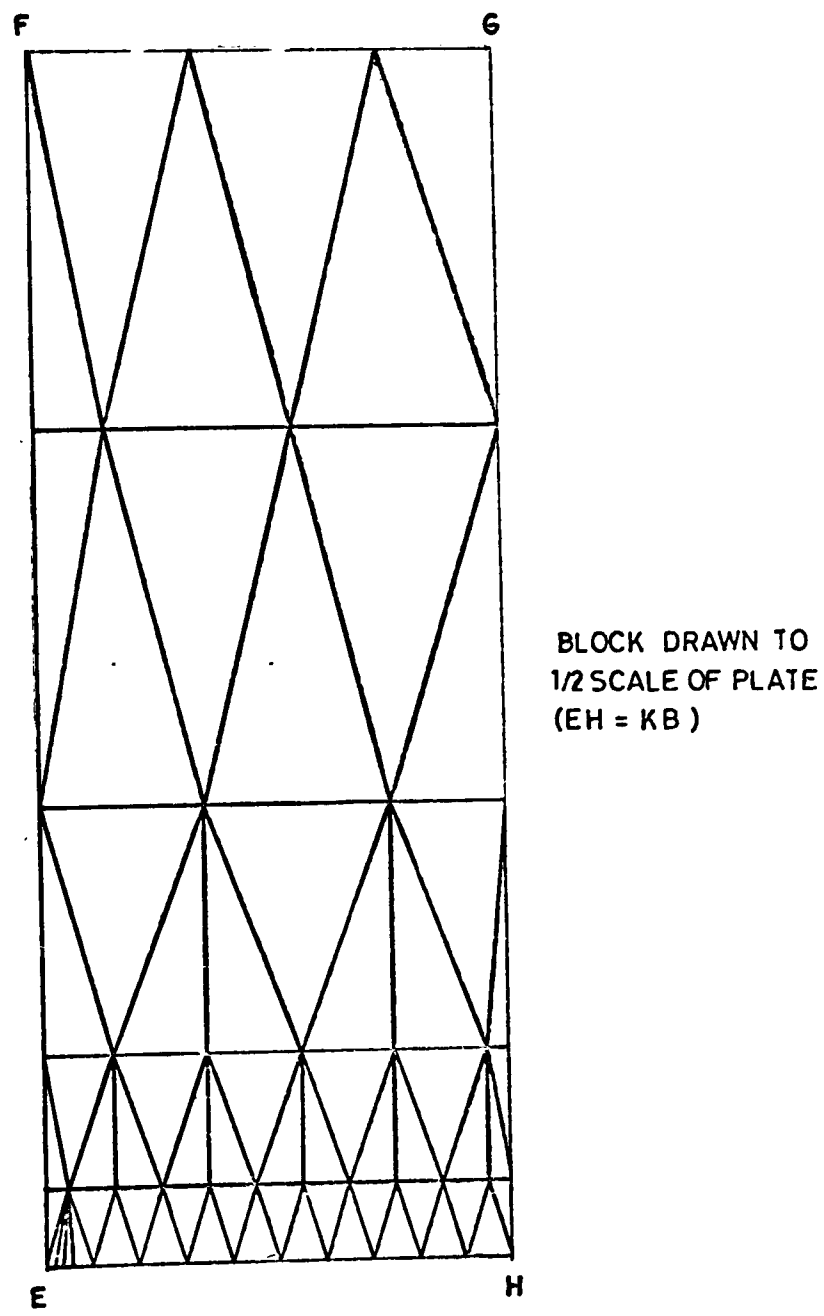


Fig. 7.3 Mesh for Block (14 Interface Nodes)

this line are coincident, in the unloaded condition, with nodes in the block along line EH. The problem was solved with n, the number of nodes on the interface, equal to 10, 13 and 14. The best solutions were obtained with n = 14 and further detailed calculations were based on this mesh which is the one illustrated in fig. 7.2 and 7.3.

As mentioned in the previous chapter, the solution is in three stages, the finite element technique being used in the first and third. The boundary conditions are as follows: Stage (1) - computation of influence coefficients

(a) Block

(1) Surfaces EF and FG are stress free.

(2) Zero normal displacement and shear stress on line GH.

(3) Point G has zero displacement normal to the interface.

(4) Unit loads, first parallel to and then normal to the interface, are applied in turn to each node on the surface EH, the remaining nodes being load free. The resulting sets of nodal displacements are the required influence coefficients for the block.

(b) Plate

(1) Surface AK is stress free.

(2) Zero normal displacement and shear stress on surfaces DC and BC.

(3) Zero shear stress on surface AD.

(4a) With zero normal stress on surface AD, unit loads, first parallel to and then normal to

the interface, are applied in turn, to each node on surface KB, the remaining nodes being load free. The resulting sets of nodal displacements are part of the set of required influence coefficients for the plate.

(4b) With surface KB stress free, a uniformly distributed unit load is applied to surface AD. The resulting displacements of nodes on surface KB complete the set of influence coefficient for the plate.

Stage (3) - calculation of stresses in the plate.

(1) Boundary conditions b1 to b3 apply.

(2) The nodal shear and normal forces obtained from stage (2) are applied at the interface nodes.

(3) Nodal normal forces, similarly obtained are applied to nodes on surface AD.

7.2.3 Assembled radiused specimens

The meshes for the full and incomplete radiused plates are shown in fig. 7.4 and 7.5. There are eleven equispaced nodes on the interface and the block mesh for these problems differs accordingly from that shown in fig. 7.3.

The method of solution is identical with that used for the sharp cornered assembly.

7.3 SHARP CORNERED SOLID

7.3.1 Stress distributions

Fig. 7.6 illustrates a solid sharp cornered specimen and indicates the notation used when plotting results. Values of stress on the interface, non dimensionalised with respect to some mean value, are plotted against x/a,

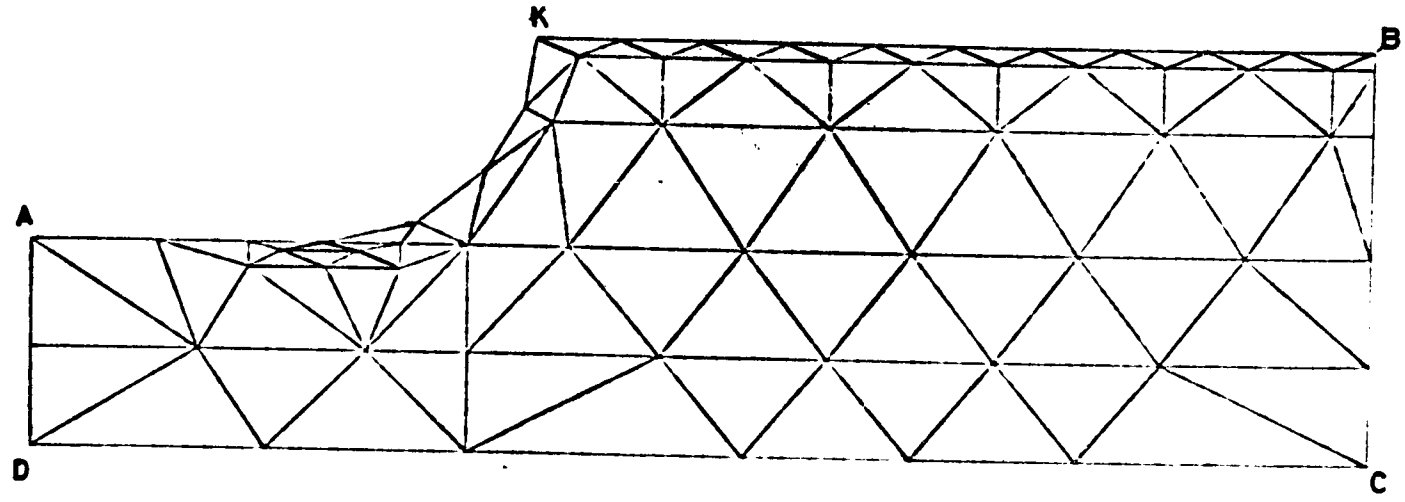


Fig. 7.4 Mesh for full radiused plate
(10 Interface Nodes)

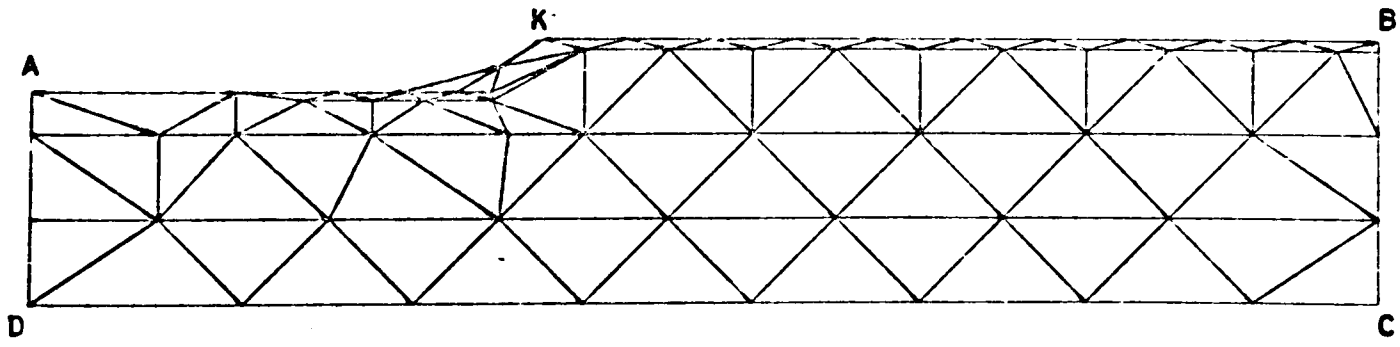


Fig. 7.5 Mesh for incomplete radiused plate
(10 Interface Nodes)

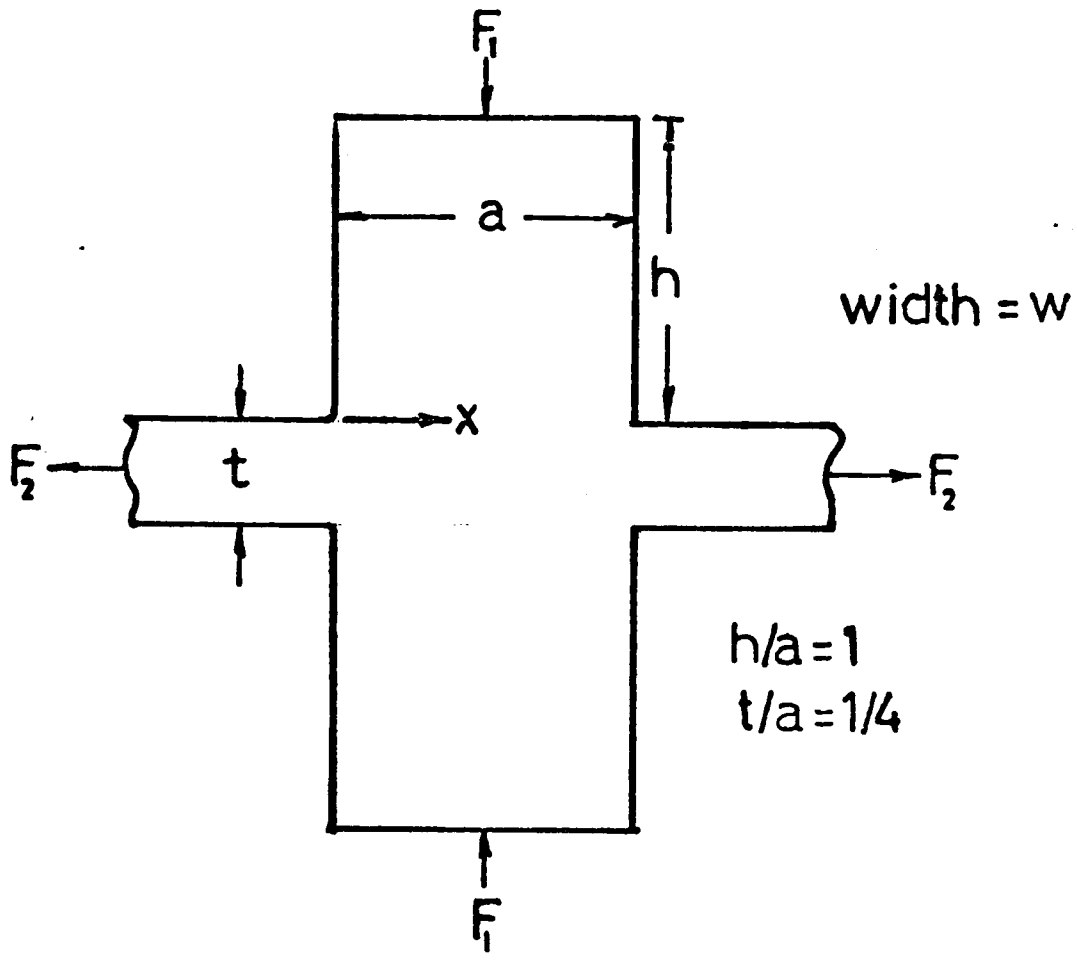


Fig. 7.6 Sharp cornered solid (notation)

where x is the distance along the interface measured from the corner and a is the full width of the blocks. (N.B. Although in this case there is no real interface, the line corresponding to the interface in an assembly is referred to as such). Since the distributions are symmetric they are only plotted for x/a = 0 to 0.5. Results are plotted for different values of λ where λ is the ratio of the nominal axial stress away from the blocks, σ_o, to the nominal normal (clamping) pressure, $(-\sigma_n)$[+].

$$\text{i.e. } \lambda = \frac{\sigma_o}{-\sigma_n} \quad \lambda = \frac{F2 \cdot a \cdot w}{F1 \cdot t \cdot w}$$

where w is the specimen thickness. Since, in all the specimens considered, a/t = 4, $\lambda = 4 \cdot F2/F1$. Note that using the ratio of σ_o to $-\sigma_n$ causes λ to be positive for tensile axial loads.

[+]For sharp cornered specimens (solid and assembly) $\lambda = 3$

Fig. 7.7 shows the distribution of normal stress, (σ_y) non dimensionalised with respect to its nominal mean value, (σ_n) for λ between 2 and - 2. For λ = 0.0 (i.e. no axial load), the pressure is constant over most of the interface but peaks sharply near the corner. The finite element method cannot give values of stress right in the corner where an exact (elastic) solution would presumably give infinite values of stress. However, the slope of the curve in that region is very high, suggesting an infinite value of normal stress at the corner.

As λ increases (i.e. a tensile axial load is applied), this pressure peak is very rapidly reduced and for values of $\lambda > 2$ becomes negative. i.e. for $\lambda > 2$ the normal stress at the corner is tensile. This was the first indication that separation of the block and plate might occur in the assembly during the tensile half cycle of loading. For negative values of λ the pressure peak at the corner is emphasised.

The variation of axial stress, (σ_x) for different λ is shown in fig. 7.8. In this plot the stress is non dimensionalised with respect to the axial stress away from the blocks (σ_o). For $\lambda > 1$ and $\lambda < -1$ the axial stress distribution is indistinguisable from that illustrated for λ = + 8. The salient features of this curve are the peak at the corner and the reduced level of stress inside the blocks due to the load here being carried by a wider section. For $1 > \lambda > -1$, i.e. when the mean normal stress is greater than the mean axial stress, the component of axial stress due to the normal load begins to predominate, particularly at the corner, and for very small positive values of λ the direction of the axial

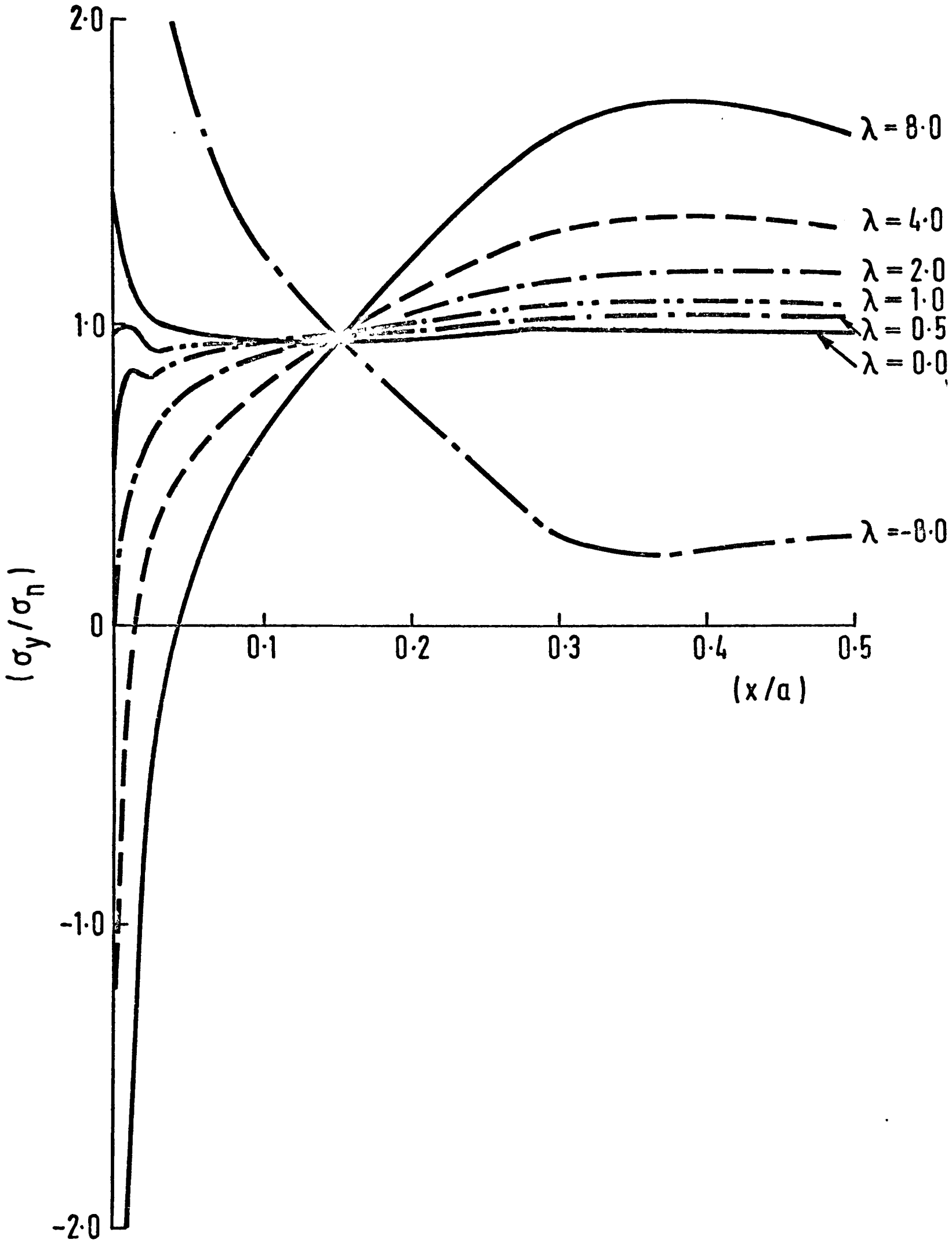


Fig. 7.7 Normal stress in a sharp cornered solid

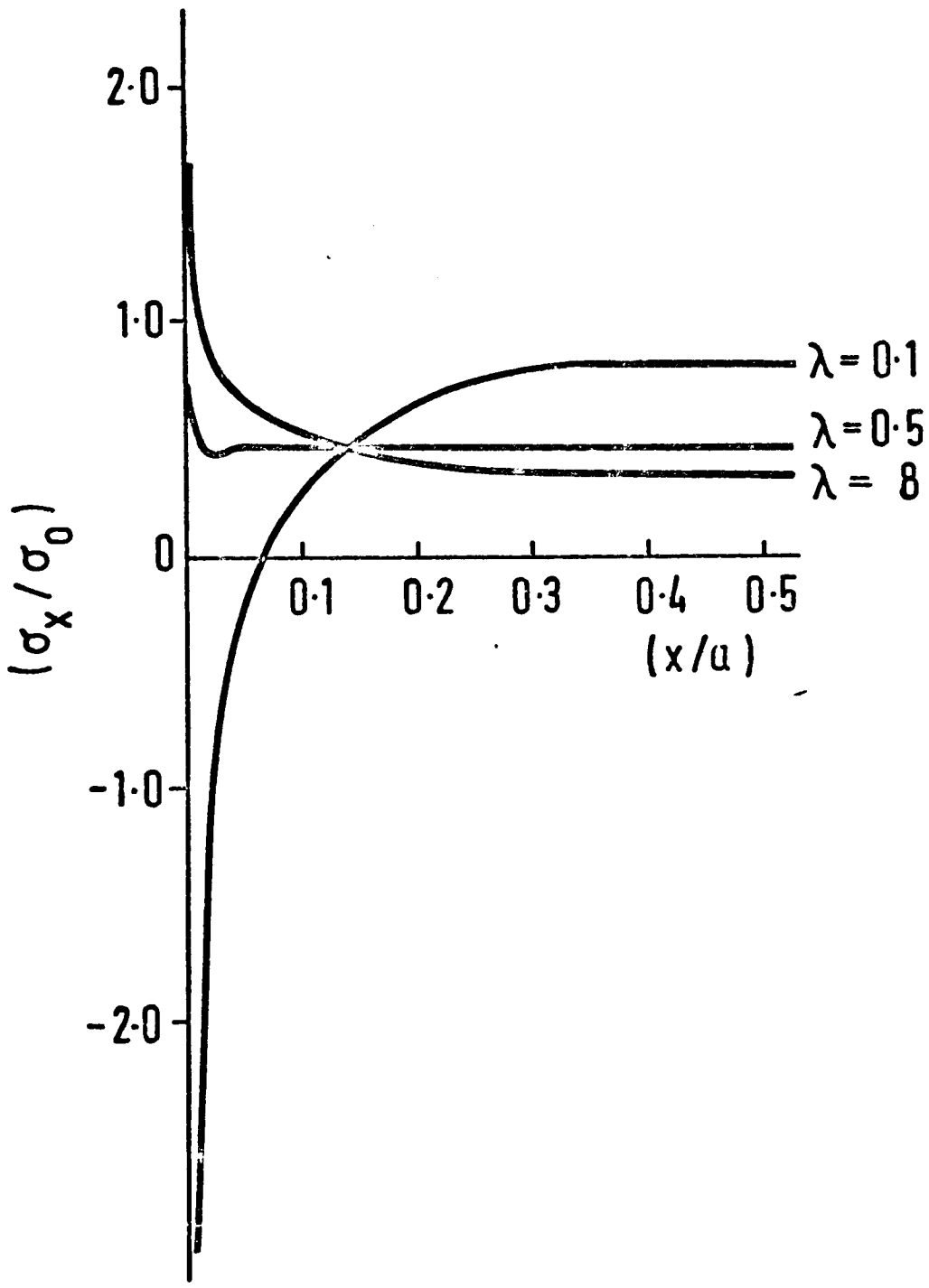


Fig. 7.8 Axial stress in a sharp cornered solid

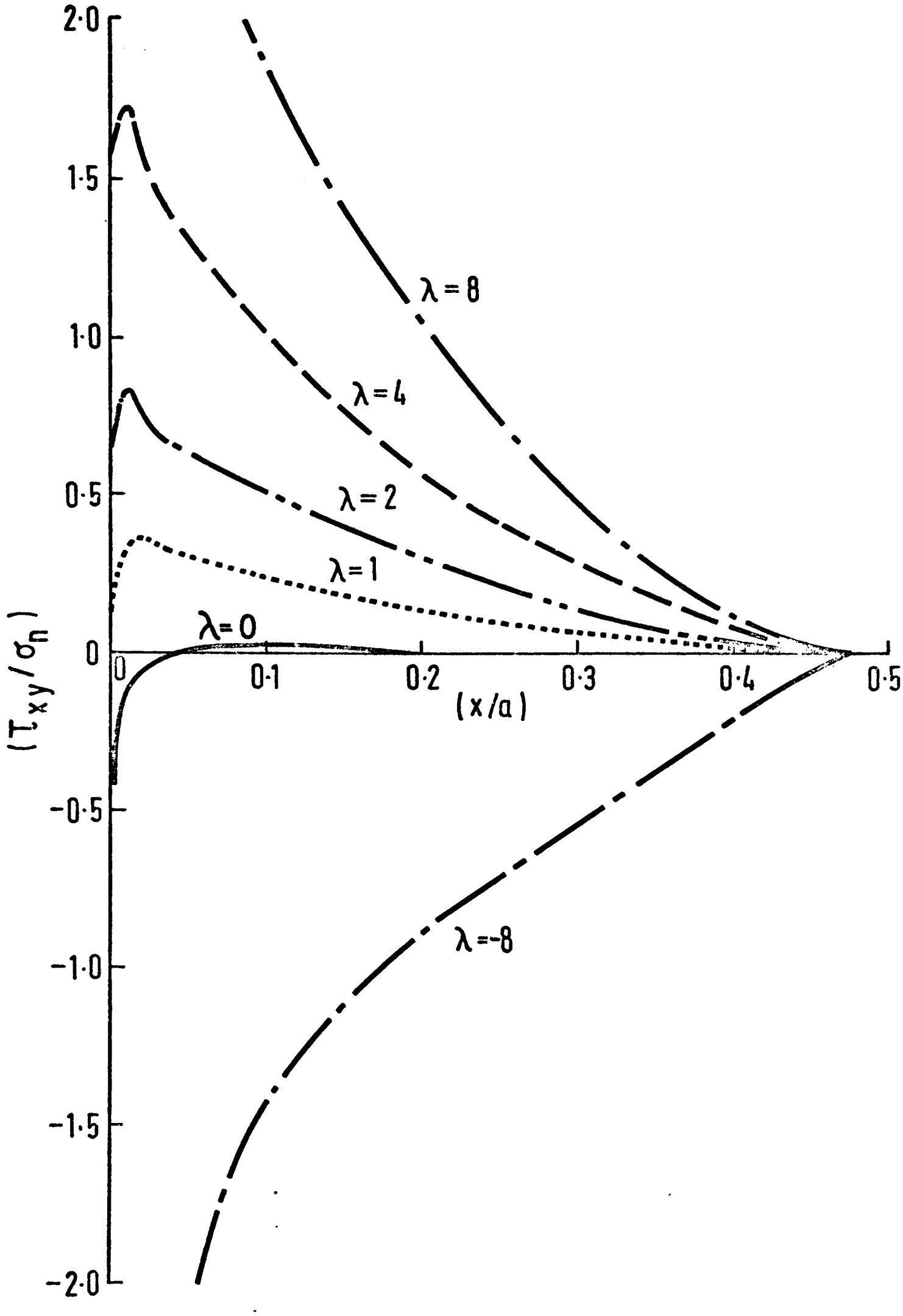


Fig. 7. 9 Shear stress in a sharp cornered assembly

stress there is reversed.

In fig. 7.9 the shear stress parallel to the interface, τ_{xy}, non dimensionalised with respect to the mean normal pressure ($-\sigma_n$) is plotted for λ in the range $8 > \lambda > -8$. For all values of λ the shear stress increases in magnitude as the corner is approached, its direction depending upon the direction of axial load.

7.3.2 Estimate of slip in an assembly

An interesting aspect of the results for this configuration is revealed by comparing the curves of figs. 7.7 and 7.9. From the arguments of Chapter 1 it is concluded that an estimate of the extent of the slip region in an assembly may be obtained by comparing the shear and normal stresses found in a geometrically similar solid in the region corresponding to the interface in the assembly. i.e. slip will occur in the assembly wherever $\tau_{xy} > \mu\sigma_y$ in the solid. Assuming a value for μ of unity+, it is seen that, for $\lambda = 8$, $\tau_{xy} > \mu\sigma_y$ for $x/a < 0.2$. Bearing in mind the redistribution of shear stress when slip occurs, it is apparent that for $\lambda = 8$ slip could be expected in an assembly over most of the interface.

From these curves it is apparent that slip would not be eliminated until $|\lambda| < 0.5$ (approximately).

7.4 SHARP CORNERED ASSEMBLY

7.4.1 Introduction

The notation used in this section is the same as that used for the solid sharp cornered specimen (fig. 7.6).

+In the fatigue tests μ was determined experimentally to be 0.8.

Due to the nature of the method used to determine stresses in assemblies, values of stress in the plate, at points nominally on the interface, are, in fact, at points, a distance d, just below the interface where d/t = 0.014. However, values of slip amplitude, etc., refer to points actually on the interface.

When considering assemblies, it is necessary, because of non linearities associated with the slip, to consider complete load cycles. The problems solved all dealt with alternating axial load and constant normal load and the ratio of the peak, nominal, positive, axial stress, during a cycle, to the mean normal stress is designated by λ^*. The ratio of instantaneous nominal axial stress to peak nominal axial stress is designated by ϕ. (Thus $\lambda = \lambda^* \times \phi$) Stress distributions are plotted for various λ^* and $\phi = 1$ and - 1.

An important parameter in any slip problem is the coefficient of friction, μ. In the fretting fatigue tests described in Chapters 3 and 4, μ was found experimentally to be about 0.8 and all the following results, unless otherwise stated, are based on this value.

Where possible all results are plotted in non dimensional form. Stresses are plotted as stress concentrations, usually with respect to the appropriate nominal value. Displacements, slip amplitudes etc. are non dimensionalised with respect to the size of assembly, the elastic modulus, and the applied stress causing the displacement. Thus slip amplitude, (s) is plotted as $(\frac{s}{a} \frac{E}{\sigma_o})$ where a is the interface length, E the elastic modulus, and σ_o the nominal axial stress causing the slip.

In fig. 7.10 the axial displacement, d_c, of the point in the plate originally coincident with the corner of the block is plotted in non dimensionalised form, against Ø during the first $1\frac{1}{4}$ load cycles for two values of λ^*. After $1\frac{1}{4}$ cycles the loop has been closed and the displacement has the same value as it had after $\frac{1}{4}$ cycle. The assembly can then be said to have shaken down after $1\frac{1}{4}$ cycles and the cycle from $\frac{1}{4}$ cycle to $1\frac{1}{4}$ cycles can be taken as representative of all following cycles, provided λ^* does not change.

Although the main interest, as far as the fatigue tests are concerned, lies in determining the peak values of stress during a cycle of loading, it is none the less interesting to consider what is happening on the interface during the first $1\frac{1}{4}$ cycles.

Referring to fig. 7.10, OA represents the displacement that occurs due to the application of the clamp load F_1. During this phase of loading no slip occurs. Starting to apply the tensile axial load F_2, further displacement, represented by AB, occurs, still with no slip. At B the surfaces start to slip at the outer edge of the interface and along BC the slip region spreads along the interface until, at C, it covers almost the whole contact area.

From C to D the axial load is removed and slip in the opposite sense to that which occurred along BC starts from the outer edge of the interface and spreads inwards as the load falls. However, at the same time, slip continues, in the original sense (secondary slip) near the centre of the interface and continues to do so until

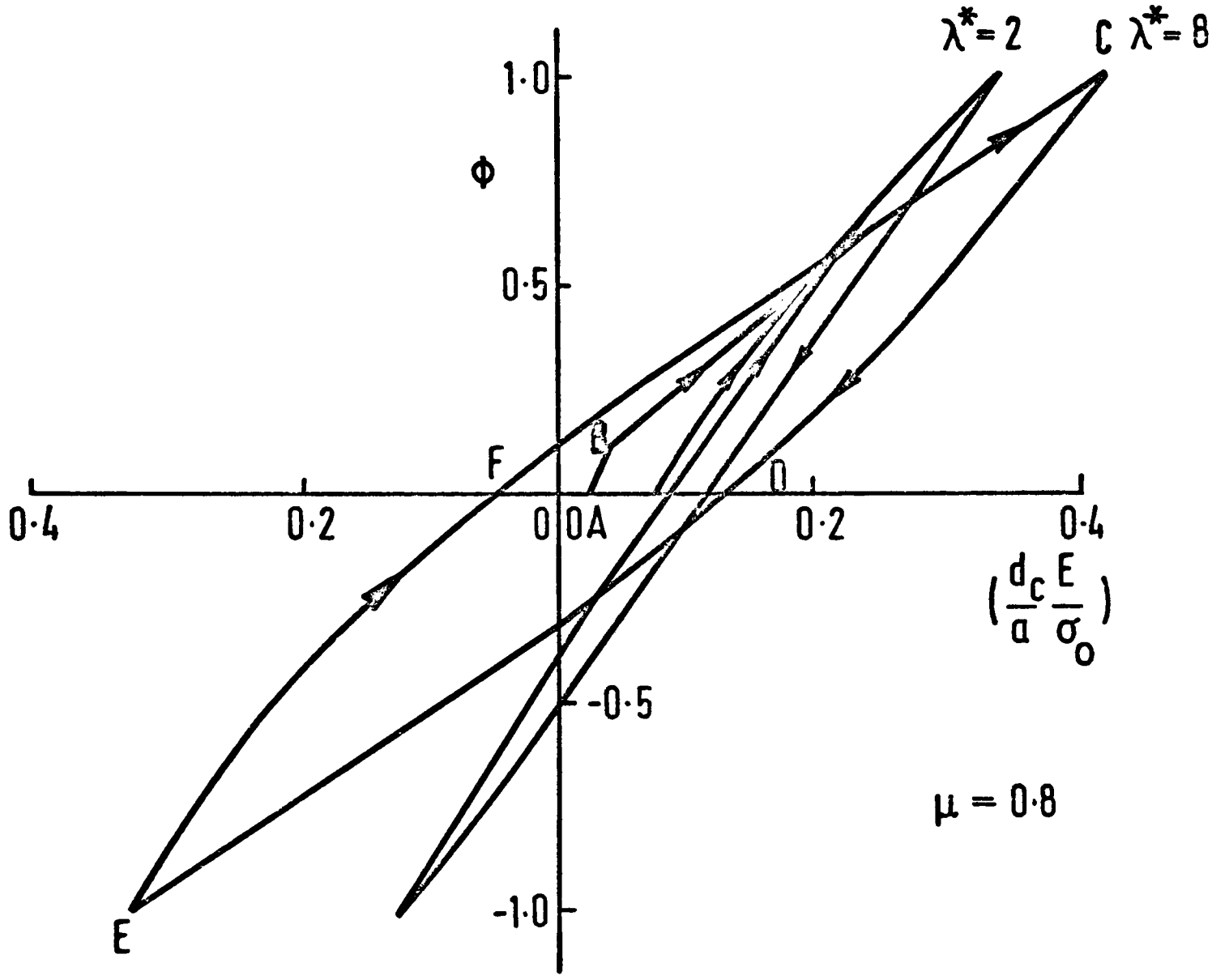


Fig. 7.10 Load-displacement loops for sharp cornered assemblies

point D is passed when the axial load, having passed through zero, starts to build up compressively. During the compressive loading phase, the 'reversed' slip region continues to spread into the contact area and at E covers practically the whole interface. Along EFC, the axial load goes from compressive to tensile and slip occurs in the same sense as that during the first $\frac{1}{4}$ cycle, again starting at the corner. During this part of the cycle there is no further slip on any other part of the interface as there was between C and D. At C the conditions are exactly as they were after the first $\frac{1}{4}$ cycle.

It is thus evident that, when the axial load oscillates between $\pm$ F and the clamping load, F_1, remains constant, the load displacement curve traverses the loop C-D-E-F-C. The area of this loop represents the frictional energy lost per cycle which, in turn, determines the damping capacity of the assembly. This feature is considered further in Section 7.6.

7.4.2 Slip and separation

Fig. 7.11 shows the extent of the slip region l_s/a at the instant of maximum axial stress (both tensile and compressive) during a load cycle plotted against λ for three values of μ. (l_s = the length of interface, measured from the corner, on which slip occurs.) As would be expected, the extent of the slip region increases with axial load but for slip to occur over the whole interface requires the axial load to tend to infinity. This is because, for reasons of symmetry, the shear stress on the interface, τ_{xy}, will tend to zero as the centre

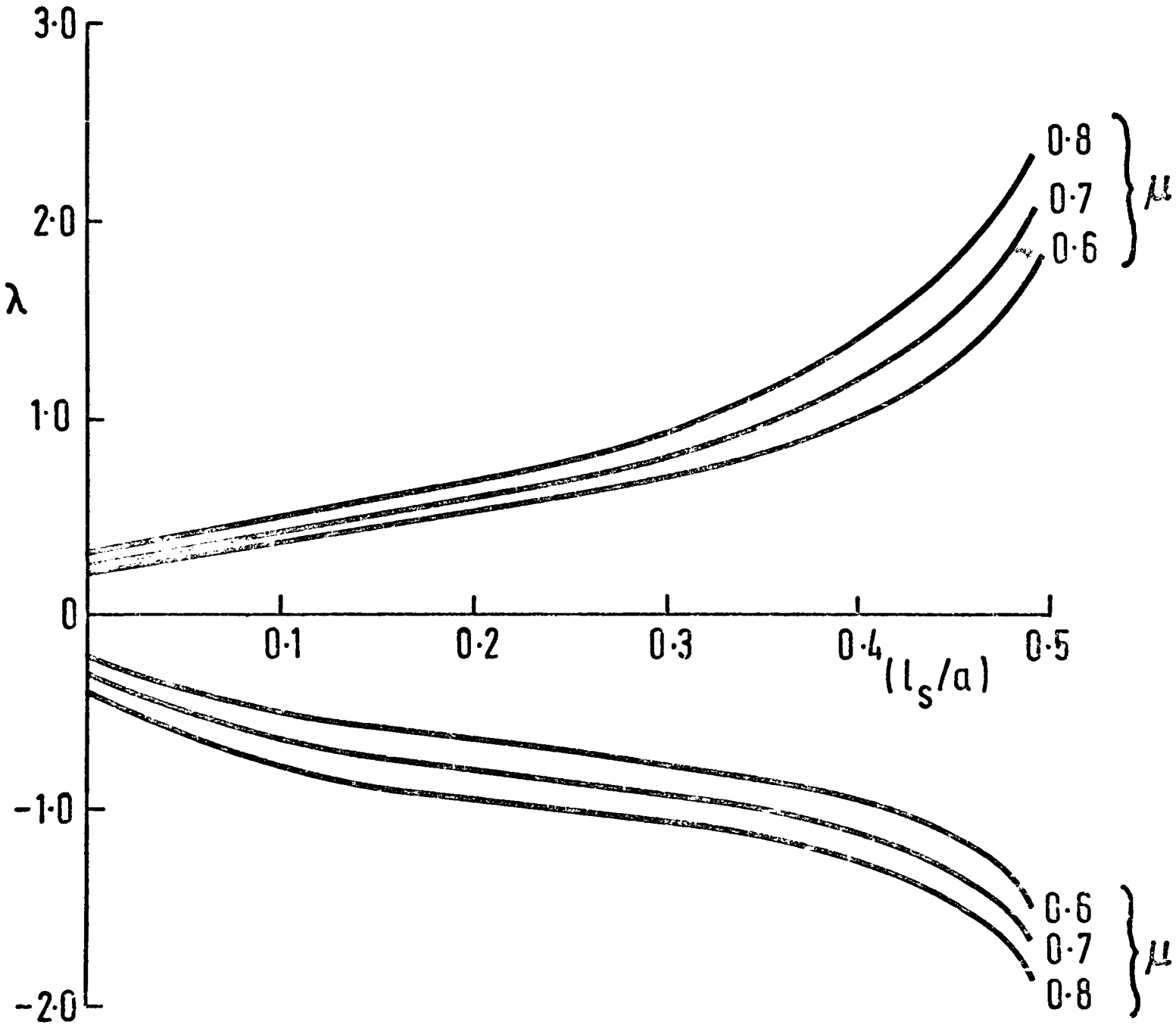


Fig. 7.11 The extent of the slip region in a sharp cornered assembly at the instant of maximum tensile and compressive axial load

line (x/a = 0.5) is approached, whereas the normal pressure, σ_y, remains finite. Since, for slip to occur $\tau_{xy} = \mu\sigma_y$ slip can only occur on the centre line of the interface if the axial load is infinite. The effect of change in μ is also predictable, the slip region decreasing in size for increasing μ, and needs no further comment.

The variation of slip amplitude along the interface, for various λ^* and $\phi = 1$, is shown in fig. 7.12. The slip amplitude (s) defined as the horizontal displacement of a node in the plate relative to the corresponding node in the block, is plotted in non dimensional form, $(S.E/a.\sigma_o)$ against x/a where E is the elastic modulus and σ_o the nominal axial stress in the plate.

It was found that, for this geometry, there was no slip due to the application of the normal load alone (i.e. when $\lambda = 0$) but slip occurs for quite low values of axial load and when λ reaches 8 slip covers more than 90% of the interface. The variation of slip amplitude along the interface appears to be nearly linear but close to the slip/no-slip boundary diverges from this slightly. The pattern of slip during the compressive loading phase is very similar to that shown for tensile loads. The variation of slip amplitude at times other than those of peak loads is illustrated by fig. 7.13. This shows the change in slip amplitude occurring when ϕ is reduced from 1 to 0.95 in the second $\frac{1}{4}$ of a cycle in which $\lambda^* = 8$. At the outer edge of the interface, the slip amplitude falls, as expected, with the falling axial load

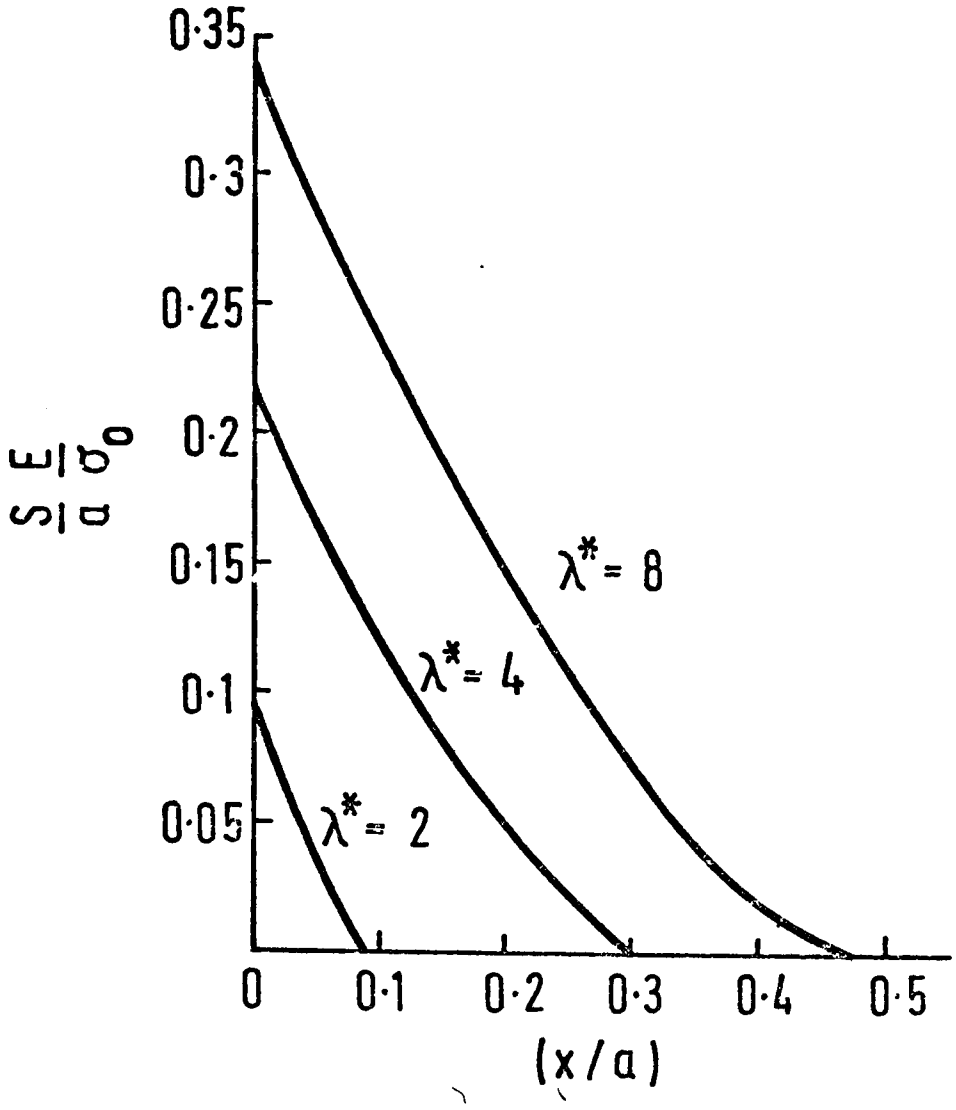


Fig. 7.12 Variation of slip amplitude along the interface of a sharp cornered assembly

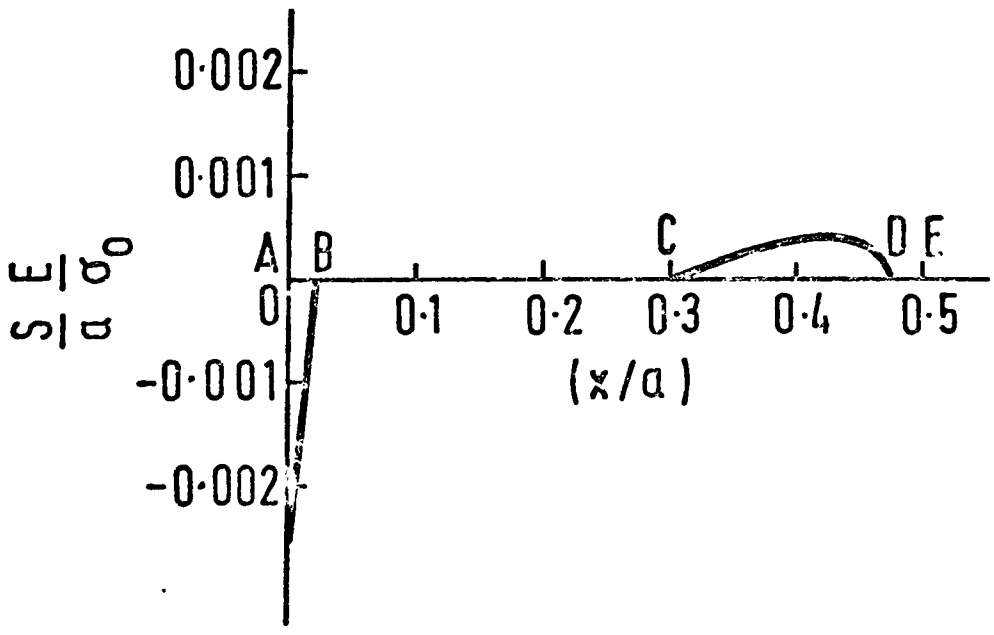


Fig. 7.13 Change in slip amplitude when Ø changes from 1.0 to 0.95 during a cycle with $\lambda^* = 8$

but near the centre of the interface it continues to increase. This is because the redistribution of stress, as the axial load is reduced, causes the normal pressure near the corner to rise (cf. sharp cornered solid). This reduces the pressure further along the interface faster than the shear stress falls and results in additional (secondary) slip. Interesting as the pheonomenon is, it is of little import since it does not coincide with the instant of maximum stress. However, such second order effects have to be considered, as was mentioned in the previous chapter, so that their associated boundary conditions can be included in the solution.

In addition to the surfaces slipping, it is found that, for values of λ greater than 1, the surfaces near the corner separate under tensile load. The amplitude, (S_p) and extent of separation, is plotted in non dimensional form, for various values of λ^* and $\emptyset$ = 1, in fig. 7.14. For λ^* = 8 the separation extends over nearly 2% of the total interface. The possibility of separation occurring was indicated by the results for the solid sharp cornered specimen under tensile axial loads in which large tensile normal stresses were found near the corner.

The explanation for the phenomenon of separation is found in fig. 7.15 which shows plots of the vertical displacement (V), of points on the interface surface of the block, due to the application of single point loads at three points on the surface. The loads act parallel to the surface of the block and outwards from the block centre line. The displacements are relative to the point at the centre of the top surface of the block.

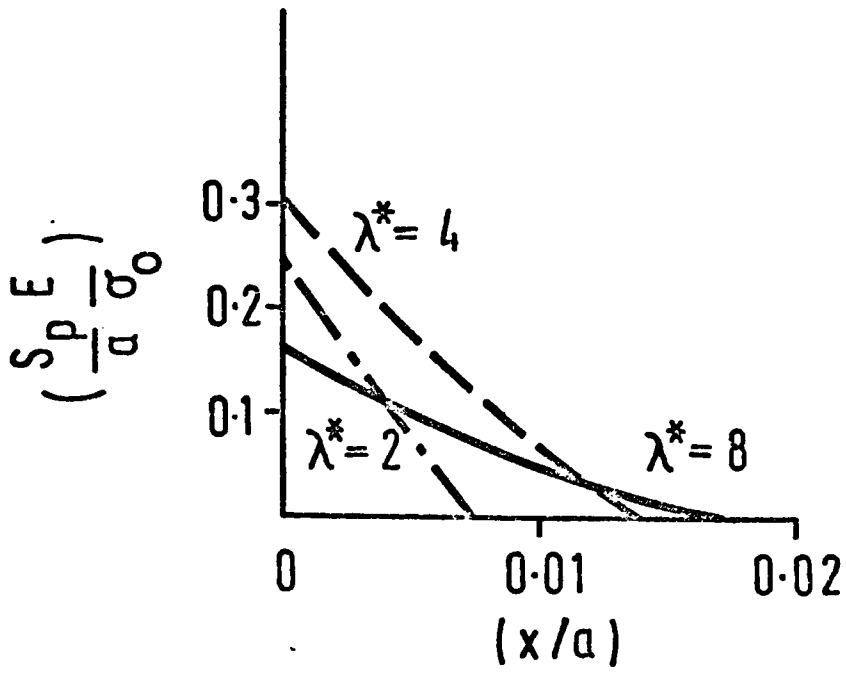


Fig. 7.14 Separation of surfaces during tensile axial loading

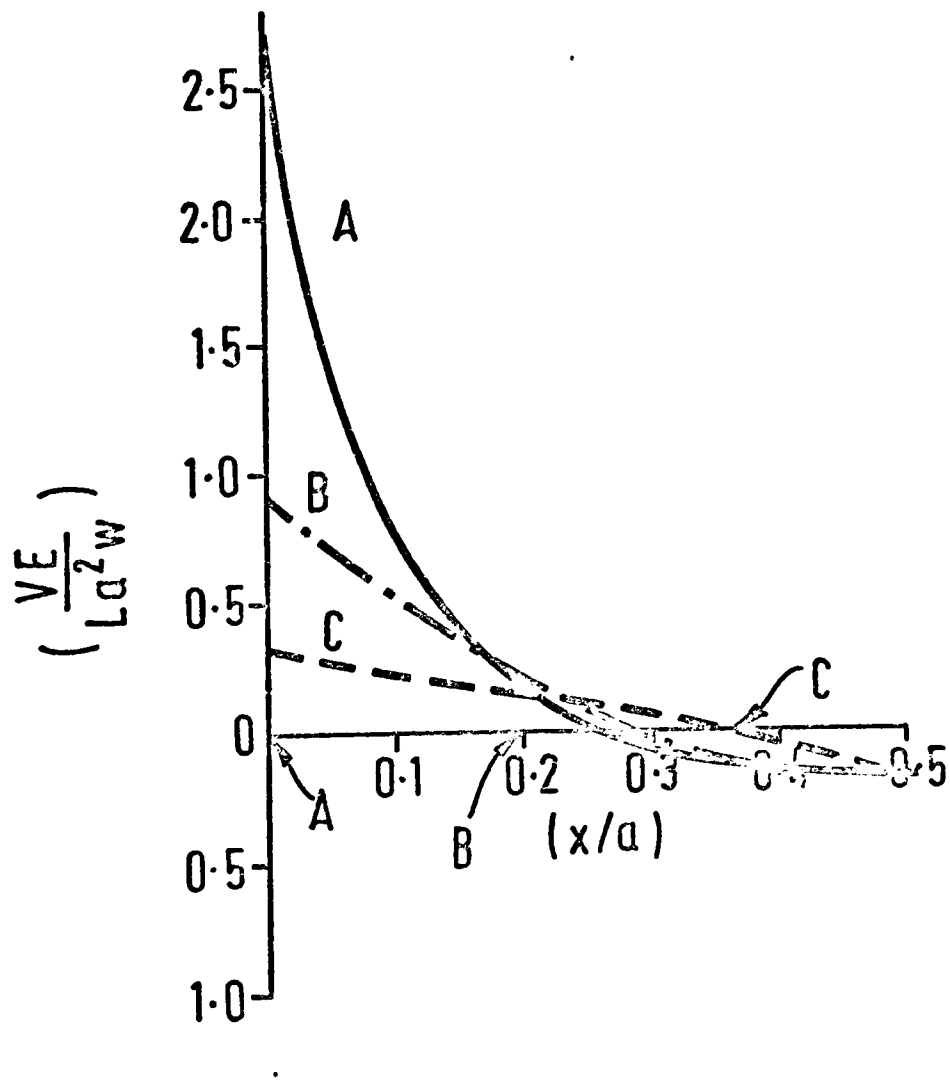


Fig. 7.15 Vertical displacements of the interface surface of a block due to point tangential loads on that surface

The plot is non dimensionalised by plotting $(\frac{VE}{La^2w})$ against (x/a) where E is the elastic modulus, w the thickness of the block and L the magnitude of the point load. The three curves shown are for loads acting at points A, B, and C, which are at (x/a) = 0.0, 0.2 and 0.35, respectively. The significant feature of these curves is that they show the corner of the block (x/a = 0) to undergo positive vertical displacements.

When an assembly is in tension the block will be subjected to an outward acting shear stress along the whole interface transmitted across the interface by friction. This will clearly cause a positive vertical displacement of the corner of the block relative to points in the block well removed from the interface.

At the same time, due to the clamping force, the block will have a rigid body displacement causing it to indent the plate. According to the relative magnitude of the indenting and the positive displacement of the corner of the block, the corner may or may not separate from the plate. Since the frictional force transmitted across the interface is dependent on the normal pressure, both components of the final displacement are dependent in a complex way on the ratio of the mean clamping stress to the axial stress. This point is illustrated by fig. 7.14. For $\lambda^* = 8$ the region over which separation occurs is larger than for $\lambda^* = 4$ although the amplitude of separation is smaller. Presumably, for $\lambda^* = 8$, the normal stress on the interface being small, both effects are small but the predominant effect is that of the shear stress. Thus the separation, while being relatively small in magnitude, extends well along the interface. As

the normal load is increased the separation of low magnitude, away from the corner, is suppressed by the increased indenting effect, but the increased normal pressure, and hence shear stress, increases the magnitude of separation at the corner. As the normal pressure is increased further, to $\lambda^* = 2$, the indenting effect begins to dominate and the separation is reduced in both magnitude and extent.

Clearly similar arguments can be applied, in modified form, to explain the tensile normal stress in the solid of this shape described in Section 7.3.1. There the coefficient of friction is infinite and, instead of separation occurring, high tensile stresses develop, but otherwise the explanation is qualitatively the same.

If the mechanism described above is the reason for separation the coefficient of friction (μ) should be an important parameter in determining whether or not separation occurs. For low values of μ the shear stress transmitted across the interface by friction must also be low and so the tendency for the surfaces to separate will be slight. Calculations using a value of 0.2 for μ showed no separation and the decrease in normal pressure towards the corner was not nearly as great as when $\mu = 0.8$.

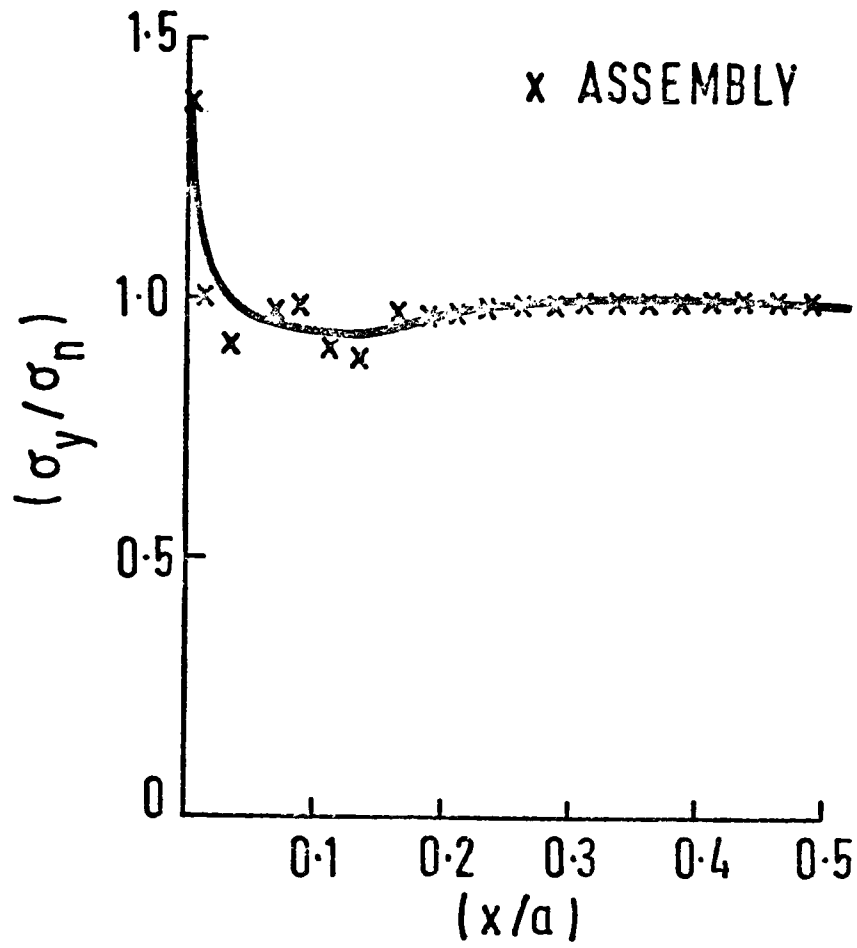
It may be worth recording that the above explanation for separation was not obvious to the author for some time. The first reaction when finding separation being predicted by theory was to explain it in terms of a Poisson ratio effect. Consider the assembly under tensile axial load. Between the blocks, the mean axial stress in

the plate, and hence the lateral contraction due to Poisson's ratio, is less than that away from the blocks due to some of the load being transferred to the blocks by friction. Since this will result in the plate being thicker between the blocks than away from them, it seemed that an explanation for separation had been found.

However, subsequent computation of the sharp cornered assembly problem, with Poisson's ratio equal to zero, showed that separation still occurred although it was slightly reduced in amplitude. Clearly, the effect of Poisson's ratio on separation is only of secondary importance.

7.4.3 Solutions to some simplified stress problems compared to those obtained by other methods

It is possible to compare the computed stress distributions, for the sharp cornered assembly in certain special cases, to results obtained by other methods and thereby estimate the reliability of the technique used. When the assembly is subjected to the normal load only it is found that there is no slip on the interface (fig. 7.11). The associated stress distributions should therefore be identical with those obtained for the solid sharp cornered specimen under a similar load. In fig. 7.16 the normal pressure and shear stress on the interface in the solid specimen are shown with the results from the assembly superimposed. In regions of low stress gradient agreement is good but, where rapid changes of stress occur, the solutions for the assembly oscillate slightly about the solution for the solid.



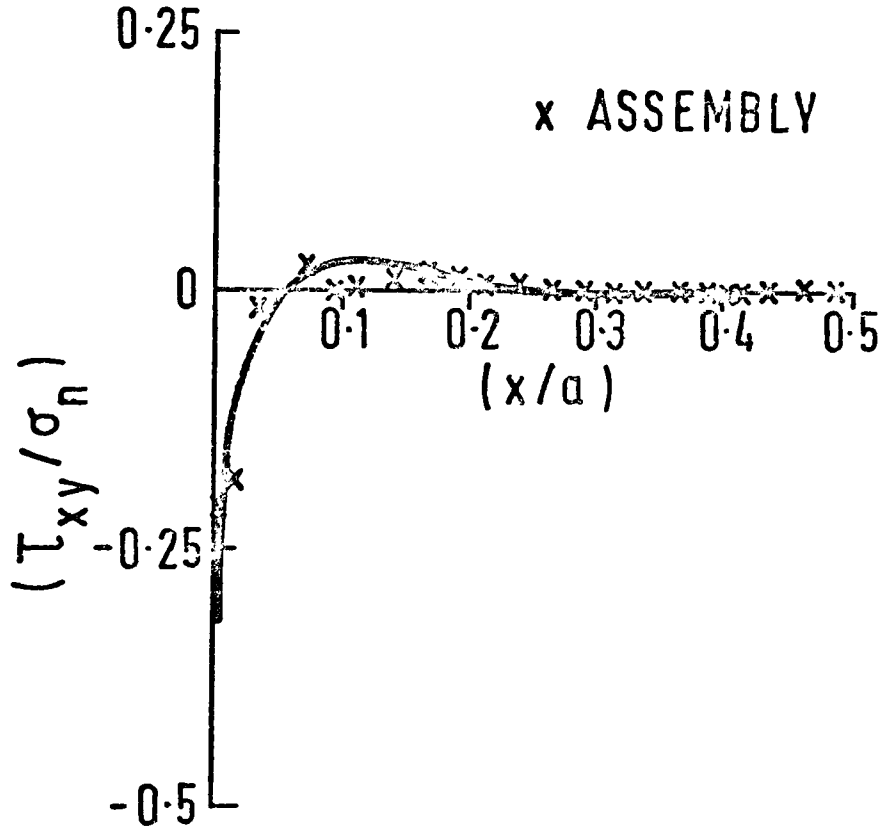


Fig. 7.16 Normal and shear stress in sharp cornered solid and assembly under a normal load only

However, the oscillation is such that, when smoothed by an estimated best fit curve, the agreement is very close.

A further check is provided by computing the normal stress distributions when the block is assumed to be rigid and adhesion is either total ($\mu = \infty$) or negligible ($\mu = 0$). This problem has been solved by Conway et al (36). In fig. 7.17 the author's results are compared to those reported in (36) and the agreement is good. It should be noted that Conway's results are for Poissons ratio = 0.3, as against 0.32 in this work, and also that they were taken from the figures in (36) which are small and may have acquired slight errors in printing.

These were the only comparisons that could be made with other methods of solution but they indicate that the errors are small and, in the main, take the form of oscillation about the exact solution. In the subsequent solution of problems where the axial stress was included, the oscillation was very slight and, in general, occurred only in one principal stress if that stress was small compared with the other principal stress. In the following results, any oscillation that occurred has been smoothed out and the stress distributions given are the best fit curves to the point values obtained.

7.4.4 Stress distributions

The normal stress distribution (σ_y) along the interface of a sharp cornered assembly is shown in figs. 7.18 and 7.19 for tensile and compressive axial stress respectively and for four values of λ^* between 1 and 8. The stress is non dimensionalised with respect to its nominal mean value (σ_n). For tensile axial stress ($\phi=1$), as λ^* increases

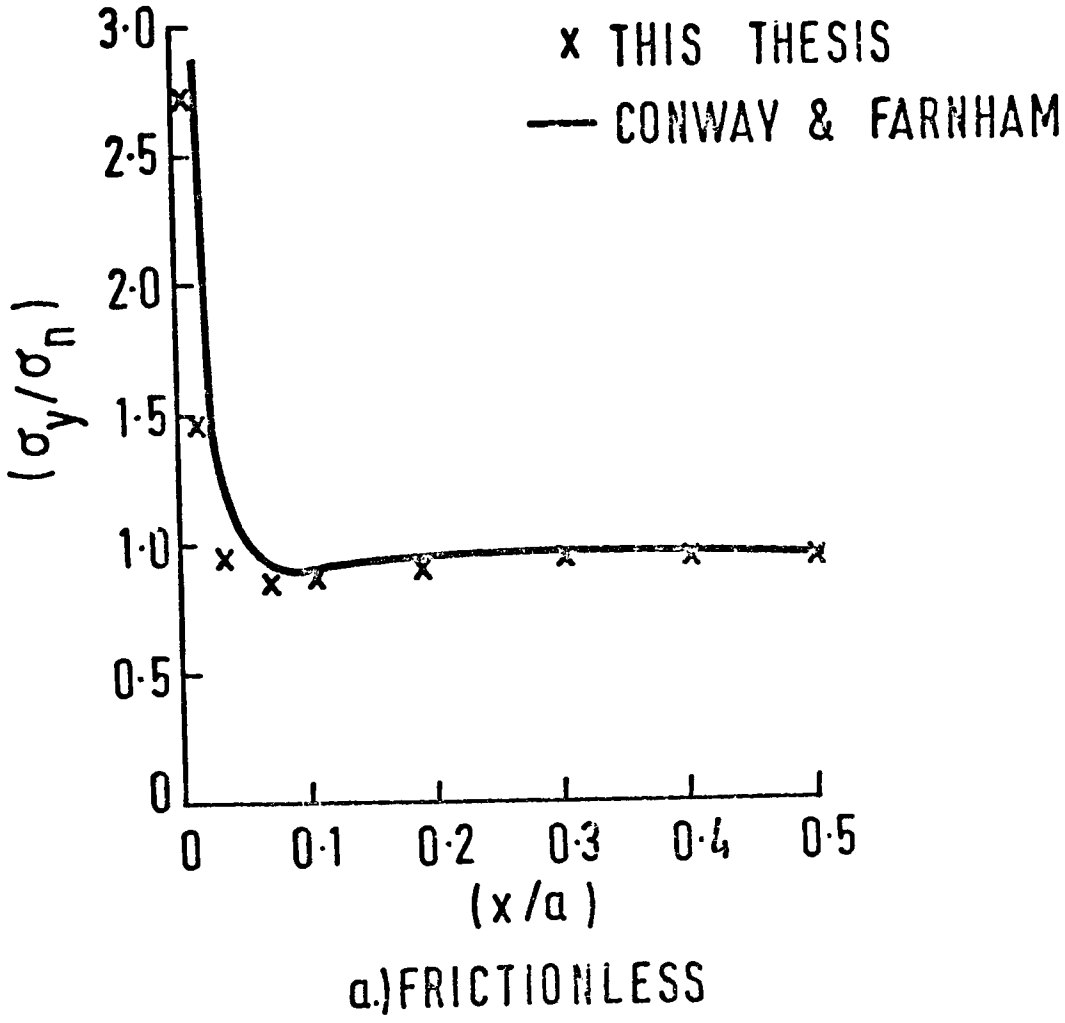


Fig. 7.17 Normal pressure distribution due to a rigid block indenting an elastic plate

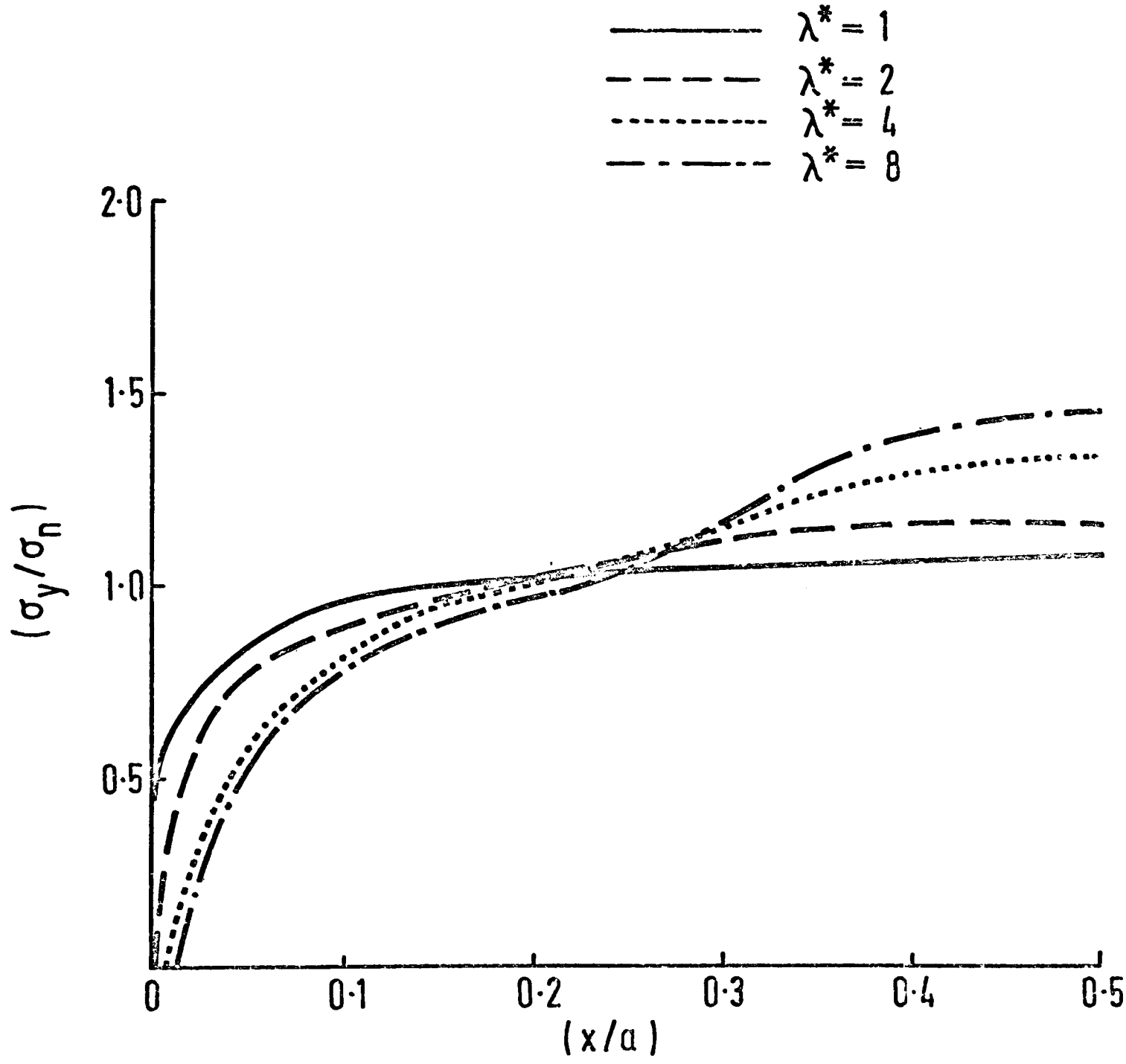


Fig. 7.18 Normal stress in a sharp cornered assembly under tension

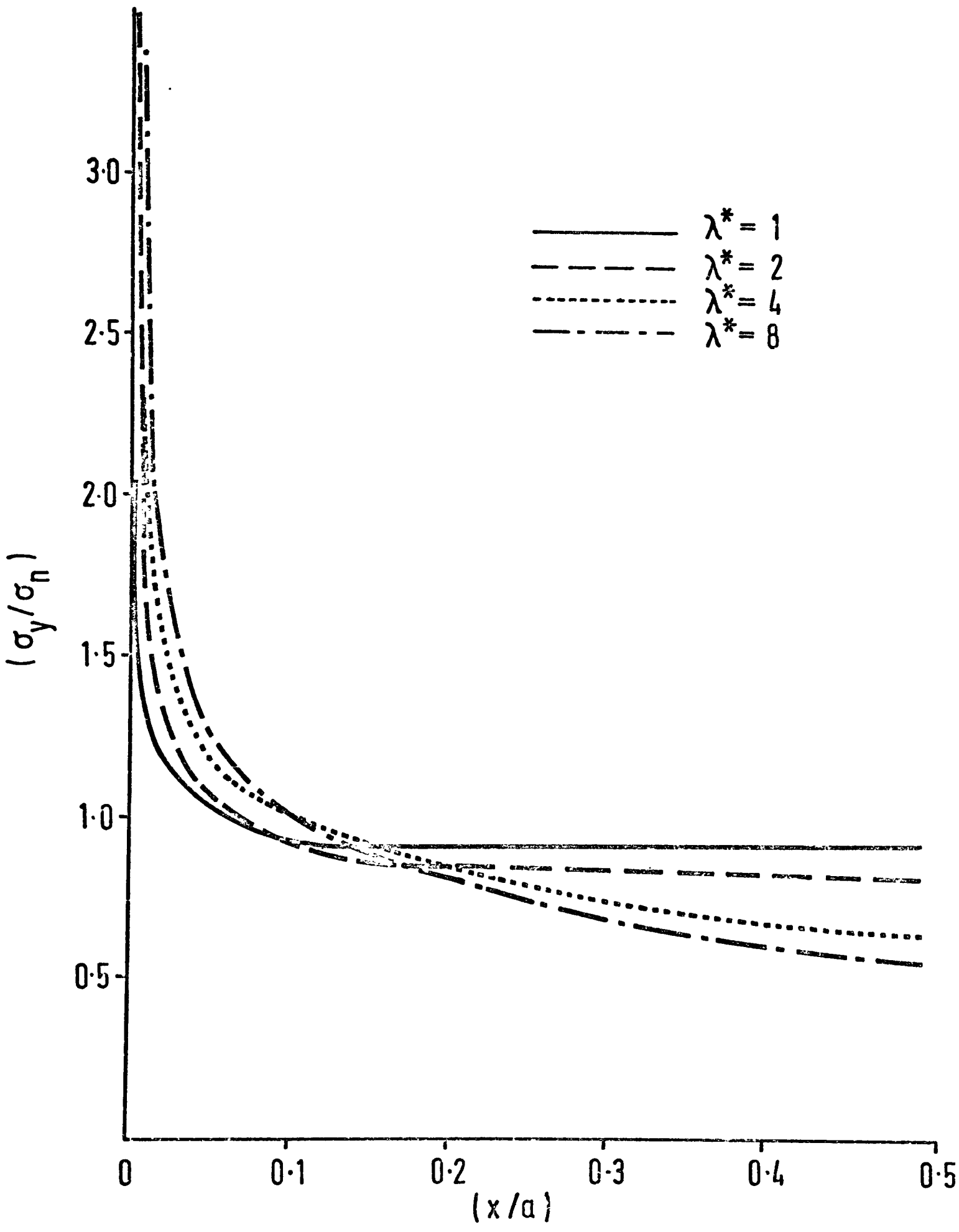


Fig. 7.19 Normal stress in a sharp cornered assembly under compression

the pressure at the edge of the interface is reduced for the reasons explained in the Section 7.4.2, until, when $\lambda^* = 2$, it falls to zero there and the surfaces start to separate. For compressive axial stress ($\phi = -1$) the reverse occurs and the normal pressure peaks sharply at the corner. As λ^* increases this peak increases rapidly, a stress concentration greater than 4 being indicated when $\lambda^* = -8$.

The axial stress distributions, σ_x, non dimensionalised with respect to the mean axial stress away from the blocks, σ_o, are plotted for tensile and compressive axial loads (ϕ=1 and -1) in figs. 7.20 and 7.21 respectively. Again λ^* takes values between 1 and 8 and, in this case, the effect of this variation is most marked. For high tensile values of nominal axial stress ($\lambda^* = 8$) the expected stress peak at the corner has been almost entirely eliminated by the separation there. Indeed, because of separation, the peak, such as it is, (stress concentration of 1.07) occurs slightly inside the nominal contact area at the point where actual contact starts. Even when the nominal axial and normal stress are equal (λ^*=1) the axial stress concentration at the corner is only 1.9, this compares, of course, to a value which tends to infinity in the solid case.

Over a length of the interface coinciding approximately with the slip region, the tensile axial stress falls, for all values of λ^*, to about 0.4 of its nominal value and then remains sensibly constant along the no-slip region.

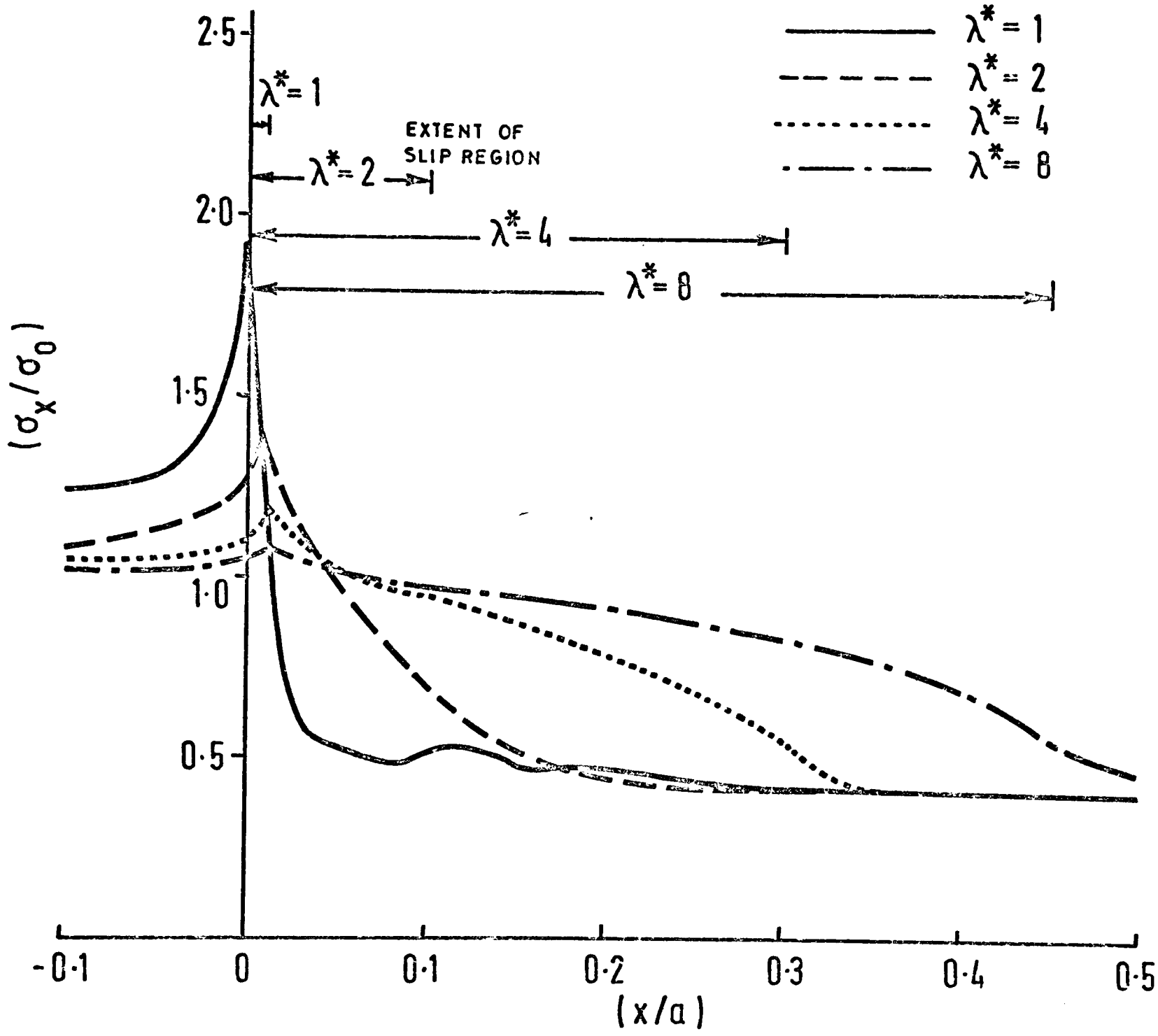


Fig. 7.20 Axial stress in a sharp cornered assembly under tension

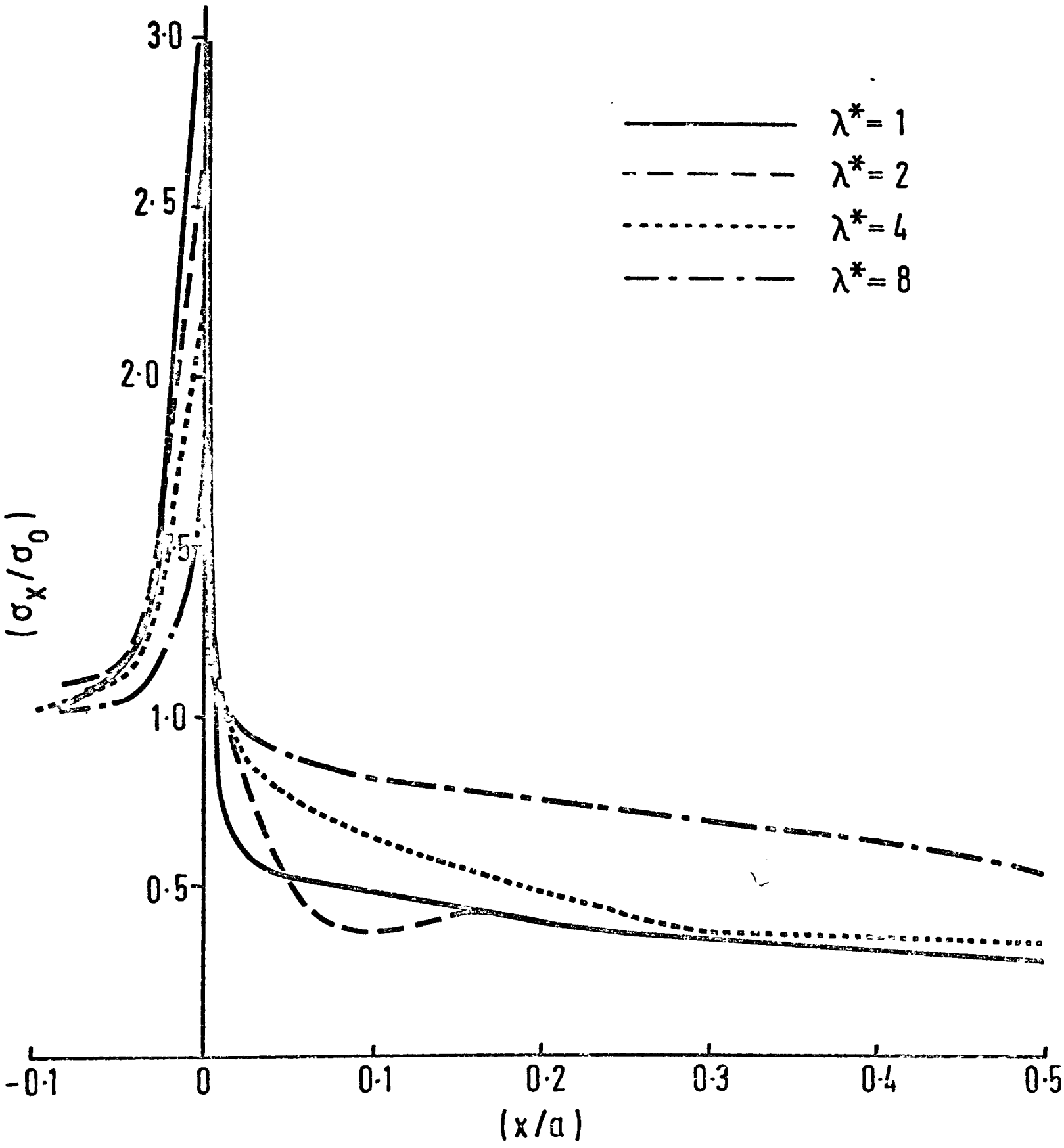


Fig. 7.21 Axial stress in a sharp cornered assembly under compression

When the axial stress is compressive, high axial stress concentrations occur at the corner which increase with increasing λ^*. For $\lambda^* = 8$ the stress concentration appears to be in excess of 3. Again, the axial stress falls between the corner and the end of the slip region and in the no-slip region has a value of about 0.3 of the nominal value.

The maximum shear stress on the interface, τ_{max}, again non dimensionalised with respect to the nominal value of maximum shear stress away from the blocks, σ_o, is plotted in figs. 7.22 and 7.23. Under tensile loading and high values of λ^*, these stress distributions are also affected by separation at the corner. Expected high concentrations only appear for low ratios of axial to normal stress and even when $\lambda^* = 1$ the stress concentration is only 2.5. When the axial load is compressive, high concentrations of maximum shear stress, which increase in magnitude as λ^* increases, appear at the corner. When $\lambda^* = 8$, a stress concentration greater than 4 is indicated.

7.5 RADIUSED ASSEMBLIES

7.5.1 Extent of slip region and amplitude of slip

For radiused assemblies, the shakedown process was again found to be complete after $1\frac{1}{4}$ cycles (fig. 7.28), the cycle from $\frac{1}{4}$ cycle to $1\frac{1}{4}$ cycles being typical, therefore, of all those following. Figs. 7.24 and 7.25 show the variation of slip amplitude along the interface of incomplete and fully radiused assemblies, for various values of λ^* and $\phi = 1$. Since the radiused plates are thicker between the blocks than away from them, the

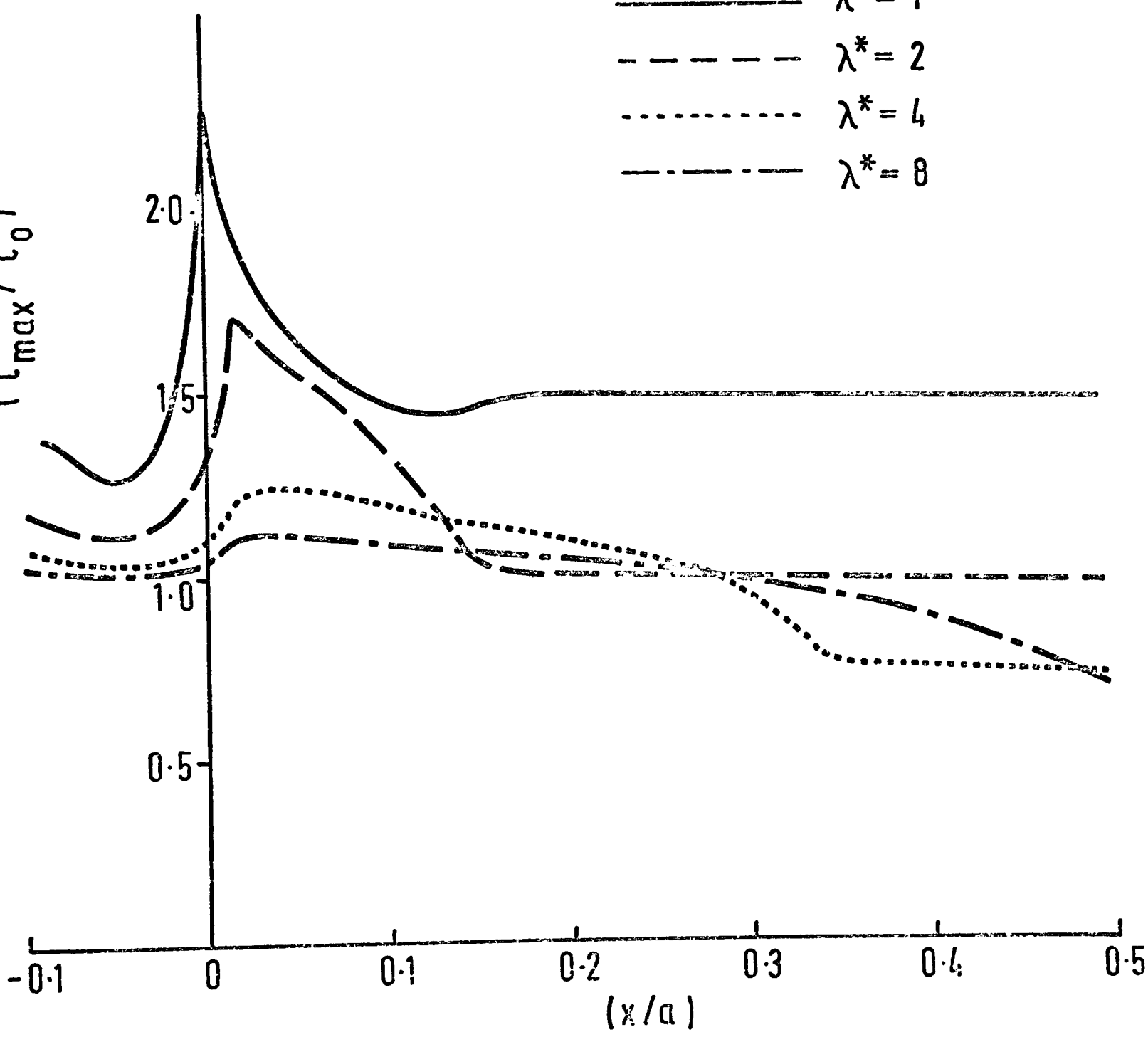


Fig. 7.22 Maximum shear stress in a sharp cornered assembly under tension

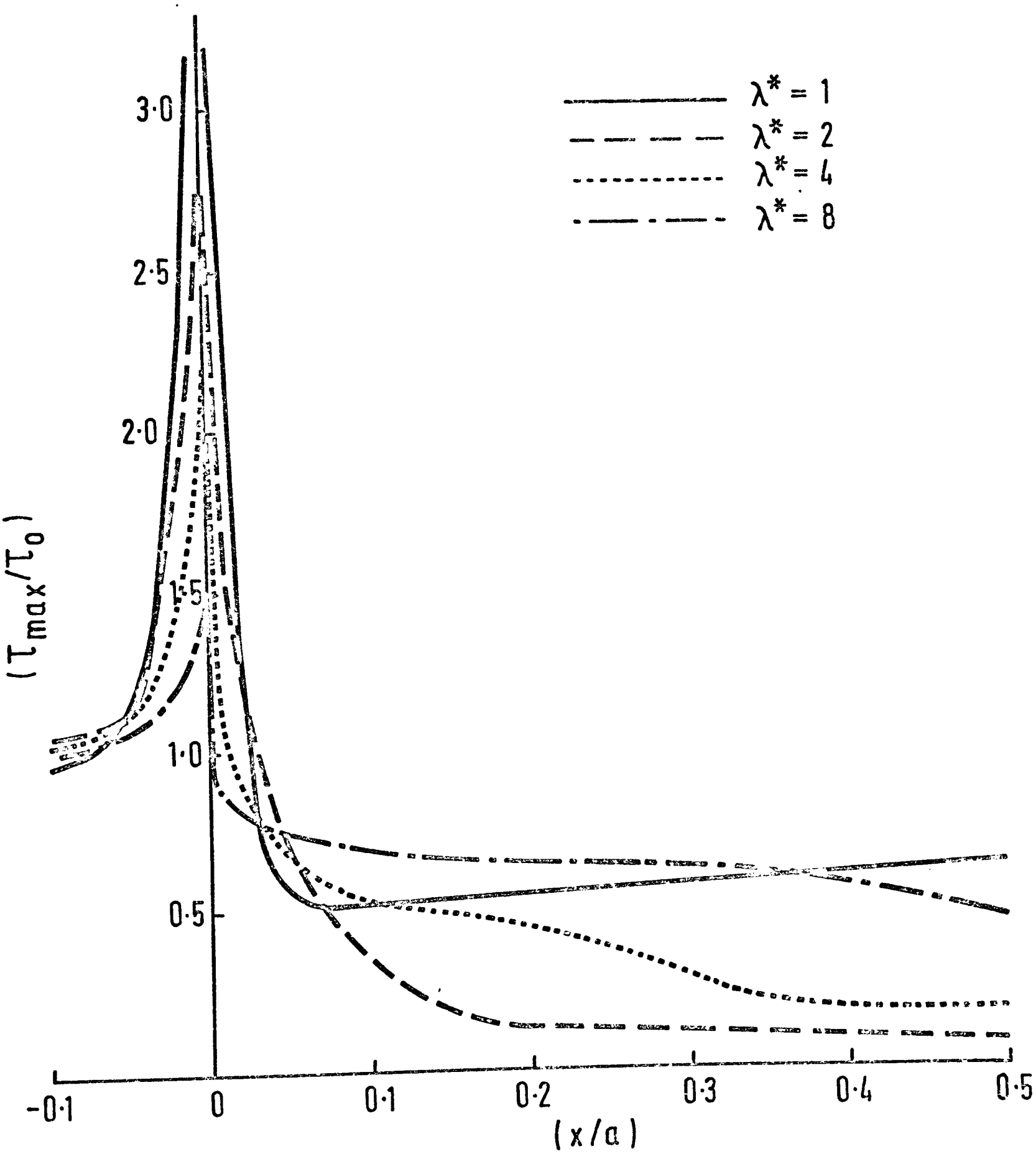


Fig. 7.23 Maximum shear stress in a sharp cornered assembly under compression

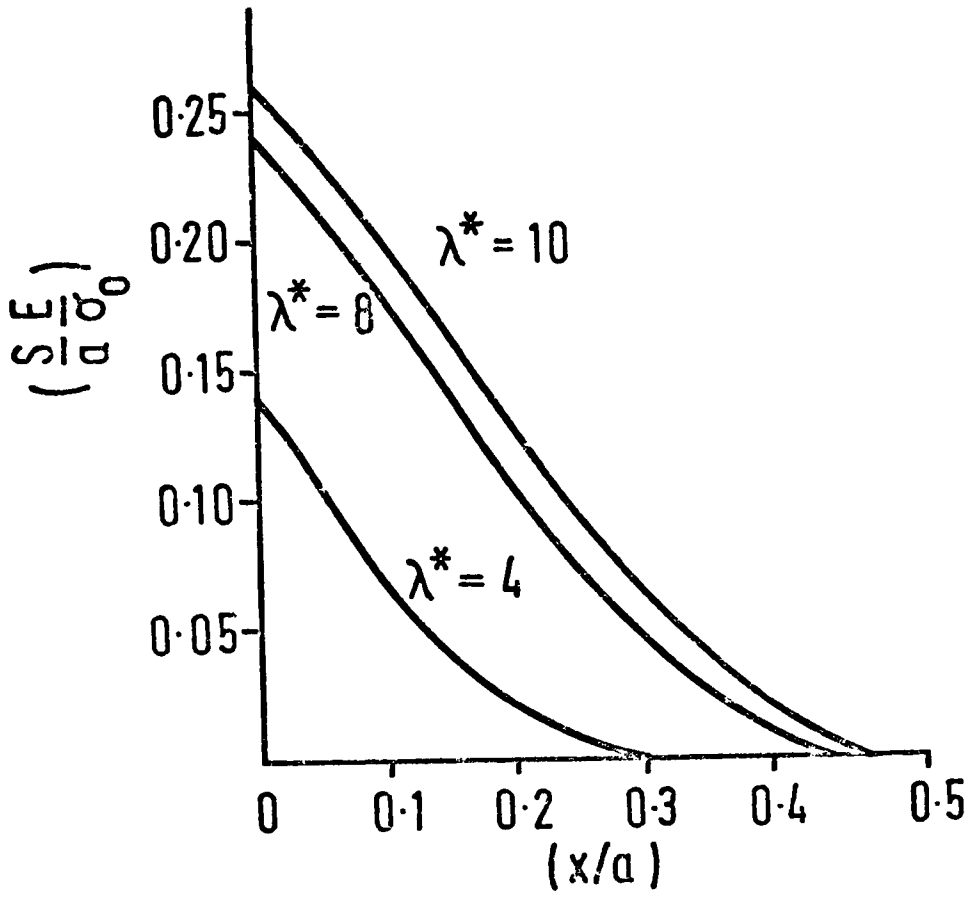


Fig. 7.24 Incomplete radius assembly, slip amplitudes

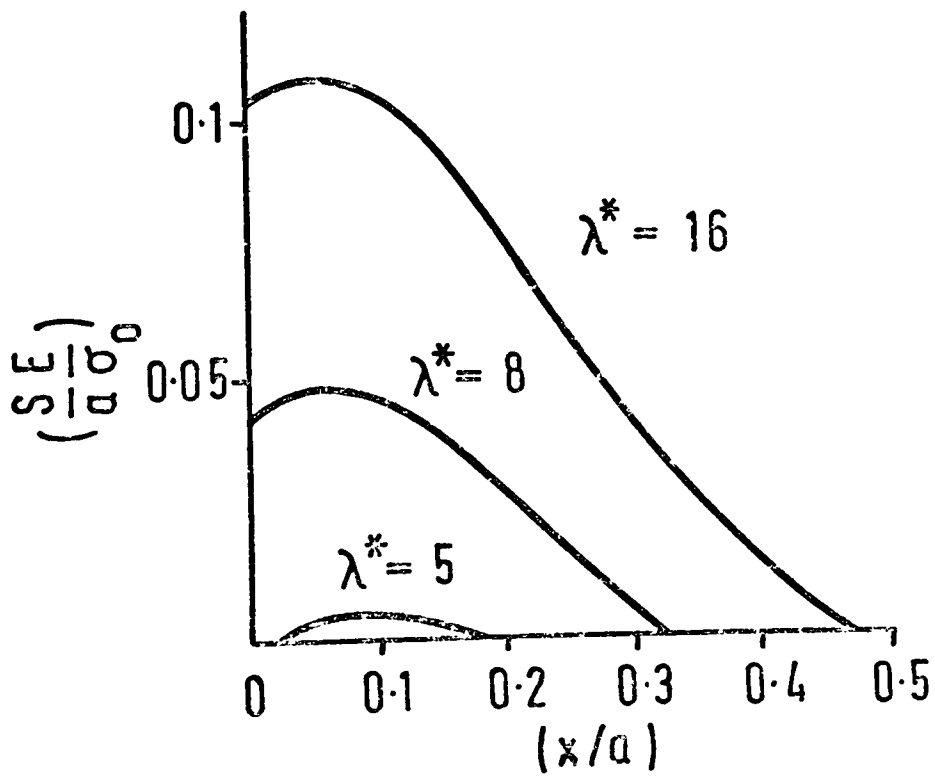


Fig. 7.25 Full radius assembly slip amplitudes

nominal axial and shear stresses there, will be lower for given values of λ^*, than the corresponding stresses in the flat plate of the sharp cornered assembly. Thus, as would be expected, the amplitudes of slip for the same value of λ^* are less in the radiused specimens than in those with sharp corners; considerably so for the fully radiused case. Of particular interest is the case of $\lambda^* = 5$ in the fully radiused case when slip is found to start from a point inside the interface leaving the outside edge of the interface unslipped. Even for higher values of λ^*, the maximum amplitude of slip does not occur at the edge of the interface.

Since the fatigue tests on radiused assemblies were carried out with the ratio of the nominal axial to nominal normal stress, in the region between the blocks, (ξ), equal to that in the sharp cornered case when $\lambda^* = 8$, it was necessary to determine the stress distributions in those cases. The values of λ^* corresponding to this situation are 10 and 16 for the incomplete and complete radiused assemblies respectively. The corresponding slip distributions are shown in figs. 7.24 and 7.25 and, as in the case of $\lambda^* = 8$ for the sharp cornered assembly, the region of slip extends over most of the interface.

Again the pattern of slip during compressive axial loading is very similar to that for tensile loading.

7.5.2 Stress distributions

The distributions of σ_x, σ_y and τ_{max}, on the interface of the incomplete and fully radiused assemblies, are plotted in fig. 7.26 and 7.27 respectively. The

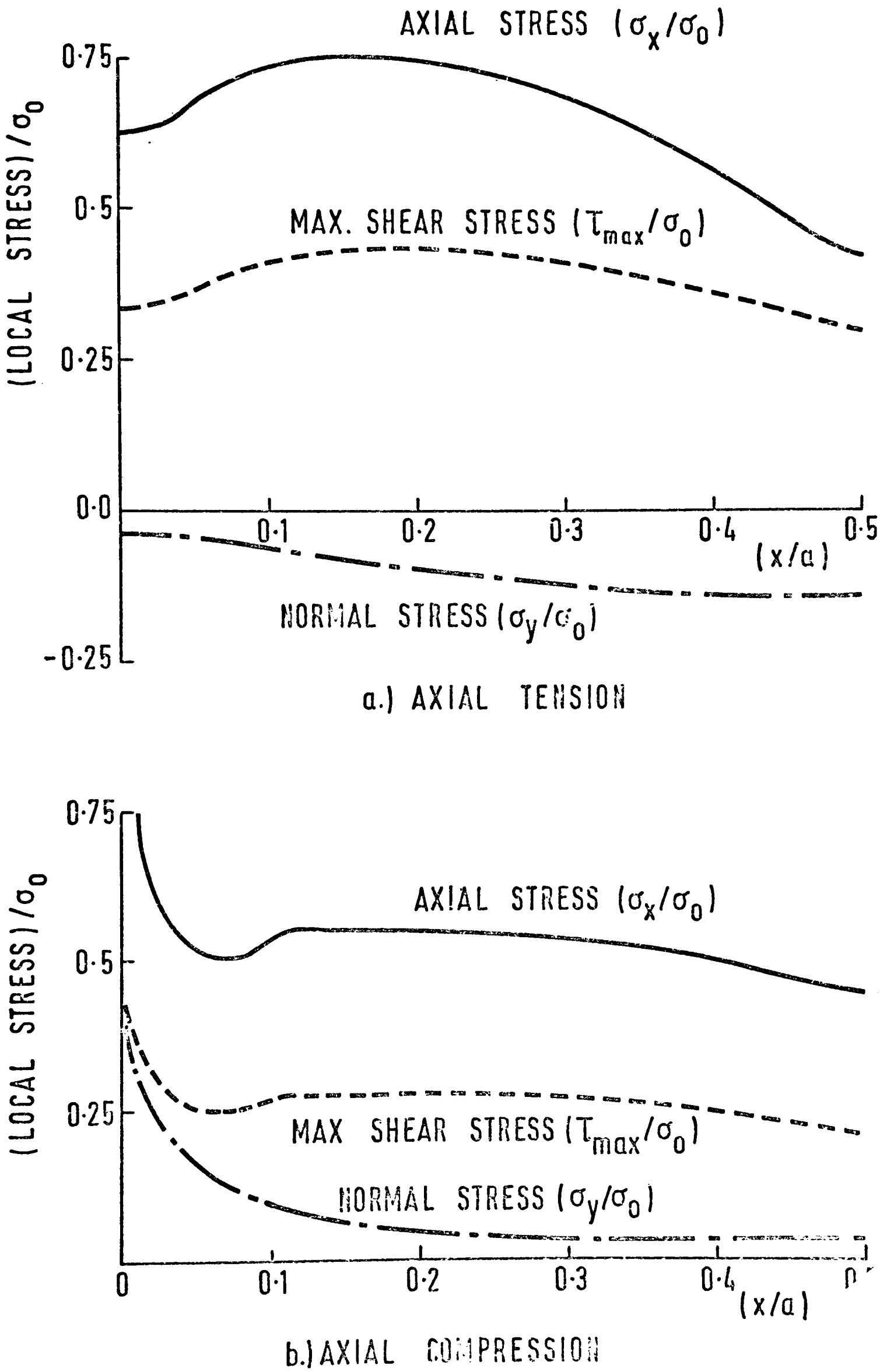
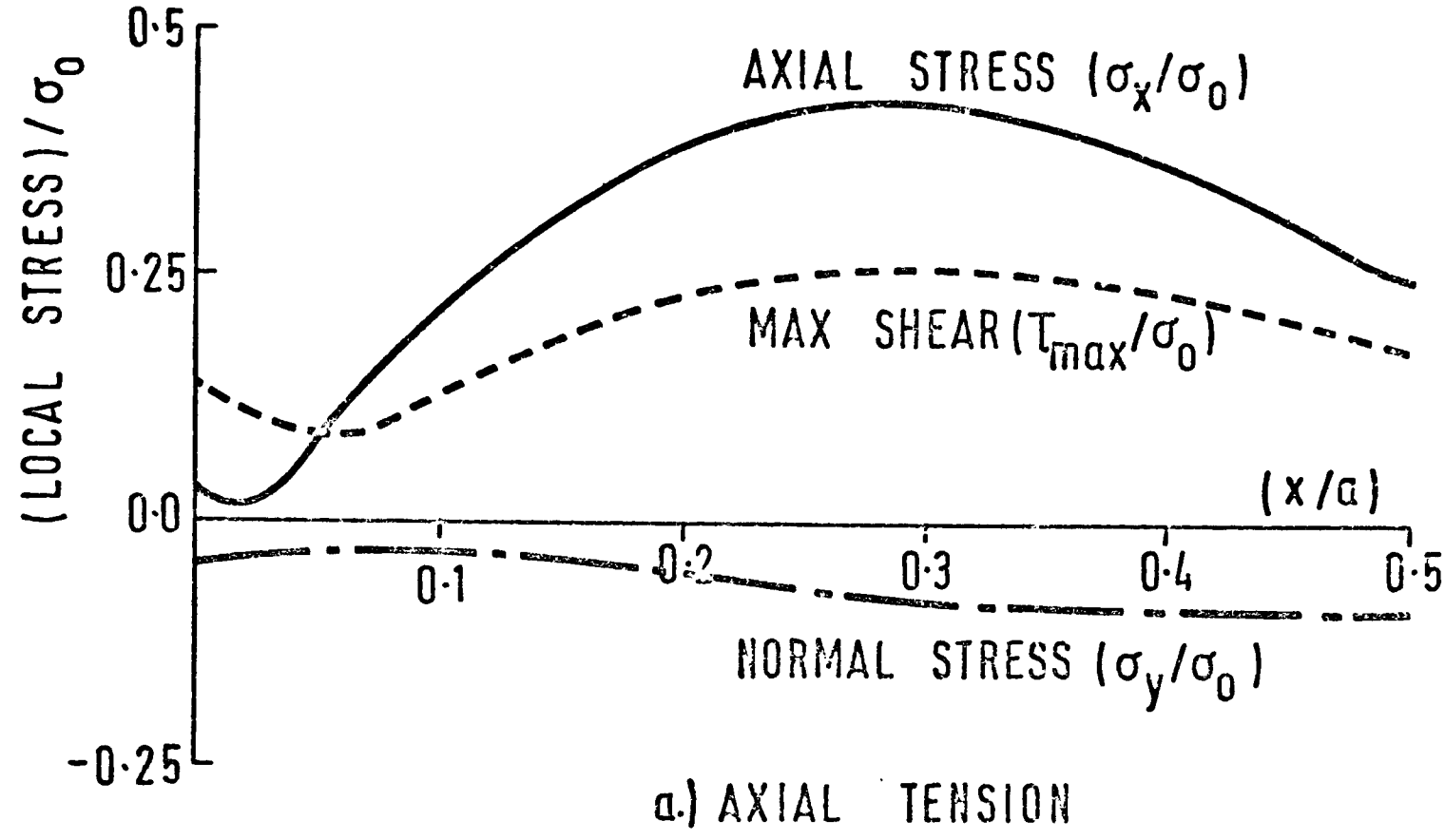


Fig. 7.26 Stress distributions in an incomplete radius assembly (λ = 10)



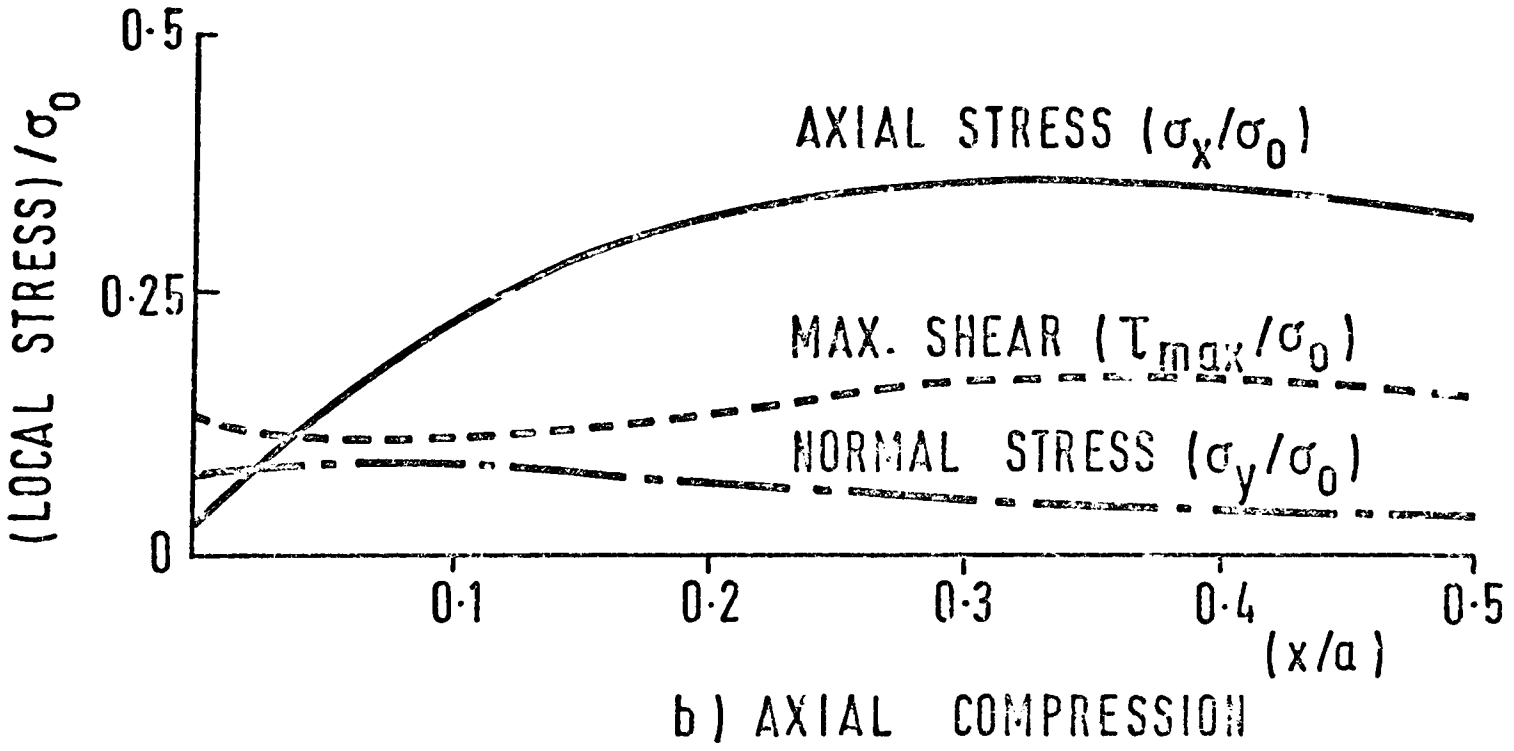


Fig. 7.27 Stress distributions in a full radius assembly (λ = 16)

values of λ^* are those corresponding to the experimental conditions (i.e. 10 and 16 respectively) and the distributions shown are those occurring at the instant of maximum tensile and compressive axial load (i.e. $\phi = 1$ and -1). As for the sharp cornered assembly, the values of stress actually refer to points a distance d below the interface, where d/t = 0.01 and 0.02 for the incomplete and fully radiused plate respectively. (t' is the thickness of the plate between the blocks.) All the stresses are non dimensionalised with respect to σ_o, the nominal axial stress away from the blocks.

The stress distributions require little comment. In the case of the incomplete radius, the stress concentrations which might have been expected at the end of the interface are not found during the tensile half cycle, the reasons being those already given in connection with the same phenomenon in the sharp cornered assembly. For the fully radiused case the distributions, qualitatively at least, behave much as expected, the axial and maximum shear stresses reaching maximum values about one quarter of the way along the interface. The normal stress is sensibly uniform over the whole interface.

7.6 DAMPING PROPERTIES OF ASSEMBLIES

Figs. 7.10 and 7.28 show load-displacement loops associated with the first 1¼ load cycles applied to the three assemblies investigated. The displacement, d_e, is the displacement of the point in the plate which is coincident with the corner of the block before any load is applied to the assembly. The area of each loop is

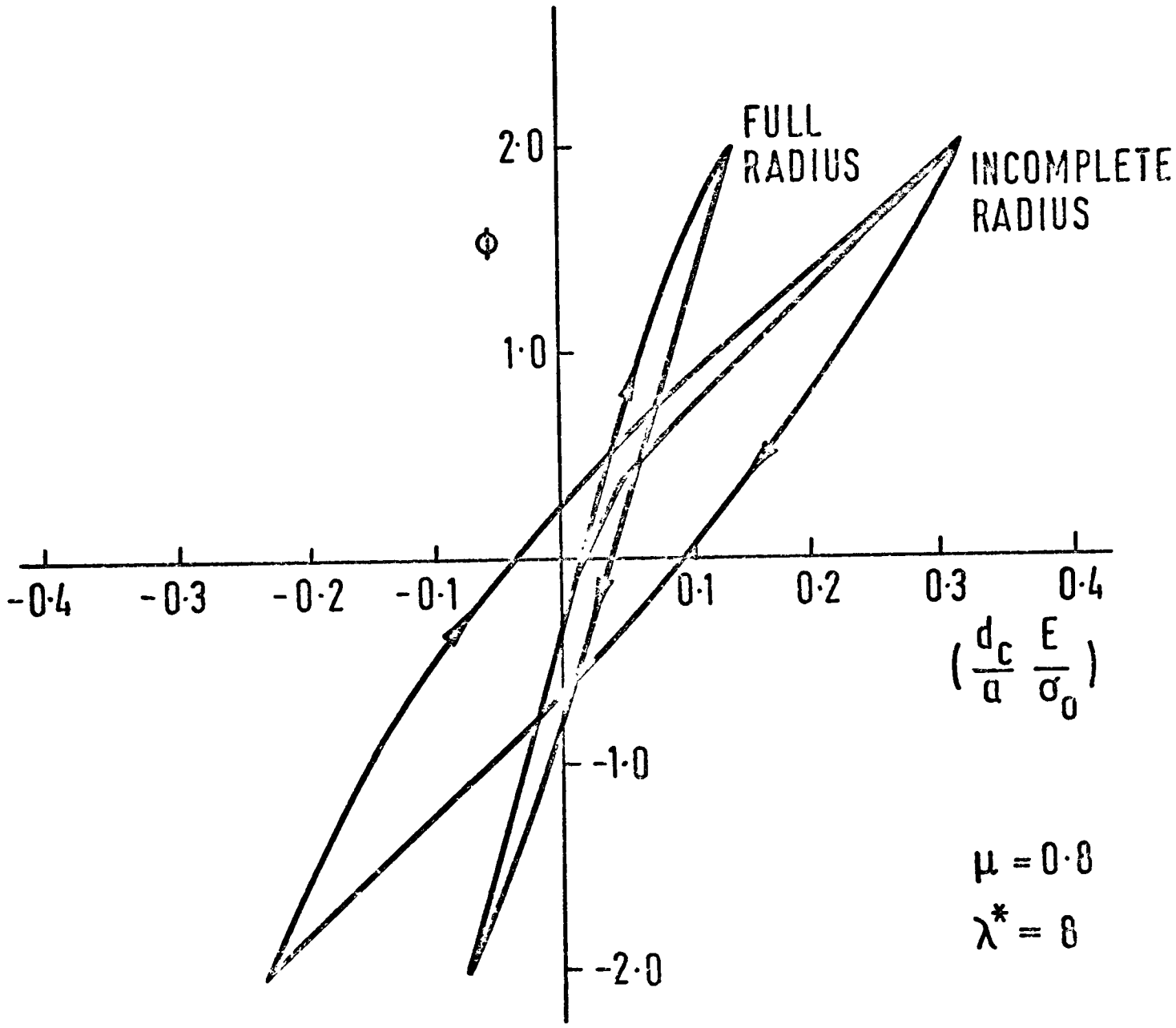


Fig. 7.28 Load-displacement loops for radiused assemblies

related to the frictional energy loss per cycle and indicates the clamping capacity of the assembly when subjected to a given system of loading. Unfortunately it is beyond the scope of this thesis to consider the damping properties of clamped assemblies except in a general qualitative sense. From fig. 7.10 it is seen that, as would be expected, increasing the clamping force in the sharp cornered assemblies reduces the damping by causing a reduction in the size of slip region and the slip amplitude.

For λ^* = 8 it is seen from fig. 7.28, that the damping capacity of the full radius assembly is less than that of the incomplete radius assembly and comparison with fig. 7.10 shows that both have damping capacities less than the sharp cornered assembly. Here again the damping capacity has decreased with the decrease in the size of slip region and slip amplitude, this time caused by the interface moving into a region of lower stress.

7.7 COMPARISON OF THEORETICAL SOLUTIONS WITH EXPERIMENTAL RESULTS

The number of experimental results, which can be directly compared to the theoretical solutions, is very small. However, where comparison is possible, agreement is good and inspires confidence in the theoretical work.

The comparisons which can be made fall into the following groups:

(1) Comparison of maximum shear stress distributions obtained theroetically with those obtained using photoelastic models.

(2) Comparison between the size of the slip region determined theoretically and that observed in the fatigue tests when the specimens were disassembled.

(3) Comparison between theoretically determined slip amplitudes and those measured during fatigue tests.

Referring to the first group, araldite models of the three types of assemblies were made and loaded in such a way that they represented the fatigue specimens at the moment of maximum tensile axial load with $\lambda = 8$. (Appendix 3.) The coefficient of friction in araldite was found, experimentally, to be about 0.2 and this figure was used to determine theoretically the maximum shear stress on the interface under these conditions. Corresponding values, obtained experimentally from the models, are shown plotted with the theoretical distributions in fig. 7.29. The agreement is extremely good.

Comparing the theoretical and experimental slip regions proved less satisfactory. The ground finish used on the mating surfaces in the fatigue tests did not show clearly the slip, no-slip boundary. However when the surfaces were polished and lapped before assembly the boundary was very easy to see. Fig. 4.16 shows the interface region of four such sharp cornered assemblies after running for 10^5 cycles at the same alternating axial load but at values of ξ of 8, 4, 2 and 1. The difference in size of slip region is plain to see and agrees well with theory.

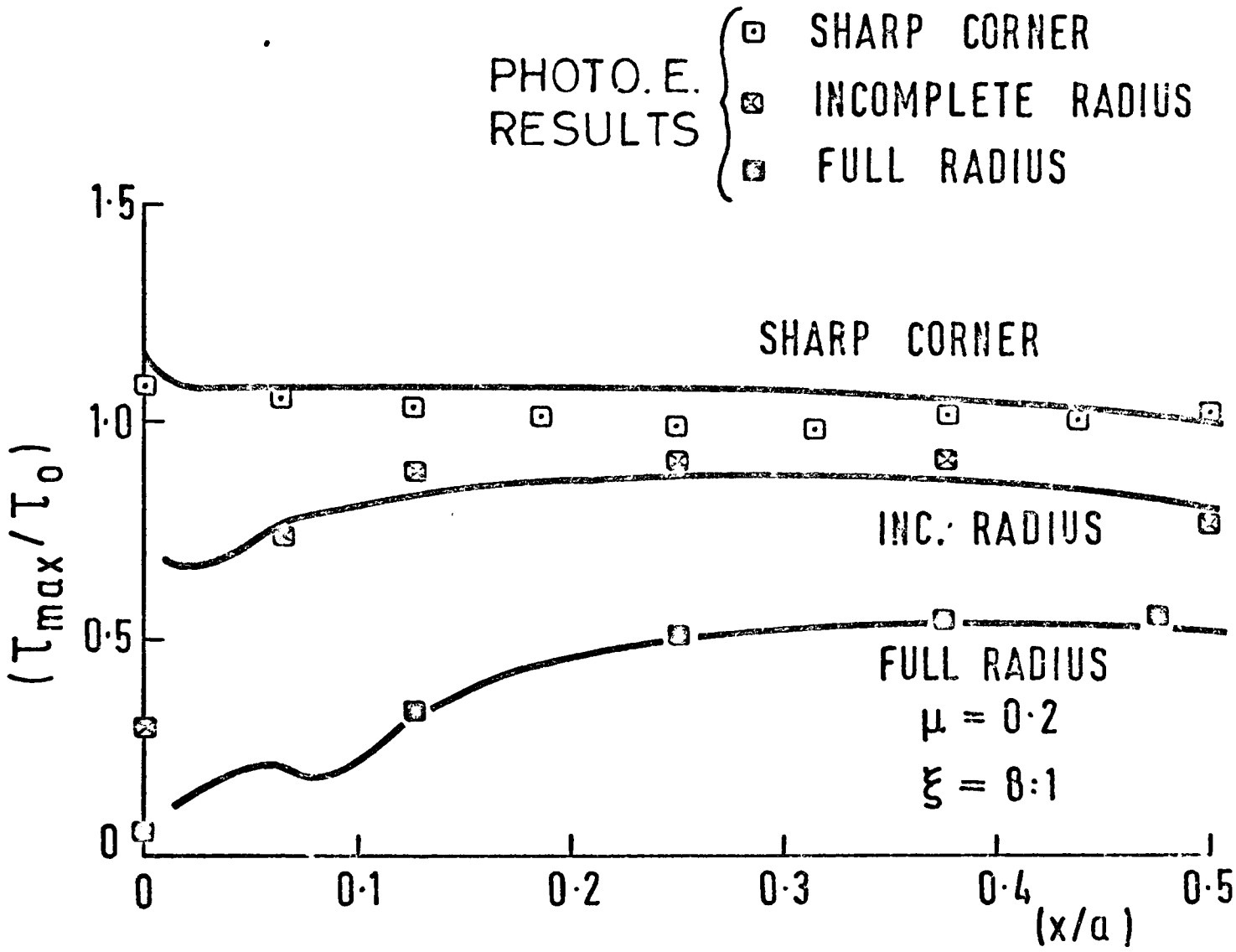


Fig. 7.29 Maximum shear stress determined photo-elastically and theoretically in sharp cornered, full and incomplete radiused assemblies

For the radiused assemblies, the theoretical and experimentally observed slip regions were again of similar size. In the full radiused assembly it was noticed that the heaviest fretting was a small distance from the edge of the interface where the theoretical results predict the largest slip amplitudes.

Experimentally determined slip amplitudes are plotted in fig. 7.30 along with the theoretical variations of slip amplitude for the three main types of assembly. Bearing in mind that the slip measurements were only thought to be accurate to within ± 15%, the agreement between theory and experiment is good.

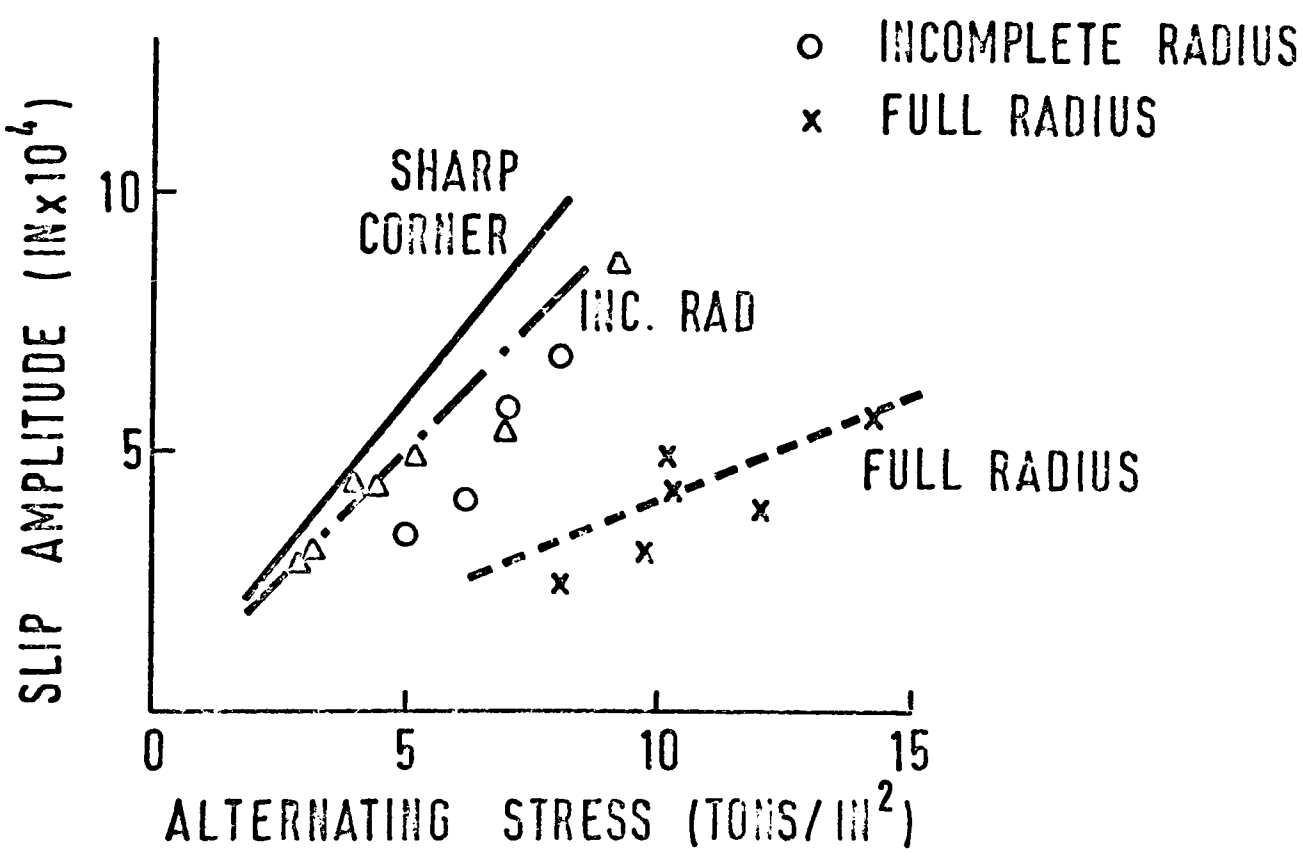


Fig. 7.30 Comparison between experimental and theoretical slip amplitudes

7.8 ASSESSMENT OF THE METHOD AND SOME GENERAL COMMENTS

In general, the method developed and described in this and the two preceding chapters was very successful. It produced (relatively) quickly the desired solutions to an extremely complex problem previously unsolved and probably intractable by analytic methods for a long time. Specifically, the main drawbacks were that the method could not give answers either right on the interface or right in the corners. Also, there was a tendency for the point values of stress to oscillate about the true solution, particularly in regions of high stress gradient. The first difficulty was largely overcome by use of a very fine mesh near the interface which also helped to overcome the second.

Choosing the correct mesh size and recognising the difference between oscillating solutions and true solutions which are changing rapidly, is largely a matter of experience, which can be gained quite quickly by solving a few standard problems.

Probably the feature of this method which will ensure its continued use for a long time is the ability to deal with arbitrary geometric shapes.

Commenting on the results and solutions worked in this chapter, the most surprising feature is certainly the occurrence of separation of the surfaces in the sharp cornered assembly under tensile axial load. As far as the author knows, this has never previously been predicted theoretically. However, the experimental results of the fatigue tests suggest that separation does occur

and an explanation for separation has been given which also explains the high tensile normal stress at the corner in the sharp cornered solid under similar loading. Because of separation the high stress concentrations which were expected in the sharp cornered assemblies do not occur. Without this theoretical analysis, an accurate interpretation of the fatigue results would therefore have been impossible and it is doubtful whether any specific conclusions about the causes or consequences of fretting could have been reached.

Chapter 8

DISCUSSION OF RESULTS AND A REVISED HYPOTHESIS TO EXPLAIN FRETTING FAILURES

8.1 INTRODUCTION

The results of the fatigue tests, described in Chapter 4, proved difficult to interpret because the stress distributions in the assemblies were not known. It had been thought that qualitative estimates of stresses in assemblies, based on photoelastic analysis of geometrically similar solids, would provide an adequate basis for the design of specimens and the subsequent analysis of the results.

When it became apparent that such estimates gave extremely inaccurate results, the theoretical analysis described in Chapters 5-7 was initiated. The theoretical stress analysis confirmed that the estimated stress distributions in assemblies were grossly inaccurate. High stress concentrations, which occur in solid components at rapid changes of section, need not occur in similar assemblies even when the interface of such an assembly is coincident with the region of stress concentration in the solid. It was, of course, expected that the assemblies would not exhibit the full stress concentration associated with the similar solid because of stress relief associated with slip. However, due to the phenomenon of separation described in Section 7.4.2, the stress relief is much greater than expected and stress concentrations in assemblies may be negligible even when there are rapid changes in section. For this reason, the fatigue behaviour of geometrically similar solids

and assemblies may be very different.

In the tests described in Chapters 3 and 4, solid specimens always failed at the point of highest stress. The bulk stress at which failure occurred could be predicted (with certain provisos if the stress concentration was high) from the unnotched fatigue strength of the material and the theoretical stress concentration factor. Assemblies, on the other hand, often failed from points where there was no apparent stress concentration, at stresses considerably lower than the fatigue strength of the material. However, in all such case, the failure originated in a region of fretting.

The theoretical stress analysis confirmed the lack of stress concentration at the origin of such fretting fatigue failures. For example, in the sharp cornered assembly with $\lambda = 8$, the theoretical stress concentration at the origin of failure, at the instant of maximum tensile load, was only 1.07 and yet the bulk failure stress was less than $\frac{1}{3}$ of the fatigue strength of the material.

Initially, it had been assumed that high strength reductions associated with fretting fatigue were due to stress concentrations associated with the overall geometry of the assembly. The theoretical analysis showed that this was not so and the only alternative explanation was that fretting substantially reduces the fatigue strength of a material.

The results of the fatigue tests of Series 3, in which fretting was applied in the absence of a propagating stress, showed that the strength reducing effect of

fretting is not a result of the damage to the surface which characterises fretting. Indeed, even without the results of Series 3, it would be difficult to believe that such surface damage could result in fatigue strength reduction factors as high as 3. The roughest surface finish rarely reduces fatigue strength by a factor greater than 1.5.

Having established that fretting applied in the presence of a propagating load can cause large strength reductions it is useful to determine the magnitude of such strength reductions. From the results of the fatigue tests and the theoretical stress analysis of various assemblies, estimates can be made of the stress at the origin of the fretting failures. In Section 8.2 the magnitude of these stress are compared with the fatigue strength of the material to obtain values of the strength reduction factor due to fretting.

In Section 8.3, the original hypothesis is examined in the light of the theoretical and experimental results and, although supported by some results, is found to be an inadequate explanation for fretting fatigue in general. The contact stresses associated with discontinuous contact are discussed quantitatively in Section 8.4 and a revised hypothesis, based on a consideration of such stresses, is proposed in Section 8.5. The remaining sectionsconsider evidence in favour of the new hypothesis and its consequences; finally section 8.10 summarises the conclusions drawn from this investigation.

8.2 STRENGTH REDUCTION FACTORS ASSOCIATED WITH FRETTING

The results of this investigation showed that fretting applied in the presence of a propagating load, but remote from any geometric stress concentration, can cause failures at stresses well below those normally required for fatigue failure. It would be useful to evaluate exactly the strength reduction caused by fretting. The tests of Series 4 were designed for this purpose. However, as explained in Section 4.5, strain gauge readings showed that the stress at the point of failure was varying about a non zero mean stress, thereby implying that the normal stress also was varying. Consequently, the variation of maximum shear stress, on specimens of this type, can only be estimated very crudely. (The use of strain gauge rosettes to measure the shear stress is ruled out because of the localised nature of the stress of interest and the presence of the interface.)

The stresses in specimens of Series 4 are therefore no less complex and uncertain than those of the radiused assemblies in Series 1. However, for the specimens of Series 1, the stress distributions were analysed theoretically and are plotted in Chapter 7. (Similar calculations for specimens of Series 4 were not possible in the time available because the problem is no longer a plane problem and has lost one axis of symmetry.) Figs. 7.26 and 7.27 show the stress distributions in the full and incomplete radiused assemblies when the coefficient of friction is 0.8 and the ratio of nominal axial stress on the interface to the mean normal pressures is 8:1; these are the conditions

under which the tests were run. Failure of both types of radiused assembly, when it originated on the interface, did so from a point coincident with the point of maximum theoretical stress. This suggests that the theoretical stresses are closely representative of the actual stresses set up during testing.

From the theoretical results and the experimental fatigue limits it is possible to estimate the value of the strength reduction factor (K_f) due to fretting. K_f, based on both axial stress and maximum shear stress was calculated by comparing the theoretical semi-range of stress at the origin of failure in various assemblies with the fatigue strength of the material. Such calculations are only reliable if the stress gradient near the origin of failure is low. When that is the case slight errors in selecting the position of the origin of failure do not affect, significantly, the calculated value of K_f. For this reason, the results of the sharp cornered assembly were not used to determine K_f due to fretting. In that case, the stress gradient at the corner, during the compressive half cycle of loading is very high.

Values for K_f due to fretting, calculated in the manner described above from the results for the two types of radiused assembly, are tabulated in Table 8.1 along with the theoretical values of the mean axial stress at the origin of failure. Additional values, estimated from the results of Series 4, are also shown, For the Series 4 specimens the axial stresses are calculated from the measured strains and the maximum shear stresses were

estimated assuming that, at the origin of failure, the normal stress is equal to its mean nominal value. From the theoretical stress determinations for other geometries, it is clear that the normal stress at any point will vary during a cycle. However, the variation is not predictable with any accuracy in the specimens of Series 4 and the nominal value is taken as a first approximation. Since the nominal value of the normal stress is only $\frac{1}{8}$ of the nominal peak axial stress, changes in the value of normal stress have a second order effect on the maximum shear stress. (N.B. Change in normal pressure greatly affects the axial stress. However changes in axial stress are measured by the strain gauges.)

Table 8.1

Strength Reduction Factors due to Fretting

Specimen Type	Mean Axial Stress tons/in^2	K_f based on	
		σ_x	τ_{xy}
Full Radius	+ 0.39	2.6	2.6
Inc. Radius	+ 0.50	3.1	2.9
Series 3	+ 0.60	3.6	3.4

From the results tabulated in Table 8.1, it seems that fretting applied in the presence of a propagating stress can reduce fatigue strengths by a factor as high or higher than 3. The difference between the values of K_f obtained from different specimens is hard to explain. The value of K_f increases as the mean axial tension increases but, although mean stress is known to affect

fretting fatigue strength greatly (7), (22), the magnitude of mean stress in all the specimens is very low. From graphs of fretting fatigue strength against mean stress (7) it appears that an axial mean stress of 0.6 tons/in^2 would reduce the fretting fatigue strength by less than 9%. This variation in mean stress is clearly not the only cause of the difference in values for K_f in Table 8.1.

Other factors which might affect the fatigue strength, such as amplitude of slip, normal pressure and size of slip region, are reasonably constant for all three types of specimens.

It seems most likely, therefore, that the major difference in the results for K_f due to fretting obtained from different specimens is due to differences between the calculated or estimated stress at the origin of failure and that which exists in practice. Such differences are due to the assumptions which are made in order to make the calculation possible. In all calculations, the coefficient of friction was assumed to be 0.8 over the whole interface which is unlikely to be true in practice. It is known that the coefficient of friction changes as fretting occurs and examination of interfaces after several thousand cycles of reversed slip shows regions where slip has occurred without causing serious fretting. In such regions the coefficient of friction is probably much less than in regions of severe fretting. For specimens of Series 4, the estimated stress at the origin of failure is, clearly, only approximate.

Summing up, it seems that fretting which occurs on the surface of a component in which there is a bulk

propagating stress can cause strength reduction factors which may be as high or higher than 3. Most instances of such strength reductions cannot be explained in terms of stress concentrations associated with the overall geometry of the assembly.

8.3 A REVIEW OF THE HYPOTHESIS PROPOSED IN CHAPTER 1 IN THE LIGHT OF EXPERIMENTAL RESULTS

Many of the experiments, carried out in the course of this investigation, showed that fretting fatigue failures could occur in fretting regions remote from any obvious geometric stress concentration. At the same time the tests of sharp cornered assemblies with high clamp loads suggested that, in certain cases, failure could be due, primarily, to geometric stress concentration even in the presence of fretting which was at most a secondary cause of failure (Section 4.6).

Tests described in (23,24,25), in which flat specimens were fretted by cylinders, resulted in fatigue strength reductions (based on the nominal stress in the specimen) which could be related quantitatively to the theoretical stresses in the contact region formed by the cylinder and the specimen. That is to say, failure occurred when the external loads were such that the peak stress in the contact region was approximately equal to the fatigue strength of the material. Furthermore the origin of failure coincided with the point of maximum stress and the inclination of fatigue cracks to the surface was consistent with the principle stress directions. Similar results were obtained by O'Connor and were mentioned in Chapter 1.

It appears that, in certain circumstances, particularly when the contact area is small, the so-called fretting fatigue strength of an assembly can be predicted from a knowledge of the macroscopic stress fields in the contact region. That fretting fatigue strength was a function of macroscopic stress concentration was the central theme of the original hypothesis. However, while that hypothesis may explain certain fretting fatigue failures, it clearly does not explain them all. It is proposed to put forward a new hypothesis which explains all the fatigue results so far discussed.

8.4 STRESS CONCENTRATIONS ASSOCIATED WITH DISCONTINUOUS CONTACT

When surfaces are initially pressed together, contact is assumed to occur only on a relatively small fraction of the total nominal contact area, the normal load being carried only on surface asperities. In Chapter 1, it was suggested that this situation will give rise to two types of stress concentration; the microscopic stress concentrations associated with the individual contacting asperities and the macroscopic stress concentration associated with the overall geometry of the assembly. Because of the extremely small size of an asperity, the associated microscopic stress concentrations can almost certainly be neglected when considering the fatigue behaviour of the assembly. However the above arguments fail to consider the effect of oscillating relative slip on the size of the contact regions. In (11), experimental evidence is given which suggests that, with the onset of slip, asperity contact is immediately replaced by contact on r elatively

larger areas. It is reasonable to suppose that these larger areas of contact will coincide with the peaks formed by the large scale waviness of the surface (16,44). An approximation to the stresses which may arise from contact of this nature can be gained by considering a block with a rough surface pressed against a perfectly flat plate (Fig. 8.1). Due to loads applied to the plate, the surfaces of the plate and the block experience relative slip.

One contact region can be likened to a cylinder of radius R being pressed into the surface of a half space with force P and loaded tangentially with force T, which is of such magnitude that the cylinder is sliding relative to the plate; i.e. $T = \mu P$, where μ is the coefficient of friction (fig. 8.2). If it is assumed that, even in the presence of the tangential load T, the normal pressure will be distributed in Hertzian fashion in the contact region, the following expressions are obtained:

$p_o = 2P/\pi a$ where 2a is the width of the contact area and p_o the maximum normal pressure.

$2a = \sqrt{8RP\ (1-\nu^2)/\pi E}$ where ν and E are Poissons ratio and Youngs modulus.

For this situation, the axial stresses on the contact surface can be calculated from the following equation obtained by Poritsky (35) or Smith and Liu (45):

$$\sigma_x/P_o = -2\mu(x/a) - \sqrt{1-(x/a)^2}$$

For completely reversed tangential loading and slip, the range of stress at x = - a (the edge of the contact region) is given by $4\mu p_o$, the mean stress there being zero.

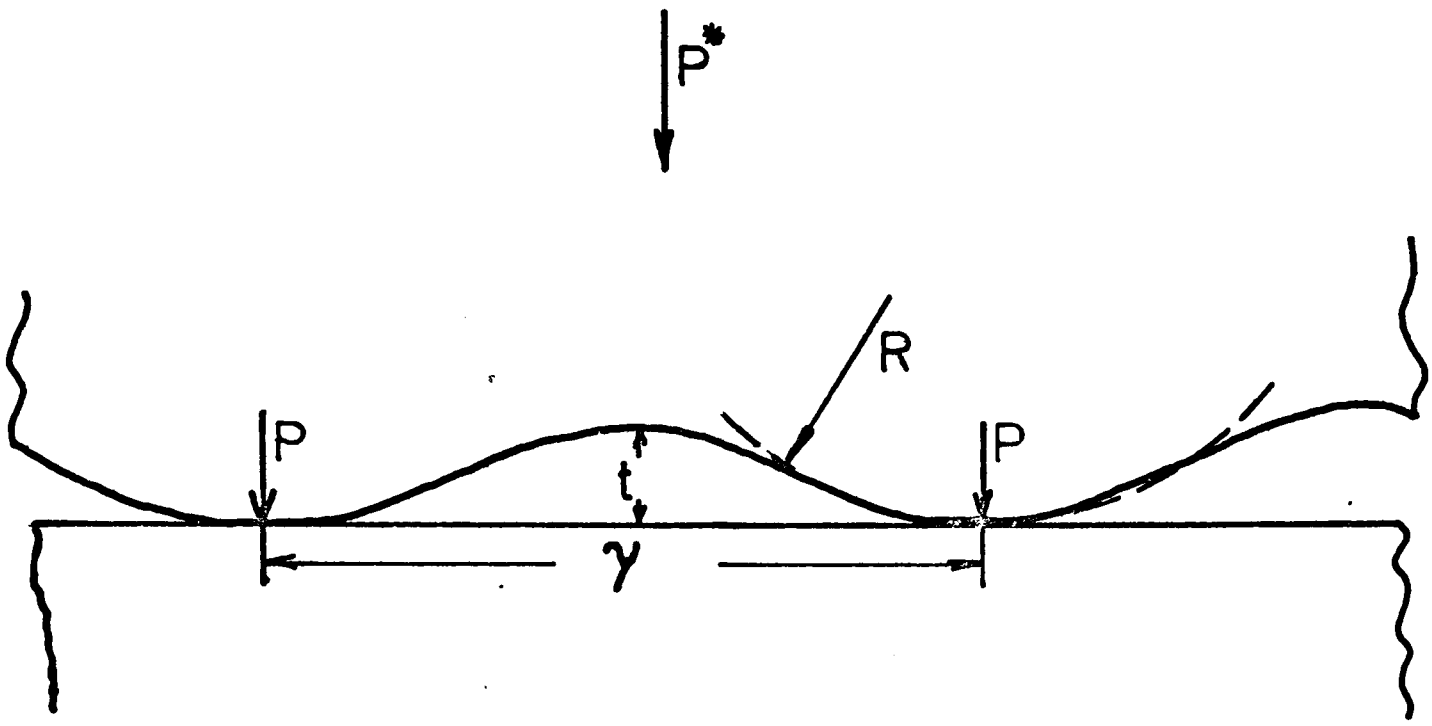


Fig. 8.1 An idealised model of surfaces on which contact is discontinuous

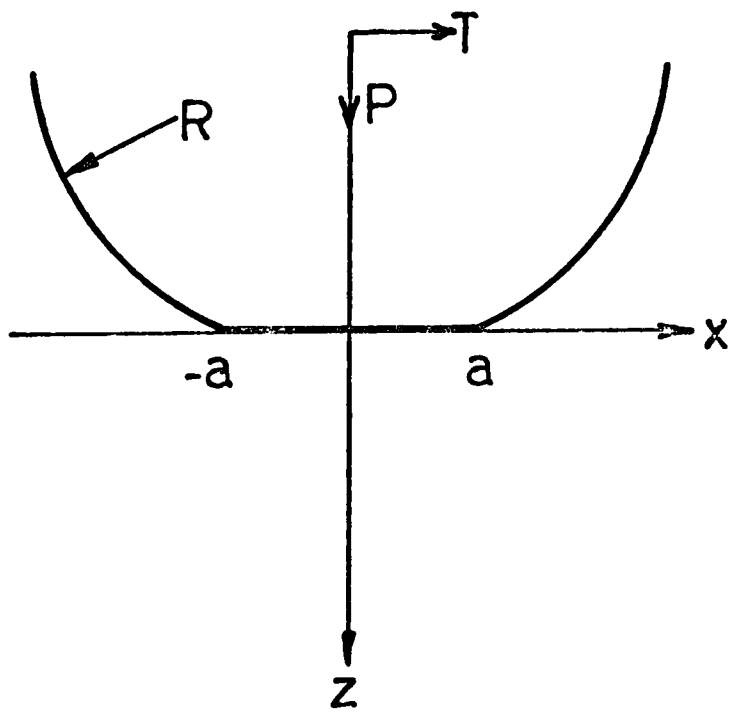


Fig. 8.2 A cylinder indenting a flat surface

This analysis can be applied to the contacting surfaces in fig. 8.1. The normal force (P) at each point of contact is equal to

$\gamma \frac{P^*}{l}$ where l is the total nominal contact length,

P^* the total normal force and γ the wavelength of the surface waviness.

If the slip is caused by strain in the plate due to a nominal axial stress in the plate (σ_a) and the ratio of σ_a to the nominal normal stress is ξ, then

$$P^* = \frac{\sigma_a \, l}{\xi}$$

and

$$P = \gamma \frac{\sigma_a}{\xi}.$$

For $\gamma \gg t$, the equivalent radius, R, is approximately given by:

$R = \frac{\gamma^2}{8t}$ where t is the peak to peak amplitude of surface waviness.

The maximum range of axial stress at the edge of the contact region is given by:

$$\sigma_R = 2\sigma_a + 4\mu p_o$$

and the axial stress concentration factor K_t, based on the nominal axial stress, is given by:

$$K_t = 1 + 2\mu p_o / \sigma_a$$

Substituting the expression for P and R into the expressions for p_o and 2a and then substituting for p_o into the expression for K_t gives:

$$K_t = 1 + 8\mu \left(\frac{t}{\gamma \cdot \xi \cdot \sigma_a \cdot \pi \cdot k}\right)^{\frac{1}{2}} \qquad 8.1$$

where $k = (1 - \nu^2)/E$

As an example, taking values of ν and E as those of L65 (i.e. $\nu = 0.32$, $E = 10.7 \times 10^6$ lbs/in^2) and a

value of μ of 0.8, as was found experimentally, values of K_t can be determined for various surface conditions. If σ_a is taken to be 7,000 lbs/in^2 (roughly the fretting fatigue limit of L65) and ξ equal to 8 (as in most of the tests in this investigation), the values of K_t, determined for $t = 10^{-4}$ inches and $\gamma = 10^{-1}$ and 10^{-2} inches, are 2.6 and 6.1 respectively. The respective contact widths are 16×10^{-3} and $.5 \times 10^{-3}$ inches.

Clearly the model used to arrive at the above values of K_t is very approximate. It might be argued that contact will occur at points randomly distributed over the interface rather than in accordance with a wave pattern, as shown in fig. 8.1. In that case the contact areas would tend to be circular rather than rectangular and the contact would be akin to spherical rather than cylindrical contact. However one would expect stress concentrations of a similar order of magnitude to those calculated for cylindrical contact.

It seems, therefore, that discontinuous contact due to large scale waviness of surfaces (as distinct from asperities) can give rise to axial stress concentrations, when the surfaces slip, which are high enough to explain the strength reductions associated with fretting. What is more (unlike asperity contact) the size of associated contact areas is such that the contact stress field affects a sufficiently large volume of material for it to influence fatigue behaviour.

8.5 A NEW HYPOTHESIS TO EXPLAIN FRETTING FATIGUE FAILURES

It is now suggested that so-called fretting fatigue is due to the following mechanism. When surfaces are pressed together and undergo relative slip, contact initially occurs at a large number of small contact areas. Associated with each contact area there is a high stress concentration but, because the volume of material affected by the high stress is very small, such stress concentrations only result in small, non propagating cracks and the damage to the surface which typifies fretting. As fretting and wear continues and the surfaces bed-in, the areas of contact grow fewer but larger in area. The magnitude of the stress concentration associated with each contact region falls as the contact areas increase in size but the volume of material within the contact stress field increases. The length of the cracks formed within the contact regions therefore increase and eventually are of sufficient length to be propagated by the bulk stress in the component. The results of fretting fatigue tests indicate that the critical size of contact area required for complete failure has associated with it a stress concentration factor of the order of 3. (This figure may only apply for L.65.) In the following discussion, the stress concentrations associated with the relatively large contact within the nominal contact region will be referred to as macro-micro stress concentrations.

It should be noted that the above explanation for fretting fatigue is very similar to qualitative explanations expressed (at least in private) by J.E. Field, co-author

of (7,8,9,10). Section 8.4 provides quantitative support for such a hypothesis.

8.6 EVIDENCE IN SUPPORT OF THE NEW HYPOTHESIS

There is a certain amount of experimental evidence to support the hypothesis proposed in the previous section. When fretted surfaces are examined, they are found to be extremely rough, and contact at any given time is clearly only occurring within a number of discrete areas. This is the condition required for the generation of large contact stress on the interface. (N.B. It is thought that, although the initial areas of contact coincide with the large scale waviness of the surface, subsequent discontinuous contact may also be caused by the formation of fretting pits.)

A further experimentally observed phenomenon also supports the hypothesis. Microscopic examination of sections taken through fretted areas such as those described in Section 4.8 always show the fatigue cracks leaving the surface in a direction inclined at an angle of between 30^{o} and 60^{o} to the surface.

In (25) the angle at which fatigue cracks leave the surface is compared to, and found consistent with, the direction of principle stress at the point at which the crack originates. The contact in (25) is between a flat specimen and a cylindrical fretting pad which is the model on which the explanation of fretting fatigue was based. It appears, therefore, that the experimentally observed angles at which fatigue cracks leave fretted surfaces are consistent with this model.

In addition to the above mentioned evidence, the hypothesis proposed in the previous section would suggest that the following phenomena should be observed in fretting fatigue tests.

1. The contact areas take time to reach the critical size for which the combination of stress concentration and size effect is the most damaging. Therefore the strength reduction due to fretting should increase with the duration of the fatigue test. This is observed in all the fretting fatigue tests carried out in this investigation. The strength reduction due to fretting is roughly twice as great for failure at 10^6 cycles as it is at 10^5 cycles.

2. The rate at which contact areas grow is related to the rate of wear. This in turn is related to the amplitude of slip. Therefore, for zero amplitude of slip, one would expect to find no strength reduction and for finite amplitudes of slip one would expect to find that the strength reduction, for a given number of cycles, increases as slip amplitude increases. Fretting fatigue tests with different slip amplitudes (7) show fatigue strength falling as the slip amplitude increases. (Above a certain slip amplitude, the fatigue strength starts to increase again but this is thought to be due to embryonic fatigue cracks being destroyed by rapid wear before they can start to propagate.)

3. The effect that the macro-micro stress concentrations have on fatigue strength depends upon the volume of

material within the contact stress field. The fatigue strength of an assembly begins to be reduced by fretting when the size of the macro-micro stress fields is significant compared with a typical dimension of the assembly. Thus, other parameters being equal, one would expect that for a given number of cycles, the fatigue strength of larger components would be reduced less by fretting than that of smaller components. There were no tests in this investigation in which the specimen size was altered. However, references such as (29) describe full scale tests on collar and shaft assemblies which indicate that strength reduction factors due to fretting having a value close to 2 are normal under those conditions. Unfortunately, it is rare, in reports of such fatigue tests, to find a detailed analysis of the theoretical stress at the origin of failure. As a consequence, it is difficult to determine the strength reduction due to fretting. However, from the evidence available, it does appear that the effect of fretting on fatigue strength decreases as the component size increased.

8.7 THE COMBINED EFFECTS OF FRETTING AND GEOMETRIC STRESS CONCENTRATION

In the preceding sections, a possible explanation for fretting failures has been proposed. It is suggested that fretting fatigue is due to stress concentrations which are associated with the discontinuous contact between surfaces undergoing relative slip. It is interesting to consider the additional effect of geometric stress concentrations which are due to the overall shape of the assembly.

Very little information is available on the effect of superimposed stress raisers. However, the strength reduction associated with fretting (i.e. with the macro-micro stress concentrations) is relatively high and it is known that, above a certain limit, increase in stress concentration ceases to lower the fatigue strength (32). This phenomenon is known as the size effect. For instance, the sharp cornered solid specimens of Series 1, in which the stress concentration is theoretically infinite, showed a strength reduction factor of only 3.5 (see Section 4.2.1).

If, then, the additional geometric stress concentration affects a volume of material of equivalent size to that affected by the macro-micro stress fields, significant additional fatigue strength reduction is unlikely although failure will probably originate at the geometric discontinuity. (e.g. the sharp cornered assembly of Series 2.) However, if the geometric stress raiser has a typical dimension such that it raises the stress within a region which is much larger than that influenced by the macro-micro stress fields, the strength reduction factor based on the nominal stress will be greater than that due to fretting alone.

The relative size of the regions affected by fretting and geometric stress concentration, and their effect on fatigue behaviour, is largely determined by the proportion of the interface on which slip occurs. If slip occurs on a small proportion of the interface, it implies that the stress relief due to slip is small. Consequently, the fatigue behaviour is determined principally by the stress

fields associated with the geometry of the assembly. (e.g. Series 5 when $\xi = 1.$)

If the slip region is large, there are two possibilities. Firstly, if the normal pressure distribution is affected by the fatigue load, as in the tests carried out in this investigation, the geometric stress concentration may be drastically reduced and the reduction in fatigue strength of the assembly is then almost entirely due to fretting. Alternatively, if the normal pressure is not influenced by the fatigue load, as in the case of a torque applied to an axisymmetric shrink-fit assembly (see Section 8.9), the stress concentration due to geometry may still be relatively high, even though the slip region is extensive. In such a case, the effects of fretting and geometric stress concentration may be additive although the fatigue strength may not fall much below that associated with fretting alone, due to the size effect. An investigation of the second situation is proposed as a topic for further work in Section 8.9.

A further possibility, if the geometric stress raiser is high, is that it may result in high residual stresses following yielding during the first few load cycles. In that case, the propagation of the fretting fatigue cracks may be affected by the residual stress and the strength reduction factor will change accordingly.

8.8 SOME CONSEQUENCES OF THE NEW HYPOTHESIS

In Chapter 1, it was suggested that, if fretting failures are due to geometric stress concentrations associated with the overall shape of an assembly, the

fatigue strengths of solids and assemblies of the same overall shape should be similar and could both be improved by geometric stress relief such as fillet radii. It is clear now that this is not necessarily true. Fretting can result in strength reduction factors of up to 3 and assemblies are quite often much weaker than a similar solid. (e.g. the incomplete radius specimens fig. 4.6.) Geometric stress relief will be beneficial if it moves the interface into a region of lower stress but, unless such a change eliminates slip, the stress on the interface must be no greater than $\frac{1}{3}$ that of the highest stress elsewhere in the assembly if a fretting failure is to be prevented.

A further point raised in Chapter 1 was a criticism of methods of evaluating fretting fatigue strength, typified by the work of Field et al (7,8,9,10). It was argued that, using fretting blocks with small 'feet' at either end resulted in a complex contact stress field which confused the results. However, tests of this type carried out in Series 6 resulted in a strength reduction factor of 2.6 and it appears that the results of such tests give good indications of the strength reductions associated with fretting. The contact area in such tests is comparable to that between a cylinder and a flat plate and probably results in similar stress distributions.

The advantages of such a method are several. With such a small contact area, the normal pressure distribution cannot be greatly affected by the axial loading and the bulk axial stress is not significantly modified by the

shear transmitted across the interface. The bulk stress which ultimately causes the fretting fatigue crack to propagate is therefore known quite accurately and effectively fluctuates about a zero mean. (Assuming of course that there is no externally applied mean load.) By changing the block length, slip amplitude can be carefully controlled and is independent of the area of fretting. However, in view of the arguments used to explain fretting fatigue failures, the test might be improved if the flat fretting pads were replaced by pads having cylindrical surfaces.

8.9 SUGGESTIONS FOR FURTHER WORK

Further work in which specimens are fretted by pads having cylindrical or spherical surfaces would provide useful results. It has been argued that contact of this type is typical of situations in which the nominal contact area is much larger, although in those situations, the equivalent radius of the contacting surfaces is very large. It would be interesting therefore to observe the change, if any, in fatigue strength with changes in the radius of the fretting pads and hence the contact area. Also, further investigation of the effect of slip amplitude and normal pressure could yield useful results. With small contact areas, parameters such as these can be varied virtually independently. The results of all such tests would be analysed in the light of associated contact stress analysis.

It would also be interesting to investigate the combined effects of fretting and a severe geometric stress

concentration. Using plane specimens under axial or bending loads, such an investigation is difficult due to the coupling between the normal stress distribution and the axial stress. For instance, in the sharp cornered tests of Series 1, the application of tensile load caused the surfaces of the block and specimen to separate at the corner, thus eliminating the expected stress concentration. When the normal load was increased sufficiently to prevent separation, the slip was reduced to such an extent that fretting was minimal (Series 5). A test in which severe fretting and geometric stress concentration should occur together is the torsional fatigue test of a collar and shaft shrink-fit assembly. The torsional loading will not modify the original shrinkage stresses and it is thought that a large stress concentration will occur at the corner.

The partial relief of the stress concentration by slip will result in fretting occurring just inside the contact region. For the results to be interpreted quantitatively, an associated stress analysis would have to be carried out. Methods similar to those used to analyse the plane stress problems in this investigation could probably be used.

8.10 CONCLUSIONS

1. Fretting applied in the presence of a propagating stress can result in large reductions of fatigue strength, even in the absence of an obvious geometric stress concentration.

2. Associated with fretting which is caused by cyclic loading about zero mean load, there will be a strength reduction factor at the fatigue limit which may be as high as 3. (N.B. This figure was determined using Aluminium alloy L-65.)

3. Strength reductions due to fretting are explained by considering the effect of discontinuous contact between components of an assembly and the high (macro-micro) concentrations of stress at the edge of such contact regions when the components undergo oscillating, relative slip. In the presence of a bulk stress, cracks formed at the edge of the contact regions propagate and result in premature failure. In the absence of such a stress the cracks do not propagate and simply result in surface damage. If the components of the assembly are separated, subsequent application of a bulk alternating stress shows such damage to have a minimal effect on fatigue strength.

4. The combined effect of fretting and geometric stress concentration depends on the relative size of the associated stress fields. This is usually determined by the proportion of the interface over which slip occurs. In general, if the slip region is large the geometric stress concentration is low and fretting is the dominant factor. If the slip region is small the fatigue strength is determined principally by the overall geometric stress concentration.

5. Assessing the fatigue strength of assemblies by considering them as solids may give wrong answers. Similarly, geometric stress relief, as used in solid components to improve fatigue strength, may not raise the fatigue strength of the assembly to that of the equivalent solid, due to the effect of fretting. However geometric stress relief certainly improves the fatigue strength of assemblies even if fretting is not eliminated.

6. No totally effective, novel method for avoiding fretting failures is suggested by the work described in this thesis. Inhibiting crack initiation by surface treatment, or preventing fretting by the use of thin flexible interleaves, appear, from the work of other authors, to be partially successful. The use of geometric stress relief in conjunction with such methods will further improve the fatigue strength but, unless the geometry is changed extensively, fretting is unlikely to be eliminated entirely.

APPENDIX I

A COMPUTER PROGRAM TO SOLVE PLANE STRESS OR STRAIN PROBLEMS

The program used for the computation of the influence coefficients in stage 1 of the contact problem and the stresses in the plate in stage 3, was based extensively on a program written in Fortran by Y.K. Cheung at the University of Swansea. The program is discussed at some length in (40) and (42). For this reason the discussion here will be very limited. The version of the program listed at the end of this Appendix is written in Egdon 3, a Fortran dialect in use at Oxford, and makes use of disc file facilities rather than magnetic tapes which are used in the original version. The use of disc storage reduces the computing time for a given problem by a factor of approximately two. Sections of the original program which allow consideration of anisotropy and body forces, are omitted since they are not required in the problems solved in this investigation. Other changes are extremely minor. A flow diagram of the program is shown in fig. A1.1.

To solve a plane stress or plane strain problem, the component which is being analysed is divided up into a triangular mesh. The nodes and elements of the mesh are numbered consecutively. In order to reduce the storage required, the problem is solved using a scheme of matrix partitioning. The mesh is therefore divided into partitions, the maximum number of nodes in any one partition being 26. (For a note on the advantages and theory of partitioning see (40,42).) Other input data include the elastic properties, prescribed nodal displacements,

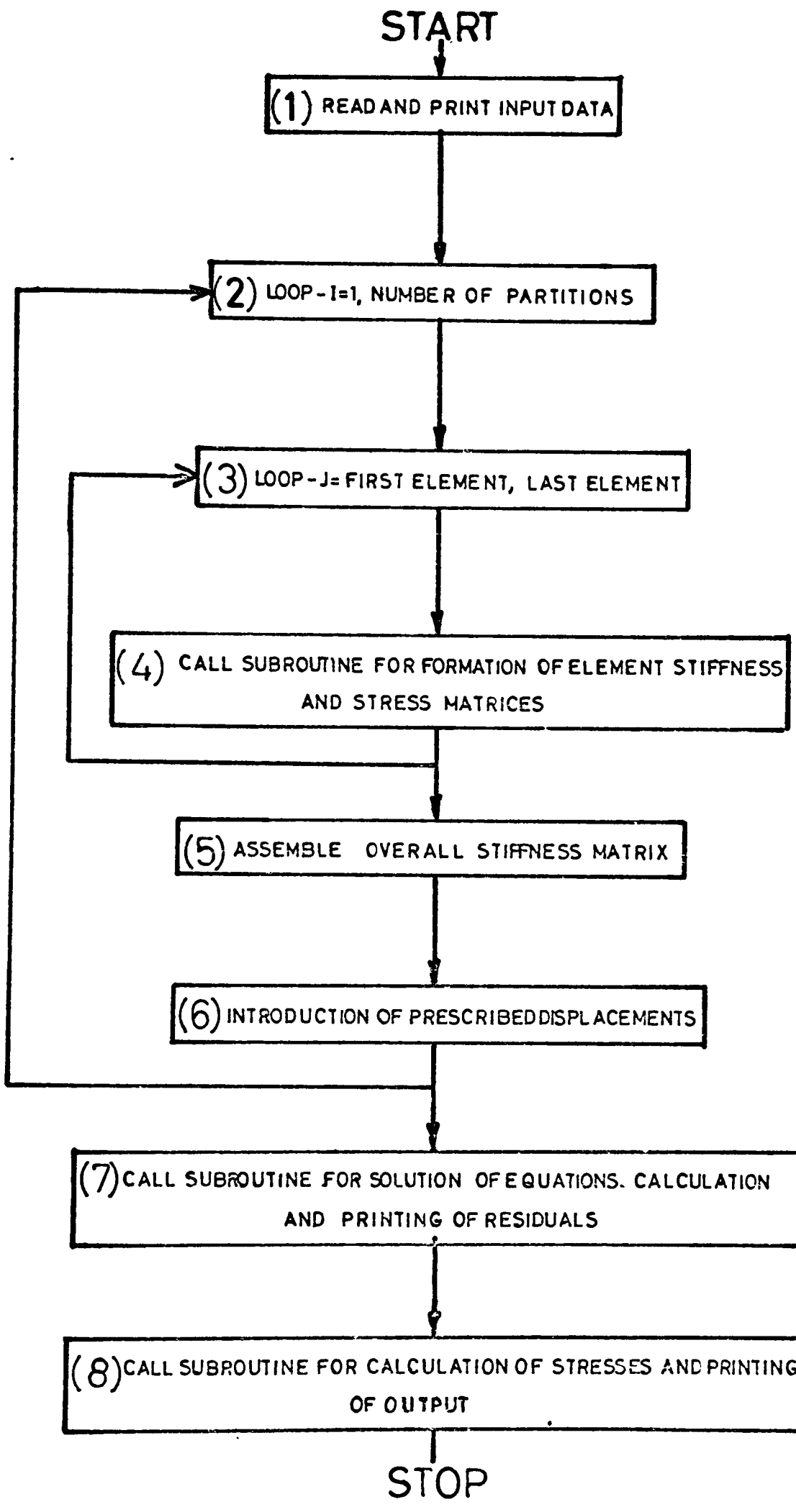


Fig. A1.1 Flow diagram of program to solve plane stress or plane strain problems using finite elements

external loads etc. The input is prepared as follows:

Input

1. 1 Card

Columns		
1 - 4	Number of problems to be run in one execution of program,	I4

2. 1 Card

Columns		
1 - 50	Title	50H

3. 1 Card

Columns		
1 - 4	Number of partitions ($\leq$15)	I4
5 - 8	Number of nodal points ($\leq$ 350)	I4
9 - 12	Number of elements ($\leq$ 450)	I4
13 - 16	Number of nodal points with prescribed displacements ($\leq$ 45)	I4
17 - 20	Number of load vectors ($\leq$ 4)	I4
21 - 24	0: plane strain. 1: plane stress	I4
25 - 28	Number of degrees of freedom per node	I4
29 - 32	Format number for nodal co-ordinates	I4
33 - 36	0: punch output. 1: do not punch output	I4

4. 1 Card for each nodal point (in ascending order).

Columns		
	x co-ordinate of nodal point) choice of	
	y co-ordinate of nodal point) format, see listing	

5, 1 Card for each element (in ascending order)

Columns		
1 - 4	Element number	I4
5 - 8)	Nodal points in anti-clockwise	I4
9 - 12)	rotation	I4
13 - 16)		I4

6. 1 Card for each nodal point with prescribed displacement.

Columns		
1 - 4	Nodal point number	I4
5 - 8 (	Displacement in x direction	
(	0: fixed	
(	1: free	I4

9 - 12	(Displacement in y direction (0: fixed (1: free	I4
13 - 28	Prescribed value of displacement in x direction	F 16.8
29 - 44	Prescribed value of displacement in y direction	F 16.8

7. 1 Card for each partition (in ascending order)

Columns

1 - 4	First element in partition	I4
5 - 8	Last element in partition	I4
9 - 12	First nodal point in partition	I4
13 - 16	Last nodal point in partition	I4

8. 1 Card

Columns

1 - 16	Young's modulus in x direction	F 16.5
17 - 32	Poisson's ratio in x direction	F 16.5
33 - 48	Shear modulus	F 16.5
49 - 64	Thickness	F 16.5

9. 1 Card

Columns

1 - 4	Number of nodal points with concentrated loads	I4

10. 1 Card for each nodal point with concentrated load.

Columns

1 - 4	Nodal point number	I4
5 - 20	Load in x direction	F 16.8
21 - 36	Load in y direction	F 16.8

Repeat 2 - 10 for each separate problem.

Output

The printed output of the listed program consists of the following:

(1) Nodal displacements.
(2) Residuals obtained by substituting solutions back into the equations.
(3) Stresses σ_x, σ_y and τ_{xy} at the centroid of each element.
(4) The principal stresses and the direction of the principal axes at the centroid of each element.

To compute influence coefficients the program was modified slightly. Sub-routine STRESS was omitted and

and sub-routine SOLVE modified so that the nodal displacement of the last partition only were computed. When partitioning the mesh it was arranged that the last partition contained only the nodes which are on the interface of the assembly. The interface nodal displacements (influence coefficients) were punched on cards along with the node number and a number representing the position and direction of the applied unit load. There were, of course, corresponding slight modifications to the main program, among which was an increase in certain storage areas so that a given mesh could be solved for 22 separate load vectors simultaneously. 22 sets of influence coefficients (corresponding to 11 nodes on the interface) could then be determined in one operation.

To compute stresses in the plate (stage 3) the program was modified slightly so that the output contained values of stress non dimensionalised with respect to various nominal values. This involved very small changes in sub routine STRESS.

Notation

NPROB	Number of problems to be done in one execution of program.
NPART	Total number of partitions.
NPOIN	Total number of nodal points.
NELEM	Total number of elements.
NBOUN	Total number of nodal points with prescribed displacements.
NCOLN	Total number of load vectors.
NP	NP = 0. Plane strain case; NP = 1, Plane stress case.
NFREE	Number of degrees of freedom per node.

NFORM	Indication of format used in nodal co-ordinate data.
NPUNCH	NPUNCH = 0, Punch output NPUNCH = 1 Do not punch output.
NONO	Node number.
X	x, y, co-ordinates of nodal points.
NOD	The three nodal numbers defining a triangular element, counting anticlockwise.
NEP	
NF(I)	Nodal point number I with prescribed displacement.
NB	NB(I,1) = 0, Displacement in x direction is prescribed. NB(I,2) = 0, Displacement in y direction is prescribed. NB(I,1) = 1, Displacement in x direction is not prescribed. NB(I,2) = 1, Displacement in y direction is not prescribed.
BV	BV(I,1) = Prescribed displacement in x direction. BV(I,2) = Prescribed displacement in y direction.
NSTART	Number of first element in each partition.
NEND	Number of last element in each partition.
NFIRST	Number of first node in each partition.
NLAST	Number of last node in each partition.
E1	Young's modulus.
P1	Poisson's ratio
GE	Shear modulus
THICK	Thickness of component.
NCONC	Number of nodal points at which there is a non zero external load.
K	Node number of nodes at which there is a non zero external load.
U	Magnitude of external loads.

PROGRAM LISTING

```
C                    MAIN PROGRAM
C   *   *   *   *   *   *   *   *   *   *   *   *   *   *   *   *   *   *   *
      DIMENSION X(350,2),XE(3,2),NF(30),NB(30,2),BV(30,2),NOD(450,3),
     1NSTART(15),NEND(15),NFIRST(15),NLAST(15)
      COMMON C(6,6),DBA(3,6),DB(3,6),A(6,2),B(3,6),ST(50,100),U(700,4
      READ 10,NPROB
   10 FORMAT(9I4)
      DO 20 LA=1,NPROB
      PRINT 100
      READ 101
      PRINT 101
  100 FORMAT(1H1)
  101 FORMAT(50H
      MARK1=0
      MARK4=0
C          READING AND PRINTING OF DATA
C   *   *   *   *   *   *   *   *   *   *   *   *   *   *   *   *   *   *   *
      READ 10,NPART,NPOIN,NELEM,NBOUN,NCOLN,NP,NFREE,NFORM,NPUNCH
      PRINT10,NPART,NPOIN,NELEM,NBOUN,NCOLN,NP,NFREE,NFORM,NPUNCH
      DO 30 I=1,NPOIN
      IF(NFORM-1) 11,12,13
   11 READ 351,NONO,X(I,1),X(I,2)
      PRINT351,NONO,X(I,1),X(I,2)
      GO TO 30
   13 READ 352,NONO,X(I,1),X(I,2)
      PRINT352,NONO,X(I,1),X(I,2)
      GO TO 30
   12 READ 35,X(I,1),X(I,2)
      PRINT35,X(I,1),X(I,2)
   30 CONTINUE
   35 FORMAT(4F16.8,F8.4)
  351 FORMAT(I4,2F7.4)
  352 FORMAT(I4,2F16.8)
      DO 40 I=1,NELEM
      READ  46,NUM,(NOD(I,J),J=1,3)
   40 PRINT 46,NUM,(NOD(I,J),J=1,3)
   46 FORMAT(5I4,2F16.8)
   45 FORMAT(3I4,2F16.8,I4)
      DO 50 I=1,NBOUN
      READ  45,NF(I),NB(I,1),NB(I,2),BV(I,1),BV(I,2)
   50 PRINT 45,NF(I),NB(I,1),NB(I,2),BV(I,1),BV(I,2)
      DO 60 I=1,NPART
      READ  10,NSTART(I),NEND(I),NFIRST(I),NLAST(I)
   60 PRINT 10,NSTART(I),NEND(I),NFIRST(I),NLAST(I)
      READ 3500,E1,P1,GE,THICK
      PRINT 3500,E1,P1,GE,THICK
 3500 FORMAT(4F16.5)
      READ  10,NCONC
    6 NPOIN2=NPOIN*2
      DO 68 I=1,NPOIN2
      DO 68 J=1,NCOLN
   68 U(I,J)=0.
      DO 69 J=1,NCOLN
      DO 69 I=1,NCONC
      READ  33,K,U(2*K-1,J),U(2*K,J)
   69 PRINT 33,K,U(2*K-1,J),U(2*K,J)
   33 FORMAT (I4,2F16.8)
C   *   *   *   *   *   *   *   *   *   *   *   *   *   *   *   *   *   *   *
C              FORMATION OF MATRICES
C   *   *   *   *   *   *   *   *   *   *   *   *   *   *   *   *   *   *   *
```

```
      INTER = 0
      MLB=0
      NLB=0
      DO 70 II=1,NPART
      DO 75 I=1,50
      DO 75 J=1,100
   75 ST(I,J)=0.
      NST=NSTART(II)
      NEN=NEND(II)
      K=NFIRST(II)
      L=NLAST(II)
      MINUS= K-1
      DO 80 LK=NST,NEN
      MARK1 = LK-1
      MM =LK-INTER
      DO 85 I=1,3
      JJ=NOD(LK,I)
      XE(I,1)=X(JJ,1)
   85 XE(I,2)=X(JJ,2)
      TH=THICK
      YM1=E1
      PR1=P1
      G=GE
C  *  *  *  *  *  *  *  *  *  *  *  *  *  *  *  *  *  *  *  *  *  *
C       CALCULATION OF ELEMENT STIFFNESS AND STRESS MATRICES
C  *  *  *  *  *  *  *  *  *  *  *  *  *  *  *  *  *  *  *  *  *  *
      CALL FEM(XE,YM1,PR1,G,NP,TH,MM,MARK1)
      DO 80 LL=1,3
      DO 80 KK=1,3
      IF (NOD(LK,KK)-K) 80,131,131
  131 IF (NOD(LK,KK)-L) 132,132,80
  132 M = NFREE*(NOD(LK,KK)-K)
      N = NFREE*(NOD(LK,LL)-K)
      I = NFREE*(KK-1)
      J = NFREE*(LL-1)
      IF (N) 80,900,900
  900 DO 5 NJ = 1,NFREE
      DO 5 MI = 1,NFREE
      MMI = M+MI
      NNJ = N+NJ
      IMI = I+MI
      JNJ = J+NJ
    5 ST(MMI,NNJ) = ST(MMI,NNJ) + C(IMI,JNJ)
   80 CONTINUE
C  *  *  *  *  *  *  *  *  *  *  *  *  *  *  *  *  *  *  *  *  *  *
C                 INTRODUCTION OF PRESCRIBED DISPLACEMENTS
C  *  *  *  *  *  *  *  *  *  *  *  *  *  *  *  *  *  *  *  *  *  *
      DO 290 I=1,NBOUN
      M=NF(I)-K
      MM=NF(I)-1
      IF (M) 290,242,242
  242 IF (M-24)243,243,290
  243 DO 230 J = 1,NFREE
      IF (NB(I,J)) 230,345,230
  345 NMI = NFREE*M+J
      ST(MMI,NMI) = ST(NMI,NMI)*.1E+12
      DO 233 JJ= 1,NCOLN
      JNJ=NFREE*MM+J
  233 U(JNJ,JJ) = ST(MMI,NMI)*BV(I,J)
```

```
  230 CONTINUE
  290 CONTINUE
      INTER=NEN
      MI = NFREE*MINUS+1
      NJ=NFREE*L
      M=NJ-MI+1
      IF (II - NPART) 115,116,115
  115 NA=NFREE*(NLAST(II+1)-MINUS)
      GO TO 117
  116 NA=N+1
  117 N=NA-M
      MM=M+1
      WRITE DISC 4,MARK4,NLB,NLB,M,N,((ST(I,J),I=1,M),J=1,M),((ST(I,J)
     1I=1,M),J=MM,NA),((C(I,J),I=MI,NJ),J=1,NCOLN)
      MARKAD=M**2+N*(NA-MM+1)+NCOLN*(NJ-MI+1)+4
      MLB=M
      NLB=N
   70 MARK4=MARK4+MARKAD/640 + 1
C          *   *   *   *   *   *   *   *   *   *   *   *   *   *   *
C       SOLUTION OF TRIDIAGONAL MATRICES AND CALCULATION OF RESIDUALS
C          *   *   *   *   *   *   *   *   *   *   *   *   *   *   *
      CALL SOLVE(NPART,NCOLN)
C          *   *   *   *   *   *   *   *   *   *   *   *   *   *   *
C           CALCULATION OF STRESS
C          *   *   *   *   *   *   *   *   *   *   *   *   *   *   *
      CALL STRESS(NPART,NFIRST,NLAST,NCOLN,NELEM,NOD,NFREE,NPOIN,
     1NPUNCH)
   20 CONTINUE
      STOP
      END
```

```
      SUBROUTINE FEM(XE,YM1,PR1,G,NP,TH,MM,MARK1)
      DIMENSION D(3,3),BTDBA(6,6),XE(3,2),R(3,3),ZX(3),ZY(3),RI(3,3),
     1XES(3,2)
      COMMON C(6,6),DBA(3,6),DB(3,6),A(6,6),B(3,6),ST(50,100),U(700,4)
      DO 20 J=1,6
      DO 21 I=1,3
      B(I,J)=0.
      DB(I,J)=0.
   21 DBA(I,J)=0.
      DO 20 I=1,6
      A(I,J)=0.
      BTDBA(I,J)=0.
   20 C(I,J)=0.
      DO 22 J=1,3
      DO 22 I=1,3
      R(I,J)=0.
   22 D(I,J)=0.
      ORX = (XE(1,1) + XE(2,1) + XE(3,1))*.333333
      ORY = (XE(1,2) + XE(2,2) + XE(3,2))*.333333
      DO 5 I=1,3
      XE(I,1) = XE(I,1) - ORX
    5 XE(I,2) = XE(I,2) - ORY
      ZX(1) = XE(2,2) - XE(3,2)
      ZX(2) = XE(3,2) - XE(1,2)
      ZX(3) = XE(1,2) - XE(2,2)
      ZY(1) = XE(3,1) - XE(2,1)
      ZY(2) = XE(1,1) - XE(3,1)
      ZY(3) = XE(2,1) - XE(1,1)
      ZK = XE(2,1)*XE(3,2) - XE(3,1)*XE(2,2)
      Z=3.*ZK
      A(1,1)=ZK/Z
      A(2,1)=ZX(1)/Z
      A(3,1)=ZY(1)/Z
      A(4,2)=A(1,1)
      A(5,2)=A(2,1)
      A(6,2)=A(3,1)
      A(1,3)=ZK/Z
      A(2,3)=ZX(2)/Z
      A(3,3)=ZY(2)/Z
      A(4,4)=A(1,3)
      A(5,4)=A(2,3)
      A(6,4)=A(3,3)
      A(1,5)=ZK/Z
      A(2,5)=ZX(3)/Z
      A(3,5)=ZY(3)/Z
      A(4,6)=A(1,5)
      A(5,6)=A(2,5)
      A(6,6)=A(3,5)
      B(1,2)=1.
      B(3,3)=1.
      B(3,5)=1.
      B(2,6)=1.
      IF (NP) 75, 81,75
C  *  *  *  *  *  *  *  *  *  *  *  *  *  *  *  *  *  *  *  *  *  *  *
C              ELASTICITY MATRIX FOR PLANE STRAIN CASE
C  *  *  *  *  *  *  *  *  *  *  *  *  *  *  *  *  *  *  *  *  *  *  *
   81 DEN = 1. - PR1 - 2.*PR1**2
```

```
      D(1,1) = YM1*(1.-PR1)/DEN
      D(2,1) = YM1*PR1/DEN
      D(1,2) = D(2,1)
      D(2,2) = YM1*(1. - PR1**2)/((1.+PR1)*DEN)
      D(3,3) = G
      GO TO 72
C  *  *  *  *  *  *  *  *  *  *  *  *  *  *  *  *  *  *  *  *  *
C                ELASTICITY MATRIX FOR PLANE STRESS CASE
C  *  *  *  *  *  *  *  *  *  *  *  *  *  *  *  *  *  *  *  *  *
   75 DEN=(1.-PR1*PR1)
      D(1,1)=YM1/DEN
      D(2,1)=PR1*YM1/DEN
      D(1,2)=D(2,1)
      D(2,2)=YM1/DEN
      D(3,3)=G
   72 DO 30 J=1,6
      DO 30 I=1,3
      DO 30 K=1,3
   30 DB(I,J)=DB(I,J) + D(I,K)*B(K,J)
      DO 40 J=1,6
      DO 40 I=1,3
      DO 40 K=1,6
   40 DBA(I,J)=DBA(I,J) + DB(I,K)*A(K,J)
C  *  *  *  *  *  *  *  *  *  *  *  *  *  *  *  *  *  *  *  *  *
C              STRESS MATRIX IS FORMED
C  *  *  *  *  *  *  *  *  *  *  *  *  *  *  *  *  *  *  *  *  *
      IF (NH) 126,126,127
  127 WRITE DISC 1,MARK1,((DBA(I,J),I=1,3),J=1,6),ORX,ORY
  126 CONTINUE
      VOL = .5*TH*Z
      DO 50 J=1,6
      DO 50 I=1,6
      DO 50 K=1,3
   50 BTDBA(I,J)=BTDBA(I,J) + B(K,I)*DBA(K,J)*VOL
      DO 60 J=1,6
      DO 60 I=1,6
      DO 60 K=1,6
   60 C(I,J)=C(I,J) + A(K,I)*BTDBA(K,J)
C  *  *  *  *  *  *  *  *  *  *  *  *  *  *  *  *  *  *  *  *  *
C        STIFFNESS MATRIX C IS FORMED
C  *  *  *  *  *  *  *  *  *  *  *  *  *  *  *  *  *  *  *  *  *
      RETURN
      END
```

```
      SUBROUTINE SOLVE(NPART,NCOLN)
      DIMENSION AM(50,50),BM(50,50),YM(50,50),TF(50,4),RS(50,4),F(50,4)
     1DIS(50,4)
      COMMON C(6,6),DA(3,6),DB(3,6),A(4,6),B(3,6),ST(50,100),U(700,4)
      EQUIVALENCE(AM,ST),(BM,ST(2501)),(TF,U),(DIS,U(701)),
     1(RS,U(1401)),(F,U(2101))
      MARK2=0
      MARK4=0
      DO 140 I=1,50
      DO 141 J=1,NCOLN
      TF(I,J)=0.
  141 RS(I,J)=0.
      DO 140 J=1,50
  140 YM(I,J)=0.
      DO 144 LL=1,NPART
      READ DISC 4,MARK4,NLB,NLB,M,N,((AM(I,J),I=1,M),J=1,M),((BM(I,J),
     1I=1,M),J=1,M),((F(I,J),I=1,M),J=1,NCOLN)
  150 DO 424 I=1,M
      DO 425 J=1,NCOLN
      F(I,J)=F(I,J)-TF(I,J)
  425 DIS(I,J)=F(I,J)
      DO 424 J=1,M
  424 AM(I,J)=AM(I,J)-YM(I,J)
      CALL MATINV(AM,M,DIS,NCOLN)
C  *   *   *   *   *   *   *   *   *   *   *   *   *   *   *   *   *   *   *   *
C            MATINV----------STANDARD IBM INVERSION PROGRAM          *
C  *   *   *   *   *   *   *   *   *   *   *   *   *   *   *   *   *   *   *   *
      WRITE DISC 2,MARK2,NLB,NLB,M,N,((AM(I,J),I=1,M),J=1,M),((BM(I,J),
     1I=1,M),J=1,M),((F(I,J),I=1,M),J=1,NCOLN)
      MARKAD=M**2+M*N+M*NCOLN+4
      MARK4=MARK4+MARKAD/640+1
      MARK2 = MARK4
      IF(NPART-LL)437,437,432
  432 CALL MATMU(AM,F,DIS,M,N,NCOLN)
      CALL MATTM(BM,DIS,TF,N,M,NCOLN)
      DO 110 J=1,M
      DO 110 I=1,M
      YM(I,J) = 0.
      DO 110 K = 1,M
  110 YM(I,J)=YM(I,J)+AM(I,K)*BM(K,J)
      DO111 J=1,N
      DO111 I=1,N
      AM(I,J)=0.
      DO 111 K=1,M
  111 AM(I,J)=AM(I,J)+BM(K,I)*YM(K,J)
      DO112 I=1,N
      DO 112 J=1,M
  112 YM(I,J)= AM(I,J)
  144 CONTINUE
  437 MARK4 = 0
      WRITE DISC 3,0,((DIS(I,J),I=1,M),J=1,NCOLN)
      MARK3 = 1
      IF(NPART-1) 600,600,601
  601 NA=NPART-1
      MARK2 = MARK2 = MARKAD/640 - 1
      DO 441 LL=1,NA
      MARKAK = NLB**2+NLB*NLB+NLB*NCOLN+4
      MARK2 = MARK2 = MARKAK/640 - 1
      READ DISC 2,MARK2,NLB,NLB,M,N,((AM(I,J),I=1,M),J=1,M),((BM(I,J),
```

```
     1I=1,M),J=1,N),((F(I,J),I=1,M),J=1,NCOLN)
      CALL  MATM(BM,DIS,TF,M,N,NCOLN)
      DO 444 J=1,NCOLN
      DO 444 I=1,M
  444 F(I,J) = F(I,J) - TF(I,J)
      CALL MATM(AM,F,DIS,M,M,NCOLN)
      WRITE DISC 3,MARK3,((DIS(I,J),I=1,M),J=1,NCOLN)
  441 MARK3 = MARK3 + 1
      PRINT 515
  515 FORMAT(10H RESIDUALS)
      MARK3 = MARK3 - 1
      DO 600 LL=1,NPART
      READ DISC 4,MARK4,NLB,NLB,M,N,((AM(I,J),I=1,M),J=1,M),((BM(I,J)
     1I=1,N),J=1,N),((F(I,J),I=1,M),J=1,NCOLN)
      MARKAD = N**2 + M*N + M*NCOLN + 4
      MARK4 = MARK4 + MARKAD/640 + 1
      MARK3 =MARK3 - 1
      IF(MARK3.GE.0)READ DISC3,MARK3,((TF(I,J),I=1,N),J=1,NCOLN)
      IF(MARK3) 5200,5120,5120
 5200 DO5130 J=1,NCOLN
      DO5130 I=1,N
 5130 TF(I,J) = 0.
 5120 DO 510 J=1,NCOLN
      DO 510 I=1,M
      F(I,J) = F(I,J) - RS(I,J)
      DO 512 K=1,M
  512 F(I,J) = F(I,J) - AM(I,K)*DIS(K,J)
      DO 510 L=1,N
  510 F(I,J) = F(I,J)-BM(I,L)*TF(L,J)
      CALL MATTM(BM,DIS,RS,N,M,NCOLN)
      DO 5000 I=1,N
      DO 5000 J=1,NCOLN
 5000 DIS(I,J) = TF(I,J)
  500 PRINT 31,((F(I,J),I=1,M),J=1,NCOLN)
   31 FORMAT(1H ,12E9.2)
  600 CONTINUE
      RETURN
      END
```

```
      SUBROUTINE STRESS(NPART,NFIRST,NLAST,NCOLN,NELEM,NOD,NFREE,NPOIN,
     1NPUNCH)
      DIMENSION NOD(450,3),NFIRST(15),NLAST(15)
      COMMON C(6,6),DBA(3,6),DB(3,6),A(6,6),B(3,6),ST(50,100),U(700,4)
       MARK3 = 0
      DO 600 II=1,NPART
      JJ=NPART+1-II
      M=NFREE*(NFIRST(JJ)-1) + 1
      N = NFREE*NLAST(JJ)
      READ DISC 3,MARK3,((U(I,J),I=M,N),J=1,NCOLN)
  600 MARK3 = MARK3 + 1
      PRINT 615
  615 FORMAT(5H NODE,16H X-DISPLACEMENTS,16H Y-DISPLACEMENTS)
      PRINT 32,((I,U(2*I-1,J),U(2*I,J),I=1,NPOIN),J=1,NCOLN)
   32 FORMAT(1H ,I4,2F16.8)
      PRINT 625
  625 FORMAT(16H ELEMENT NUMBER ,16H  FIRST  NODE   ,16H  SECOND NODE
     1,16H  THIRD  NODE   ,36H  X  AND  Y  COORDINATES OF CENTROID)
      PRINT 635
C  *  *  *  *  *  *  *  *  *  *  *  *  *  *  *  *  *  *  *  *  *  *
C     PRINCIPAL ANGLE IS THE ANGLE BETWEEN Y AXIS AND STRESS-1
C  *  *  *  *  *  *  *  *  *  *  *  *  *  *  *  *  *  *  *  *  *  *
  635 FORMAT(16H    X-STRESS    ,16H    Y-STRESS    ,
     116H    XYSTRESS    /16H    STRESS-1    ,16H    STRESS-2    ,
     216H PRINCIPAL ANGLE,16X,16HMAX SHEAR STRESS)
      DO 20 LL=1,NELEM
      MARK1 = LL-1
      READ DISC 1,MARK1,((DBA(I,J),I=1,3),J=1,6),ORX,ORY
      DO 620 J=1,NCOLN
      DO 620 I = 1,3
      JJ = NOD(LL,I)
      C(2*I-1,J) = U(2*JJ-1,J)
  620 C(2*I,J) = U(2*JJ,J)
      DO 630 J=1,NCOLN
      DO 630 I=1,3
      DB(I,J)=0.
      DO 630 K=1,6
  630 DB(I,J)=DB(I,J)+DBA(I,K)*C(K,J)
      PRINT 10, LL,(NOD(LL,J),J=1,3),ORX,ORY
      CALL PRIN(DB,A,NCOLN)
      PRINT 31, ((DB(I,J),I=1,3),(A(I,J),I=1,3),J=1,NCOLN)
      SSM = 0.5*(A(1,1)-A(2,1))
   25 PRINT 33,(A(I,1),I=1,3),SSM
      IF(NPUNCH) 2,2,20
    2 PUNCH 331,LL,ORX,ORY,(A(I,1),I=1,3)
   20 CONTINUE
   31 FORMAT(1H ,3F16.8)
   33 FORMAT(1HP,3F16.8,16X,F16.8)
  331 FORMAT(I4,5F12.6)
   10 FORMAT(1H ,4I4,2F16.8)
      RETURN
      END
```

```
      SUBROUTINE MATINV(A,N,B,M)
C     MATRIX INVERSION WITH ACCOMPANYING SOLUTION OF LINEAR EQUATIONS
C
C     INITIALIZATION
C
      DIMENSION IPIVOT(50),A(50,50),B(50,4),INDEX(50,2),PIVOT(50)
   10 DETERM=1.0
   15 DO 20 J=1,N
   20 IPIVOT(J)=0
   30 DO 550 I=1,N
C
C     SEARCH FOR PIVOT ELEMENT
C
   40 AMAX=0.0
   45 DO 105 J=1,N
   50 IF (IPIVOT(J)-1) 60, 105, 60
   60 DO 100 K=1,N
   70 IF (IPIVOT(K)-1) 80, 100, 740
   80 IF (ABS(AMAX)-ABS(A(J,K))) 85,100,100
   85 IROW=J
   90 ICOLUM=K
   95 AMAX=A(J,K)
  100 CONTINUE
  105 CONTINUE
  110 IPIVOT(ICOLUM)=IPIVOT(ICOLUM)+1
C
C     INTERCHANGE ROWS TO PUT PIVOT ELEMENT ON DIAGONAL
C
  130 IF (IROW-ICOLUM) 140,260,140
  140 DETERM=-DETERM
  150 DO 200 L=1,M
  160 SWAP=A(IROW,L)
  170 A(IROW,L)=A(ICOLUM,L)
  200 A(ICOLUM,L)=SWAP
  205 IF(M) 260, 260, 210
  210 DO 250 L=1,M
  220 SWAP=B(IROW,L)
  230 B(IROW,L)=B(ICOLUM,L)
  250 B(ICOLUM,L)=SWAP
  260 INDEX(I,1)=IROW
  270 INDEX(I,2)=ICOLUM
  310 PIVOT(I)=A(ICOLUM,ICOLUM)
  320 DETERM=DETERM*PIVOT(I)
C
C     DIVIDE PIVOT ROW BY PIVOT ELEMENT
C
  330 A(ICOLUM,ICOLUM)=1.0
  340 DO 350 L=1,N
  350 A(ICOLUM,L)=A(ICOLUM,L)/PIVOT(I)
  355 IF(M) 380, 380, 360
  360 DO 370 L=1,M
  370 B(ICOLUM,L)=B(ICOLUM,L)/PIVOT(I)
```

```
C
C
C       REDUCE NON-PIVOT ROWS
C
  380 DO 550 L1=1,N
  390 IF(L1-ICOLUM) 400, 550, 400
  400 T=A(L1,ICOLUM)
  420 A(L1,ICOLUM)=0.0
  430 DO 450 L=1,N
  450 A(L1,L) = A(L1,L)-A(ICOLUM,L)*T
  455 IF(M) 550, 550, 460
  460 DO 500 L=1,M
  500 B(L1,L)=B(L1,L)-B(ICOLUM,L)*T
  550 CONTINUE
C
C       INTERCHANGE COLUMNS
C
  600 DO 710 I=1,N
  610 L=N+1-I
  620 IF (INDEX(L,1)-INDEX(L,2)) 630, 710, 630
  630 JROW=INDEX(L,1)
  640 JCOLUM=INDEX(L,2)
  650 DO 705 K=1,N
  660 SWAP=A(K,JROW)
  670 A(K,JROW)=A(K,JCOLUM)
  700 A(K,JCOLUM)=SWAP
  705 CONTINUE
  710 CONTINUE
  740 RETURN
  750 END
```

```
      SUBROUTINE PRIN(D,C,N)
      DIMENSION D(3,6),C(6,6)
      DO 650 J=1,N
      C(1,J)=(D(1,J)+D(2,J))*.5 + SQRT((D(1,J)-D(2,J))**2/4.
     1 + D(3,J)**2)
      C(2,J) = (D(1,J)+D(2,J))*.5 - SQRT((D(1,J)-D(2,J))**2/4.
     1 + D(3,J)**2)
  650 C(3,J) = 57.3*ATAN((C(1,J)-D(2,J))/D(3,J))
      RETURN
      END
```

```
      SUBROUTINE MATM (D,B,DB,L,M,N)
      DIMENSION D(50,50),B(50,4),DB(50,4)
      DO 110 J=1,N
      DO 110 I=1,L
      DB(I,J)=0.
      DO 110 K=1,M
  110 DB(I,J) = DB(I,J)+D(I,K)*B(K,J)
      RETURN
      END
```

```
      SUBROUTINE MATT (D,B,DB,L,M,N)
      DIMENSION D(50,50),B(50,4),DB(50,4)
      DO 110 J=1,N
      DO 110 I=1,L
      DB(I,J)=0.
      DO 110 K=1,M
  110 DB(I,J)=DB(I,J)+D(K,I)*B(K,J)
      RETURN
      END
```

APPENDIX 2

A PROGRAM TO SOLVE THE CONTACT PROBLEM

A program was written to solve the contact problem previously described in Chapter 6 as stage 2 in the overall solution of stresses in a plate indented by a block. Equations are set up, with nodal forces as the unknowns, using the influence coefficients computed in Stage 1 and the boundary conditionswhich are detailed in Chapter 6. The program described, and listed at the end of this Appendix, is the version which employs iterative methods to solve the problem when the axial load is applied incrementally (see Section 6.3). The program is written in Egdon 3 and a flow diagram is shown in fig. A2.1. The formulation of the equations and the iteration processes are described in detail in Section 6.5.

To solve the equations directly slight changes are required in the section in which the equations are set up and the iteration section is, of course, omitted. In this case the length of the slip region is specified and the axial force is part of the solution (see Section 6.2.3).

Input

The input to the version of the program listed at the end of this Appendix, is as follows:-

1. 1 Card

   Columns

   1 - 4 The number of problems requiring different sets of influence coefficients I4

2. 1 Card

   Columns

   1 - 50 Title 50H

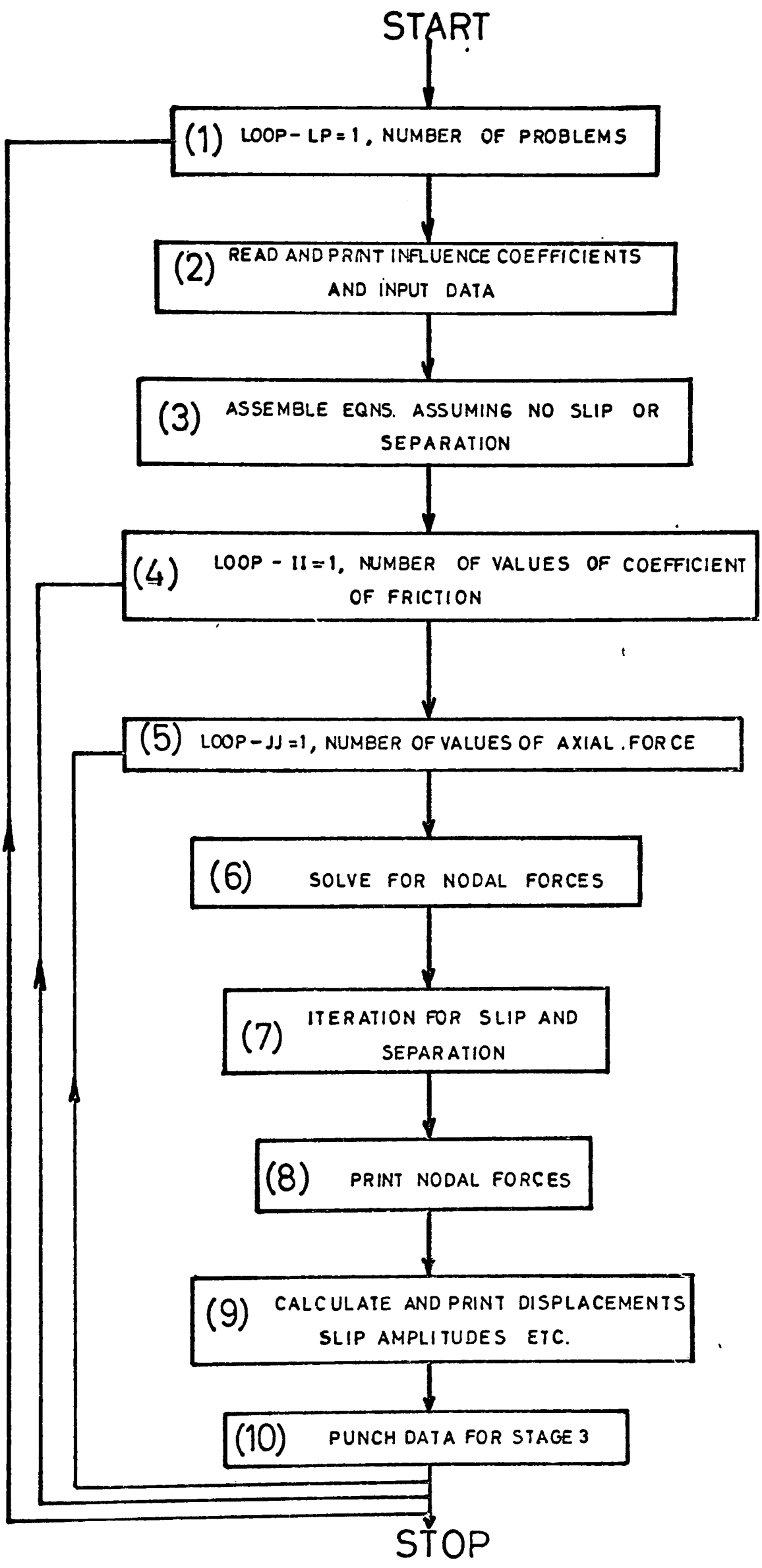


Fig. A2.1 Flow diagram for program to solve nodal forces in the contact region

3. 1 Card

Columns

1 - 4	The number of nodes on the interface	I4
5 - 8	The number of separate loading cycles starting from zero load	I4

4. 2 Cards for each node on the interface. The influence coefficients which are ready punched in the correct order and format in Stage 1.

5. 1 Card

Columns

1 - 4	The number of nodes on the end face of the plate	I4
5 - 8	The node number of the first node (in the plate) on the interface	I4

6. 1 Card

Columns

1 - 4))	The node numbers of the nodes on the end face of the plate	I4
5 - 8) etc.)		

7. 1 Card

Columns

1 - 5))	The axial force at each node on the end face of the plate for unit total axial force acting on the end face of the plate	F5.2
6 - 10) etc.)		

8. 1 Card

Columns

1 - 4	The number of different values of the coefficient of friction	I4
5 - 8	The number of different values of axial force to be considered in the load cycle	I4

9. 1 Card

Columns

1 - 5) 6 - 10) etc.)	Values of coefficient of friction	F5.2

10. 1 Card

Columns

1 - 5) 6 - 10) etc.)	Values of axial force	F 5.2

Output

The printed output of this program lists the following:-

(1) The value of the coefficient of friction and axial force.
(2) The value of the determinant of the matrix of coefficients of the equation for nodal forces.
(3) The residuals obtained having substituted the solutions back into the equations.
(4) The vertical displacement of the point on the top surface of the block at which the load F_1 is applied.
(5) The nodal forces at each node.
(6) x and y displacements of the interface nodes in the plate and block, and the slip amplitude at each node.
(7) Three simple checks to ensure that the boundary conditions are satisfied.

The value of the determinant, the residuals and the checks merely indicate the accuracy of the solution. If the value of the determinant is very small compared to typical elements of the matrix, errors are likely to be large. As might be expected, it was found that the magnitude of the determinant decreased as the number of nodes on the interface increased. In addition to the printed output, the nodal forces on the interface and the end of the plate are punched on cards in a suitable format for use in Stage 3 which uses the program listed in Appendix 1 to compute stresses in the plate.

Notation

The following notation is used.

NPROB	The number of problems requiring different sets of influence coefficients.
NPOIN	The number of nodes on the interface.
NLOOP	The number of separate loading cycles starting from zero load.

NENPT	The number of nodes on the end face of the plate
NBINT	The nodal number of the first node (in the plate) on the interface
NOD(I)	The nodal numbers of nodes on the end face of the plate
AXF(I)	The axial force at each node on the end face of the plate for a unit total axial force acting on the end face of the plate
NCF	The number of different values of the coefficient of friction
NFCE	The number of different values of total axial force to be considered in the load cycle
CF(I)	The values of the coefficient of friction
FORCE(I)	The values of the total axial force
Arrays, A1, A2, B1, B2, C1, C2, D1, D2, E, G.	Influence coefficients
Arrays ST) STT) STS)	The elements of the matrix of coefficients in the set of simultaneous equations for the nodal forces
Array U	The right hand side of the above equations
Array SLIP	The value of nodal slip amplutdes
DELTA	The displacement of the point on the top surface of the block at which load F_1 is applied
Array F2	The total axial force
Array P	The normal nodal forces
Array Q	The tangential nodal forces

PROGRAM LISTING

```
C       PROGRAM TO SOLVE FOR NODAL FORCES
        DIMENSION CF(10),NSP(10),NN(20),NP(20),A1(20,20),C1(20,20),
       1B1(20,20),D1(20,20),A2(20,20),C2(20,20),B2(20,20),D2(20,20),
       2G(20),E(20),F(20),H(20),P(20),Q(20),F2(10,10),RES(50),
       3ST(42,42),U(42),C(42),STT(1806),NOD(10),AXF(10)
       4,FORCE(20),CHECK2(20),SLIP(20)
       5,STS(42,42)
        COMMON W(1764)
        READ1,NPROB
        DO 1000 LP=1,NPROB
        PRINT6
        READ7
        PRINT 7
        READ1,NPOIN,NLOOP
C   *   *   *   *   *   *   *   *   *   *   *   *   *   *   *   *   *   *   *   *   *
C    READING AND PRINTING INFLUENCE COEFFICIENTS
C   *   *   *   *   *   *   *   *   *   *   *   *   *   *   *   *   *   *   *   *   *
        READ 8,(((NN(I),NP(J),A1(I,J),C1(I,J)),I=1,NPOIN),J=1,NPOIN)
        PRINT8,(((NN(I),NP(J),A1(I,J),C1(I,J)),I=1,NPOIN),J=1,NPOIN)
        READ 8,(((NN(I),NP(J),B1(I,J),D1(I,J)),I=1,NPOIN),J=1,NPOIN)
        PRINT8,(((NN(I),NP(J),B1(I,J),D1(I,J)),I=1,NPOIN),J=1,NPOIN)
        READ 8,(((NN(I),NP(J),A2(I,J),C2(I,J)),I=1,NPOIN),J=1,NPOIN)
        PRINT8,(((NN(I),NP(J),A2(I,J),C2(I,J)),I=1,NPOIN),J=1,NPOIN)
        READ 8,(((NN(I),NP(J),B2(I,J),D2(I,J)),I=1,NPOIN),J=1,NPOIN)
        PRINT8,(((NN(I),NP(J),B2(I,J),D2(I,J)),I=1,NPOIN),J=1,NPOIN)
        READ 8,((NN(I),NP(I),E(I),G(I)),I=1,NPOIN)
        PRINT9,((NN(I),E(I),G(I)),I=1,NPOIN)
C   *   *   *   *   *   *   *   *   *   *   *   *   *   *   *   *   *   *   *   *   *
C    READ AND PRINT INPUT DATA
C   *   *   *   *   *   *   *   *   *   *   *   *   *   *   *   *   *   *   *   *   *
        READ1,NENPT,NBINT
        READ4,(NOD(I),I=1,NENPT)
        PRINT4,(NOD(I),I=1,NENPT)
        READ 3,(AXF(I),I=1,NENPT)
        PRINT3,(AXF(I),I=1,NENPT)
        DO 100 LC=1,NLOOP
        READ1,NCF,NFCE
        READ3,(CF(J),J=1,NCF)
    2   PRINT 3,(CF(J),J=1,NCF)
    1   FORMAT(4I4)
        READ3,(FORCE(I),I=1,NFCE)
        PRINT3,(FORCE(I),I=1,NFCE)
    3   FORMAT(15F5.2)
    4   FORMAT(10I4)
    6   FORMAT(1H1)
    7   FORMAT(50H
    8   FORMAT(2I4,2E23.15)
    9   FORMAT(1I4,2E23.15)
   10   FORMAT(1I4,1E23.15)
        Z=.1E+7
C   *   *   *   *   *   *   *   *   *   *   *   *   *   *   *   *   *   *   *   *   *
C   EQUATIONS FOR SOLUTION OF NODAL FORCES SET UP ASSUMING NO SLIP
C   OR SEPARATION
C                   FORMATION OF MATRIX
C   *   *   *   *   *   *   *   *   *   *   *   *   *   *   *   *   *   *   *   *   *
        N=2*NPOIN+2
        DO 101 I=1,N
        DO 101 J=1,N
  101   ST(I,J)=0.
```

```
      DO 13 I=1,NPOIN
      DO 11 J=1,NPOIN
      ST(I,2*J-1)=C1(I,J)-C2(I,J)
   11 ST(I,2*J)=D1(I,J)-D2(I,J)
   13 ST(I,2*NPOIN+1)=-G(I)
  341 ST(2*NPOIN+1,2*NPOIN+1)=1.
      N1=NPOIN+1
      N4=NPOIN*2-1
      DO 16 I=N1,N4
      K=I-NPOIN
      DO 14 J=1,NPOIN
      ST(I,2*J-1)=A1(K,J)-A2(K,J)
   14 ST(I,2*J)=B1(K,J)-B2(K,J)
   16 ST(I,NPOIN*2+1)=-E(K)
      DO 18 J=1,NPOIN
   18 ST(2*NPOIN+2,2*J)=1.
      ST(2*NPOIN+2,2*NPOIN+2)=-1.
      N1=NPOIN+1
      DO 20 I=N1,N
   20 U(I)=0.
      DO 201 I=1,N
      DO 201 J=1,N
  201 STS(I,J)=ST(I,J)
C  *  *  *  *  *  *  *  *  *  *  *  *  *  *  *  *  *  *  *  *  *
C  FROM HERE ON PROCESS REPEATED FOR EACH VALUE OF COEF OF FRICTION
C  AND AXIAL FORCE
C  *  *  *  *  *  *  *  *  *  *  *  *  *  *  *  *  *  *  *  *  *
      DO 100 II=1,NCF
      DO 12 I=1,NPOIN
   12 SLIP(I)=0.
      CMU=CF(II)
      DO 100 JJ=1,NFCF
      DO 203 I=1,N
      DO 203 J=1,N
  203 ST(I,J)=STS(I,J)
      DO 19 I=1,NPOIN
   19 U(I)=Z
      ST(2*NPOIN+1,2*NPOIN+2)=-FORCE(JJ)
      N1=NPOIN+1
      DO 202 I=N1,N4
      K=I-NPOIN
  202 ST(I,NPOIN*2+2)=-SLIP(K)
  343 N1=2*NPOIN
      DO 161 I=1,N1
      DO 161 J=1,N
  161 ST(I,J)=ST(I,J)*Z
  162 ST(2*NPOIN,2*NPOIN-1)=1.
C  *  *  *  *  *  *  *  *  *  *  *  *  *  *  *  *  *  *  *  *  *
C        MATRIX IS FORMED
C  *  *  *  *  *  *  *  *  *  *  *  *  *  *  *  *  *  *  *  *  *
      PRINT33
      PRINT34,CMU,FORCE(JJ)
   33 FORMAT(16HCOEF OF FRICTION,13H  AXIAL FORCE)
   34 FORMAT(5X,F5.3,12X,F6.3)
```

```
      M=0
      DO 57 NITS=1,5
      DO 571 NIT=1,10
C  *  *  *  *  *  *  *  *  *  *  *  *  *  *  *  *  *  *  *  *  *
C  DETERMINANT EVALUATED USING LIBRARY ROUTINE
C  *  *  *  *  *  *  *  *  *  *  *  *  *  *  *  *  *  *  *  *  *
      CALL MDO1A(ST,N,DET,42)
      PRINT52
      PRINT50,DET
   52 FORMAT(11HDETERMINANT)
   50 FORMAT(E9.2)
      NA=N*(N+1)
      DO 212 I=1,NA
  212 STT(I)=0.
   51 DO 211 I=1,N
      DO 211 J=1,N
      IJ=(J-1)*N+I
  211 STT(IJ)=ST(I,J)
C  *  *  *  *  *  *  *  *  *  *  *  *  *  *  *  *  *  *  *  *  *
C   MATRIX INVERSION AND SOLN. OF EQNS. USING LIBRARY ROUTINE
C     SOLNS ARE C(J)
C  *  *  *  *  *  *  *  *  *  *  *  *  *  *  *  *  *  *  *  *  *
      CALL NEWLEQ(STT,U,C,N)
C          CALCULATION OF RESIDUALS
      DO 501 I=1,N
  501 RES(I)=0.
      DO 503 I=1,N
      DO 502 J=1,N
  502 RES(I)=RES(I)+ST(I,J)*C(J)
  503 RES(I)=RES(I)-U(I)
      PRINT505
  505 FORMAT(9HRESIDUALS)
      PRINT504,(RES(I),I=1,N)
  504 FORMAT(12E9.2)
C  *  *  *  *  *  *  *  *  *  *  *  *  *  *  *  *  *  *  *  *  *
C  CALCULATION OF NODAL FORCES AND CHECKS
C  *  *  *  *  *  *  *  *  *  *  *  *  *  *  *  *  *  *  *  *  *
      DELTA=1./C(2*NPOIN+2)
      F2(JJ,II)=DELTA*C(2*NPOIN+1)
      FC2=F2(JJ,II)
      DO 21 J=1,NPOIN
      Q(J)=DELTA*C(2*J-1)
      P(J)=DELTA*C(2*J)
   21 CHECK2(J)=(Q(J)/P(J))/COU
      PRINT 22
   22 FORMAT(16H      DELTA       ,16H        F2        )
      PRINT23,DELTA,FC2
   23 FORMAT(3E16.8)
      PRINT24
      PRINT23,((Q(J),P(J),CHECK2(J)),J=1,NPOIN)
   24 FORMAT(16H  SHEAR FORCE    ,16H  NORMAL FORCE  ,
     1 16H       CHECK2       )
   31 FORMAT(I4,2F16.8)
C  *  *  *  *  *  *  *  *  *  *  *  *  *  *  *  *  *  *  *  *  *
C            ITERATION FOR SLIP
C  *  *  *  *  *  *  *  *  *  *  *  *  *  *  *  *  *  *  *  *  *
C   ND AND NE USED TO ENSURE PRIMARY SLIP OCCURS FIRST
C    *  *  *  *  *  *  *  *  *  *  *  *  *  *  *  *  *  *  *  *
      NSLP=0
      ND=0
      NE=0
```

```
      DO 111 I=1,NPOIN
      IF(ABS(CHECK2(I))-1.00000001)111,111,112
  112 IF(D(I))114,114,115
  114 IF(NE)120,120,121
  120 FRIC=CMU
      ND=ND+1
      GO TO 123
  115 IF(ND)122,122,121
  122 FRIC=-CMU
      NE=NE+1
  123 NSLP=NSLP+1
      NI= NPOIN+I
      DO 113 J=1,N
  113 ST(NI,J)=0.
      ST(NI,2*I-1)=1.
      ST(NI,2*I)=FRIC
  111 CONTINUE
  121 M=M+NSLP
      IF(NSLP)116,116,117
  117 PRINT118,NIT
      PRINT119,N
  571 CONTINUE
  118 FORMAT(18HITERATION FOR SLIP,I4)
  119 FORMAT(16HNO OF SLIP NODES,I4)
C  *  *  *  *  *  *  *  *  *  *  *  *  *  *  *  *  *  *  *  *  *
C       ITERATION FOR SEPARATION
C  *  *  *  *  *  *  *  *  *  *  *  *  *  *  *  *  *  *  *  *  *
  116 NNEG=0
      DO 80 I=1,NPOIN
      XX=D(I)
      IF(XX)81,80,80
   81 NNEG=NNEG+1
      NPOINI=NPOIN+I
      DO 56 J=1,N
      ST(NPOINI,J)=0.
   56 ST(I,J)=0.
      ST(I,2*I)=1.
      ST(NPOINI,2*I-1)=1.
   55 U(I)=0.
   80 CONTINUE
      IF(NNEG)54,54,53
   53 PRINT58,NITS
   58 FORMAT(24HITERATION FOR SEPARATION,I4)
   57 CONTINUE
   54 PRINT28
      PRINT29
C  *  *  *  *  *  *  *  *  *  *  *  *  *  *  *  *  *  *  *  *  *
C   CALCULATION OF DISPLACEMENTS AND SLIP
C  *  *  *  *  *  *  *  *  *  *  *  *  *  *  *  *  *  *  *  *  *
      DO 32 I=1,NPOIN
      U1=0.
      U2=0.
      V1=0.
      V2=0.
      DO 26 J=1,NPOIN
      U1=U1+A1(I,J)*Q(J)+B1(I,J)*P(J)
      V1=V1+C1(I,J)*Q(J)+D1(I,J)*P(J)
      V2=V2+C2(I,J)*Q(J)+D2(I,J)*P(J)
   26 U2=U2+A2(I,J)*Q(J)+B2(I,J)*P(J)
```

```
      U2=U2+E(I)*FC2
      V2=V2+G(I)*FC2
      SLIP(I)=U1-U2
      CHECK1=V1-V2-DELTA
      PRINT27,I,U1,U2,V1,V2,SLIP(I),CHECK1
   32 CONTINUE
      CHECK3=0.
      DO 35 J=1,NPOIN
   35 CHECK3=CHECK3+P(J)
      PRINT36
      PRINT37,CHECK3
   36 FORMAT(16H     CHECK3       )
   37 FORMAT(2E10.8)
   28 FORMAT(4HNODE,32H                X-DISP                ,
     132H                Y-DISP                ,16H       SLIP       ,
     216H      CHECK1      )
   29 FORMAT(20H            BLOCK       ,16H       PLATE      ,
     116H       BLOCK       ,16H       PLATE      )
   30 FORMAT(3I4,2F16.8)
   27 FORMAT(I4,7F16.8)
C  *  *  *  *  *  *  *  *  *  *  *  *  *  *  *  *  *  *  *  *  *  *
C     PUNCH DATA FOR STRESS CALCULATIONS
C  *  *  *  *  *  *  *  *  *  *  *  *  *  *  *  *  *  *  *  *  *  *
   99 PUNCH93,II,CMU
      PUNCH200,FC2
  200 FORMAT(F16.5)
      DO 91 I=1,NPNPT
      FF=-FC2*AXF(I)
   91 PUNCH31,NOD(I),FF
   98 FORMAT(I4,F8.2)
      DO 25 J=1,NPOIN
      NOND=J+NBINT-1
      P(J)=-P(J)
   25 PUNCH31,NOND,Q(J),P(J)
  100 CONTINUE
 1000 CONTINUE
      YYYYYYY
      STOP
      END
```

APPENDIX 3

PHOTOELASTIC DETERMINATION OF STRESS IN FATIGUE SPECIMENS

Photoelastic methods were used in an attempt to determine the stress distributions in solid and assembled fatigue specimens possessing the geometries illustrated in fig. 3.7. Full scale models of the specimens were made from $\frac{1}{4}$" sheet araldite which was sensibly free of residual stress. Stresses induced by the machining process were removed by annealing. The models of both the solids and the assemblies were loaded in an identical way to the corresponding fatigue specimens. The axial load was tensile and the ratio of the nominal axial stress on the interface to the nominal normal pressure (ξ) was 8:1. Photoelastic analyses give values of relative retardation which are proportional to the maximum shear stress (τ_{max}). Fig. A3.1 depicts a model under load. Results were obtained for the variation of τ_{max} on the interface of assemblies or on a line corresponding to the interface in the solid models and compared with the maximum shear stress away from the blocks (σ_o). Where the maximum value of τ_{max}/σ_o was not on the interface or the line corresponding to it this value was noted. The results are shown in Table A3.1.

Specimen	Max.value of τ_{max}/σ_o on interface	Position of max.value on interface	Max.value of τ_{max}/σ_o if elsewhere	Position of max. value elswhere
Sharp cornered solid Sharp cornered assembly	2.5 1.09	Corner Corner	- -	- -
Inc.rad.solid Inc.rad.assembly	1.2 0.9	End of 'interface' $\frac{1}{8}$" from end of interface	- 1.1	- Toe of radius
Full radius solid Full radius assembly	0.41 0.55	$\frac{1}{4}$" from end of interface $\frac{1}{4}$" from end of interface	1.2 1.2	Toe of radius Toe of radius

Table A3.1

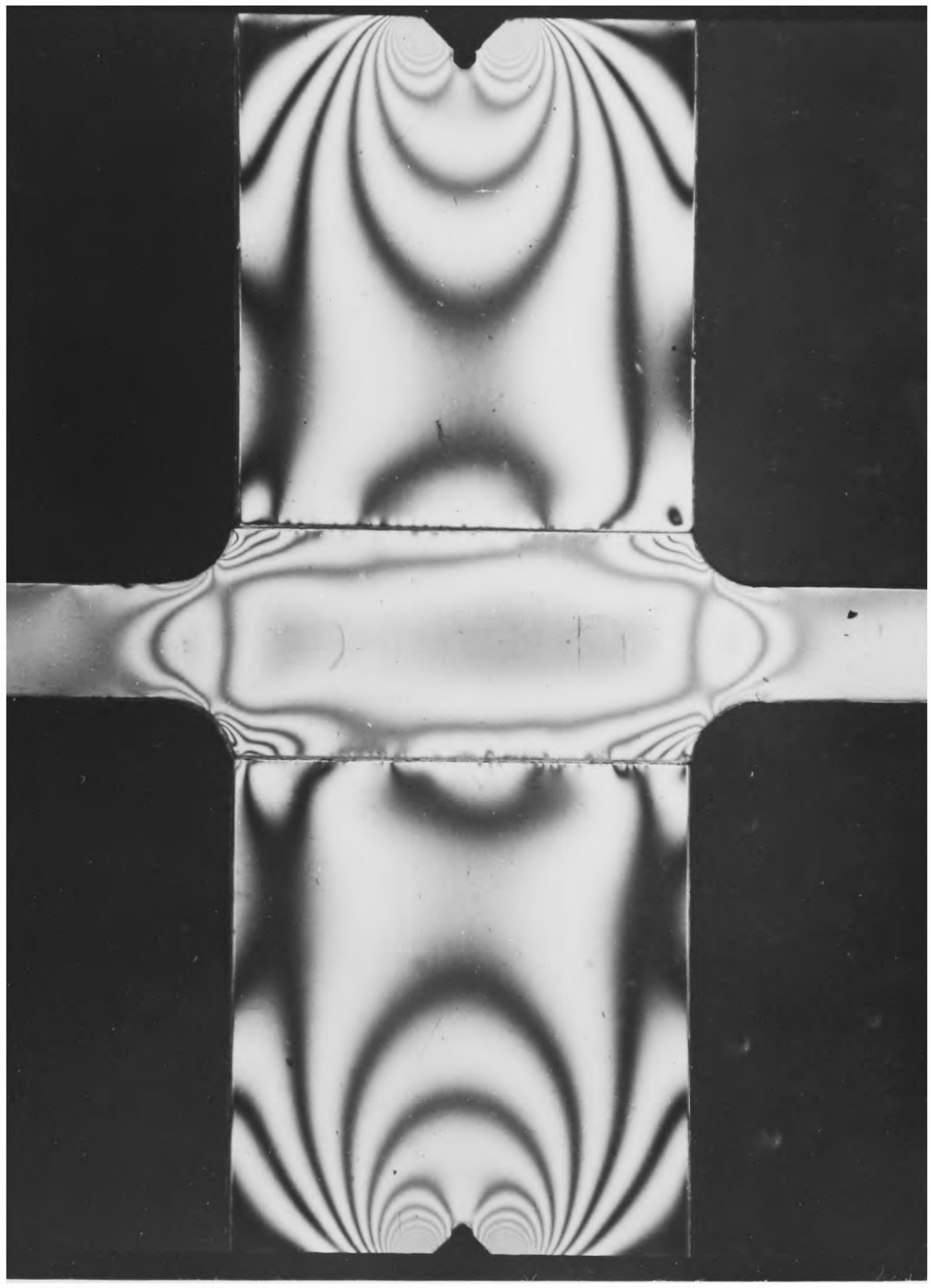


Fig.A3.1 Photoelastic model of a full radiused assembly under load.

Where stress concentrations were high (e.g. the sharp cornered solid) accurate values are very difficult to estimate because the fringes become very close together. Thus it is thought that the results for the stress concentration in the sharp cornered solid and incomplete radius solid, in which the maximum stress occurred where the stress gradient was high, indicate values which are lower than the true value - a theory supported by the fatigue results. However the most surprising feature of the results was the low stress concentrations in the assemblies, particularly the sharp cornered assembly.

At the time the tests were carried out, such low stress concentrations were thought to be due to the low coefficient of friction between two araldite surfaces. The value of the coefficient of friction in the araldite assemblies was found to be about 0.2 by an experimental method similar to that described in Section 3.2.7. It was thought that such a low value of the coefficient of friction would allow much greater stress relief due to slip than would occur in fatigue specimens where the coefficient of friction is 0.8 (after the surfaces have experienced several thousand cycles of reversed slip). The results for assemblies were therefore ignored until fatigue test results suggested they might have been approximately correct.

The theoretical analysis of stress in assemblies (Chapters 5-7) showed that the photoelastic results for assemblies were, in fact, very good and that the low coefficient of friction was only a secondary cause of the low

stress concentrations found in the araldite models.

The photoelastically determined stress distributions in assemblies are plotted in fig. 7.29 and compared to theoretical results which were obtained assuming a value of 0.2 for the coefficient of friction. A comparison of these results with those in figs. 7.22, 7.26 and 7.27, which illustrate the variation of maximum shear stress in assemblies with a coefficient of friction of 0.8, reveals the small variation in stress, associated with a change in the coefficient of friction from 0.2 to 0.8.

REFERENCES

1. M.B. Coyle and S.J. Watson. 'Fatigue strength of turbine shafts with shrunk-on discs', Proc.I.Mech.E., 1963-64, Vol.178, Part 1, p.147.
2. H. Ouchida. 'Fatigue strength and size effect of shrink fitted specimens'. Bull.Japan Soc.Mech.Engrs., 1962, Vol.5, p.587.
3. J.D. McAllan. 'Fatigue strength of shafts with shrunk-on rings', N.E.L. Report No.259, Min.Tech., 1966.
4. W.W. Maxwell, B.R. Dudley, A.B. Cleary, J. Richards, J. Shaw. 'Measures to counter fatigue failures in railway axles'. Proc.I.Mech.E., 1967-68, Vol.182, Part 1, p.89.
5. E.S. Burdon. 'The effect of various surface coatings on the fatigue strength of press fitted model wheel and axle assemblies'. British Railway Board Research Report, No. E448D, 1963.
6. O.J. Horger. 'Fatigue of large shafts by fretting corrosion'. Proc.Int.Conf.Fatigue Metals, 1956, 352, (I.Mech.E., London).
7. A.J. Fenner, J.E. Field. 'A study of the onset of fatigue damage due to fretting'. Proc.N.E.Coast Inst. of Engrs. and Shipbuilders, 1960, Vol.76, p.183.
8. J.E. Field, D.M. Waters. 'Fretting fatigue strength of En 26 steel'. N.E.L. Report No.275, Min.Tech., 1967.
9. J.E. Field. 'Effect of direction of fretting on the fatigue strength of L.65 Aluminium Alloy'. N.E.L. Report No.120, Min.Tech., 1963.
10. J.E. Field, D.M. Waters. 'The fretting-fatigue strength of a 100 tons/in^2 EN.30B steel'. N.E.L. Report No.340, Min.Tech., 1968.

11. K.L. Johnson, J.J. O'Connor. 'Mechanics of fretting'. Proc.Appl.Mechanics Group Conv., Newcastle 1964, Paper 11, (I.Mech,E., London).

12. J.J. O'Connor, K.L. Johnson. 'The role of surface asperities in transmitting tangential forces between metals'. Wear, 6 (1963), p.118.

13. P.G. Forrest. 'Fatigue of Metals'. Pergammon, 1962.

14. G.A. Tomlinson, P.L. Thorpe, H.J. Gough. 'An investigation of the fretting corrosion of closely fitted surfaces'. Proc.I.Mech.E., 1936, Vol.141, p.223.

15. K.H.R. Wright. 'An investigation of fretting corrosion'. Proc.I.Mech.E., 1952-53, Vol.1B, p.556.

16. I-Ming Feng, B.G. Rightmire. 'An experimental study of fretting'. Proc.I.Mech.E., 1956, Vol.170, p.1055.

17. A.J. Fenner, K.H.R. Wright, J.Y. Mann. 'Fretting corrosion and its influence on fatigue failure'. Proc.Int.Cont.Fatigue Metals, 1956, p.386 (I.Mech.E., London).

18. R.B. Waterhouse. 'Influence of local temperature increase on the fretting corrosion of mild steel'. J.Iron & Steel Inst., April 1961, p.301.

19. R.B. Waterhouse, P.A. Brook, G.M.C. Lee. 'The effect of electro deposited metals on the fatigue behaviour of mild steel under conditions of fretting corrosion'. Wear, Vol.5, 1962, p.235.

20. J.E. Bowers, N.J. Finch, A.R. Goreham. 'The prevention of fretting fatigue in aluminium alloys'. Proc.I.Mech.E. 1967-68, Vol.182, Part 1, p.703.

21. J.A. Collins, B.M. Marco. 'The effect of stress direction during fretting on subsequent fatigue life'. Preprint No.69, presented at 67th Annual Meeting of A.S.T.M., June 1964.

22. J.A. Collins. 'Fretting fatigue damage factor determinations'. Paper No.64-WA/MD-10, A.S.M.E., 1964.

23. W.D. Milestone. 'An investigation of the basic mechanism of mechanical fretting and fretting fatigue at metal-to-metal joints'. Thesis 1966, Ohio State Univ.

24. K. Nishioka, K. Hirakawa. 'Fundamental Investigation of fretting fatigue'. Bull.Japan Soc.M.E., 1969, Vol.12, No.50, p.180.

25. K. Nishioka, K. Hirakawa. 'Fundamental investigation of fretting fatigue, Part 3'. Bull.Japan.Soc.M.E., 1969, Vol.12, No.51, p.397.

26. E.M. Eden, W.H. Rose, F.L. Cunningham. 'The endurance of metals'. Proc.Inst.Mech.Engr., Vol.4 (1911), p.875.

27. R. Kühnel. 'Axle breakages of railway vehicles and their causes'. Glasers Annalen, Nos.1312, 1313 (1932).

28. O.J. Horger. 'Influence of fretting corrosion on the fatigue strength of fitted members'. A.S.T.M. Symp. on Fretting Corrosion, STP 144 (1952), 40.

29. R.E. Peterson, A.M. Wahl. 'Fatigue of shafts at fitted members, with a related photoelastic analysis'. Proc.A.S.M.E., 1935, J.Appl.Mech., 1935, Vol.57, A-1.

30. S. Wise, E.S. Burdon. 'The dual roles of design and surface treatment in combating fatigue failures. J.Inst.Loco Engrs., 1964-65, Vol.54, p.142.

31. D.J. White. 'Fatigue strength of small pinned connections made from alloy steel FV520B'. Proc.I.Mech.E., 1967-68, Vol.182, Part 1.

32. W.J. Harris. 'Metallic Fatigue'. Pergamon, 1961.

33. H. Hertz, quoted in 43, p.372 ff.

34. J.J. O'Connor. 'Compliance under a small torsional couple of an elastic plate pressed between two identical elastic spheres'. A.S.M.E., J.Appl.Mech. Vol.33, E, No.2, p.377.

35. H. Poritsky. 'Stresses and deflections of cylindrical bodies in contact with application to contact of gears and of locomotic wheels'. J.Appl.Mech., Vol.17, No.2, 1950, p.191.

36. H.D. Conway, S.M. Vogel, K.A. Farnham, S.So. 'Normal and shearing contact stresses in indented strips and slabs'. Int.J.Eng.Sci., Vol.4, p.343, 1966.

37. H.D. Conway, K.A. Farnham. 'The contact stress problem for indented strips and slaps under conditions of partial slipping'. Int.J.Eng.Sci., Vol.5, p.145, 1967.

38. R. Khadem. D.Phil.Thesis, Oxford University, 1967.

39. O.C. Zienkiewicz, Y.K. Cheung. 'The finite element method for analysis of elastic isotropic and orthotropic slabs'. Proc.Inst.Civ.Eng., Vol.28, p.471, 1964.

40. O.C. Zienkiewicz, Y.K. Cheung. 'The finite element method'. McGraw Hill, (London), 1967.

41. R.K. Livesley. 'Matrix Methods in Structural Analysis', Pergamon, 1964.

42. Y.K. Cheung. 'Computer Program Report No.1'. Centre for Numerical Methods in Engineering, University of Wales, Swansea, 1967.

43. S. Timoshenko, J.N. Goodier. 'Theory of elasticity'. 2nd Edition, 1951, McGraw-Hill.

44. F.P. Bowden, D. Tabor. 'Friction and lub ication of solids'. O.U.P., 1950.

45. J.O. Smith, C.K. Liu. 'Stresses due to tangential and normal loads on an elastic solid with application to some contact stress problems'. J.Appl.Mech., Vol.20, No.2, (1953), p.157.